DOE/ER/61488--T1-PL5

A CONCEPTUAL SEDIMENTOLOGICAL-GEOSTATISTICAL MODEL OF AQUIFER HETEROGENEITY BASED ON OUTCROP STUDIES

by

J. Matthew Davis

Submitted in Partial Fulfillment
of the Requirements for the

Doctorate of Philosophy in Hydrology

New Mexico Institute of Mining and Technology
Department of Geoscience

Socorro, New Mexico

January 1994

DISCLAIMER

TABLE OF CONTENTS

PART I
INTRODUCTION

PART II
GENERAL METHODOLOGY

PART III
SIERRA LADRONES STUDY

PART IV
OTHER STUDIES

PART V
DISCUSSION AND CONCLUSIONS

LIST OF FIGURES

LIST OF TABLES

ACKNOWLEDGEMENTS

This research was funded by the Subsurface Science Program, Office of Energy Research, U.S. Department of Energy under contracts DE-FG04-89ER60843 and DE-FG03-92ER61488. The initial work on this project was supported by the New Mexico Water Resources Research Institute (#1345681).

I would like to thank my committee for the opportunity to work with them on this project that involves such a wide range of disciplines. Drs. Fred M. Phillips and John L. Wilson provided insight and direction throughout the various phases of research. I thank Dr. Dave W. Love for his guidance and assistance in the field and Dr. Allan L. Gutjahr for his valuable input.

This project involved several students that greatly contributed to the results presented in this dissertation. I am fortunate to have had the opportunity to work with and learn from them. The initial architectural element mapping was undertaken and artfully performed by Ruth C. Lohmann. Madeline B. Gotkowitz was in charge of the small-scale permeability studies and contributed quality data and analyses. I would also like to thank Susan J. Colarullo for her discussions on various aspects of heterogeneity and fluid flow.

I would also like thank my family and friends for their support throughout my stay at New Mexico Tech. Most of all, thanks are due to my wife Ruth Lohmann Davis for her unending support.

ABSTRACT

Spatial variation of hydraulic properties has been recognized as a dominant control on fluid flow through natural porous media. One approach to quantifying the subsurface variability inherent in geologic materials is geostatistical modeling. A variety of geostatistical, or stochastic, models have been developed to represent heterogeneity. Each of the models is based on a different mathematical formulation and result in different spatial patterns. Ubiquitous to the models are assumptions regarding the nature of the underlying probability distribution and the correlation structure. One of the main difficulties in applying these models is the lack of a rationale for choosing one over another based on physical evidence. Another difficulty arises from the amount of data necessary to estimate the parameters.

Incorporation of geological information has been proposed as one method of providing both ground truth to the geostatistical models and estimating the necessary parameters from minimal data. The objective of this study was two-fold. The first objective was to obtain intensive data sets of the spatial distribution of permeability and observed geological features in a variety of geological settings then, second, to investigate the relationship between the observed sedimentological characteristics and quantitative models of heterogeneity.

Three outcrop studies were conducted in deposits of different depositional environments. At each site, permeability measurements were obtained with a lightweight, syringe-based, air-minipermeameter developed as part of this study. In addition, the geological units were mapped with either surveying, photographs, or both. Geostatistical analysis of the permeability data was performed to estimate the characteristics of the probability distribution function and the spatial correlation structure. The information obtained from the geological mapping was then compared with the results of the geostatistical analysis for any relationships that may exist.

The main field site was located in the Albuquerque Basin of central New Mexico at an outcrop of the Pliocene-Pleistocene Sierra Ladrones Formation. The geologic framework of

lithofacies and architectural elements were adopted for the mapping. Four principal architectural elements were defined: 1) a high-energy channel element consisting of primarily sand and gravel lithofacies; 2) a low-energy channel element consisting of primarily sand lithofacies; 3) an overbank fine element consisting of sand, silt and clay lithofacies; and 4) a paleosol element consisting of ancient soils with various parent materials. The architectural elements were mapped over a 20 meter vertical section along approximately two kilometers of outcrop and approximately 2,000 permeability measurements were obtained. Results of the statistical analysis indicated that 1) the architectural elements exhibit different mean log-permeability distributions that approximate a log-normal distribution; 2) the spatial correlation structure exhibits at least two scales corresponding to the variability associated with the assemblage of lithologic facies within architectural elements and the variability associated with the assemblage of architectural elements; 3) at the lithofacies scale, the shape of the correlation function appears to coincide with the character of the internal fluvial bounding surfaces; and 4) at the architectural-element scale, the correlation structure exhibits non-orthogonal anisotropy that appears to coincide with the axis of deposition.

The second study was conducted on the walls of waste pits in alluvial fan deposits at the Nevada Test Site. Approximately 500 permeability measurements were obtained from two pit walls each approximately 50 meters wide by 10 meters high. The geologic units consisted primarily of sheet flood and debris flow deposits. Results of the statistical analysis indicate that: 1) the sheet flood and debris flow deposits exhibit different mean log-permeability; 2) the variance of the log-permeability distribution within the sheet flood and debris flow units is higher than the variance estimated from the lithofacies-scale studies at the main field site and the combination of these two distributions results in a variance of log-permeability of approximately 1.1; and 3) the correlation structure appears to exhibit two scales with correlation lengths on the order of centimeters and meters, respectively.

The third study was conducted on an outcrop of an eolian deposit (Miocene) south of Socorro, New Mexico. Approximately 200 permeability were obtained over an area approximately 30 meters wide by five meters high. One type of facies (grain-fall) dominated

the outcrop resulting in a low variance of log-permeability. The estimated correlation structure exhibited two distinct scales with correlation lengths on the order of centimeters and meters, respectively.

The results of the three studies were then used to construct a conceptual model relating depositional environment to geostatistical models of heterogeneity. The deposits associated with a particular depositional environment are characterized geologically by the occurrence and spatial assemblage of lithofacies and architectural elements. In the conceptual model, the occurrence of lithofacies and architectural elements provides insight into the character of the underlying probability distribution, whereas the spatial assemblage of lithofacies and architectural elements provides insight into the character of the spatial correlation structure. The model presented is largely qualitative but provides a basis for further hypothesis formulation and testing.

Inherent in the analysis of sedimentary deposits are the bounding surfaces that separate hierarchical units (e.g. lithofacies and architectural elements). Results of the studies also indicate that these bounding surfaces may provide a geologic framework for future theoretical developments.

CHAPTER 1: INTRODUCTION

One of the major challenges facing hydrogeology today is that of groundwater contamination. The migration of a contaminant plume is controlled by the mean groundwater seepage velocity. Spatial variations in local groundwater velocities are associated with spatial variations in hydraulic conductivity. This differential advection results in a mechanical mixing known as macrodispersion. In general, macrodispersion is directly related to the heterogeneities encountered by the migrating plume.

Understanding and predicting contaminant migration and dispersion requires an understanding of subsurface heterogeneity at the scale of the contaminant plume. Spatial variability of hydrologic properties results from spatial variability of geologic materials (e.g. Lake et. al., 1991). Since geological materials of a particular aquifer are fixed, the heterogeneity is deterministic. That is, at every location there is one value of hydraulic conductivity.

However, obtaining the entire set of values is not feasible and a statistical representation of heterogeneity is often employed. Such statistical representations of heterogeneity provide a means of statistically characterizing contaminant plume evolution. In essence, the lack of knowledge regarding the hydrologic properties in the subsurface translates into uncertainty in the behavior of a contaminant plume. As the accuracy of subsurface characterization increases, the ability to understand and predict contaminant plume behavior increases.

Statistical models of subsurface heterogeneity are based on an assumption that hydraulic conductivity at each location in space is a realization of a random process which follows some probability distribution. In addition, the value of a realization at a given location is statistically dependent on neighboring values. The distance over which the values are statistically related is called the correlation length. Conceptually, this spatial correlation of hydraulic conductivity corresponds to the relative homogeneity within lithologic facies. Values of hydraulic conductivity separated by distances less than the average dimension of the lithologic facies are statistically correlated, whereas those separated by distances exceeding the average dimension of lithologic facies are uncorrelated.

A wide variety of statistical models have been proposed in the literature, each based on different methods for generating spatially correlated random variables and each exhibiting overall differences in appearance. The most common model is the multi-variate Gaussian model which represents the hydraulic conductivity as a log-normal distribution at each location, with a single scale of correlation. The spatial variation of hydraulic conductivity in these models is continuous and relatively smooth. The primary benefit of such a conceptualization is that the equations of flow and transport can be solved analytically (e.g. Bakr et al., 1978; Gelhar and Axness, 1983). The disadvantages of the multi-variate Gaussian model are the tendency for regions of extreme (high and low) values to be isolated and volumetrically under-represented (Journel and Alabert, 1988) and the inability to represent abrupt spatial changes in hydraulic conductivity.

Multi-variate Gaussian models can also be used to represent multiple-scale heterogeneity. Several workers (e.g. Wheatcraft and Tyler, 1988; Hewitt and Behrens, 1990; Neuman, 1990) have proposed that a fractal model may be more appropriate for geological media. Fractal models of heterogeneity have the advantage of being amenable to theoretical analysis. However, while geological features are known to occur at a variety of scales, the degree to which they are self-similar has yet to be evaluated.

Burrough (1983a,b) assessed the applicability of the fractal model to represent the spatial variation of soil properties along a one-dimensional transect, but preferred a nested non-fractal model in which the finite number of correlation lengths correspond to the scales of the dominant pedogenic processes. The non-fractal nested model (Burrough, 1983b) preserves both abrupt (discrete) changes in soil properties at large scales and the gradual (continuous) processes at small scales. Colarullo and Gutjahr (1991) have also proposed a multi-dimensional discrete model of heterogeneity based on a Markov random field.

In addition to the numerous models developed for quantifying solute transport in aquifers, petroleum researchers are also active in the development of statistical models of geological heterogeneity. Haldorsen and Damsleth (1990) provide a comprehensive review of the statistical models used to represent geological heterogeneity of petroleum reservoirs.

The proliferation of statistical models has proceeded much more rapidly than has the accumulation of data necessary to evaluate the relationship between the models and actual geologic deposits. Without such a relationship it is difficult to justify which statistical model best represents heterogeneity in different geologic deposits.

The task of theoretically discriminating between statistical models based on subsurface measurements of hydraulic conductivity alone is arduous if not impossible. Similarly, estimation of the hydraulic conductivity probability distribution and correlation length generally requires hundreds of measurements at a given scale (e.g. Sudicky, 1986; Rehfeldt et al, 1989; Rehfeldt and Gelhar, 1992). The costs and risks associated with sampling contaminated aquifers are often prohibitive. Alternative methods for the discrimination between, and the parameterization of, statistical models of heterogeneity would greatly enhance our understanding of contaminant migration and our ability to effectively remediate contaminated aquifers.

One such alternative method is the incorporation of geologic information. Geologic information has long been used in the characterization of aquifer properties. However, the focus has generally been on problems of water supply and utilizing large-scale stratigraphic relationships to estimate transmissivity (Phillips et al., 1989; Anderson, 1989).

In problems of groundwater contamination, the scale of interest is on the order of meters to hundreds of meters. For clastic sedimentary deposits, this scale of geologic variability generally falls under the purview of sedimentology. Sedimentological models of depositional environment are based largely on the occurrence and spatial assemblage of lithologic units. If lithologic information can be used to estimate hydrologic properties, then "soft" information regarding the relative abundances and hydrologic properties of lithologic units implies information for the estimation of suitable spatial distributions of hydraulic conductivity in the subsurface.

For example, if the major depositional controls of an aquifer can be inferred from paleogeographic information, limited on-site data, and analog outcrop studies, then the overall sedimentological characteristics can be inferred from sedimentological models. The next step would be to relate the information obtained from the sedimentological models to quantitative

models of heterogeneity.

Incorporating geologic information into the discrimination between models and parameterization of the models should begin with a conceptual understanding relating characteristics of sedimentological models with statistical models of heterogeneity. Initially, primary effects such as depositional environment would be treated separately from the secondary effects of diagenesis. Outcrop studies of geology and air-permeability provide the most realistic source of two-and-three-dimensional information on geologic heterogeneity.

Several such outcrop studies have been conducted. Goggin et al. (1988a) conducted an outcrop study of the eolian Jurassic Page Sandstone in northeastern Arizona and found that the three primary types of stratification exhibit different mean permeabilities (Chandler et al., 1989). Kittridge et al. (1989) studied heterogeneity in an outcrop of the carbonate Permian San Andres Formation in southeastern New Mexico and found a wide range of permeability exhibiting two different scales of correlation. In addition, variation in permeability did not closely correspond to changes in bedding. Dreyer et al. (1990) studied heterogeneity in the Middle Jurassic Ness Formation (Yorkshire, England) consisting of delta-plain distributary sand bodies and found good correlation between permeability and lithologic facies.

OBJECTIVE

While each of these studies have contributed to the understanding of heterogeneity in different depositional environments, a comprehensive analysis relating the spatial assemblage of lithologic units to the overall statistical properties has not been performed.

The objective of this study was two-fold. The first objective was to obtain intensive data sets of the spatial distribution of permeability and observed geological features in a variety of geological settings, and then, second, to investigate the relationship between the observed sedimentological characteristics and quantitative models of heterogeneity.

METHODS

In each of the outcrop studies, three main steps of analysis were employed to different

degrees. First a conceptual model of the depositional environment was developed using paleogeographic information and previous studies in the area. Second, an accurate spatial representation of the lithologic units and their hydrologic properties was obtained through mapping and measurements, repsectively. Third, the mapped spatial representation of lithologic units were combined with the permeability measurements to yield a relationship between statistical characteristics of permeability and deposition processes.

The main study area is an outcrop of the Pliocene-Pleistocene Sierra Ladrones Formation in the Albuquerque Basin of central New Mexico. Located west of Belen, New Mexico, the Cejita Blanca escarpment exposes the fluvial deposits of the ancestral Rio Grande system. Erosion of the largely uncemented deposits has resulted in a badlands style topography offering good three-dimensional exposure. Geologic mapping was conducted on a two kilometer long by 20 meter high section of the outcrop. In situ air-permeability measurements were taken for statistical characterization of heterogeneity.

Two outcrop studies in deposits of different geological origin were conducted to complement the main study area. The first of these complimentary studies was conducted on alluvial fan deposits at the Nevada Test Site, Nevada. In two existing waste-disposal pits, geologic mapping and air-permeability sampling was performed. In each pit, one wall was studied, each approximately 50 meters wide and 10 meters high. Approximately 250 permeability measurements were obtained in each of the pits. The second complimentary study was conducted on an outcrop of Miocene eolian deposits located on the Bosque del Apache Wildlife Refuge south of Socorro, New Mexico. The excavation for the construction of the highway and railroad provided good exposures about 20 meters wide and 10 meters high. On one of these exposures, approximately 200 measurements of permeability were obtained and the lithologic units mapped.

ORGANIZATION

This work contains the results of a large project involving several faculty and graduate students at New Mexico Tech. A few words are in order regarding the contributions of the

various researchers. The dissertation is subdivided into five parts.

Following the introduction, Part II presents the general methodology developed for the study of the main field site. Chapter 2 describes in detail the methodology developed for mapping the main field site and the geostatistical methods adopted for this study. Chapter 3 describes the air-minipermeameter and is a paper currently "in press" in the journal Ground Water (Davis et. al., 1994). The author and Principal Investigators Drs. John Wilson and Fred Phillips are largely responsible for the work described. The circuitry design was developed with the assistance of Mike Fort.

Part III of the dissertation focuses on the main field site of the project, the Sierra Ladrones Formation. Chapter 4 is a summary of the site geology and is an extension of the geology presented in the Master's Theses of Davis (1990) and Lohmann (1992). The field guidance of Dr. Dave Love throughout the project was invaluable in the development of the methodology, geologic definitions, and mapping. The petrographic analysis was performed by James Harris. The facies-scale heterogeneity studies described in Chapter 5 were conducted by the author and Madeline Gotkowitz and are more fully described in Gotkowitz (1993). The architectural-element scale heterogeneity study (Chapter 6) is from the paper published in the Geological Society of America Bulletin (Davis et al., 1993) and is an extension of the work of Lohmann (1992).

Part IV of the dissertation presents the results of the two other outcrop studies of heterogeneity in different types of deposits. The study of the alluvial fan deposits at the Nevada Test Site (Chapter 7) was conducted by the author through an arrangement with Reynolds Electrical Engineering Company and Sandia National Laboratories. Appropriate acknowledgements for the various aspects of the work are provided in the chapter and in Davis (1992). The third study (Chapter 8) was conducted on an outcrop of eolian deposits for additional comparison of heterogeneity styles in different depositional environments. Madeline Gotkowitz assisted in the data collection.

PART II

GENERAL METHODOLOGY

CHAPTER 2: GEOLOGIC MAPPING AND GEOSTATISTICAL ANALYSIS

INTRODUCTION

This chapter describes the geologic mapping methods employed for the study of the main field site and the general methods of geostatistical analysis. The main field site for this study is an outcrop of Pliocene-Pleistocene Sierra Ladrones Formation located along the Cejita Blanca Escarpment west-southwest of Bosque, New Mexico. Chapter 4 describes the site location and geology in detail.

Early in the study, it was recognized that the deposits are on the order of one meter thick and exhibit lateral continuity on the order of 100's of meters. Since one of the primary objectives of this study was to quantify geological heterogeneity by detailed mapping, an accurate and cost-effective spatial mapping technique was considered a primary concern.

Several possible methods for mapping were evaluated on their ability to provide high resolution spatial data and their cost-effectiveness. In recent years highly sophisticated equipment has become commercially available for measuring spatial structures and spatial locations. Two recent technologies that were considered in some detail are non-topographic photogrammetry and Global Positioning Systems.

Non-topographic photogrammetric methods can have a high degree of resolution (Karara, 1989). However, the data acquisition and reduction requires highly sophisticated cameras and computer facilities. This method was not considered to be cost-effective at the time of this study.

Another relatively new technology with mapping applications is the Global Positioning System (GPS). GPS antennae measure the simultaneous distance to four or more satellites. From the combination of these distance measurements, the horizontal position of the antenna on the earth's surface can be calculated to centimeter resolution. In general the potential vertical resolution of GPS is on the order of one meter. The vertical resolution of

GPS is controlled by the resolution of the mathematical models for the surface of the earth and associated earth-tides. For local studies, the vertical resolution can be enhanced by differential measurements from a base antenna at a known (vertical) location. While GPS currently allows for high-resolution spatial positioning, at the outset of this study the availability of satellites in orbit limited the sampling window to approximately four hours per day. In addition, the equipment with sufficient resolution was prohibitively bulky and expensive. With the advancement of the technology, the size and cost of the necessary equipment are being reduced. In the future, GPS may provide a powerful tool for the detailed spatial mapping of geological features over a range of spatial scales.

For the main field site of this study, a combination of traditional mapping techniques were employed to obtain the necessary accuracy and numbers of measurements. Traditional surveying techniques were used to obtain spatially located measurements on the outcrop. U.S. Geological Survey 7.5 minute topographic maps and aerial stereo-photo pairs were used to assist in the construction of topographic base maps. The specific methods and emphasis placed on the methods varied between the two mapping phases of the study.

Data reduction and graphical presentation were performed on a series of IBM compatible PC's. Survey data reduction was performed with a spreadsheet program and maps were generated using the GSMAP software package (Selner and Taylor, 1991a; 1991b) and plotted on a large format (36" x 22") pen plotter.

MAPPING

Phase I (August 1989-August 1991)

The objective of the mapping during Phase I was to obtain the detailed spatial assemblage of lithologic units encompassing a 400 x 400 meter peninsular protrusion of the main escarpment. The map resulting from Phase I is presented in Chapter 6.

Mapping of Phase I was initiated on the outcrop face opposite of Outcrop I of Davis (1990). The initial survey location was assigned a horizontal location of (0,0) and elevation of 4985 feet (1519.4 meters). The instrument azimuth at the initial station was zeroed

approximately to magnetic north. A Sokkia TM20H theodolite was used to measure relative azimuth and true zenith angles. Distances were obtained by optical distance measurements via instrument stadia and graduated staff. The stadia method in general is restricted to approximately 100 meters for accurate readings. Heat shimmer prohibited accurate distance measurements over 120 meters.

A network of survey locations was constructed by conducting a traverse of 22 survey stations from the initial survey location. At each survey station, the instrument was zeroed to a previously surveyed station and 20-100 measurements were obtained on the outcrop. Fifteen of the survey stations were established around the perimeter of the outcrop and seven on the top of the outcrop. The locations of significant geologic contacts, locations of scours and pinchouts, and topographic features were measured and documented. A schematic illustration of the survey network is presented in **Figure 2.1**.

The base map for Phase I was constructed by hand contouring the survey network data (approximately 1000 locations). Ground photos and aerial stereo-photo pairs were used to augment the survey data. The base map was digitized using GSMAP for later editing and addition of geologic information.

Geologic mapping during Phase I was conducted by first transferring the geologic contacts survey notes onto the base map. The surveyed geologic data served as a basis for field measurements and subsequent mapping. Stratigraphic sections were measured up the outcrop face with a Jacob staff and level at approximately 30 meter horizontal intervals. The measured section data was then transferred onto the base map using significant surveyed lithologic units as control and occasional conditioning points. Mapping of Phase I was completed by mapping the lithologic units between measured sections. Again survey information was used to augment and constrain the locations of field observations. The lithologic units on the map were then digitized as polygons for graphical representation and quantitative analysis via GSMAP. A more detailed description of the Phase I mapping methods is provided in Lohmann (1992).

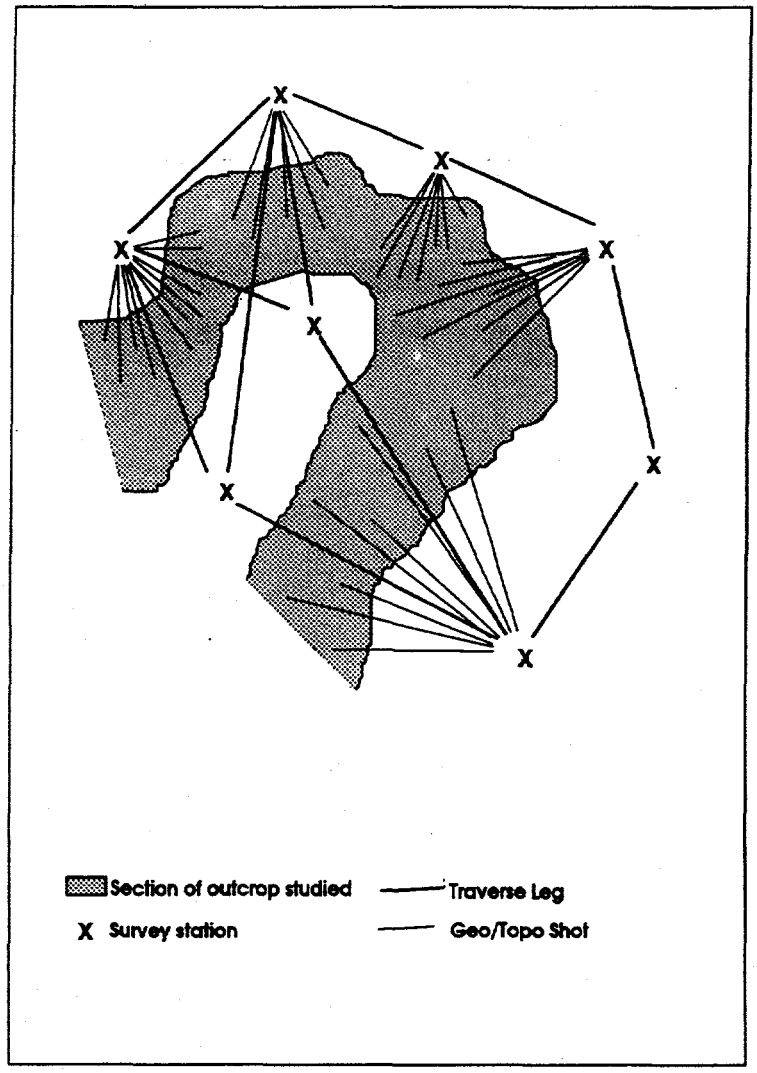

Figure 2.1 Illustration of survey campaign.

Phase II (January 1991-August 1992)

Results of the mapping in Phase I were used to modify the mapping methodology of Phase II. The principal finding driving the modification was that the lithologic units generally persist for hundreds of meters in the horizontal direction. This suggested that 1) horizontal resolution on the order of five meters was sufficient to capture the lateral variation, and 2) distinct lithologic units could be used reliably as marker beds. The objective of Phase II was to extend the Phase I mapping exercise one kilometer to the south. The addition of a Sokkia Red 2A electronic distance meter allowed for the accurate measurement of distances up to one kilometer. This allowed the traverse technique employed in Phase I to be applied to a much larger area without the constraint of the 120 meter maximum separation between survey stations. Also, in an effort to minimize the amount of survey data necessary, the U.S. Geological Survey 7.5 minute topographic map of the area (Veguita Quadrangle, New Mexico: N3430-W10645) was used in the construction of the base map.

The base map for Phase II was constructed by enlarging the 1:24000 topographic quadrangle map to a scale of 1:1200. The steep topography contoured in 10 foot intervals resulted in some discontinuous contour lines on the published USGS map. Also, with the 20x enlargement, the contour lines became very thick. To clarify topography, the enlarged published contour lines were traced on mylar with a 0.5 millimeter pen. Contour lines were inferred in locations where they were discontinuous on the published map. The series of traced contour maps were then digitized on GSMAP for future modification and incorporation of survey and geologic information.

Surveying for Phase II was initiated at a benchmark (BM-I25-54) located just east of the fence-line and west of Interstate 25 near the Socorro-Valencia County border. It is not known whether or not this benchmark defines the county line. The instrument azimuth was zeroed on a prominent hill approximately four kilometers north of the benchmark. The azimuthal reference angle was then determined from the 7.5 minute published topographic map.

The survey network established for Phase II was similar to that of Phase I (Figure

2.1). A traverse was conducted to the north along the base of the main escarpment. The traverse resulted in eleven survey stations along the base of the escarpment and four on top. The stations were numbered in the tens beginning with 40 and increasing to the north. When several survey stations were located in similar north-south positions, the numbers increased by one from west-to-east. As in Phase I, locations of geologic and topographic significance were surveyed from the established survey stations. Surveying efforts focused on the lithologic units used as marker beds and significant scours and pinchouts. In general, good agreement was observed between published elevations and surveyed locations. The agreement was particularly good where 1) the inferred location on the topographic map was reasonably easy to identify, and 2) topography was relatively gentle.

The survey locations were directly imported into the digitized topographic map data base (GSMAP). The digitized topographic lines and the survey location number and elevation were displayed on the screen in a common coordinate system. The survey data served as conditioning criteria for the published, enlarged, digitized topographic data. The program GSMEDIT of the GSMAP package allows the on-screen selection and editing of individual points along a selected line. With this editing process, the topographic contour lines were modified to fit the survey data. With few exceptions, points were not moved more than 7 horizontal meters. The exceptions occurred where the topography is the steepest and the published contour lines exhibit the most error. In these regions, the density of survey data collected was increased.

Three 60 x 90 centimeter base maps were plotted at a scale of 1:685 for field mapping. Survey locations were plotted with their respective identification numbers and elevations. As in Phase I, the geologic significance of each survey location was transferred onto the base map. Stratigraphic sections were measured with a Jacob staff and level at approximately 100 meter intervals. This information was also transferred onto the base map. The areas between the measured sections were mapped in the field by tracing contacts laterally.

GEOSTATISTICAL ANALYSIS

Geostatistics is the branch of statistics which studies and describes random variables correlated in space and/or time. The reader is referred to one of the many textbooks on the subject for a detailed discussion of the statistical measures (e.g. Journel and Huijbregts, 1978; Cressie, 1991; Deutch and Journel, 1992) In the study of heterogeneity the random variable is hydraulic conductivity, or as in this study, permeability. Geostatistical models of heterogeneity represent the value of permeability at a given location as a realization of a spatially correlated random variable. In most geostatistical models, the probability distribution and the correlation structure of the random variable are estimated from spatially located data.

In this study, a log-normal probability distribution is the hypothesis the data is tested against. The mean and variance of log-permeability are estimated from the data. Then the cumulative probability for each measurement is estimated empirically and compared with the theoretical normal distribution calculated with the estimated mean and variance. The results of the univariate analysis are presented on two graphs. The first graph of the pair is the empirical cumulative distribution on probability scale. The second graph is a box plot of the empirical cumulative distribution. An example of both of these graphs and the associated definitions are given in **Figure 2.2**

The spatial correlation was estimated with the variogram estimator (Journel and Huijbreghts, 1978). The variogram graphically expresses the dissimilarity between data values as a function of separation distances in space. The variogram is estimated by calculating the variance of the differences of values that are separated by a certain lag distance. For example, at lag zero, provided there is no measurement error, the differences of values with themselves are zero, resulting in zero variance. At small lags the differences become non-zero but remain relatively small. As the separation distance increases, the differences between values and the variance of those differences also increase. The range of a variogram refers to the separation distance (lag) at and above which values of the variogram no longer increase. The sill of a variogram refers to the maximum value of the variogram and, for a stationary process, corresponds to the variance of the population. The variogram estimated from the data is

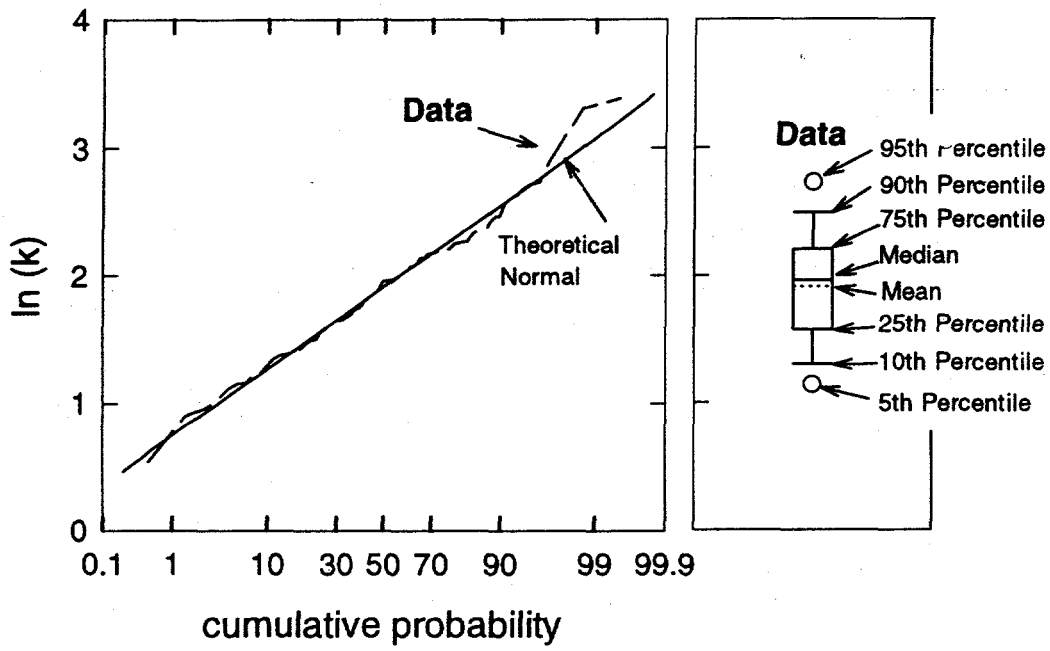

Figure 2.2. Example presentation of univariate statistical analysis performed on data set in this study.

usually fit with a mathematical function that is referred to as the variogram model. In this study, the two models used most often are the exponential and "bell-shaped" variogram models.

Geostatistical analysis in this project was performed with two published software packages depending on the amount of data and the dimensionality of the data. For relatively small one and two-dimensional data sets containing less than 200 points, the software package Geo-EAS (Englund and Sparks, 1988) was used. Geo-EAS allows for the change of parameters and model fitting through a series of on-screen menus. For larger data sets and those with three spatial coordinates, the variograms were calculated with the GSLIB software package (Deutsch and Journel, 1992).

Both programs used to estimate the variogram employ a search window for the pairing of irregularly spaced data. For each lag class, ξ, a search window (Figure 2.3) is defined and the data are grouped accordingly. In this study the search window was kept as narrow as possible.

In addition to the geostatistical software, other programs served an important role in the analysis of the spatial data. The programs TRIMAKE and TRIMAT (Macedonio and Pareshi, 1991) were used for estimating topographic elevations on a rectangular grid from digitized elevation contour data. The geologic maps constructed using GSMAP consist of two-dimensional polygons, each representing a different lithologic unit. A rectangular grid of points were then overlain on the polygon data and analyzed to determine in which polygon each point lay. The PTPOLY program used for this was developed from the algorithm described by Sedgewick (1990) and is documented by Lohmann (1992).

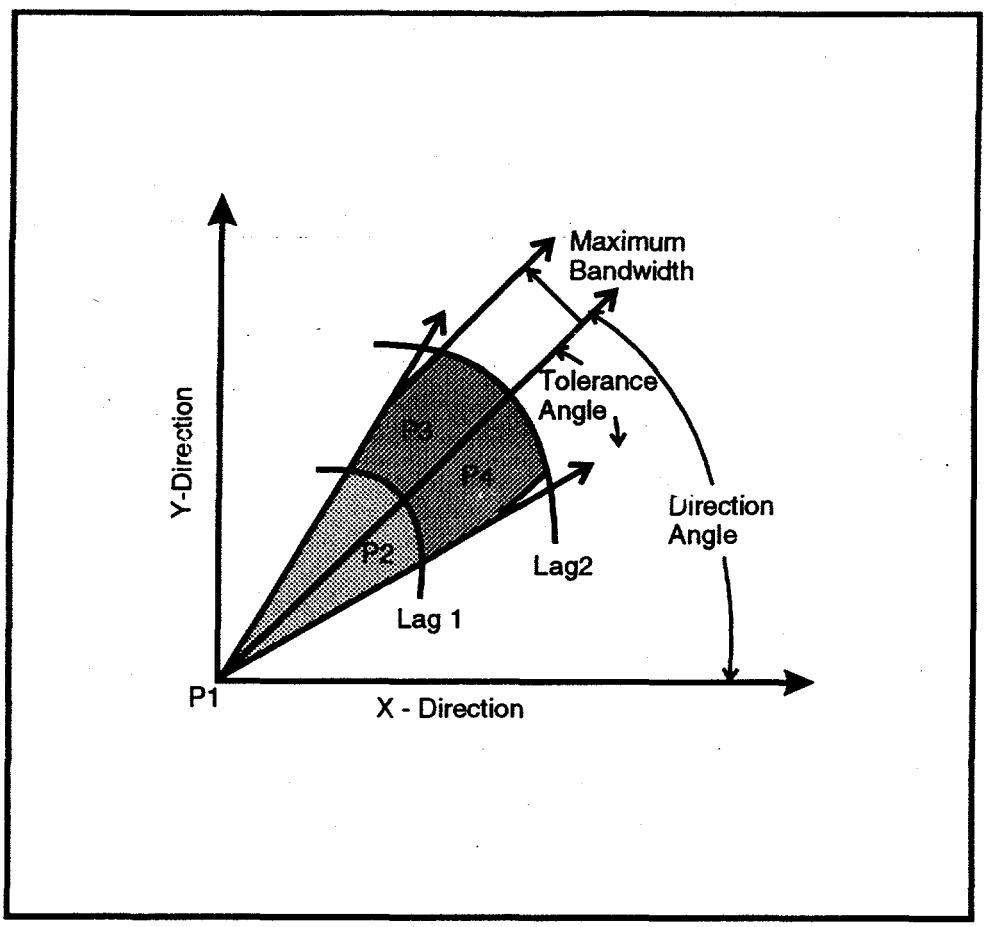

Figure 2.3. Schematic illustration of search window parameters.

CHAPTER 3: AIR-MINIPERMEAMETER[1]

INTRODUCTION

As the economic importance of groundwater quality becomes more pronounced, more sophisticated models of flow and transport are necessary. Generally, these models require abundant hydraulic conductivity data to estimate parameters for either spatial statistical models or deterministic numerical models. Obtaining large numbers of hydraulic conductivity measurements in the subsurface is often economically prohibitive. One method of supplementing on-site subsurface measurements is to incorporate geologic information obtained from studies of analogous geologic material exposed in outcrop.

One economical method for collecting large numbers of permeability measurements on outcrops is by means of an air-minipermeameter. In situ measurements of permeability in dry material can be performed rapidly and economically when air is the fluid. When measuring the hydraulic conductivity or permeability, two conditions must be satisfied. First, the solution to the flow equation (Darcy's law) must be known for the particular flow geometry. The second condition is an accurate knowledge of the applied pressure and the flow-rate through the porous medium.

Eijpe and Weber (1971) developed one of the first air-minipermeameters capable of quick and non-destructive permeability measurements on consolidated and unconsolidated sands. Goggin et al. (1988a) performed an experimental and generalized theoretical analysis of flow associated with a minipermeameter in which air is injected into an outcrop or core plugs via a bored rubber stopper. The rubber stopper applicator is referred to as the tip seal and allows for non-destructive, small-scale measurements of permeability. The boundary conditions associated with the tip seal are shown in **Figure 3.1**. As in the case of Eijpe and Weber (1971), Goggin et al. (1988a) utilized a compressed air tank as a source and measured the pressure and flow rate with diaphragm gauges and rotameters, respectively. The device described in Goggin et al. (1988a) consists of a 60 x 60 x 25 centimeter box housing the flow

[1]From, Davis, J.M., J.L. Wilson, and F.M. Phillips, 1994, A portable air-minipermeameter for rapid in-situ field measurements: Ground Water, in press.

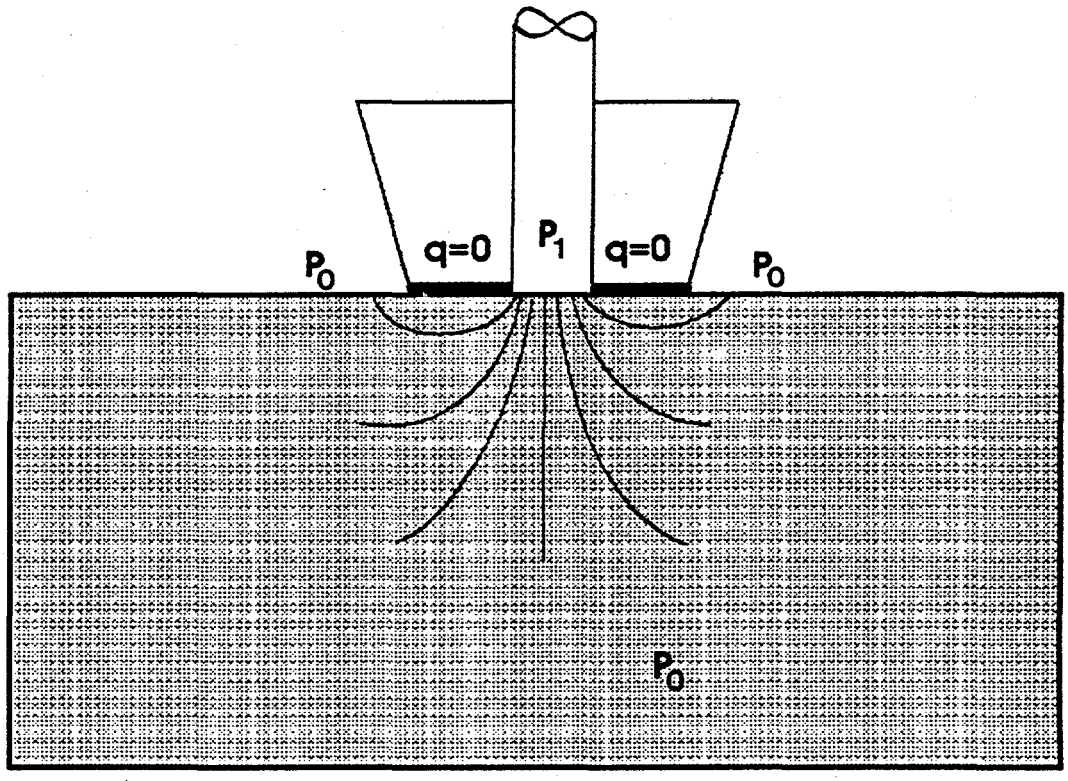

Figure 3.1. Boundary conditions associated with tip seal design and schematic of flow lines.

meters and pressure gauges and a large (scuba-size) compressed air tank (L.W. Lake, Univ. Texas, Austin, personal communication).

In studies to quantify the spatial distribution of permeability in outcrops analogous to petroleum reservoirs, several outcrop studies have been conducted using the minipermeameter of Goggin et al. (1988b) or a similar instrument. Goggin et al. (1988a) obtained several thousand measurements of air-permeability on an outcrop of the eolian Page Sandstone (Jurassic) in Northeastern Arizona. Using the same device Kittridge et al. (1989) performed a comparison of outcrop and subsurface permeability in the carbonate San Andres Formation (Permian) of southeastern New Mexico. Dreyer et al. (1990) used a similar air minipermeameter to assess the relationship between depositional facies and permeability in the delta-plain distributary channels of the Ravenscar Group (Jurassic) in Yorkshire, England. By collecting large numbers of permeability measurements on an outcrop, these studies yielded insight into the relationship between observed geologic features and geostatistical characteristics of permeability heterogeneity in cemented sedimentary rocks typical of petroleum reservoirs.

In groundwater hydrology, however, aquifer sediments are often weakly lithified and generally exhibit higher permeability than sedimentary rocks of petroleum reservoirs. In order to prevent grain movement and excessively high flow rates, air-permeability measurements in weakly lithified sedimentary deposits typical of aquifers require smaller applied pressures than those used to measure lithified sedimentary rocks typical of petroleum reservoirs. In principle, lower pressures could be achieved by simply changing the gas delivery regulators and associated diaphragm gauges of the existing air-minipermeameters. However, a different design is employed here to not only achieve lower applied pressures but also to greatly increase the portability of the air-minipermeameter for use on steep and unstable slopes.

A mechanical pressure source was developed to replace the compressed air source. The piston of a ground glass syringe falls steadily under its own gravitational force through the syringe casing with negligible leakage between the syringe piston and casing. The falling piston applies a small constant pressure and the flow rate is calculated by timing the rate the

piston falls. Injecting air with the low-pressure glass syringe through a tip seal allows for the calculation of permeability from the model of Goggin et al. (1988b).

PERMEAMETER DESIGN

The lightweight, syringe-based air-minipermeameter (LSAMP) described in this chapter is presented schematically in **Figure 3.2**. The device consists of three main components: a glass syringe which applies the pressure to the sample, a timing device which measures the rate at which the syringe piston displaces a known volume, and a tip seal through which air is injected into the outcrop.

The syringe component of our prototype device consists of a Becton-Dickenson® 100 cm^3 ground glass syringe which is ground further with 800-grit corundum. When the syringe is oriented vertically, the syringe piston falls relatively freely through the casing due simply to the gravitational force exerted on the piston. Some friction between the piston and casing is present and can be quantified.

In order for the piston to fall steadily in the presence of the abundant dust and loose sand typically encountered in the field, an air-filter is placed in-line to remove particulates from the air drawn into the piston between measurements. At the upper end of the syringe, a plastic bag is taped around the syringe casing with sufficient room for the piston to be drawn up to its full extent. The plastic bag prevents particulate matter from falling into the top of the syringe while ensuring that the top of the piston is exposed to atmospheric pressure.

The second component of the LSAMP is the timing circuit. The volumetric flow rate is measured by timing the rate at which the piston passes two known locations on the syringe. Knowledge of the volume displaced and the time required allows calculation of the flow-rate. The timing circuit consists of two pairs of light sensors affixed to the inside of the instrument and straddling the syringe. The sensors are wired to a stopwatch through the circuit board. As the piston passes the first set of sensors, a signal is sent to start the stopwatch. Then, as the piston passes the second set of sensors, another signal is sent to stop the stopwatch. The specifics of the prototype device circuitry are described in detail in Appendix A.

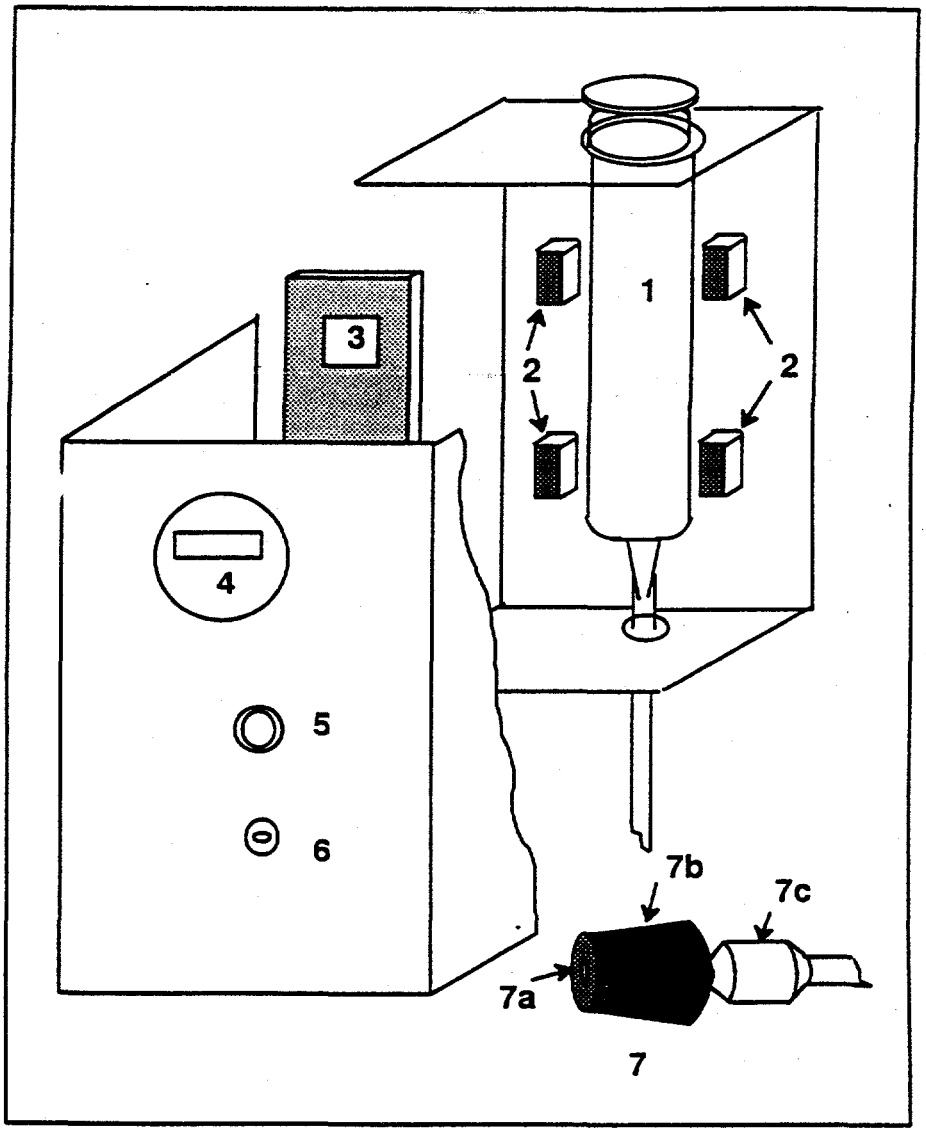

Figure 3.2. Schematic diagram of air-minipermeameter. 1. 100cc ground glass syringe; 2. photo-sensors; 3. circuit board; 4. stopwatch; 5. reset button; 6. on/off switch; 7. tip seal assembly; 7a. foam rubber with 0.03 cm ID grommet; 7b. #6 rubber stopper; 7c. quick disconnect.

The third main component of the LSAMP is the tip seal. The tip seal (Figure 3.2; part #7) is the means of applying the air to the sample surface. The tip seal of the prototype device is designed specifically for weakly lithified sands. First, in order to obtain a no-flow boundary along the annulus of the seal, a soft foam-rubber pad approximately five millimeters thick is adhered to the base of the rubber stopper. The foam rubber pad readily conforms to the sandy surface. A 0.66 centimeter diameter brass grommet is placed in the center of the foam rubber pad to ensure a circular orifice of fixed radius while sampling. Second, the rubber stopper used is larger in diameter (No. 6) than those previously applied in sampling consolidated rocks; the increased diameter distributes the application force over a larger surface preventing penetration of the tip seal annulus into the sample material. A quick-disconnect fitting connects the tip seal to the permeameter via 0.64 centimeter (1/4 inch) flexible tubing.

The glass syringe and circuitry are encased in a 12.7 x 15.2 x 23 centimeter (5 x 6 x 9 inch) box with a total weight of approximately two kilograms. The length of the tubing to the tip seal is one meter. Measurements of permeability are obtained by orienting the device (i.e. the syringe) vertically with a bubble level, extending the syringe piston, placing the tip seal to the outcrop, releasing the piston, and recording the time measured to displace the fixed volume. The measured time is used to calculate the volumetric flow-rate and the applied pressure. For example, with our prototype device measured times of 60.0 and 0.75 seconds correspond to permeabilities of 0.5 and 200 darcys, respectively. The LSAMP differs from other field permeameters in that it is an entirely self contained apparatus designed for a single user. The LSAMP can either be placed on a four-legged stand or suspended from a neck-strap.

CALIBRATION AND ANALYSIS

According to Goggin et al. (1988b), the permeability for the tip seal flow geometry is obtained from:

$$k=\frac{2\mu q P_1}{aG_0(b_D)\ (P_1^2-P_0^2)} \tag{3.1}$$

Where:

k= Permeability [m^2]
μ= Viscosity of air [Pa·s]
q= Volumetric flow rate [m^3/s]
P_1=Pressure applied at tip seal/outcrop interface [Pa]
P_0=Atmospheric pressure [Pa]
a= Radius of tip seal orifice [m]
$G_0(b_D)$=Geometric factor [dimensionless]
b_D=dimensionless tip seal radius (b/a) [dimensionless]
b=outer radius of tip seal [m]
a=inner radius of tip seal [m]

To calculate permeability, the applied pressure, flow-rate, and geometrical factor must be known. The value of the geometrical factor is governed by the relative dimensions of the tip seal. Goggin et al. (1988b) present theoretical geometrical factors for a range of dimensionless tip seal radii. For the prototype device, the dimensionless radius is 3.5 and the associated geometrical factor is estimated to be 4.5. The tip-seal injection pressure, P_1, is governed by static forces acting on the piston, atmospheric pressure, and pressure losses resulting from flow through the instrument. The mechanical force acting on the piston is the gravitational force (F=mg) minus the frictional resistance force exerted on the piston by the syringe casing. The pressure losses resulting from flow through the instrument are due primarily to the in-line air-filter and the tip-seal assemblage. Since Equation (1) contains a difference of squared pressures it is necessary to use absolute pressure. As such, atmospheric pressure makes a direct additive contribution to the tip-seal injection pressure. All of these effects must be accounted for in the calculation of applied tip-seal injection pressure.

The pressure, in pascals, resulting from the gravitational force is calculated as:

$$P_g = \frac{F_g}{A} = \frac{mg}{A} \tag{3.2}$$

Where: m=Mass of piston [kg]
g=Gravitational acceleration [m/s^2]
A=Area of piston [m^2]

The mechanical friction and pressure loss across the in-line air-filter and tip-seal assemblage require experimental analysis. The laboratory experimental setup for the analysis of the instrument effects consisted of (1) the air-minipermeameter, (2) a set of standards, (3) a 0-9 kilopascal pressure transducer, and (4) a microcomputer equipped with an analog-to-digital data acquisition board.

As shown in **Figure 3.3**, the pressure transducer was placed first in between the nipple of the syringe and the air-filter. The pressure measured at this location was used to calculate the frictional force acting on the syringe piston. That is, the resultant pressure (F/A) is the difference between the gravitational force and the frictional force, divided by the area of the syringe. The mechanical friction in the syringe can be modeled as lubricated friction, which is proportional to some fixed power of the velocity (Symon, 1971):

$$F_f = \beta \, v^{\pm n} \tag{3.3}$$

where F_f is the frictional force [N], $v=q/A$ is the velocity [m/s], and β and n are empirical coefficients. For each measurement, the frictional force is plotted against the velocity of the piston (**Figure 3.4**). The coefficient of friction, β, for the quadratic model (n=2) was determined to be 140 [N·s^2/m^2] by performing a least squares fit to the experimental data. Incidentally, pressure losses through the orifice at the bottom of the syringe are implicitly accounted for in the friction model.

Similarly, the pressure loss resulting from flow through the in-line air-filter and tip-seal assemblage is a function of the rate at which the piston falls. **Figure 3.5** presents the pressure drop across the air filter as a function of flow-rate. A linear model is used to account for this pressure loss:

$$\Delta P = \alpha q - b \tag{3.4}$$

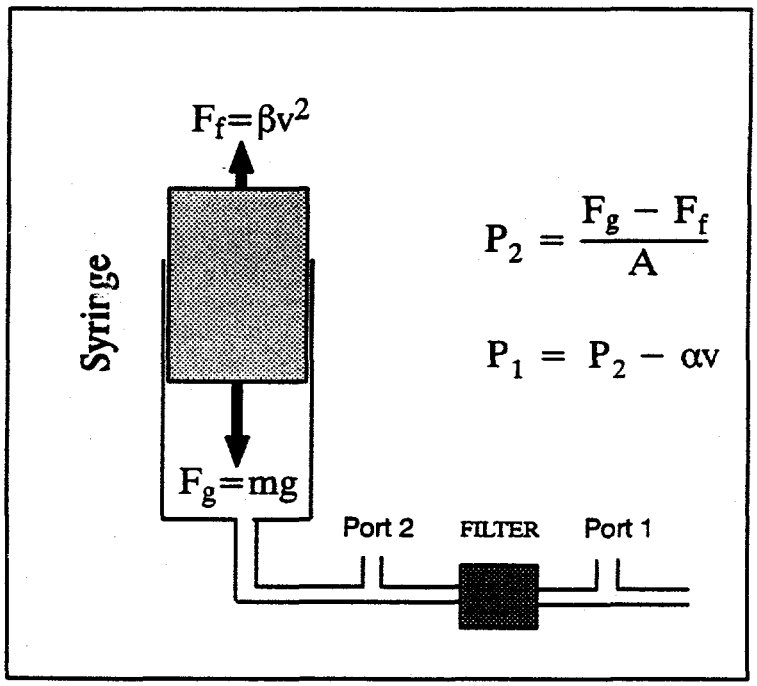

Figure 3.3. Illustration of pressure loss due to mechanical friction and flow through the instrument. Ports (1) and (2) correspond to pressure measurement locations in the estimation of α and β.

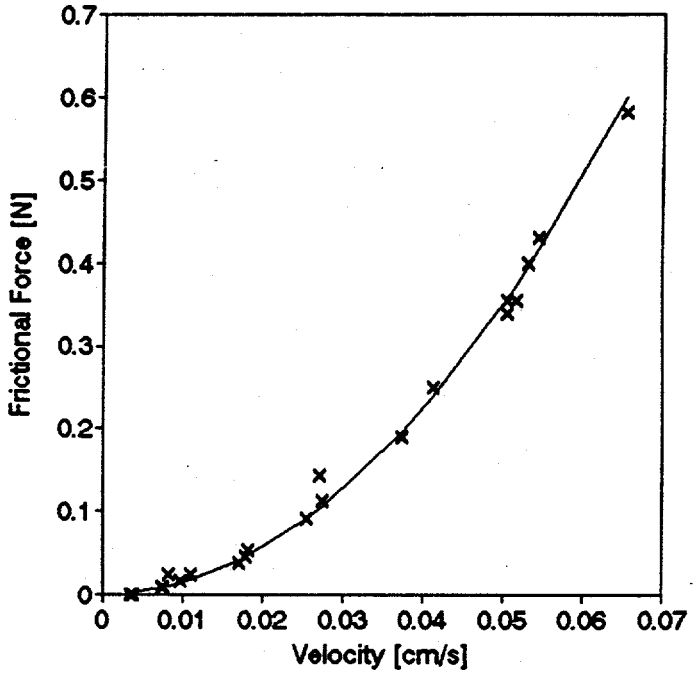

Figure 3.4. Experimental plot of frictional force versus velocity for estimation of β. Curve represents fitted quadratic model.

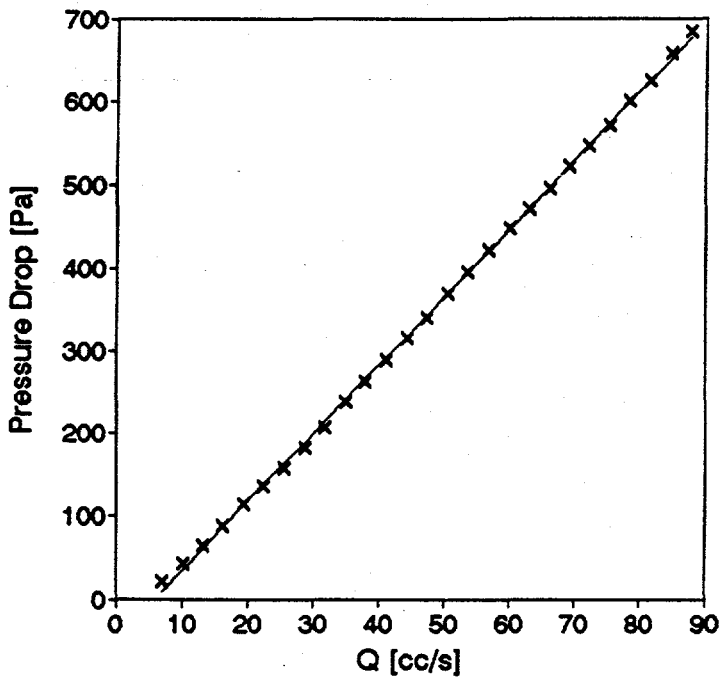

Figure 3.5. Experimental plot of ΔP versus flow rate for the estimation of α. Line represents fitted linear model.

The coefficient of resistance, α, was estimated via a least squares analysis to be 8.3×10^6 [Pa·s/m^3]. The coefficient b is a threshold pressure required to induce flow through the system and is estimated to be 50 [Pa].

For both sources of resistance, the applied pressure is a function of the rate at which the piston falls. The flow-rate is measured directly by the timing circuitry enabling the calculation of applied pressure for each measurement. For the prototype device, the applied pressure in (1) is modeled by:

$$P_1 = P_0 + P_n \tag{3.5}$$

P_o is atmospheric pressure and P_n is the net pressure due to mechanical forces and pressure losses, and

$$P_n = \frac{F_g}{A} - \frac{F_f}{A} - \Delta P = \frac{mg}{A} - \frac{\beta v^2}{A} - \alpha q + b \tag{3.6}$$

Both the net pressure and the permeability depend on the rate at which the piston passes a known volume. For the prototype device, the net pressure and permeability [from equation (3.1)] are plotted against time (**Figure 3.6**). The high degree of sensitivity at small times is a function of the inverse relationship between flow-rate and measured time and the quadratic behavior of frictional losses at high velocity (small displacement time). The approximate range of times which offer optimal sensitivity are those greater than 1.0 and less than 60 seconds. For the prototype design, this range of measured times translates into a permeability range of 200 and 0.87 darcys, respectively. The range of permeability is a function of the prototype device dimensions and piston mass. Different designs can yield different ranges by changing the various dimensions of the device and utilizing equations (3.1) - (3.6).

All of the parameters necessary for the calculation of permeability involve the measurement of the time to displace a known volume of the syringe. For highly permeable materials, calculations are extremely sensitive to the measured time. For the prototype device,

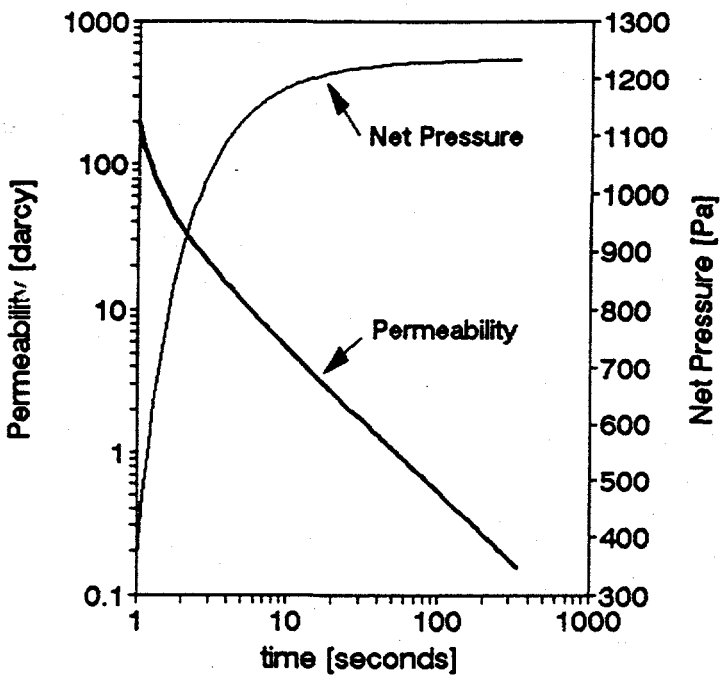

Figure 3.6. Plot of net pressure and permeability versus measured time for the prototype device.

the volume between the photo sensors was measured by two means. First, the area of the piston was multiplied by the distance the piston moved between the starting and stopping of the clock. An independent measurement of the volume was obtained by filling the syringe with water and measuring the amount of water displaced between the starting and stopping the clock. Both measurement techniques yield a volume of 55 cm^3, and the accuracy of the timing device was assessed by measuring the flow rate through a rotameter (calibrated with a soap bubble technique) for displacement times between 1 and 11 seconds. The results are presented in **Figure 3.7** and indicate that the volumetric flow rate calculated from the piston displacement time tends to slightly underestimate flow rates. This could be a result of either error in the rotameter calibration or a slight timing error. However, for all practical purposes the timing of the piston provides an adequate measure of the volumetric flow rate.

The small time required for the piston to displace the fixed volume of air also raises questions regarding the validity of the steady-state assumptions implicit in equations (3.1) - (3.6). The flow rate was observed to reach a constant level very rapidly in the rotameter measurements described above. An additional experiment was conducted to measure the transient pressure response of the prototype device. The results are presented in **Figure 3.8**. In each of the four measurements, the piston displaces the same volume. The time duration (width) of each measurement is then inversely proportional to the piston velocity. The pressure curves illustrate that the pressure reaches a fairly constant level quite rapidly and that the net pressure is a function of velocity. For the prototype device, a volume of approximately 45 cm^3 is displaced before the piston passes the first set of sensors to minimize the effects of initial transient conditions.

Calibration

The LSAMP is calibrated by comparing permeability values obtained with the LSAMP to measurements obtained with conventional methods. In order to maintain consistency in a variety of experiments, a set of laboratory fabricated sandstones were used as standards. The sandstones were fabricated by mixing sand of different grain size with a cementing agent and

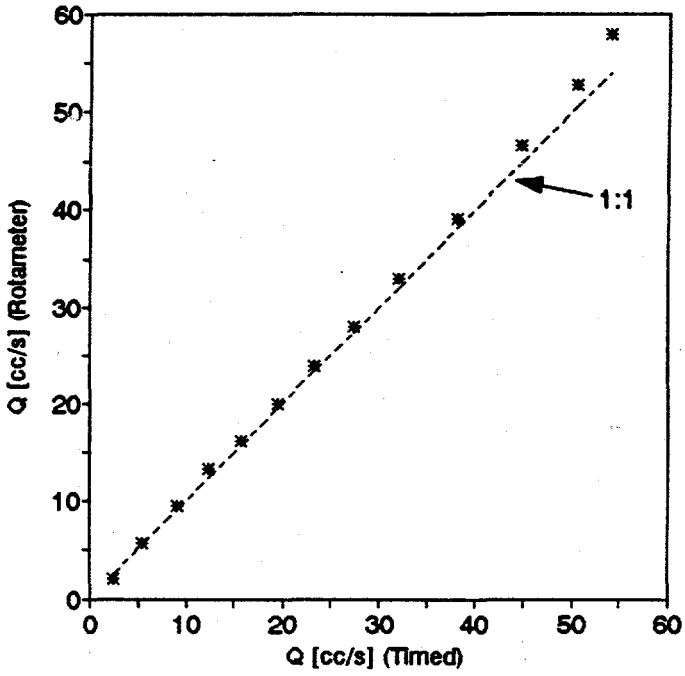

Figure 3.7. Plot of flow rate measured with rotameter versus flow rate measured with timing circuit.

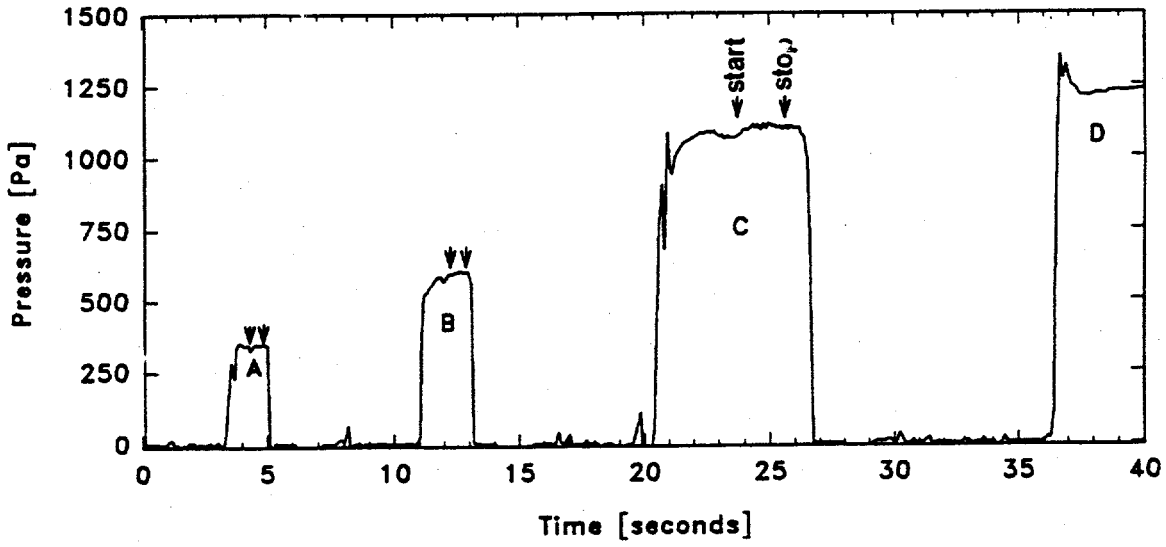

Figure 3.8. Plot of outlet pressure measured between syringe and air-filter as a function of time for the two extreme flow rates (A: "free-fall" and D: "no-flow") and two permeability measurements (B and C). Sample B has a higher permeability than sample C. Clock activity is denoted by arrows.

packing the mixture in 100 cm^3 stainless steel cylindrical rings (five centimeters in diameter and five centimeters long). One set of 16 standards was fabricated using a low viscosity epoxy as a cementing agent. For each standard, sand and epoxy were mixed thoroughly together so that just enough epoxy was present to coat the grains. The sand-epoxy mixture was then packed into a ring in four to five lifts, tamping the mixture after each lift. The minimum permeability of standards fabricated by the epoxy method was five darcys. In order to fabricate standards with a lower permeability, plaster of Paris (powdered anhydrite) was used as the cementing agent for a set of four additional standards. The anhydrite was mixed with the sand and tamped into the rings dry. Screened caps were then placed on the bottom of the rings, and the rings placed in approximately one centimeter of standing water. Capillary forces were allowed to draw interstitial water into the samples. The moistened sediment filled rings were then oven-dried. A total of 20 standards were fabricated and were used throughout the calibration process.

One-dimensional air-permeability of the fabricated standards was measured with a laboratory device following the ASTM D4525 method. The experimental set-up is shown in **Figure 3.9** and consisted of a drying tube, a low-pressure regulator, rotameters to measure air-flow-rate, and a pressure transducer. A plexiglass cap was constructed to fit over one end of the five centimeter diameter standards. Depending on the permeability of the standard, five to twenty different air-flow rates were used on each standard. For each air-flow-rate the applied pressure was measured with the pressure transducer, and the one-dimensional permeability was calculated in the standard way. In general, for higher permeability standards, fewer flow rates were measured, since the maximum flow rate (65 cm^3/s) of the rotameters was exceeded.

Air-permeability was also measured at each end of the standards with the lightweight, syringe-based, air-minipermeameter (LSAMP). The results of this calibration are shown in **Figure 3.10**. The permeability measure at each end of the standards generally brackets the one-dimensional average permeability. The lack of a well defined correlation results primarily from the heterogeneity of the packed standards. According to the analysis of Goggin et al.

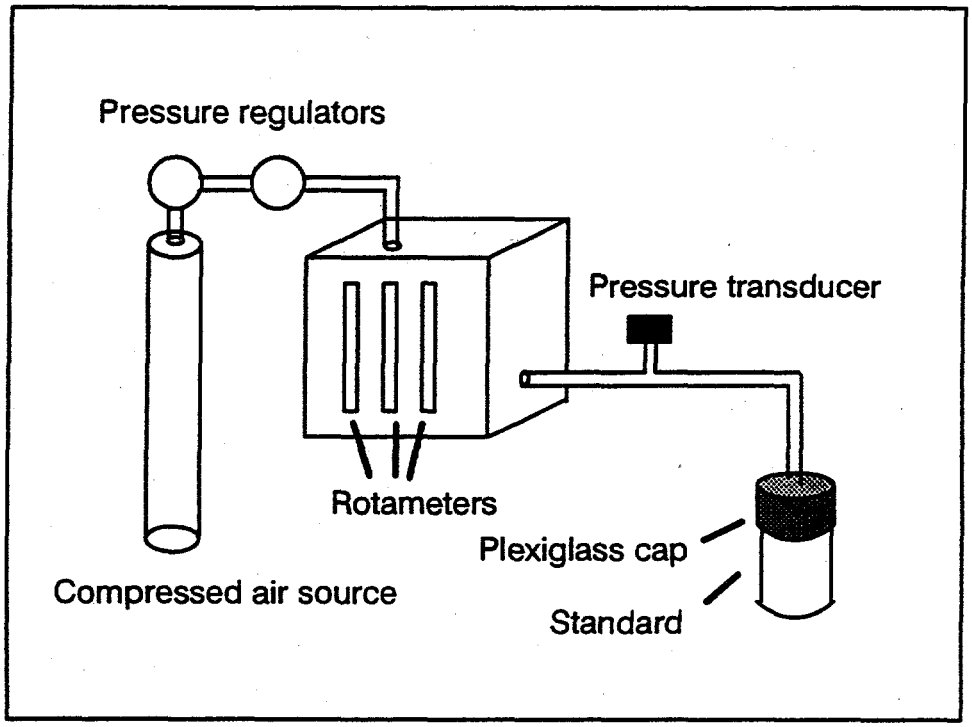

Figure 3.9. Schematic diagram of device used to measure one-dimensional air permeability.

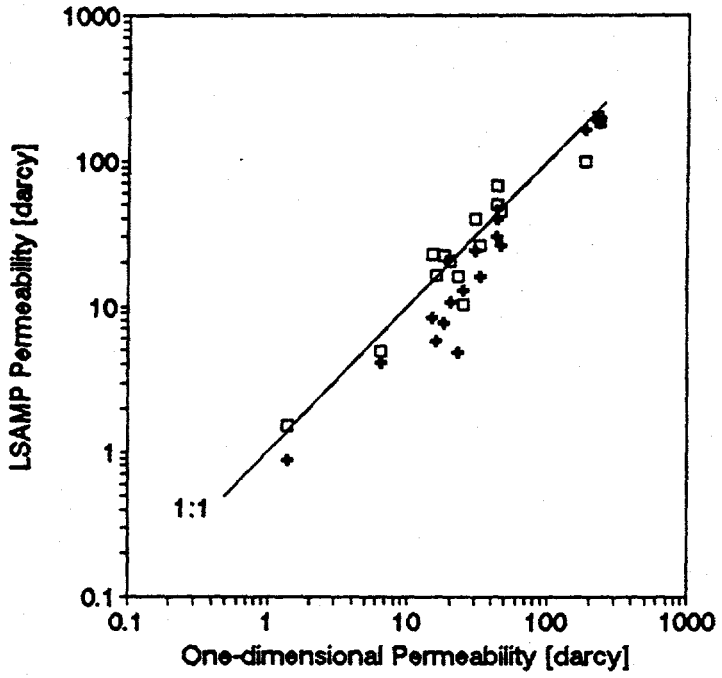

Figure 3.10. Calibration plot of air-permeabilities measured with 1-D device and LSAMP. Solid line is a one-to-one reference line. The squares represent the LSAMP measurements at one end of each core, the crosses represent the measurements at the other end.

(1988b), the volume of investigation is a hemisphere with a radius approximately four times the internal tip seal radius. For the prototype device, the volume of investigation is approximately 7.4 cm^3. The one-dimensional measurements, on the other hand, represent the permeability of the 100 cm^3 soil ring standards. The scale effect due to the different volumes is believed to greatly affect the correlation between the two methods of measuring permeability.

A second calibration experiment was conducted to compare permeability measured with the LSAMP to measurements obtained with a traditional continuous-flow air-minipermeameter (CFAMP) using the same tip seal. While permeability measured with the CFAMP is not a well established standard, the accuracy of a similar device has been documented in the works of Goggin et al. (1988a,b), Kittridge et al. (1989), and Dreyer et al. (1990). This approach ensures that both methods (LSAMP and CFAMP) are measuring the same volume of porous media. Results of the second calibration experiment are shown in **Figure 3.11**. This calibration approach results in a much stronger correlation.

Two types of non-Darcy flow phenomenon have been documented in air-minipermeameters. First, gas slippage must be considered when the mean free path of the gas is comparable to the pore size (Katz and Lee, 1990). Gas slippage in tight formations results in an overestimation of permeability. This phenomenon is considered negligible for the prototype device on two counts. First, permeabilities are not over-estimated and the mean free path of air at atmospheric pressure is on the order of 10^{-8} meters (Adamson, 1979) while the pore size of the materials sampled is on the order of 10^{-4} meters. Second, high velocity non-Darcy flow effects result in additional pressure losses and an underestimation of permeability. Traditionally, the Reynold's number is used to assess the importance of high velocity flow effects. Based on experimental observations in one-dimensional cores, Darcy's Law is valid for Reynold's numbers not exceeding a value between 1 and 10 (Bear, 1972). Since the flow geometry in the porous media resulting from the tip seal is three-dimensional (hemispherical), the applicability of the one-to-ten rule is questionable. In fact, since the seepage velocity decreases proportional to the radius squared, it is possible that for diverging

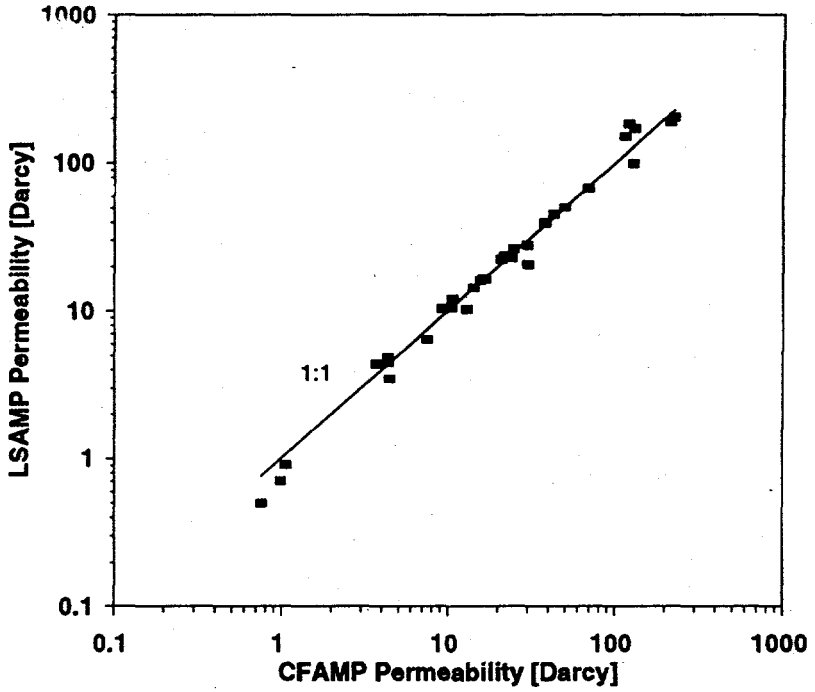

Figure 3.11. Calibration plot of air-permeabilities measured with CFAMP and LSAMP. Solid line is a one-to-one reference line.

flow conditions Darcy's Law may be applicable for apparent Reynold's numbers greater than ten. For the data presented in Figure 3.10, the Reynold's numbers for the one-dimensional measurements are consistently less than one. The Reynold's numbers near the tip seal for the corresponding LSAMP measurements range between 0.5 and 200, with the highest Reynold's numbers corresponding with the highest permeabilities. For permeabilities above 200 darcys, the LSAMP measurements appear to consistently under-estimate the one-dimensional permeabilities (Figure 3.10). Since this is near the upper end of the LSAMP measuring range, the significance of high velocity flow effects compared to other sources of measurement error is unclear.

In general, permeability measurements obtained with the LSAMP agree well with traditional one-dimensional permeability measurements and permeability measured with a traditional continuous flow air-minipermeameter. Effects of gas slippage are not observed and are not expected to be significant. Minor high velocity flow effects may be present for the highest permeabilities but further research is required on the limits of Darcy's law under the prescribed flow geometry.

Moisture Content

The presence of interstitial liquids reduces air permeability. An experiment was conducted to assess the measurement error associated with water saturation. Four epoxy-sandstone blocks (approximately 15 x 10 x 4 centimeters) were fabricated in the same manner as the columns described above. On each block permeability measurements were made at locations approximately 2.5 centimeters apart. The blocks were wetted by partially submersing them in approximately two centimeters of standing water. The wetted blocks were then set on a rack and allowed to gravity drain. The blocks were dried in steps. Drying was achieved by placing the blocks in a 90 degrees celsius oven for 20 to 30 minutes. After each heating period, the blocks were allowed to cool to room temperature. Permeability measurements were taken at one of the previously measured locations after each drying step. The use of multiple locations per block ensured against preferential drying at the measurement

point. The mass of the blocks was also measured at each drying step to calculate the gravimetric moisture content, *w*. Volumetric water content for each drying step was calculated by:

$$\theta = \frac{\rho_d^b}{\rho_l} w \tag{3.8}$$

Where: ρ^b_d=Dry bulk density of the block
ρ_l= Density of water
w = Gravimetric moisture content.

The percent error in permeability ($[k_{dry}-k_{wet}]/k_{dry}$) is plotted against the moisture content in **Figure 3.12**. The results indicate that when the volumetric water content is less than five percent, the measurement error is also less than five percent.

Performance Assessment

Performance of the LSAMP was assessed by statistically analyzing the repeatability of the instrument under laboratory conditions and the reproducibility of measurements made under both field and laboratory conditions. First, triplicate measurements under laboratory conditions were made on each end of 19 standard cores. The results of a one-way analysis of variance (ANOVA) of the measurements is presented in **Table 3.1**. For the number of degrees of freedom shown in Table 3.1, the critical F value is 2.1 (1% level of significance). The large F value obtained for both the original data and the logarithm-transformed data is a clear indication that the variability associated with measurement error is much less than the variability of the core permeabilities.

Since the LSAMP is primarily designed for use in the field, it is also desirable to assess if the calibration results are portable to the field. Two of the standard cores used in calibration were measured repeatedly under field and laboratory conditions. In conjunction

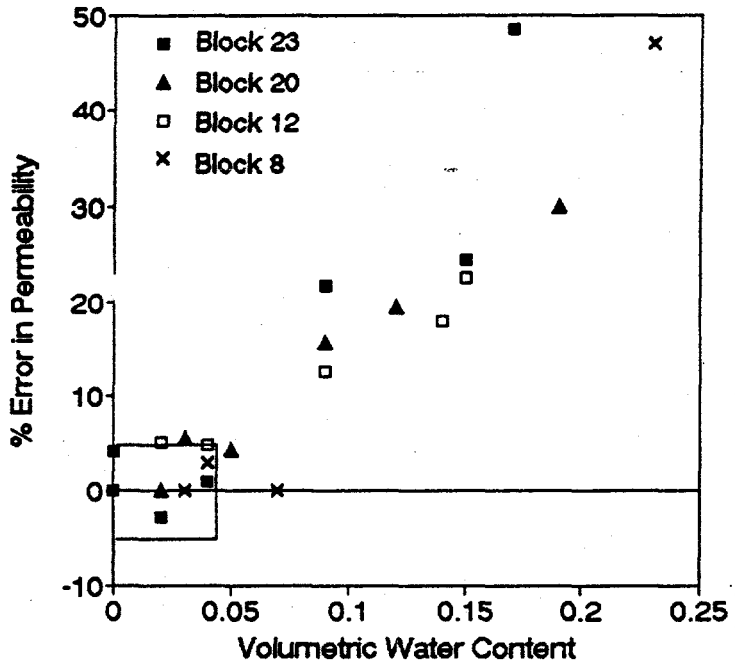

Figure 3.12. Permeability measurement error ($[k_{dry}-k_{wet}]/k_{dry}$) vs. volumetric water content. Different symbols correspond to the blocks on which measurements were taken.

Table 3.1. Summary of one-way ANOVA on triplicate measurements at each end of 19 standard cores performed under laboratory conditions.

Data	Source of Variation	Sum of Squares	Degrees of Freedom	Mean Square	F value
Original Data	Among Samples	94478	37	2553	1792
	Within Replicates	108	76	1.42	
	Total Variation	94586	113	837	
Logarithmic Data	Among Samples	18.3	37	0.50	2655
	Within Replicates	0.01	76	1.87×10^{-4}	
	Total Variation	18.3	113	0.16	

with an outcrop study of heterogeneity, twenty-two field LSAMP measurements of two standard cores were obtained at various times of day over a period of several days. Temperatures in the field ranged from 27 to 38 degrees celsius, and winds varied from 0 to 30 kilometers per hour. Twenty-two measurements of permeability were also obtained for the two standard cores under laboratory conditions.

The means and standard deviations of the permeability measurements under field and laboratory conditions for each standard are presented in **Table 3.2**. The standard deviations of the measurements under field conditions is higher than those obtained under laboratory conditions. This is interpreted as resulting from more variable sampling conditions in the field. To test the hypothesis that the sample populations have different means, a t-test was employed. Since the sample populations have different standard deviations, the results of the t-test can only be considered approximate. The results of the t-test are presented in Table 3.2. For Standard 1, the hypothesis that the populations have different means can be rejected at the 10% significance level. For Standard 2, the mean field and laboratory permeability values are 248 and 296 darcys, respectively.

Table 3.2. Statistical summary of repeated measurements on sandstone cores under laboratory and field conditions. Values are in darcys.

	Conditions	STD 1			STD 2		
		μ	σ	CV	μ	σ	CV
Original Data	Field	17.89	1.38	0.08	248.3	50.6	0.20
	Laboratory	17.91	0.41	0.02	296.0	37.1	0.12
	t- values	0.07			3.57		
Natural-log Data	Field	2.87	0.09	0.03	5.47	0.23	0.04
	Laboratory	2.87	0.02	0.01	5.68	0.12	0.02
	t-values	0.00			3.26		

The hypothesis that populations have different means cannot be rejected. From the calibration analysis, we appear to be near the upper LSAMP measuring range. The coefficient of variation however remains small under field conditions indicating that LSAMP measurements are relatively repeatable. It is possible that the field performance of the LSAMP could be further improved by correcting for temperature effects on viscosity.

CONCLUSIONS

The lightweight, syringe-based, air-minipermeameter (LSAMP) was developed for the rapid, non-destructive, in situ measurement of permeability in weakly lithified materials. For the prototype device, the syringe delivers accurately measurable pressures between 500 and 1250 pascals (0.07-0.2 psig). Such low pressures are necessary in weakly lithified, highly permeable sediments to minimize grain movement and high velocity flow effects. For studies conducted in rugged terrain, the increased portability of the LSAMP is of particular importance. The prototype device described in this paper measures permeability in the 0.5 to 200 darcy range.

Permeability measurements obtained with the LSAMP compare well with both one-dimensional core permeability measurements and traditional continuous flow air-

minipermeameter measurements. Under-estimation of permeability at the upper end of the measurement range may result from high velocity flow effects. Further work is needed to quantify the Reynold's number threshold at which flow deviates from Darcy's law under the prescribed flow geometry. If high velocity flow effects are significant, a numerical solution of Forcheimer's equation is a means to estimate permeability. Moisture content is found to play a significant role. However, for volumetric moisture contents less than five percent, the associated permeability measurement error is less than five percent. Analysis of measurement error under laboratory conditions indicates that the variability associated with instrument error is much less than the variability over the range of permeabilities measured. A slight increase in measurement error is expected and observed under field conditions. This increase is more pronounced for the upper end of the measurable range but remains at an acceptable level. Further refinement and modification of the LSAMP design should further enhance the ability to collect large numbers of quantitative permeability measurements for the study of geologic heterogeneity.

PART III

SIERRA LADRONES STUDY

CHAPTER 4: SITE GEOLOGY[2]

INTRODUCTION

An outcrop of the Pliocene-Pleistocene Sierra Ladrones Formation in the Albuquerque Basin of central New Mexico was the main field site of this study. The overall objective of this study was to develop a better understanding of how the sedimentological relationship between depositional processes and depositional products can be used to statistically characterize the spatial distribution of permeability. Three main steps of analysis were necessary.

First it was necessary to understand as well as possible the depositional environment. This information was obtained largely from previous regional studies and detailed outcrop studies and is the focus of this chapter. The second step was to obtain an accurate spatial representation of the geology and permeability (Chapters 5 and 6). This was accomplished through mapping of lithologic units and quantitative measurements of permeability, respectively. Then by combining the spatial representation of lithologic units with the measured permeability, the relationship between statistical properties and depositional processes can be obtained.

This chapter 1) defines the architectural elements of the Cejita Blanca escarpment, 2) provides a limited interpretation of the depositional environment based on a 1.25 kilometer cross section through an intensively mapped region, and 3) formulates several hypotheses regarding the implications of the observations on general basin fill processes.

GEOLOGIC SETTING

The Albuquerque Basin is located in the central portion of New Mexico. The basin is approximately 100 kilometers long and 30 - 50 kilometers wide. It is bounded to the west by the Lucero and Ladron uplifts, to the north by the San Felipe fault belt, to the east by the Sandia-Manzano-Los Pinos uplift, and to the south by the Joyita uplift and the Socorro

[2]Davis, J.M., D.W. Love, R.C. Lohmann, and J.S. Harris, Architectural-element analysis of the Sierra Ladrones Formation, paper in prep. for submission to New Mexico Geology.

Constriction. Structurally, the Albuquerque Basin is one of several en echelon basins resulting from extension of the Rio Grande Rift.

Two major episodes of rifting appear to have opened the basin to its current structural configuration (Chapin, 1989; Russell and May, 1992). The first episode occurred between the late Oligocene (30 Ma) and the early Miocene (18 Ma), and the second in the late Miocene (10 - 5 Ma). Seismic reflection data indicate that the basin is composed of a series of half grabens dipping eastward in the northern half of the basin and westward in the southern half (Russell and May, 1992). During the early stages of rifting, the Albuquerque Basin was a part of a series of closed internally drained bolsons. Sedimentation within these bolsons resulted in playa deposits in the central portions of the basins and alluvial fans adjacent to the tectonically active surrounding mountains.

Between 10 and 5 Ma, an increase in tectonic activity resulted in an increase in the rate of sedimentation (Lozinsky, 1988). As a result, the separate closed basins filled and coalesced into a single basin. At approximately 5 Ma, the ancestral Rio Grande integrated its drainage to southern New Mexico (Lozinsky et al., 1991). This shift in drainage caused fluvial deposition to replace playa deposition throughout the Albuquerque Basin.

Basin aggradation ceased between approximately 0.5 and 1 Ma (Lozinsky et al., 1991) and the Rio Grande and its tributaries began to entrench. This entrenchment left a large portion of the basin fill isolated from deposition or erosion, thereby creating a broad flat geomorphic surface known as the Llano de Albuquerque. Subsequent incision of the fluvial system has dissected the Llano de Albuquerque revealing extensive outcrops of the upper basin fill. Just north of the confluence of the modern Rio Grande and Rio Puerco are the Ceja del Rio Puerco and Cejita Blanca escarpments (**Figure 4.1**).

Previous Work

The basin fill deposits of the Albuquerque Basin have been studied since the early 1930's (e.g. Bryan and McCann, 1937; Bryan, 1938; Denny, 1940; Wright, 1946; and Stearns, 1953). The Albuquerque Basin fill was collectively known as the Santa Fe Formation (Bryan,

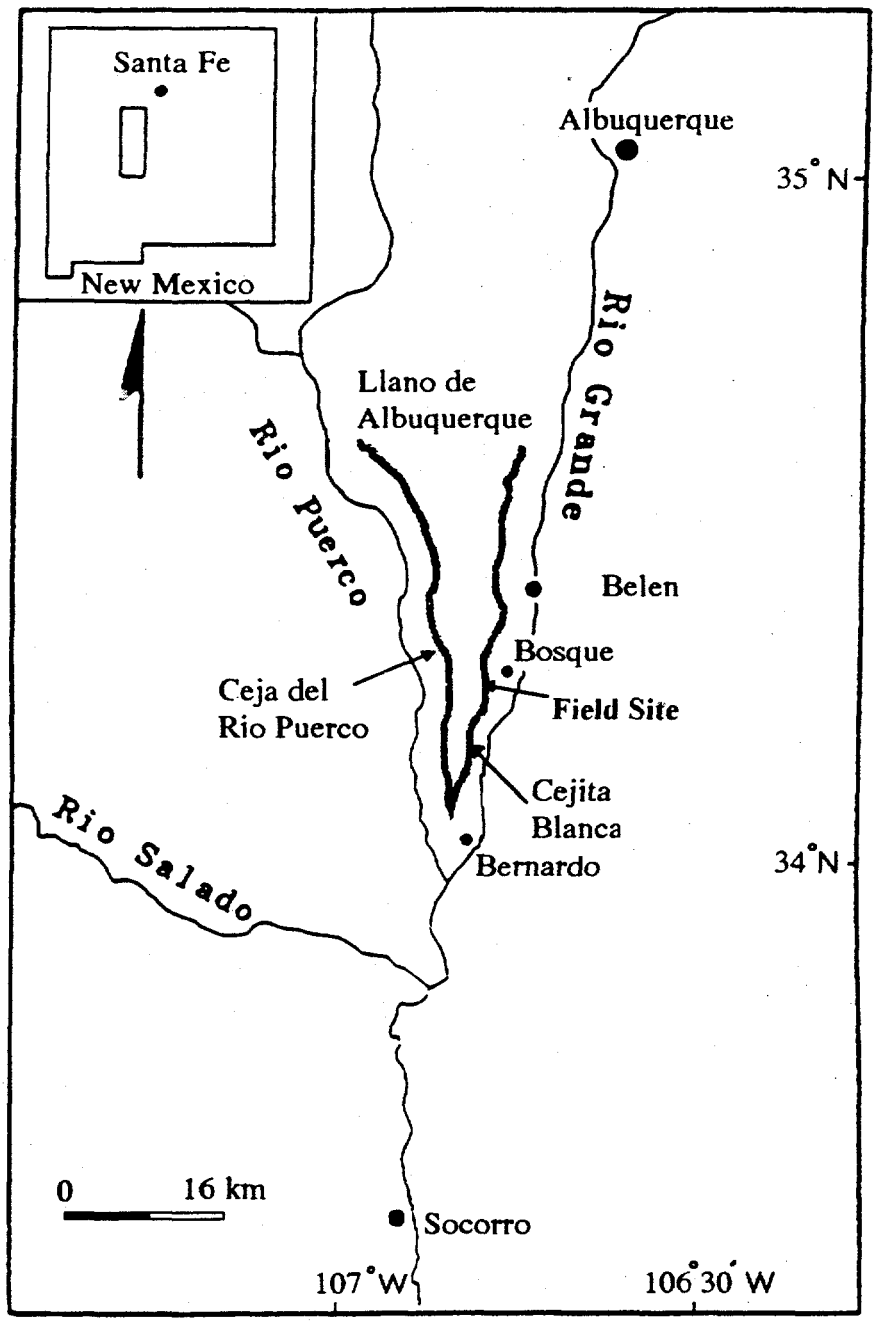

Figure 4.1. General location map. The field site is located on the Cejita Blanca escarpment west of Bosque.

1938) until 1963 when Baldwin formally proposed the Santa Fe be raised to the group status (Spiegel and Baldwin, 1963).

Machette (1978) subdivided the Santa Fe Group within the Central Albuquerque Basin into the lower Popotosa Formation and the upper Sierra Ladrones Formation. The Popotosa records deposition beginning in late Oligocene and throughout the Miocene and consists of the playa deposits interfingered with alluvial fan and eolian sediments. The Sierra Ladrones records the infilling of the Albuquerque Basin with alluvial fan and fluvial sediments between the uppermost Oligocene and the middle Pleistocene (5 to 0.5 Ma).

Several studies have been carried out which describe the lithologic facies present within the Sierra Ladrones Formation exposed in the Ceja del Rio Puerco and the Cejita Blanca. Young (1982) studied the stratigraphy and sedimentology of the Sierra Ladrones Formation exposed in the Ceja del Rio Puerco. Young (1982) recognized the presence of both alluvial fan and fluvial lithofacies. The presence of obsidian derived from the Grants Ridge area (Kerr and Wilcox, 1963) coupled with Young's paleocurrent measurements led him to conclude that the sediments were derived from the northwest, outside of the Albuquerque basin. The ancestral Rio San Jose drained the Grants Ridge area to the Rio Puerco and Rio Grande.

Lozinsky (1988) measured three vertical sections of exposed Sierra Ladrones Formation in the south-central Albuquerque Basin, one of which was located on the east-facing Cejita Blanca escarpment near Belen, New Mexico. Lozinsky (1988) noted the presence of paleosols within this section, as well as the presence of a Grants obsidian cobble in the upper 20 meters of the section. Based on the observed lithologies and petrographic analysis of thin sections of samples from these sections, Lozinsky (1988) concluded that the Belen section sediments were deposited by a large and complex fluvial system, this system most likely being the Rio Puerco/San Jose fluvial system.

Study Site

The field site for this study is located along the east-facing Cejita Blanca, just west of

Bosque, New Mexico. Figure 4.1 illustrates the location of the study area within the Albuquerque Basin. A 1.5 kilometer long, 20 meter vertical section of the escarpment was chosen for the study. **Figure 4.2** is a map of the field site and provides a reference for the studies that will be discussed later in the dissertation. The outcrop slopes are at the angle of repose or steeper. The overbank clays and paleosols as well as some cemented lenses of gravels and sands lend structural stability to the outcrop. The majority of the sediments however are uncemented. Colluvium is present in some locations as a thin veneer generally less than 10 centimeters thick and can be removed easily with a trowel or small shovel.

Results of previous studies of the upper Sierra Ladrones Formation exposed within the Ceja del Rio Puerco and the Cejita Blanca suggest that during the late Pliocene to early-Pleistocene, the positions of the Rio Grande and its tributaries were relatively similar to their present configuration. **Figure 4.3** summarizes the hypothesized drainage system of the Upper Sierra Ladrones depositional environment proposed by Lozinsky et al. (1991). Both the ancestral Rio Puerco and Rio San Jose joined the Rio Grande in the Albuquerque Basin, converging to form a single trunk stream. The approximate location of the study site is also shown on Figure 4.3. The field site is located just west of the Rio Grande Channel zone in the region of input from both the Rio Puerco and the Rio San Jose.

The general depositional setting of the upper Sierra Ladrones Formation is fairly well understood due to the geologically recent origin as well as previous outcrop and petrographic analysis. The exposures along the Cejita Blanca escarpment offer an excellent opportunity to study fluvial architecture.

METHODS

Architectural Element Analysis

The alluvial architecture scheme is used as a basis for defining the mappable units of the field site. Miall (1985) proposed that alluvial deposits consist of eight basic architectural elements which can be identified by their "grain size, bedform, position, internal sequence and, most critically, by external geometry". In a later work, Miall (1988) refined the definition of

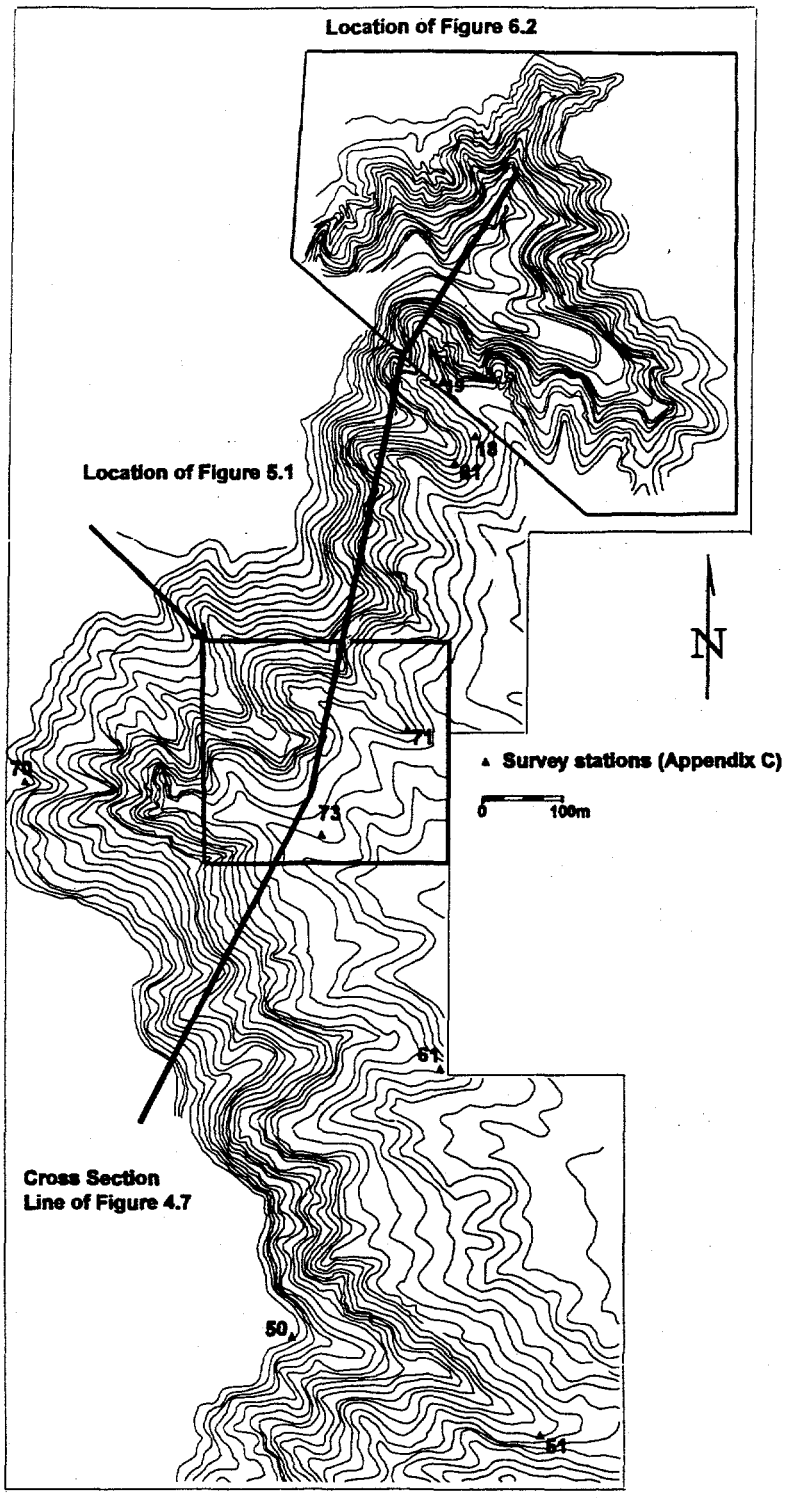

Figure 4.2. Detailed reference map of Sierra Ladrones Field Site. Locations of Figures 4.7, 5.1, and 6.2 shown.

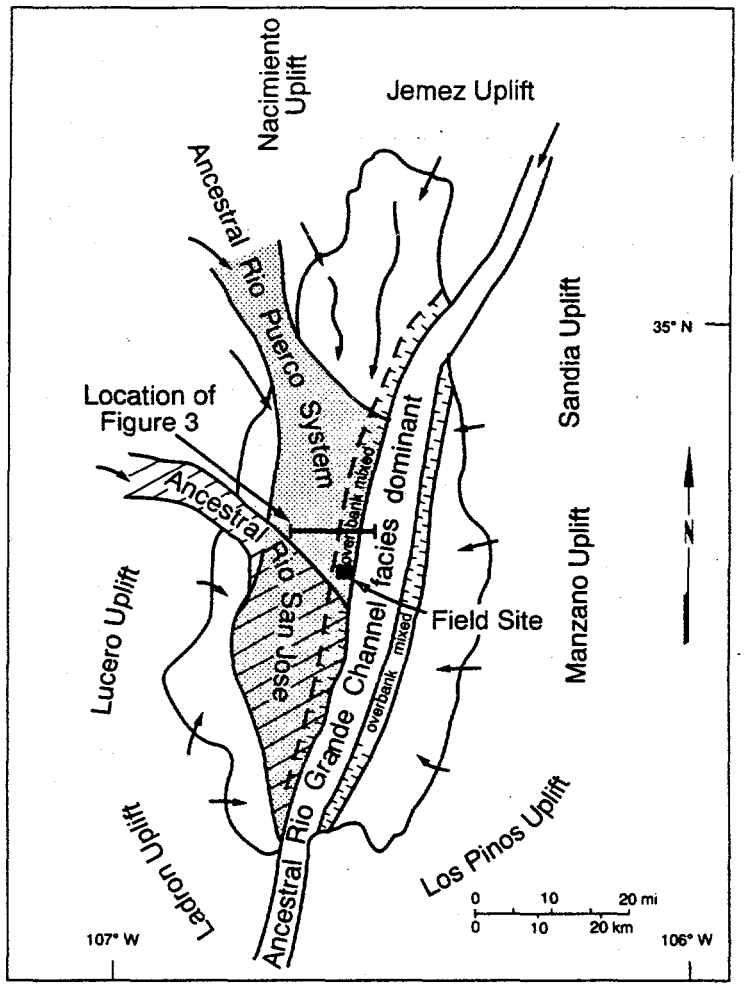

Figure 4.3. Paleogeographic setting of the Albuquerque Basin during Pliocene-Pleistocene time. Arrows indicate direction of sediment input. (Adapted from Lozinsky et al., 1991)

an architectural element as "a lithosome characterized by its geometry, facies composition and scale [that] represents a particular process or suite of processes occurring within a depositional system." A lithosome is defined as a body of sediment deposited under uniform physiochemical conditions (Bates and Jackson, 1984).

The architectural element approach is adopted here for two main reasons. First, by grouping genetically related lithofacies into architectural elements, mapping of deposits can be performed at a larger spatial scale. The larger scale spatial assemblages of architectural elements in two and three-dimensions permit analysis of basin fill at scales of hundreds of meters to kilometers. Second, from a hydrogeologic perspective, architectural elements may provide an appropriate sedimentological framework for incorporating geologic information into hydrologic modeling. Just as basin-scale stratigraphic concepts have often been used to infer hydrogeologic conditions at the basin scale (aquifer-aquitard) in modeling large scale fluid flow problems, architectural element analysis may provide a similar role in understanding the spatial distribution of hydrologic properties at the scale of tens of meters to a few kilometers.

The bulk of the field work for this study involved mapping of architectural elements around the perimeter of the outcrop as described in Chapter 2. The architectural elements are defined based on an initial facies mapping exercise. The architectural elements at the field site are generally on the order of one meter thick and extend laterally for hundreds of meters. In order to maintain adequate spatial control, traditional surveying techniques are employed.

Petrography

Sediments in the Rio Grande, Rio Puerco, and Rio San Jose drainage were petrographically analyzed to assess the provenance of the deposits studied. To develop standards for the source areas, samples of sand and gravel were collected from twenty locations in the Albuquerque Basin (**Figure 4.4**). Most samples were taken from undisturbed exposures of river terraces. Most samples were unconsolidated, however some required excavation with a small trowel or shovel due to post-depositional carbonate cementation. Four

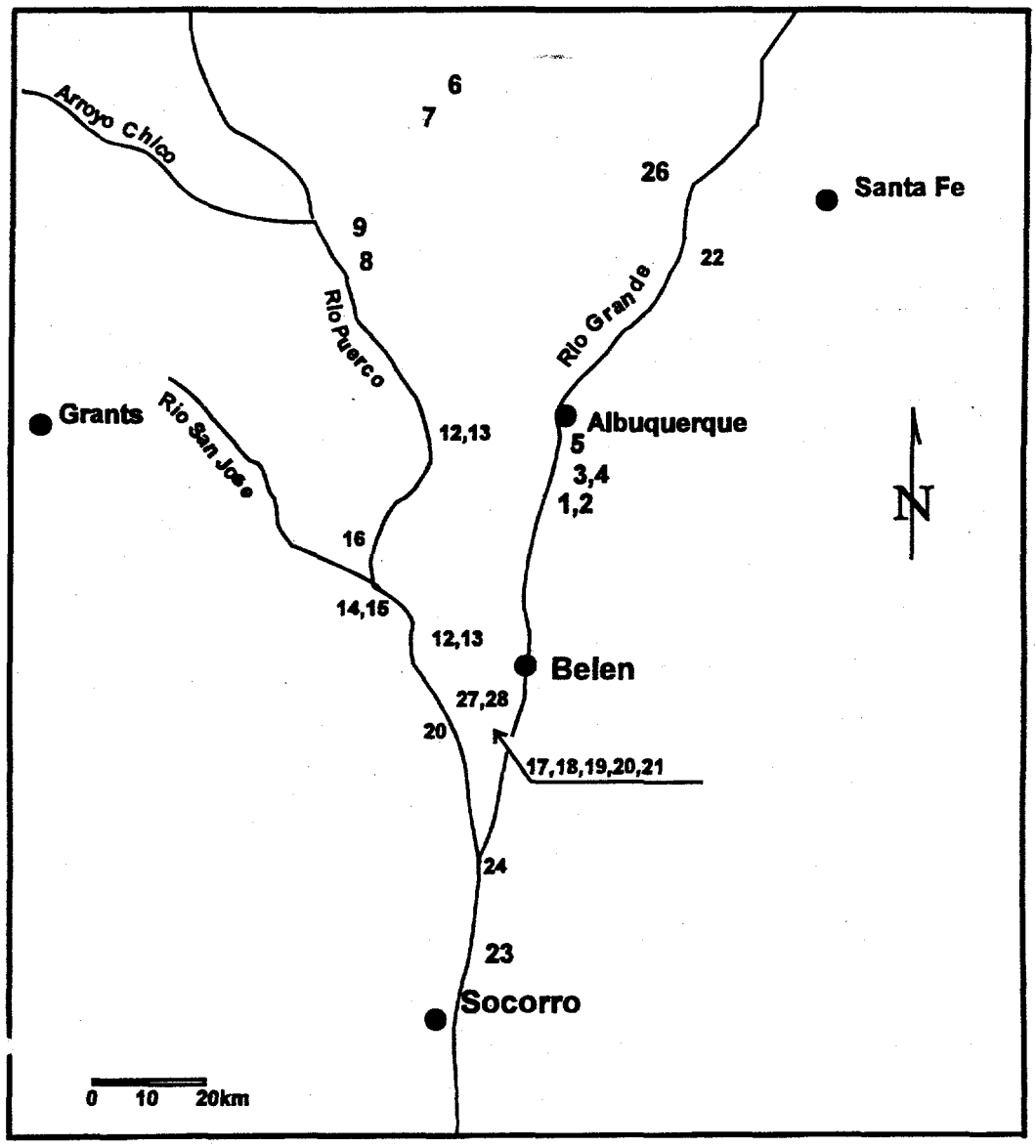

Figure 4.4. Sample locations of deposits used in petrographic sediment source terrain analysis.

samples were taken from the two high-energy channel elements (CH-I) studied at the field site (two in each the upper and lower CH-I element). An additional sample was collected approximately one kilometer north of the field site at the stratigraphic level of the upper high-energy channel element.

In order to reduce the effect of grain size on rock fragment populations, samples were split and dry sieved to remove the one-phi (0.5 millimeter) size fraction. The one-phi size fraction is optimal for standard thin-section rock-fragment analysis (Dickinson, 1985). Debris such as roots were removed from the unconsolidated grains. The prepared samples were split to obtain a representative sample to be mixed with epoxy and placed in 0.5 x 1 x 2 inch paper molds. A vacuum chamber was used to evacuate any air bubbles created during the mixing process. The hardened billets were trimmed for thin-section preparation. Thin sections were stained for both plagioclase and potassium feldspar. Each of the 30 thin sections were point counted twice for 300 grains at 3 x 3 spacing using a Swift point counter and a Nikon petrographic microscope. The first point count used the traditional method to establish percents of quartz, feldspar, and lithic fragments. The second point count used the Gazzi-Dickinson (GD) method to establish relative amounts of lithic sedimentary (Ls), volcanics (Lv), and metamorphic (Lm) rock fragments as described by Graham et al. (1976), Ingersoll (1978), and Ingersoll and Suczek (1979).

RESULTS

Architectural Element Type Descriptions

An initial facies-scale mapping exercise was conducted on an outcrop trending N35E with an average slope of approximately 45 degrees (Davis et al., 1991). The outcrop was approximately 25 meters high and 60 meters wide. The facies map constructed served as a basis for defining the architectural elements. Miall's (1978) classification scheme was used as a basis for the classification of observed lithofacies. **Table 4.1** summarizes the lithofacies observed during the outcrop study. Lithofacies Smb, Sfl, and Sm, were added to Miall's (1978) classification. Facies Smb consists of crudely crossbedded sand, sand-size clay clasts

and armored mud balls. The basal contact of the Smb facies is commonly erosional. The facies Sfl consists of finely laminated sands with abundant climbing ripples. The Sm facies consists of massive sand in which most or all sedimentary structures have been destroyed. This facies is strongly associated with the paleosol facies and is interpreted as an immature soil.

Four main types of elements were defined from the initial outcrop study: two types of channel elements, an overbank fine element, and a paleosol element. The definitions follow closely those described in Miall (1985) with the exception of the overbank fine element.

Table 4.1. Summary of lithologic facies groupings for architectural elements.

Element	Facies Present	Description Comments
CH-I	Massive gravel (Gm) Trough cross-bedded gravel (Gt) Planar laminated sand (Sp) Trough cross-bedded sand (St) Low angle cross-bedded sand (Sl) Massive sand and gravel (Sgm)	Channel element is dominantly gravelly and coarse sand facies.
CH-2	Gms, St, Sp, Sl Horizontally laminated sand (Sh) Fining upward v. fine to coarse sand (Sfl) Fine to medium sand with mud balls (Smb) Finely laminated sand, silt and clay (Fl) Clay and silt, massive, desiccated (Fm) Laminated silt, sand, and clay (Fsc)	Sand dominates with rare sand size clay clasts and gravel lag.
P	Paleosol, fine to pebbly sand, massive, carbonate stringers and nodules (P) Massive sand, immature paleosol (Sm) Fsc	Soils and stacked soils
OF	Silt, clay with rootlets (Fr) Fm, Fsc, P	Overbank fines

Miall (1985) includes the paleosol facies in the overbank fine element. This study treats paleosols as a distinct architectural element. Allen (1974) demonstrated the utility of paleosols in terms of studying the depositional environment of an alluvial sequence. In an arid to semiarid climate, the amount of time required for the formation of a mature soil is on the order of 10,000 to 100,000 years (Birkeland, 1984). In addition, the permeability of the sandy paleosols is much greater than the overbank clays and silt. Since the overall objective of this

study was to assess how the three-dimensional assemblage of lithologic units (specifically architectural elements) relates to hydrologic heterogeneity, it is preferable to treat them separately.

High-Energy Channel Element (CH-1)

The high-energy channel element is dominated by light to dark grey poorly sorted coarse sand to gravel. Coarse gravel lag deposits and trough cross bedding structures are common at the base of this element type. The deposits often fine upward into horizontally laminated clean sands. Clay interbeds and clay rip-up clasts are rare in the gravel elements. Elements of this type are generally between one and three meters thick and tend to pinchout abruptly.

An intact obsid n cobble area was found in one of the gravel elements located higher in the section. This cobble is believed to be derived from East Grants Ridge, which was last active three Ma (Lipman & Mehnert, 1980), and lies within the drainage basin of the Rio San Jose. The gravel elements (CH-1) mapped at the field site appear to be deposits of a fast-moving competent river.

Low-Energy Channel Element (CH-2)

The low-energy channel element is composed of undifferentiated scour-fill and sand-sheet deposits. A high-order bounding surface (order three or four) is not observed between these two types of deposits in the CH-2 element and thus they are not differentiated in the architectural element scheme.

The first type is characterized by sand scours filled with tan to light gray, fine to medium sand with locally abundant 0.5 to 1.5 centimeter thick clay drapes. The deposits consist of moderately to well sorted, subangular to subrounded sand grains. Sand-sized clay clasts are commonly observed in these deposits. The base of these deposits are concave upwards, with little to no observable gravel lag. Armored mud balls are also common at the base, ranging from 2 to 60 centimeters in diameter. The deposits of the scour-fill are largely

unconsolidated and range in thickness from one to nine meters. The occurrence of sand-size clay clasts and armored mud balls indicates ephemeral flow conditions.

The sand-sheet deposits are laterally extensive and consist of very-fine to fine sand with some clay drapes. The basal contacts are flat with little erosion. The upper contacts are sharp or gradational. Common sedimentary structures include continuous and discontinuous horizontal-laminated medium sands, foresets of inclined-planar-cross-bedding within fine to medium sands, ripple-cross-laminated fine to medium sands, and climbing-ripple-lamination in very-fine to fine sands. Clay drapes interbedded with very-fine sand and laminated clay and silt are common towards the top of these elements.

Overbank Fine Element (OF)

This element is composed of dark brown clay locally interbedded with tan silt and thin immature sand and clay paleosols. The most common sedimentary structure is parallel stratification between clay and silt. Interbeds of immature paleosols are especially common higher in the section. Lower in the section, this element is often a massive dark brown clay with red-brown sand-filled cracks. Elements of this type are very common and range from one to seven meters thick.

Paleosol Elements (Ps, Pc, and Pgs)

The paleosol element is further divided into three sub-element classes based primarily on parent material. These include the most common sand paleosol (Ps), a clay/silt paleosol (Pc), and a paleosol that has parent material consisting of a sand and gravel mixture (Psg).

The Ps element is an orange-red soil (5 YR 6/5 to 5YR 6/6; Munsell Soil Color Chart) and is composed of moderately to well-sorted, very-fine to fine sand. The sand grains are subangular to rounded, depending on location. Most of sandy paleosols exhibit few if any sedimentary structures in the upper two-thirds, although weak, local horizontal-lamination is visible in the lower third in some of the sandy paleosols. Rarely, sandy paleosols exhibit ghost trough-cross-stratification indicating a possible eolian parent material. Many of these

sand paleosols exhibit a marked zone of white $CaC0_3$ accumulation. The most mature of the sand paleosols at the site coincide with Stage-II of McGrath and Hawley (1987).

Due to the distinct hydrologic properties of the clays and silts, paleosols with overbank-fine parent material are mapped separately as element Pc. The most extensive clay paleosol element is a red-brown (2.5 YR, 4/6) paleosol consisting of clay and sandy clay. This element was differentiated from the clay-silt (OF) element on the basis of its red-brown color, its lack of original sedimentary structures, and its blocky texture. Only one notable element of this type was mapped. The thickness of this element ranges from 0.3 to 1.5 meters. Thin clay paleosol layers (one to three centimeters) exist within some of the OF elements.

The third paleosol element delineated in this study is the gravel-sand paleosol (Pgs). Only one element of this type was mapped. It is red/pink in color (2.5 YR, 6/6) and is composed of pebble and cobble-sized fragments in a matrix of sandy material. Preliminary analysis of this element in thin section shows that the grains in the matrix are very fine to fine sand and angular. The thin sections show that many of the grains are coated with clay, which is evidence of eluviation in the soil profile. No sedimentary structures are preserved in this largely calcite-cemented deposit.

Petrographic Analysis

Petrographic analysis of the Albuquerque Basin sediments indicates that sediment source terrain may be delineated. Results of the traditional quartz-feldspar-lithic (Q-F-L) point count are presented in **Figure 4.5**. From the Q-F-L data, no clear grouping is apparent to delineate sediment source terrain. However, the Gazzi-Dickinson (GD) point counts (**Figure 4.6**) indicate compositional zoning of lithic fragments with respect to sediment source terrain. Sediments derived from the ancestral Rio Grande system and the ancestral Rio Puerco/Rio San Jose system appear to exhibit different abundances of sedimentary, plutonic, and volcanic lithic fragments. There is insufficient difference in the relative abundances of lithic fragments among the Rio Puerco and Rio San Jose deposits to delineate them.

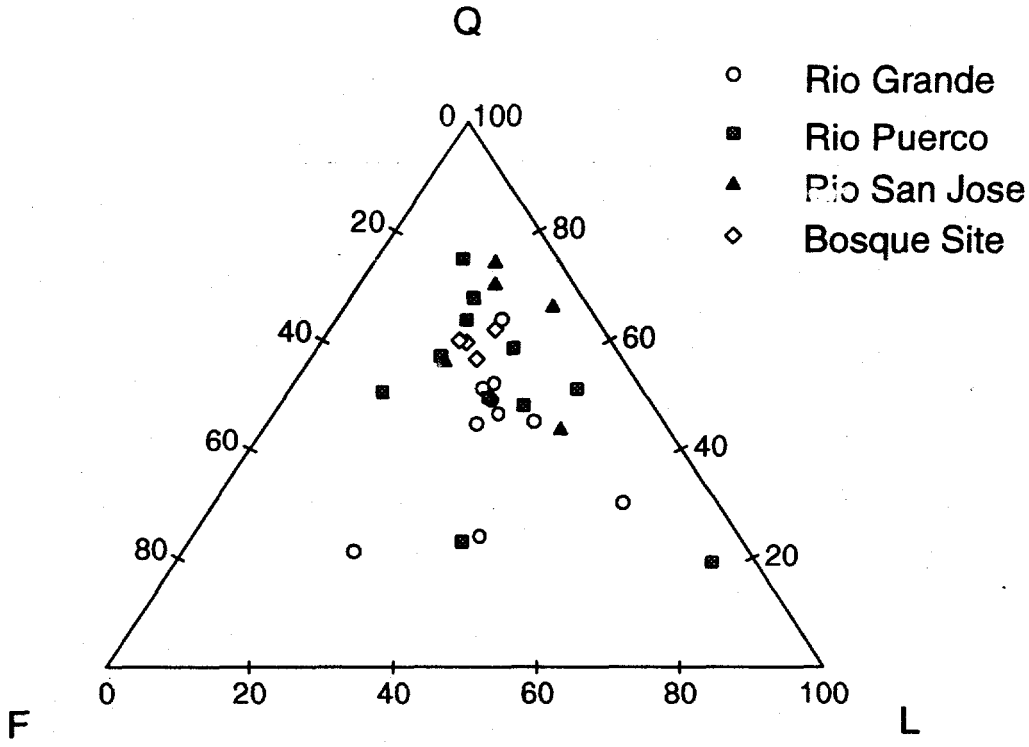

Figure 4.5. Ternary plot of the relative abundances of quartz (Q), feldspar (F), and lithic fragments (L) with respect to sample locations. (After J.S. Harris, unpublished data)

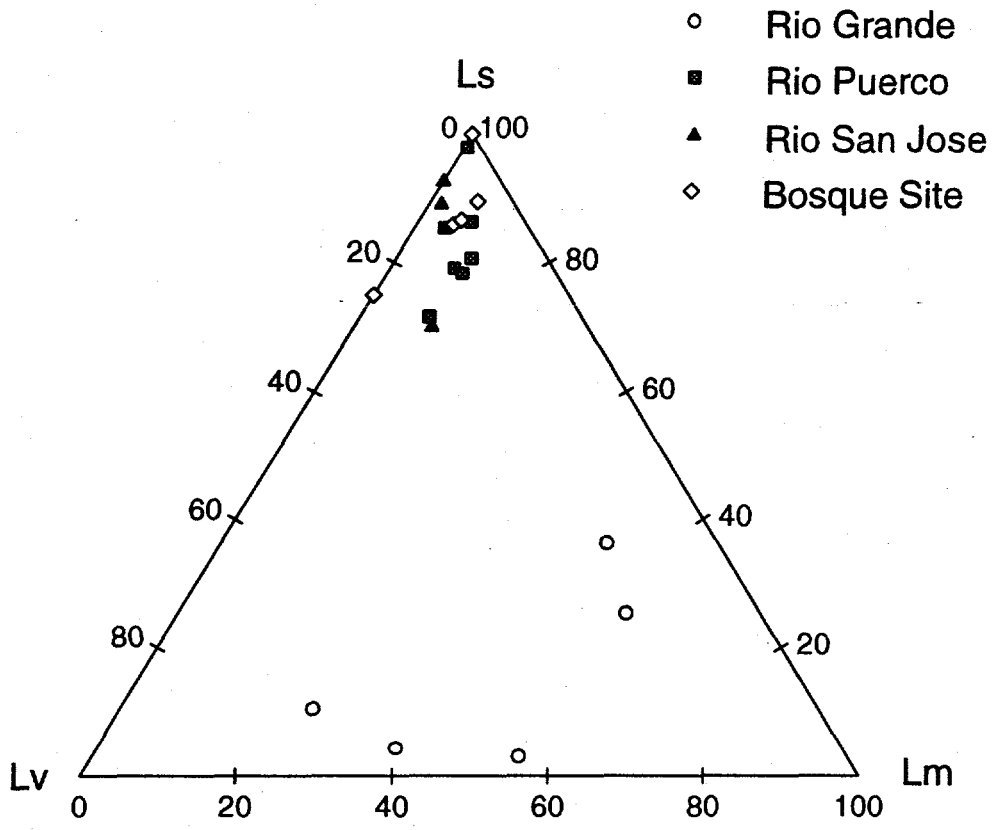

Figure 4.6. Ternary plot of the relative abundances of sedimentary (Ls), plutonic (Lp), and volcanic (Lv) lithic fragments with respect to sample locations. (After J.S. Harris, unpublished data)

With the current results, we are able to perform a preliminary assessment of the hypothesis that the high-energy (CH-I) elements represent deposits of the tributary system. However, two issues must be kept in mind when interpreting the petrographic analysis. First, the relative abundance of volcanics may be a weak criteria for the delineation of source terrain since volcanism was active in the Albuquerque Basin during the time of deposition. Currently, there are insufficient time constraints on the relative age of the deposits used to characterize the source terrain and the deposits at the field site. It is possible that the sediments used to characterize the source terrain of the Rio Grande are contemporaneous or post-date the Bandelier eruption cycles (~1.1 - 1.5 Ma) while the sediments collected from the field site pre-date the Bandelier eruptions and thus represent a time of volcanic-poor source terrain. Second, while most samples were unconsolidated, some carbonate cementation was present in some of the samples. The cementation occurred after deposition resulting in intrabasinal sedimentary fragments. The delineation of intrabasinal sedimentary fragments and those derived from the source terrain may also inhibit the use of sedimentary fragments as a delineating criteria. Intrabasinal sand-size clay clasts are believed to play a subordinate role since the samples were from high-energy sand and gravel deposits.

The resolution of the sediment source terrain analysis could be enhanced by quartz grain trace element analysis via cathodoluminescence, and clay mineralogy via X-ray diffractometry. These are possible future avenues of research.

Interpretation of Architectural Elements

The occurrence and assemblage of lithologic facies within the architectural elements and the architectural element external geometries provide a means of interpreting the depositional regime of each of the element types. The petrographic analysis is used to tentatively delineate sediment source terrain of some of the architectural elements.

The gravel (CH-1) elements appear to be axial deposits of a fast-moving competent river. Due to the lateral persistence of these elements, flow directions are not readily apparent from external geometry. The preliminary petrographic analysis indicates that the deposits are

derived primarily from the Rio Puerco/Rio San Jose tributary system.

The CH-2 elements are believed to have been deposited by either the ancestral northwestern tributaries to the Rio Grande (Rio Puerco and Rio San Jose) and/or Rio Grande floodplain sands. The occurrence of sand-size clay clasts and armored mud balls indicates ephemeral flow conditions. In addition, the occurrence of climbing ripples indicates an environment where an abundance of sediment was being deposited from suspension in slowly moving waters (McKee, 1966). Such flow conditions occur during the waning phases of a large flood (McKee et al., 1967), and in natural levee environments adjacent to the axial channel.

The sandy soil element (Ps) is interpreted as representing the pedogenesis of fluvial or eolian sands. The degree of pedogenesis observed (Stage I-II) indicate a lack of significant fluvial influx for thousands of years. Elements of this type exhibit both tabular and len- shaped geometries. The tabular elements are commonly composed of well-sorted, well-rounded quartz grains, indicating a possible eolian origin. The lens-shaped Ps elements may represent fluvial sands abandoned by the channel, which received an eolian sand influx at the surface as pedogenesis progressed.

The clay paleosol element (Pc) is interpreted as a floodplain mud which was left deprived of sediment for an extended period of time, probably due to the rapid movement of the fluvial channel away from the once proximal floodplain. The Pc element mapped grades into an OF element to the southwest suggesting that the fluvial channel may have been located further to the southwest.

The OF elements are interpreted as representing the portions of the floodplain where the primary mode of sedimentation is from the slow settling of clay and silt-sized materials from suspension. These elements may represent deposition either in the distal portion of the floodplain during relatively large flood events or the proximal portion of the floodplain during small flood events. The relative abundance, thickness, and lateral continuity of the OF elements suggest that the alluvial plain on which the river(s) flowed may have been relatively wide and flat (Mack and Seager, 1990). A wide flat alluvial plain would cause individual

flood events to easily overtop the river banks, and spread a sheet of fine sand near the channel (McKee et al., 1967) and laterally continuous layers of clay and silt at greater distances from the channel.

Architectural Element Cross Section

The spatial assemblage of the architectural elements allows for a limited interpretation of the cyclicity of deposition. A northeast-southwest cross section through the region mapped is presented in **Figure 4.7**. In between the lower and upper high-energy channel deposits (CH-I), three significant CH-II type scour fills were encountered. The architectural elements in Figure 4.7 are grouped into 7 packages, each believed to represent slightly different configurations of the fluvial/interfluvial environment.

Packages 1 and 7 are the upper and lower boundaries of the mapped deposits, respectively. These packages are believed to represent deposits of the Rio Puerco/Rio San Jose tributary system.

Package 2 is characterized by distal floodplain deposits of overbank sands, silts, and clays and paleosols. Magnetite is present in some of the sand deposits of this package, which is more indicative of ancestral Rio Grande deposits originating in southern Colorado than the northwestern tributaries originating in the San Juan Basin. This package of deposits is interpreted as representing deposits in the proximal-to-distal floodplain of the ancestral Rio Grande.

Package 3 represents a significant scour-fill event. The scour of this package trends S30E. The lower fill material is medium cross-bedded sand. The upper fill material consists of multistory deposits of fine sand, silt, and clay. This package of deposits is believed to represent the presence of either the main tributary or an associated distributary channel of the tributary system.

Package 4 represents another significant scour-fill trending S35E. A high energy CH-I element occurs at the same stratigraphic location to the south. The timing of the CH-I element relative to the CH-II element is not clear, but it is likely that the two channels are

NEXT PAGE

Figure 4.7. Cross-section of architectural elements mapped at the field site. Cross-section reference line is shown in Figure 4.2.

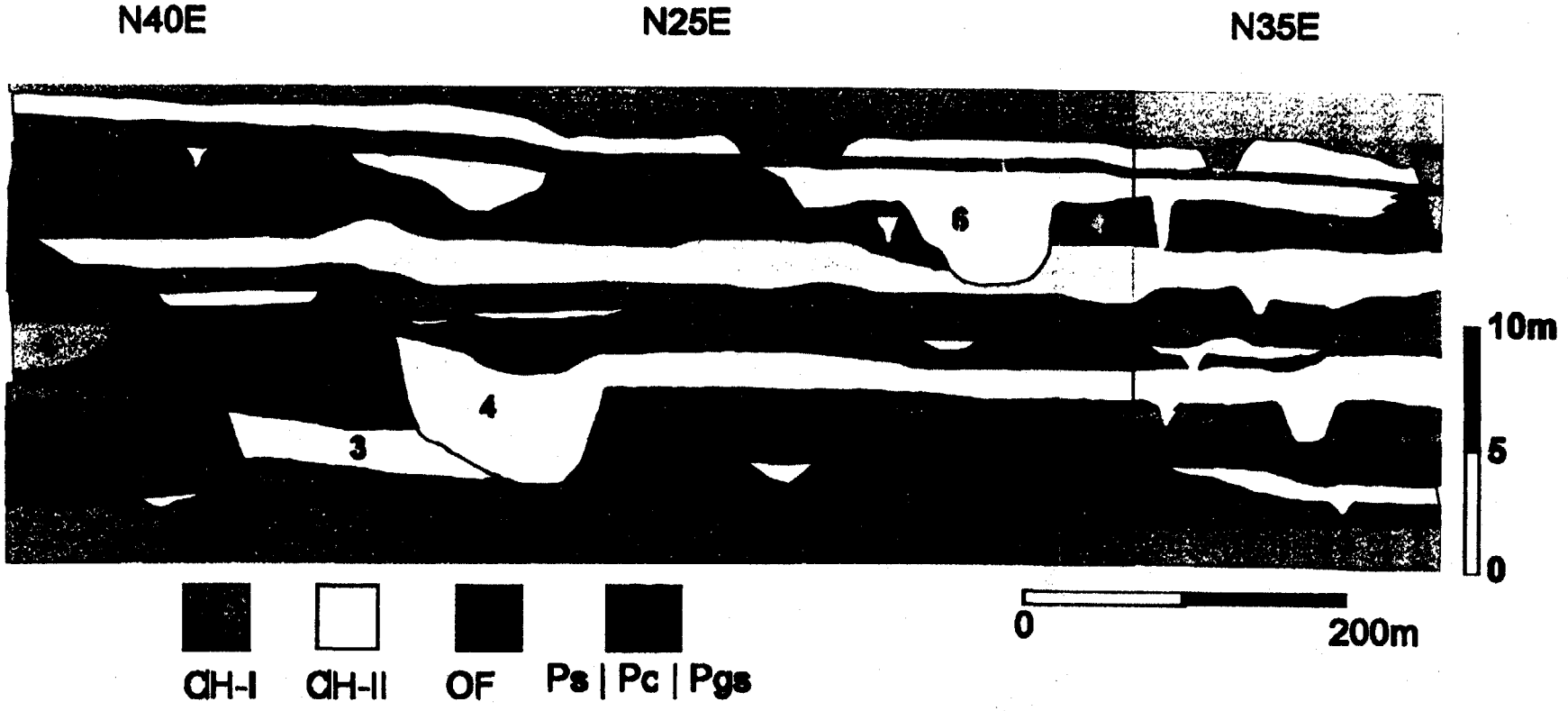
N40E
N25E
N35E
6
4
3
10m
5
0
0
200m
clH-I
clH-II
OF
Ps | Pc | Pgs

associated. The CH-I element has been traced to the south approximately one kilometer and attains a maximum thickness of approximately two meters. The overall orientation of this CH-I element is not apparent. One possibility for the relationship between the high-energy CH-I element and the low-energy CH-II element of Package 4 is that the deposits of CH-II element represent a tributary to the CH-I element.

Package 5 is characterized by overbank sands, clays, and paleosols. The low-energy CH-II element pinches out to the west indicating an associated north-south flowing channel to the east. This package could represent proximal floodplain deposits of the ancestral Rio Grande.

Package 6 represents another significant scour fill CH-II element and the associated deposits. The main channel of this package trends S55E and exhibits an asymmetric ribbon-and-wing type of morphology where the channels are plugged with sediment prior to significant lateral migration and the width to depth ratio (W/D) is generally less than 15 (Hirst, 1991). The long wing is to the northeast and the short wing to the southwest. To the southwest the overbank sands interfinger with overbank fines and paleosols within 100 meters of the main channel. The limit of the northeast wing occurs at the very northern edge of the mapped region and is approximately 200 meters from the main channel. One auxiliary channel to the CH-II scour-fill occurs to the southwest. This smaller channel deposit grades laterally into overbank fines and paleosols.

Package 7 has an erosional base with the onset of the deposition of a broad CH-II deposit. Multistory sands and gravels (CH-II) represent a laterally extensive high-energy depositional regime. Due to difficult access and lateral amalgamation, the dimensions of the individual channels are not mapped but, from the limited exposure, are believed to be on the order of five meters wide and two meters deep.

The overall abundance of overbank clays, silts and paleosols suggests that the field site was located a considerable distance from axial fluvial channels for a large portion of the time recorded by these deposits. Moreover, the sands themselves (CH-2) are characterized by predominantly lower flow regime sedimentary structures and fine-grained sand, both of which

indicate deposition in shallow, slow moving waters such as would be found on a floodplain.

DISCUSSION

This study provides the groundwork for additional studies of the deposits of the Sierra Ladrones Formation both in the vicinity of the field site described and for comparison throughout the Rio Grande Rift Basins.

Within the section dominated by fine-grained deposits (Packages 2 - 6), several general features of the channel geometries appear relevant to the large-scale depositional controls. First, there appears to be a northern migration of the channel location through time as evidenced by the relative north-south location of the channel scours. This apparent northern migration is accompanied by an apparent change in channel orientation. Using the channel-scour orientation as an indicator of average channel direction, the channels associated with Packages 3, 4, and 6 appear to have flowed in a progressively easterly direction. The second general feature observed is that two of the channels exhibit asymmetric proximal floodplain sand deposits and both have the broader side to the northeast of the channel.

These features are a possible indication of the fluvial system responding to a eastward dipping basin floor. For each location of the channel, overbank deposits spill out preferentially to the northeast. The channel appears to migrate in small avulsive steps. Each new channel location appears to be progressively to the north and exhibit a more easterly flow direction.

A larger-scale control is likely forcing the major change in depositional regime observed between the packages 1, 2 - 6, and 7. The two most likely controls are climate and channel grade. An increase in the annual precipitation of the catchment would result in an increase in the competence and capacity of the fluvial system. Increasing the dip of the basin floor tectonically would have similar effects.

CONCLUSIONS

In the study of the Sierra Ladrones Formation in the vacinity of Bosque, New Mexico,

four main types of architectural elements were delineated based on lithologic facies assemblages and external geometry. Two of the elements are interpreted as deposits of sandy channels and are differentiated based on the relative energy of deposition, high and low-energy. The overbank fine (OF) elements are interpreted as resulting from distal overbank deposits. The paleosol elements (P) are interpreted as pedogenically altered surface materials and were subdivided into three element classifications based on whether the parent material was sand (Ps), sand and gravel (Pgs), or clay (Pc).

The architectural elements were on the order of one meter thick and laterally extensive over hundreds of meters. The scours associated with the channel elements are oriented toward the southeast. The scour orientations serve as an indicator for the channel orientation. Based on the occurence of the observed architectural elements, the deposits of the Sierra Ladrones Formation studied are interpreted as resulting from a fluvial-interfluvial system. In addition, the orientation of the channel scours indicates that the northwesterly ancestral tributary system of the Rio San Jose and Rio Puerco played a significant role in the deposition. A schematic block diagram of the fluvial-interfluvial system is presented in **Figure 4.8**. Petrographic analysis of sediments obtained from the sources areas and the field site confirms this.

Some information of the evolution of the fluvial system can be gained from the study as well. There appears to be a northern migration of channel location and progressively easterly flow direction of the channel deposits. Several causes for this are possible including tectonic and/or climatic variations.

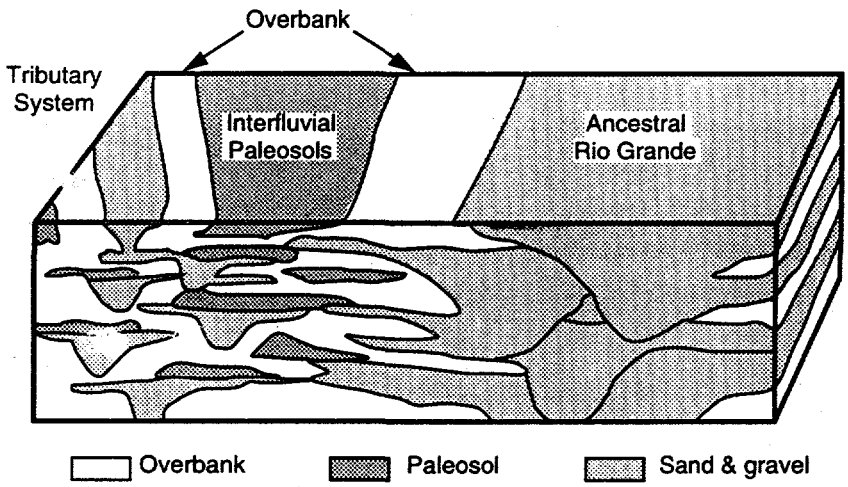

Figure 4.8. Inferred orientation and distribution of ancestral Rio Grande deposits in the vicinity of the field site. Location of cross section is shown in Figure 4.3.

CHAPTER 5: FACIES-SCALE HETEROGENEITY STUDY[3]

INTRODUCTION

The next two chapters investigate the correlation structure of the Sierra Ladrones Formation at two scales. First, the small-scale variability was studied through intensive permeability sampling of small outcrops (~ 1 m^2). Second, the large-scale variability (100's of meters) was investigated by analyzing the three-dimensional spatial assemblage of the architectural elements described in Chapter 4.

The objective of the two studies was to investigate the relationship between observed sedimentological features and the corresponding geostatistical characteristics of the heterogeneity. In the small-scale studies presented in this chapter, mapping of the sedimentological features follows the bounding surface framework (Allen, 1983; Miall, 1988). Geostatistical analysis of air-permeability data consists of the estimation of population and sub-population statistics and estimation of the overall correlation structure from spatially located air-permeability measurements. In the large-scale analysis (Chapter 6), the correlation structure is estimated by assigning mean permeabilities to the different architectural elements.

STUDY SITES

Approximately 880 measurements of permeability were obtained at six outcrop locations. Five of the study sites, referred to SS1, SS2, SS4, SS5 and SS6, were located at the main field site (Figure 4.1) referred to hereafter as the Bosque site. One study, ES1, was located approximately 10 kilometers north of Socorro, New Mexico (two kilometers northeast of Escondida, New Mexico) and is referred to as the Escondida site.

Bosque Site

The deposits of the Bosque site are interpreted as marginal ancestral Rio Grande

---

[3]Davis, J.M., M.B. Gotkowitz, F.M. Phillips, and J.L. Wilson, Correlation structure of permeability at the lithofacies scale, paper in prep. for submission to Geol. Soc. Amer. Bull.

floodplain and tributary deposits (Chapter 4). Six architectural elements have been delineated. The low-energy channel (CH-2) and sandy paleosol (Ps) elements were selected for the small-scale study based on their range of permeabilities and their overall abundance within the depositional system. Studies SS1, SS2 and SS5 were located in the CH-2 element of Package 4 (see Figure 4.7). Studies SS4 and SS6 were in the sandy paleosol element, Ps, of Package 5. The relative locations of the small-scale studies are shown in **Figure 5.1**.

CH-2 Element

The CH-2 element consists of low-energy, very-fine to medium channel sand. Sedimentary structures commonly include continuous and discontinuous horizontal lamination, foresets of inclined-planar crossbedding, ripple cross-lamination and climbing-ripple stratification. Clay drapes from 0.5 to 1.5 centimeter thick are locally abundant, and are often interbedded with very fine sand, and laminated clay and silt. With the exception of clay drapes, the deposits are relatively homogeneous and the changes between facies are subtle. These deposits are interpreted as proximal flood plain sands and tributary channel fill. (Chapter 4; Lohmann, 1992).

Ps Element

The Ps element consists of an orange-red sandy paleosol composed of moderately to well-sorted, very-fine to fine sand with scattered zones of calcium carbonate accumulation. In general, the processes involved in pedogenesis have destroyed the sedimentary structure of the parent material, although, some of these deposits display weak sedimentary structures. Based on stratigraphic location, grain size, and locally preserved sedimentary structures, Lohmann (1992) interprets the paleosol element as pedogenically modified fluvial and eolian sands.

Escondida Site

One small scale study, ES1, was conducted at a fluvial outcrop located at the

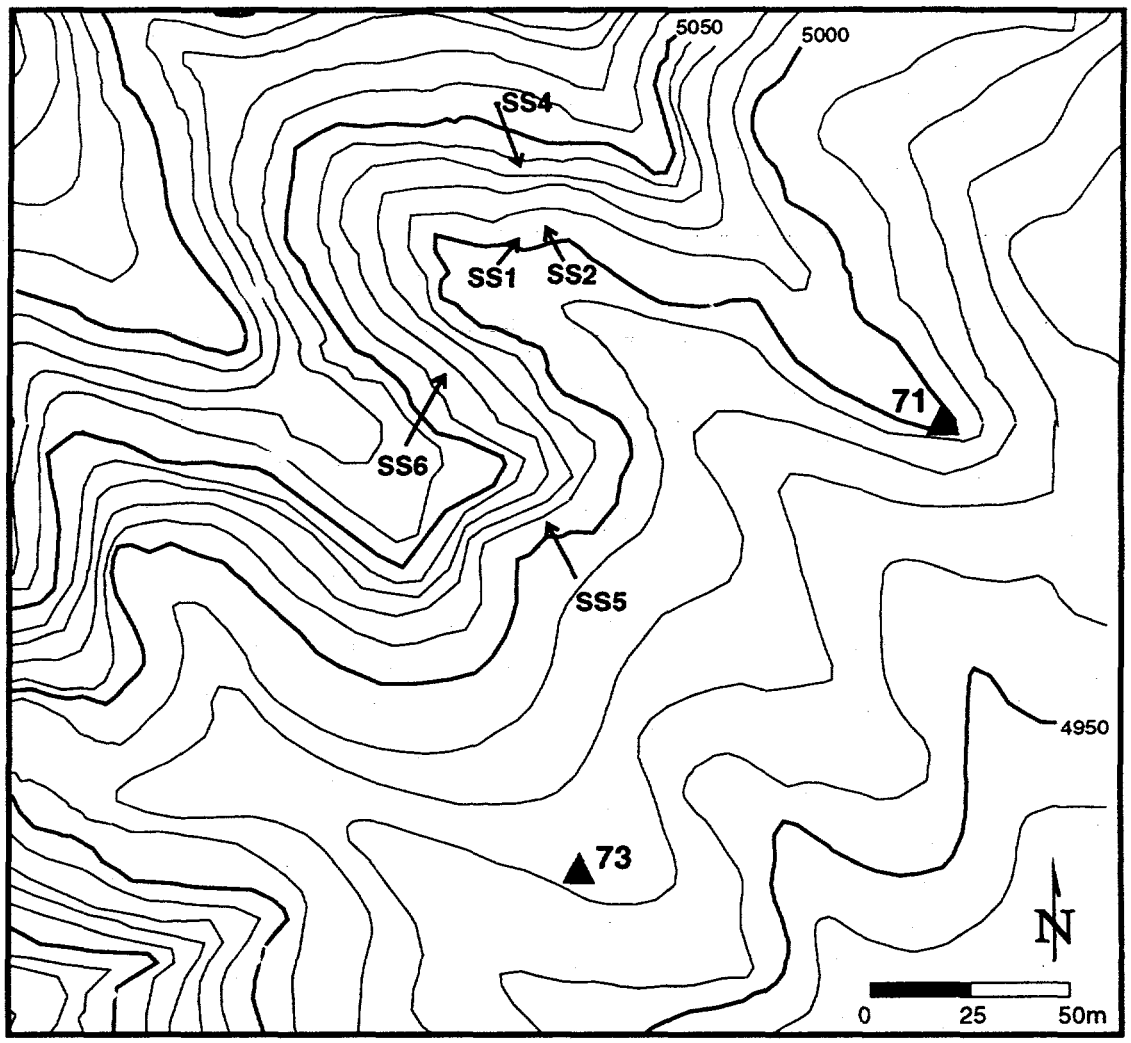

Figure 5.1. Location map of small-scale studies at the Bosque Site. See Figure 4.2 for location of this figure.

Escondida site. Based on the coarse grain size and large-scale trough cross-bedding, the deposits are interpreted as originating from the ancestral Rio Grande. The specific age of the deposits is unclear, however the deposits are stratigraphically lower than a broad geomorphic surface that is interpreted as time-correlative to the Llano de Albuquerque. This indicates that the age of the deposits at the Escondita site are comparable to the deposits of the Bosque site (Pliocene-Pleistocene).

The purpose of the Escondida study was to obtain measurements from a fluvial deposit exhibiting distinct changes in lithofacies. The study was conducted in an area of channel-fill sand, where grain size varies from very-fine to coarse. The deposit studied is analogous to the high-energy channel element (CH-1) of the Bosque site.

METHODS

The methods employed for the small-scale studies were 1) mapping of the sedimentary features of each study location, 2) obtaining in situ measurements of permeability, and 3) performing geostatistical analysis of the air-permeability data. For each study, either a single photograph or a mosaic of several photographs served as a base map for the study.

Heterogeneity observed within each study site was mapped according to the hierarchical system of bounding surfaces in fluvial deposits developed by Allen (1983) and modified by Miall (1988). The bounding surfaces model is preferred over other ad hoc definitions of hydrofacies because it is established in the sedimentological literature and provides a potential framework for generalizing the results of the geostatistical analysis.

The bounding surfaces model identifies internal divisions in sandstone bodies that separate regions of genetically related strata. At the scale of interest in the studies presented here, zeroth, first and second-order contacts (**Figure 5.2**) are of interest. Third and fourth-order surfaces coincide with the architectural element boundaries presented in Chapter 4.

Zeroth-order boundaries are non-erosional, concordant bedding contacts which might arise from deposition of a stratum parallel to the unit beneath it. First-order contacts are usually erosional and bound individual cross-bedding sets. First-order boundaries occur within

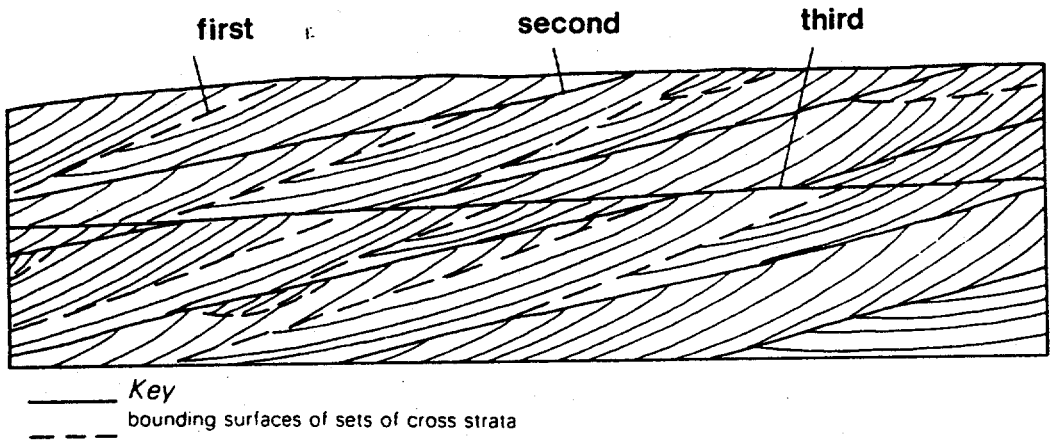

Figure 5.2. Illustration of bounding surface classification scheme. (Modified from Collinson and Thompson, 1982)

lithofacies, and are interpreted as the result of bedform migration under steady flow conditions. Boundaries of soft-sediment deformation that alter the primary sedimentary structures are considered first-order surfaces in this study. Second-order contacts separate cosets and commonly separate different lithofacies. The second-order surfaces are erosional and signify a change in flow conditions.

Measurements of permeability were obtained with the lightweight, syringe-based, air-minipermeameter (LSAMP) described in Chapter 3. Individual study sites were prepared by digging away the colluvial cover to reach a vertical face of undisturbed deposit. The prepared outcrop was allowed to dry for a few days before sampling took place to ensure that soil moisture would not affect measured permeabilities. Free-fall times are the time required for the syringe to fall with the tip seal open to the air. These were measured regularly throughout the studies to ensure against instrument malfunction.

Sampling of air-permeability was conducted in two stages. In all of the studies at the Bosque site except for SS6, the first stage of sampling employed a stratified random sampling approach for the unbiased sampling of air-permeability at a variety of spatial scales. While this method resulted in a data set with adequate spacing for variogram analysis, resolution of the correlation structure at very small lags (approximately two centimeters) was poor. As a result, a subsequent sampling campaign was conducted to improve the variogram estimate at small lags.

For the initial sampling a stratified random sampling scheme was adopted. The general method was developed for the study of alluvial fan deposits presented in Chapter 7 but differed slightly in implementation. The objectives of the stratified random sampling scheme were to obtain a spatial data set that 1) was unbiased, 2) covered as many lags as possible, 3) was computationally efficient, and 4) covered as much of the outcrop as possible. To meet these objectives a two-step sampling scheme was developed.

First, a fixed orthogonal grid of the desired number of control points was set up on the photomosaic of each study. From each node on the overlay grid, a smaller sampling grid was defined. This was determined by generating three uniformly distributed random numbers from

zero to one (U(0,1)). The first random number was used to determine the number of nodes on the sampling grid. For a number less than one-half, the sampling grid contained four points. For a number greater than or equal to one-half, the sampling grid contained nine points. The other two random numbers were used to determine the size of sampling grid. Each of the U(0,1) were multiplied by the horizontal and vertical overlay grid-element dimensions. The photomosaic was used in the field to identify the locations of control points on the outcrop. The sampling locations were measured from each control point according to the determined sampling grid characteristics.

During the the initial sampling stage, the minimum sample spacing was two centimeters in order to prevent overlap in the measurements of permeability. The range of the permeameter is suited for the measurement of weakly lithified dry sands and soils. In each of the study areas there are features of the outcrop which have associated permeabilities that are beyond the range of the permeameter, such as clay balls and clay drapes, calcite nodules, lenses of loose material, fractures, and holes. Sampling points which fell on these areas were recorded as a "non-measurement".

The second stage of permeability sampling was performed to increase the number of data separated by small distances. Air permeability measurements in the second sampling campaign were obtained along perpendicular transects at two centimeter intervals. The two sampling stages were separated by approximately one year. As a result, the small-scale study areas had undergone some changes and the locations of the second campaign could not be directly related to the coordinate system of the initial sampling. However, assuming second-order stationarity and unbiased sampling, their relative locations provide sufficient information to estimate the small scale variogram.

Measurements at the study site SS6 were taken along a series of horizontal transects that were juxtaposed laterally according to ease of sampling. The results are included here to illustrate the difference between the unbiased stratified random approach and the biased horizontal transect approach.

Measurements at study site ES1 were taken along a vertical transect. The

measurements were spaced at a variety of intervals to yield sufficient data for variogram estimation within particular subsets of the transect. This sampling design was implemented in order to better characterize the variability associated with the observed changes in depositional regime.

Geostatistical Analysis

The goal of the small-scale studies was to assess the relationship between the observed sedimentary features and the correlation structure of permeability. The observed sedimentary features include the scale of the cross-bed sets and the scale of the facies. In the context of fluvial bounding surfaces, these are regions separated by first and second-order bounding surfaces, respectively. It was hypothesized that the regions separated by bounding surfaces exhibit different mean permeability and that the dimensions of the regions are then the dominant control of the correlation structure. To test this hypothesis the probability distributions of the regions were compared against one another. Then, combined with the measured dimensions of the regions, an analysis of the relationships between the observed sedimentary features and the correlation structure was performed.

Comparison of the probability distributions between regions was performed with Kolomogorov-Smirnov (K-S) test. The K-S test relies on comparisons of the expected and the observed relative frequencies to detect differences between two distributions. Since the K-S test is non-parametric, no *a priori* assumption regarding the shape of the distribution is necessary and two empirical distributions can be compared directly (Till, 1974). The K-S test is performed by estimating the probability distribution from the ranked log-permeability data then comparing the difference in the probability estimates between the two distributions for each value of log-k. The maximum observed difference is then compared to a critical value based on the level of significance and the number of data in each data set.

The correlation structure of each of the small-scale studies was estimated with variogram estimator:

$$\gamma(\xi) = \frac{1}{N}\sum_{i=1}^{i=N} [k(x_i + \xi) - k(x_i)]^2$$

The variogram was estimated in the horizontal and vertical directions for the data obtained in each sampling stage. The two estimates are plotted together with the variogram of the initial sampling represented by filled triangles and the variogram of the second sampling stage represented by open triangles. Since the data of the initial sampling stage were not aligned on a regular grid, the pairing of data for each separtion lag, ξ, was conducted with a search window as shown in Figure 2.3. Throughout these studies, the search window was kept as small as possible while maintaining a sufficient number of pairs. Sixty pairs was the minimum number of pairs for each lag class. Sampling locations which fell on materials with extreme values of permeability, such as clay or gravel, could not be measured with the permeameter. These "non-measurements" were originally treated in the variogram estimation by assigning values of permeability found in the literature.

The inclusion of values of permeability ranging over many orders of magnitude led to very erratic variogram estimates. Reasonable estimates of the variogram can often be attained by eliminating outliers (Armstrong, 1984), and this was the approach taken in the variograms presented here. The elimination of extreme values is justified in this case because they lack spatial continuity within each study area, with no apparent correlation of their spatial distribution. For example, a scattering of clay balls with an average diameter of five centimeters might not significantly alter the effective permeability of a sand layer two meters wide, but their inclusion in the estimation of the variogram will completely mask the correlation structure of the sand layer.

In addition to the removal of outliers, the sets were analyzed for the presence of linear trends. In the data sets that did exhibit a slight trend, no significant differences were seen between the variograms estimated with the trend present or removed. Therefore, in the analyses presented, no trends have been removed.

RESULTS

Five of the small-scale studies were conducted at the Bosque site. The outcrop consists of the Pliocene-Pleistocene Sierra Ladrones Formation, and at this particular location, the deposits are interpreted to be of fluvial/interfluvial origin. Three of the small-scale studies (SS1, SS2, and SS5) were performed within a single channel scour of the low-energy channel element (CH-2). Two of the small-scale studies (SS4 and SS6) were performed in a single sandy paleosol element (Ps).

One small-scale study was performed in a area approximately 60 kilometers south of the main field site also on an outcrop of the Sierra Ladrones Formation. The deposits at this location (ES1) are interpreted as high-energy fluvial deposits of the axial drainage system.

CH-2 Element

The locations of SS1, SS2 and SS5 within the CH-2 channel element are shown in Figure 5.1. SS1 and SS2 are oriented sub-parallel to the inferred paleoflow direction, and the orientation of SS5 is interpreted as sub-perpendicular to the paleoflow direction.

SS1

SS1 was approximately 2.1 meters wide and 1.6 meters high (**Figure 5.3**). Three second-order bounding surfaces separate four regions within the outcrop. Region 1 was 0.7 meters thick and consisted of even and wavy-parallel, thickly laminated upper-fine and lower-medium sands. Soft-sediment deformation was present near a large (0.1 meter in diameter) clay ball in the lower left-hand corner of the unit resulting in two small regions bounded by first-order surfaces. Region 2 was 0.2 meter thick and consists of coarse sand and pebbles, discontinuous clay drapes, and small (from two to five centimeters in diameter) clay balls. Region 3 was 0.7 meters thick and consists of parallel, horizontal laminae. Within Region 3 grain-size fines-upward from a clean coarse sand to a fine sand at the top. Climbing ripples were present at the top of Region 3. Region 4 was approximately 0.15 meters high and consists of even, inclined parallel laminae. The average vertical dimension of the regions

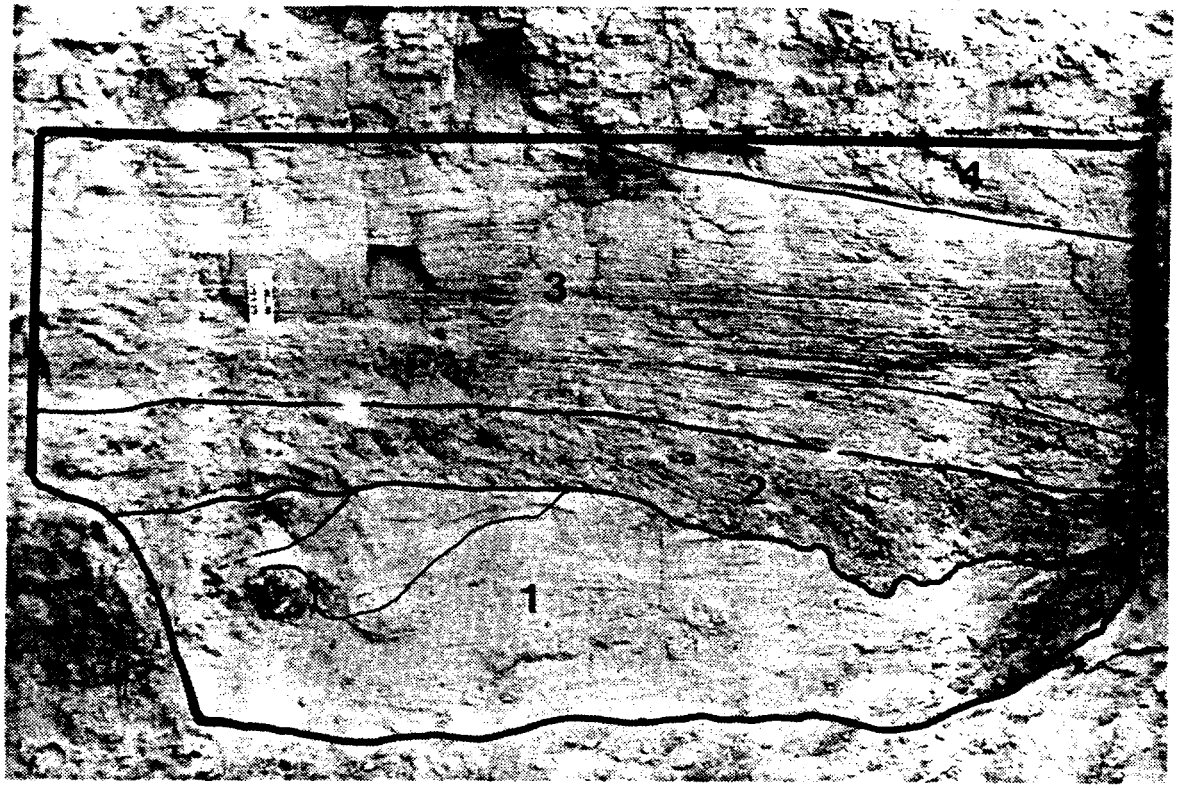

0 20cm

Figure 5.3. Photograph of SS1 outcrop. Numerically labeled regions separated by second-order bounding surfaces correspond to those described in the text.

bound by first and second-order contacts was approximately 0.34 meters.

One hundred fifty-one sample locations were identified on SS1 of which 142 air-permeameter measurements were obtained. All non-measurements were due to the presence of clay balls. Statistics and results of the comparisons of these regions for SS1 are given in **Table 5.1** . Region 4 was too small to consider. The hypothesis that Region 1 exhibits a similar distribution to the others regions can be rejected. However, the null hypothesis comparing Regions 2 and 3 cannot be rejected.

An anisotropic exponential model was fit to the directional variogram estimates of the SS1 logarithmic data. The horizontal variogram (**Figure 5.4a**) was fit with a nugget of 0.024, a sill of 0.19, and a correlation length of 16 centimeters. The vertical variogram (**Figure 5.4b**) exhibits a similar nugget (0.024) and shorter correlation length (eight centimeters). The sill estimate in both directions is approximately the same. The larger sill and shorter correlation length in the vertical direction are consistent with the observed stratification. For SS1, the ratio of the average thickness of the mapped regions to the effective range (which for the exponential model is three times the correlation length) is 0.7.

The larger correlation length and slightly lower sill in the horizontal variogram estimate for SS1 (Figure 5.4a) are consistent with the observed stratification, however the difference is small relative to the thickness-to-width ratio of the regions. This apparent underestimation of the horizontal correlation length is attributed to the variable thicknesses and slightly dipping nature of the strata. The variable thicknesses are likely to enhance search window effects in which vertically juxtaposed points are paired into a horizontal lag class. This effect is expected to be most prominent in materials exhibiting abrupt changes in permeability.

Table 5.1. Statistics of SS1 and sub-regions and results of Kolmogorov-Smirnov test.

		Population Statistics		Population Comparison	
Data set	N	μ [ln(k)]	σ^2	Region 2	Region 3
SS1 (all)	142	2.96	0.21	–	–
Region 1	61	2.69	0.20	not equal	not equal
Region 2	19	3.25	0.12	–	"equal"
Region 3	59	3.12	0.12	"equal"	–
Region 4	3	3.49	n/a	n/a	n/a

SS2

SS2 was about two meters above and to the east of SS1 and was approximately two meters high and two meters wide. It was similar to SS1 in the predominance of medium and fine sands. However SS2 was more homogeneous than SS1. The lithologic changes are more subtle and the grain-size was less variable.

Two second-order bounding surfaces were identified within SS2, dividing the outcrop into three regions (**Figure 5.5**). The lowest region, Region 1, was approximately 0.9 meters thick and consists of three sets of low-angle, cross-laminated sand. The laminae were two to four millimeters thick, alternating between bands of lower-coarse and lower-fine sands. Region 1 was overlain by a 0.4 meter area of coarse sand interbedded with thinly laminated fine sand (Region 2). The uppermost unit, Region 3, consisted of coarse trough-cross laminated sand filling a small scour (0.2 meters) and graded upward into bedded coarse and medium sand (0.1 meters). The average thickness of the regions bound by first and second-order surfaces was approximately 0.2 meters.

One hundred twenty-eight measurements were obtained on SS2 from 130 sample locations. One non-measurement was due to a calcite nodule, the other to a hole in the outcrop. Results of the statistical analysis are presented in **Table 5.2**.

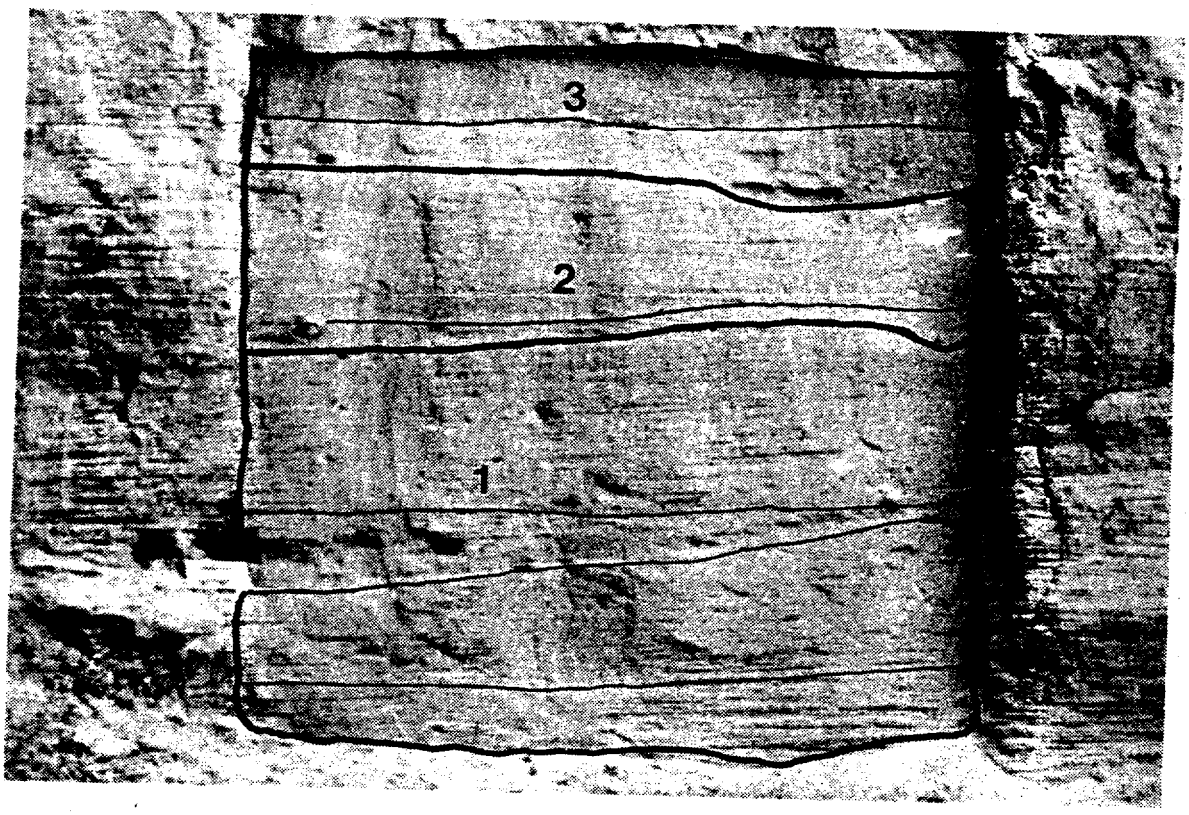

0 20cm

Figure 5.5. Photograph of SS2 outcrop. Numerically labeled regions separated by second-order bounding surfaces correspond to those described in the text.

Table 5.2 . Statistics of SS2 and sub-regions.

		Population	Statistics	Population	Comparison
Data set	N	μ [ln(k)]	σ^2[ln(k)]	Region 2	Region 3
SS2 (all)	128	3.00	0.16	--	--
Region 1	76	3.05	0.21	not equal	"equal"
Region 2	21	2.78	0.04	--	not equal
Region 3	31	3.03	0.09	not equal	--

The directional variograms of the SS2 log-permeability data (Figure 5.4 c-f) are fit with an anisotropic exponential model. The fitted model is anisotropic not only in the correlation lengths but also the sill. In the horizontal direction the variogram estimate attains a sill value of approximately 0.13 with a correlation length of 10 centimeters. The vertical variogram attains a sill of approximately 0.16 with a correlation length of eight centimeters. The statistical anisotropy observed in SS2 approximates a statistically stratified media with perfect correlation in the horizontal direction and finite correlation in the vertical direction.

As in the SS1 variogram estimates, the correlation appears stronger in the horizontal than the vertical and is consistent with the observed stratified nature of the deposits. For SS2, the ratio of the average thickness of the mapped regions to the effective range of the vertical variogram is 1.2.

SS5

The third small-scale study in the CH-2 element (SS5) was located slightly above and to the southeast of SS1. The prepared outcrop is approximately 1.2 meters high and 3.4 meters wide. The outcrop is relatively homogenous and consists predominantly of medium and fine grained sands with low-angle to planar cross-bedding throughout the outcrop (**Figure 5.6**). The deposits of SS5 differ from those of SS1 and SS2 in that there are many lateral truncations in bedding and discontinuous clay drapes. The contacts are generally discontinuous and of zeroth and first-order but were not mapped.

SS5 yielded 192 air-permeameability measurements from 198 sample locations. Non-measurements were due to the presence of insect holes in the outcrop. The mean and variance of the natural-logarithm transformed permeability (k) are 2.69 and 0.23, respectively.

The directional variogram estimates concur with the general observation that SS5 exhibits more lateral variability than SS1 and SS2. The horizontal variogram is fit with a nested exponential-bell-shaped model. The exponential component is adopted primarily for consistency with the other two small-scale studies in similar materials. The bell-shaped component is added to account for the linear behavior at larger lags. The nugget of the horizontal variogram model is 0.03 and the correlation lengths for the exponential and "bell-shaped" models are 8 and 200 centimeters, respectively. The vertical variogram is fit with an exponential model with a nugget of 0.03, a correlation length of eight centimeters and a sill equal to the estimated population variance of 0.23.

While the contacts were not mapped and the average dimensions of the regions cannot be directly compared to the variogram model, it is interesting to compare the variograms of SS5 to the other small-scale studies performed in the same channel element. First, the vertical variogram is very similar to those of SS1 and SS2 as it attains a sill equal to the population variance and exhibits a correlation of eight centimeters. The horizontal variogram, on the other hand, behaves differently than those of SS1 and SS2. An increasing variance is observed for all lags estimated in the SS5 study whereas the horizontal variograms of both SS1 and SS2 exhibited a single simple sill. Recall that SS5 was located sub-perpendicular to the inferred paleoflow direction. Geologically, it is reasonable that the correlation structure in the horizontal direction transverse to paleoflow will exhibit a more complex correlation structure.

Summary of CH-2 studies

In the SS1 and SS2 studies six regions were separated by second-order bounding surfaces. In only two cases the means were found to be "equal" and in just one case the regions with "equal" means were adjacent to one another. This indicates that, even in very

homogeneous appearing deposits, the bounding surface classification may be a good indicator of the spatial distributions of regions exhibiting different mean log-permeability. The variogram estimates all followed an exponential model for short lags. This exponential behavior is interpreted as corresponding to the abrupt changes encountered when strata were crossed.

The vertical variogram estimates from SS1 and SS2, the ratio of the average thickness of regions separated by first and second-order contacts to the effective range of the vertical variograms is 0.66 and 1.2, respectively. In SS5, the dimensions cannot readily be compared to the variogram model parameters but the vertical variogram exhibits the same correlation length as SS1 and SS2 and the horizontal variogram exhibits more variability over longer ranges.

In addition, the qualitative observations on the degree of variability and the horizontal stratification correspond to the character of the variogram estimates of log-permeability. **Table 5.3** summarizes the population statistics of the three studies and clearly shows that the most "homogeneous" appearing deposits exhibit the lowest variance. In addition, the horizontal variograms of the studies that were roughly parallel to paleoflow (SS1 and SS2) attain a sill within their respective sampling domains and the horizontal variogram of the study roughly perpendicular to paleoflow (SS5) does not reach an apparent sill.

Table 5.3. Summary of statistics for small-scale studies in the CH-II element. Permeability values in ln(k) [darcy].

	SS1	SS2	SS5
N	142	128	192
mean	2.96	3.00	2.69
variance	0.21	0.16	0.23

Ps Element

SS4 & SS6

SS4 and SS6 were located approximately 70 meters apart, across the same arroyo that separates SS5 from SS1 and SS2. The SS4 and SS6 study areas were located in a single sandy, orange-red paleosol element that lacks sedimentary structures in both locations. Grain size is very fine throughout both study areas. SS4 is 1.5 meters high and 2.4 meters wide. Calcite nodules ranging from 5 to 30 centimeters in diameter are scattered throughout the central portion of the outcrop (**Figure 5.7**). SS6 is approximately 0.7 meters high and 1.1 meters wide. Broad areas of weak calcic horizons were present throughout this exposure, and there were fewer calcite nodules (**Figure 5.8**). As noted earlier, the sampling strategies in the two studies differed. SS4 followed the unbiased stratified random approach and SS6 sampling was conducted along horizontal transects that were juxtaposed according to ease of sampling.

Whereas fluvial processes and the resulting bounding surfaces appear to control the heterogeneity in the CH-2 element, the heterogeneity within the soils likely results from pedogenic processes. The primary pedogenic processes influencing the spatial variability of permeability are bioturbation, the translocation of clay material, and precipitation of calcium carbonate. Bioturbation churns the original deposit thus destroying much of the original sedimentary structure. The physical and chemical alteration of parent material, colloid migration, and carbonate precipitation should result in a more spatially continuous processes than the abrupt changes observed in the channel deposits that resulted from erosion and deposition along distinct boundaries.

Two hundred and sixteen sample locations were identified in SS4, of which 213 air-permeameter measurements were obtained. Two of the non-measurements were due to the presence of calcite nodules, the third fell on a fracture in the outcrop. The fracture was interpreted to be a result of surface exposure. One hundred and three air-permeameter measurements were obtained in SS6 from 104 sampling locations. The non-measurement was due to calcite.

Statistics of the log-transformed data are summarized in **Table 5.4**. The

Figure 5.7. Photograph of SS4 outcrop.

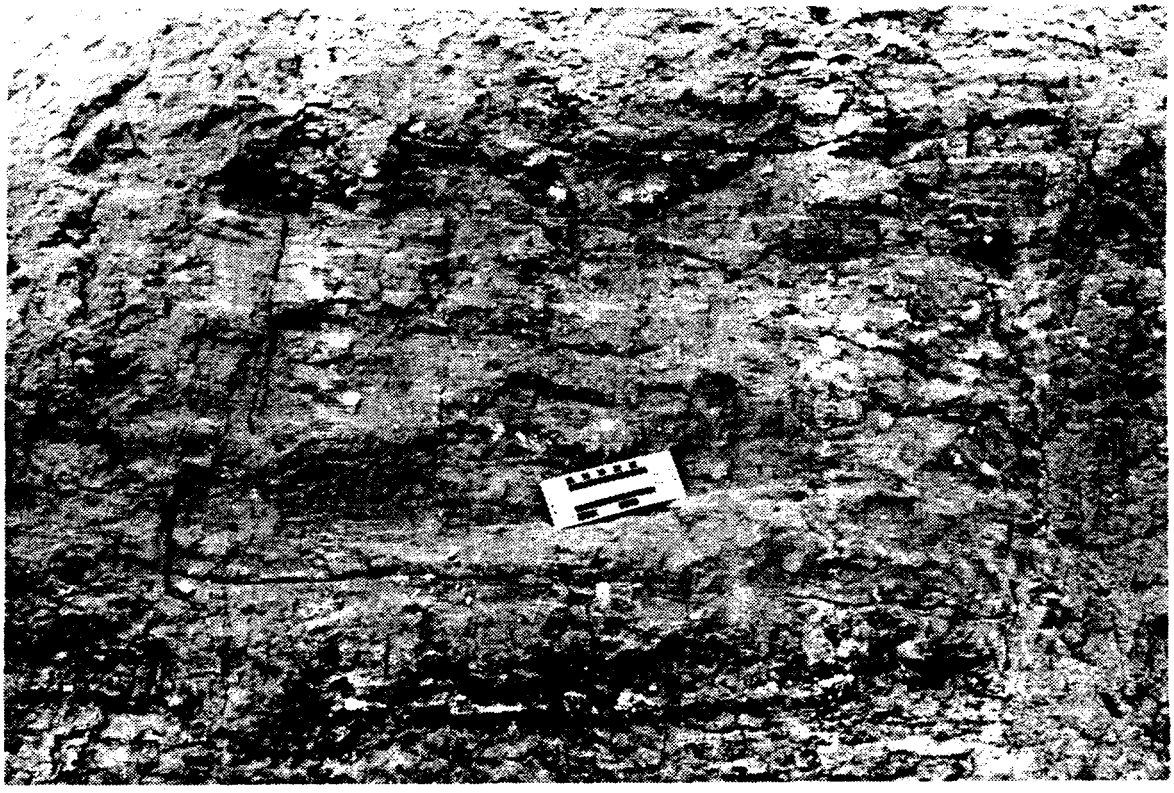

Figure 5.8. Photograph of SS6 outcrop.

Kolomogorov-Smirnov test was applied to compare the empirical cumulative distributions to the theoretical normal. The results indicate that the SS4 and SS6 data are log-normally distributed. In addition, we cannot reject the null hypothesis in comparing the empirical distributions of SS4 and SS6 with one another at the 5% significance level.

Table 5.4. Summary of statistics of Ps studies. Permeability values in ln(k) [darcy].

	SS4	SS6
N	216	134
mean	1.94	1.91
variance	0.12	0.25

Directional variogram estimates of the SS4 and SS6 studies are presented in **Figure 5.9**. Both the horizontal and vertical SS4 variograms are fit with a bell-shaped variogram model. SS4 is fit with an isotropic model with a nugget of 0.03, a sill of 0.10, and correlation length of 10 centimeters. For the SS6 directional variograms, a significant difference is observed between the variogram of the two data sets. This is interpreted as resulting from the biased sampling of the original data that tended to avoid regions that were difficult (low permeability) to sample. From the results of SS6 it is difficult to fit a variogram and one the data is presented without a model.

From a geological perspective the paleosols originate from spatially continuous processes that obscure the original abrupt changes in fabric. These processes are manifested in the paleosols as absence of bounding surfaces and an appearance of continuous variation. This spatial continuity is supported by the "bell-shaped" behavior of the variogram estimates.

The small-scale studies of heterogeneity at the Bosque provide insight into the relationship between observed sedimentological features and variogram behavior. First, the shape of the variograms differs between the deposits. This difference appears to correspond to the presence or absence of bounding surfaces. For the deposits that result from fluvial processes and exhibit geological discontinuities in the form of bounding surfaces, an

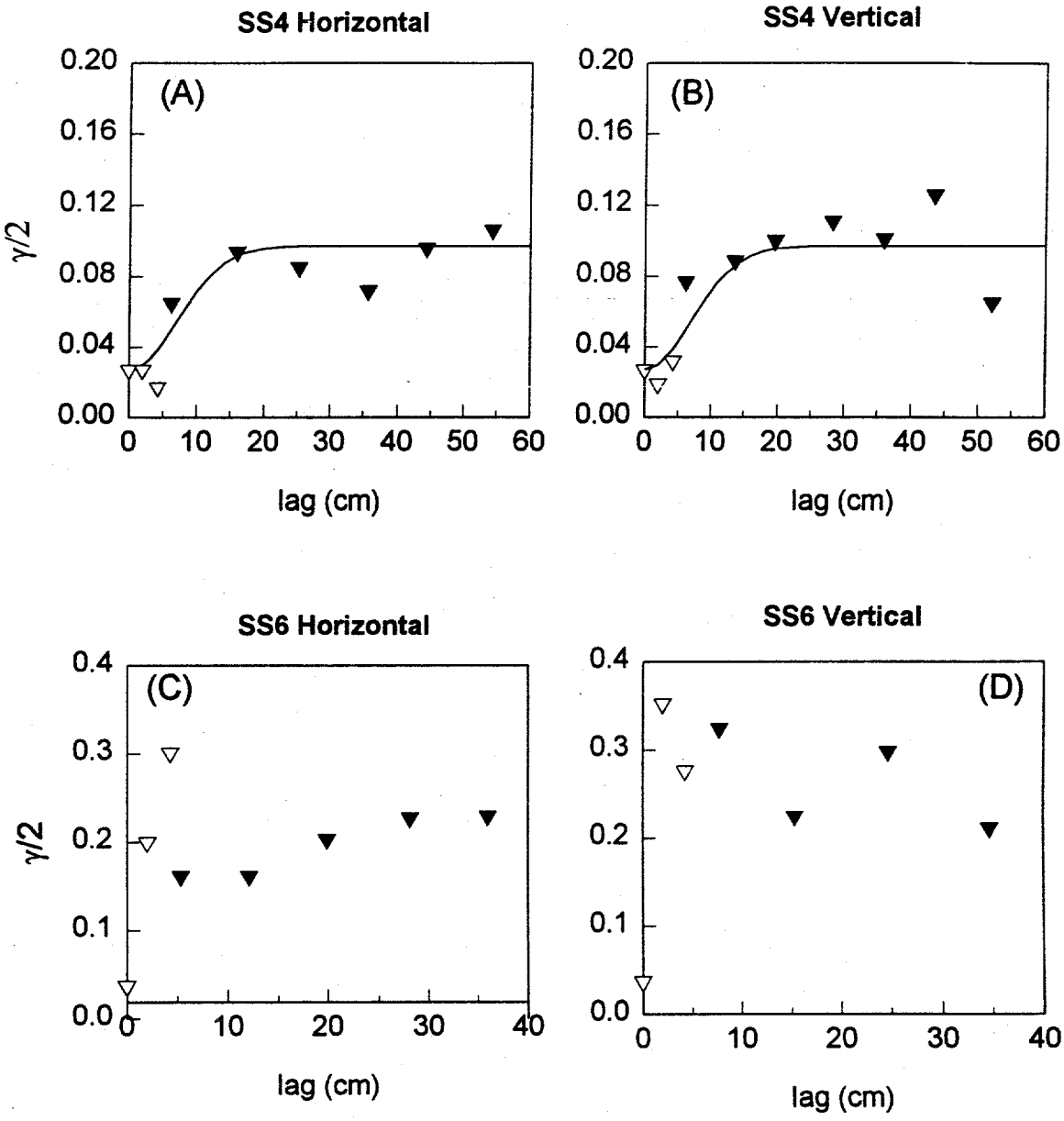

Figure 5.9. Directional variograms of the Ps element studies, SS4 and SS6

exponential model fits the variogram. On the other hand, the deposits formed by pedogenesis lack bounding surfaces and a more continuous "bell-shaped" model fits the variogram estimate.

Escondida Study (ES-1)

The objective of the Escondida small-scale study was to investigate the relationship between the fluvial bounding surfaces and the correlation structure at a site where dense sampling could be performed across several distinct bounding surfaces. The outcrop of the ES1 study area, located northeast of Escondida, New Mexico, was interpreted as deposits of the ancestral Rio Grande. The outcrop was chosen due to the distinct changes in geologic material (**Figure 5.10**).

The study involved a vertical transect 180 centimeters in length which crossed four second-order surfaces, nine first-order surfaces and two zeroth-order surfaces, as shown in **Figure 5.11**. Five regions were defined by the second-order surfaces. The uppermost 50 centimeters, Region 1, encompassed seven first-order surfaces. The sand was of fine to medium grain size with coarse lag deposits at the base of some of the first-order boundaries. Region 2 is 42 centimeters thick and contained one zeroth-order and one first-order boundary. Grain size within this region varies from coarse to pebbly sands. This is followed by Region 3, which is 56 centimeters thick and contained one first-order surface. Grain size is similar to that found in Region 2. The next 27 centimeters of the transect, Region 4, contained a single zeroth-order contact. Grain size here ranged from fine to medium sand. Region 6 consisted of the bottom five centimeters of the study area, where grain size ranged from medium to coarse sand.

Seventy-five permeability measurements were taken at a variable spacing ranging from 1.5 to 6 centimeters. Statistics of the natural-log transformed peremeability data of ES1 are shown in **Table 5.5** . The null hypothesis that the natural log-transformed data are normally distributed is rejected at the 5% significance level.

Results of the Kolomogorov-Smirnov test comparing the distributions of the regions are summarized in **Table 5.6**, indicating that Regions 1 and 4 and Regions 2 and 3 have

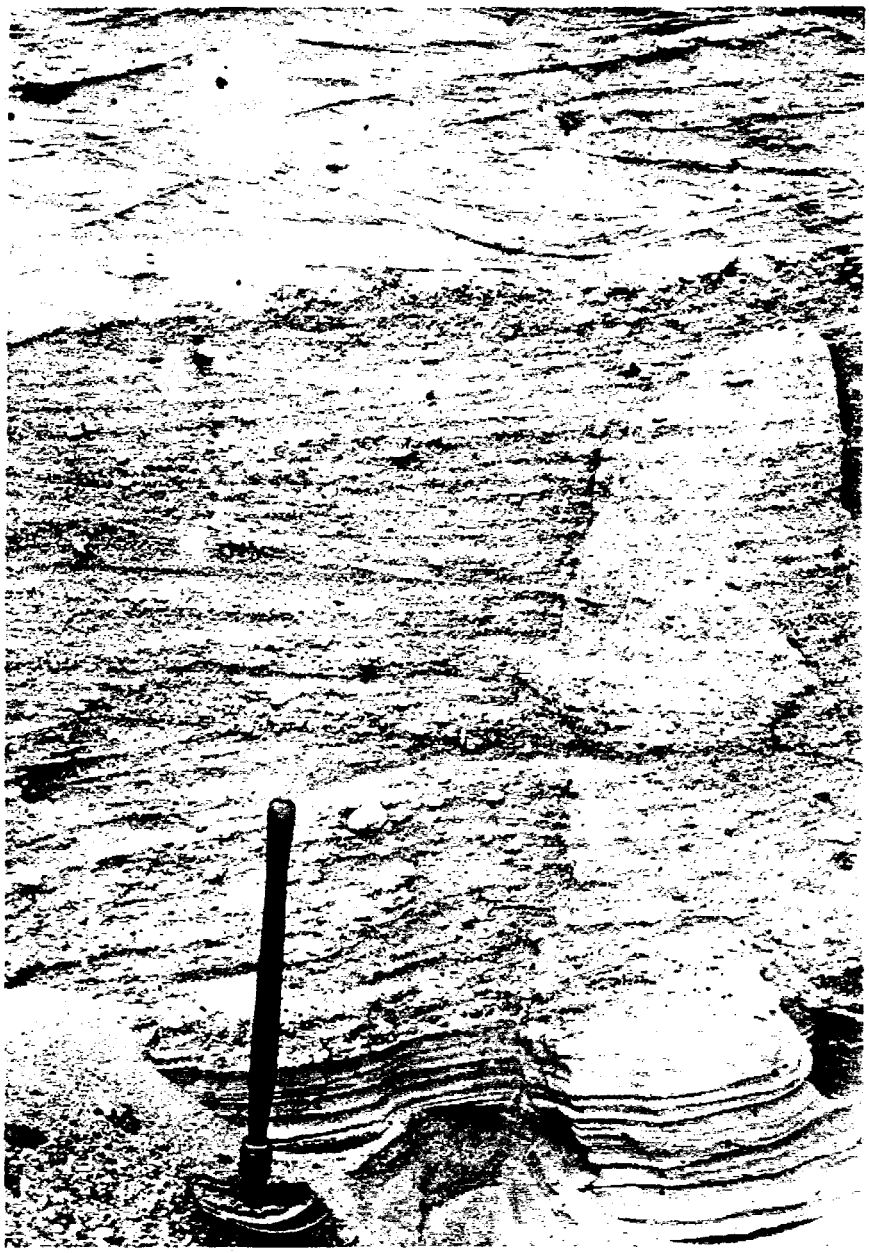

Figure 5.10. Photograph of ES1 outcrop. Shovel handle is approximately 40 centimeters long.

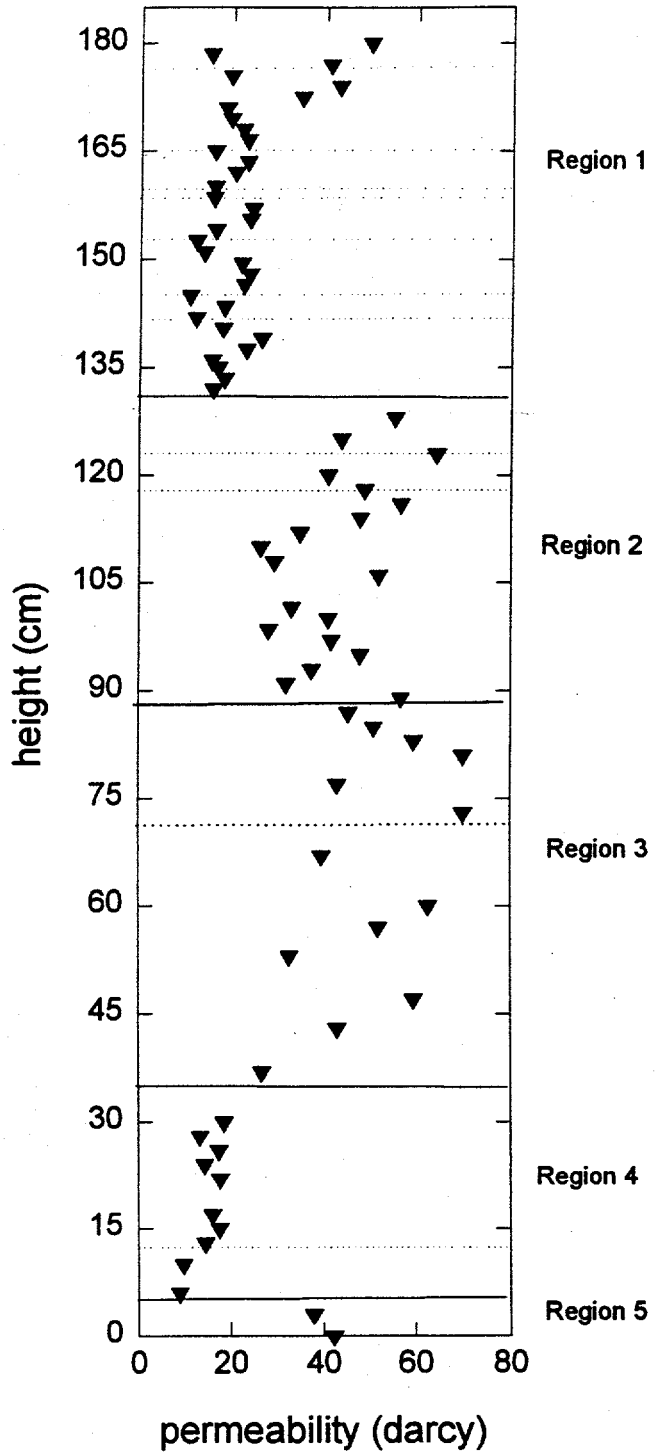

Figure 5.11. Plot of permeability along vertical transect, ES1. Dashed lines represent zeroth and first order surfaces. Solid lines represent second order surfaces.

similar distributions. Region 5 was too small to consider in this analysis. Figure 5.10 is a plot of permeability as a function of location on the transect and reflects the findings of the Kolomogorov-Smirnov test in that second-order boundaries tend to separate areas of differing mean permeability.

Table 5.5. Statistics of ES1 and ES1 sub-regions.

	ES1	Region 1	Region 2	Region 3	Region 4	Region 5
n	75	33	19	11	10	2
mean	3.28	3.01	3.73	3.82	2.67	3.69
variance	0.27	0.12	0.07	0.07	0.06	0.01

Table 5.6. Comparisons of distributions within ES1. D_{crit} is the difference between the two distributions necessary to reject the null hypothesis and D_{max} is the observed difference.

Regions	D_{crit}	D_{max}	Result
1 and 2	0.39	0.84	not equal
1 and 3	0.44	0.85	not equal
1 and 4	0.49	0.45	"equal"
2 and 3	0.49	0.25	"equal"
2 and 4	0.53	1.00	not equal
3 and 4	0.57	1.00	not equal

Variogram estimates were performed within regions bound by second-order surfaces and showed weak correlation. The variogram estimate of the entire ES1 data set is shown in **Figure 5.12**. The variogram exhibits distinct linear segments. This was interpreted as resulting from the distinct regions of different permeability observed in the transect. In addition, there appear to be different magnitudes of variability associated with the hierarchy of the bounding surfaces. That is, the change in permeability associated with first- order surfaces appears to be less than the variability associated with the second-order surfaces. This type of variation is similar to that proposed by Burrough (1983b).

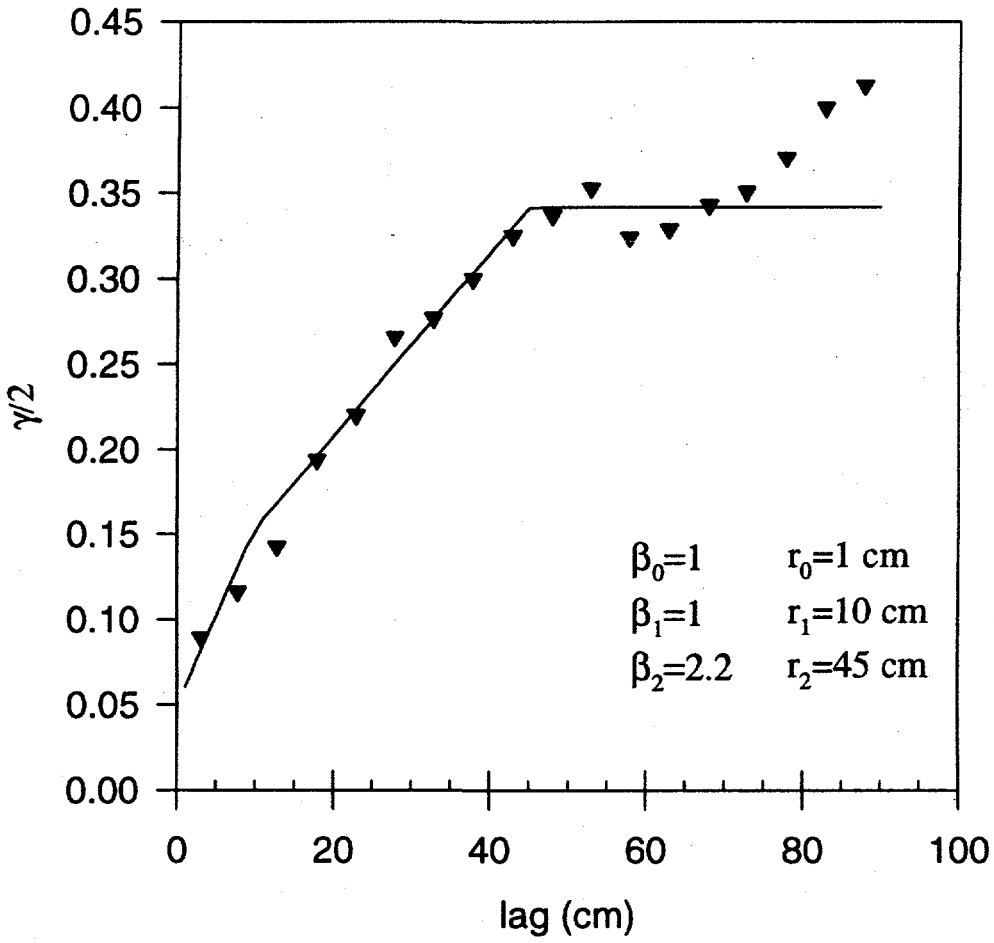

Figure 5.12. Fitted nested model to ES1 variogram estimate.

Burrough (1983b) proposed that variations in soil transects could be conceptualized as resulting from various superimposed random processes acting over multiple scales. For example, in soil science there is variability associated with parent material that may vary over intervals of kilometers. Superimposed on the variation of parent material is the variability associated with drainage patterns that may vary over intervals of hundreds of meters. Vegetation patterns may influence soil variability over scales of meters, and so on. In the conceptual model of Burrough, the large-scale variation is represented by a single mean value that persists over the length of variation (referred to as the range) then assumes another independent mean value. The result of superimposing several scales of these processes is a variogram with linear segments. The variogram model is:

$$\gamma(h) = \sigma^2 \left[\sum_{i=0}^{q} \frac{\beta_i^2 h}{r_i}\right] \qquad \frac{h}{r_i}=1 \quad \text{when} \quad h \geq r_i$$

Where: q= number of processes
σ^2=variance of the process acting of the smallest range
β=weight of the individual processes
h= lag
r=range of the individual processes

This model is adopted for the analysis of the ES1 data set. For the ES1 study, an underlying random process was assumed to represent the nugget. This process was assigned a weight, β_o, of one and a range, r_o, of one. The first and second-order bounding surfaces represent the next two processes. The range for each was estimated from the mean thicknesses of the regions separated by the bounding surface of the hierarchy. For the first process, representing the first-order bounding surfaces, the average thickness is 10 centimeters. For the next process, representing the second-order bounding surfaces, the average thickness is 45 centimeters.

The model was fit to the variogram estimate by adjusting the weights. The result is presented in Figure 5.12. In spite of the fact that the model assumes constant dimensions for

each process in the hierarchy and the processes observed (bounding surfaces) exhibit variable dimensions, the model provides a good fit to the variogram estimate. The two most important implications of this exercise are first, that the variability associated with the second-order surfaces is the largest contributor to the overall variance and, second, the average dimensions of the regions bound by second-order surfaces provide a good estimate of the variogram range.

DISCUSSION

The probability distributions of the small-scale studies are summarized in **Figure 5.13**. The groups according to geologic origin indicate similar distributions for each group and different distributions between groups. The variogram parameters for the fitted models are also summarized in **Table 5.7**. Certain attributes of the variogram can also be related to the geologic origin of the deposits. Permeability within the sandy channel deposits exhibits anisotropic exponential correlation structure with the maximum correlation length in the horizontal direction. Permeability within the sandy paleosol element exhibits "bell-shaped" correlation and in one case is fit with an isotropic model. The most heterogeneous deposit, ES1, exhibits nested linear correlation structure that differs from that observed in the other types of deposits.

Table 5.7. Summary of variogram models and parameters used to fit the small-scale studies. γ_o is the nugget, λ is the correlation length, and σ_s^2 is the sill.

		Horiz. Variogram			Vert. Variogram		
Data	Variogram Model	γ_o	λ	σ_s^2	γ_o	λ	σ_s^2
SS1	Exponential	0.02	16	0.18	0.02	8	0.18
SS2	Exponential	0.02	10	0.11	0.02	8	0.16
SS5	Nested exp., bell	0.03	8; 200	0.23	0.03	8	0.23
SS4	Bell-shaped	0.03	10	0.10	0.03	10	0.10
SS6	Bell-shaped	n/a	n/a	n/a	n/a	n/a	n/a
ES1	Nested linear	n/a	n/a	n/a	0.06	1; 10; 45	0.34

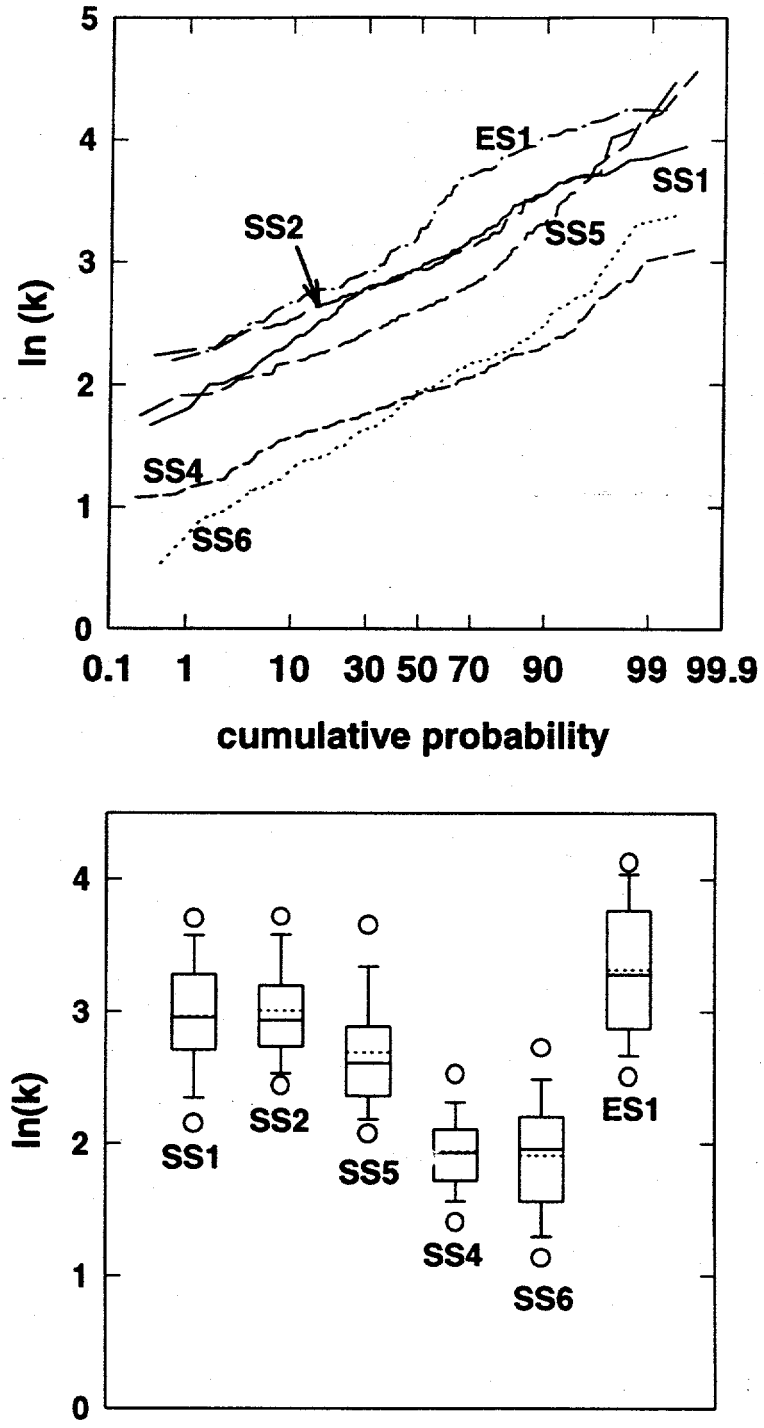

Figure 5.13. Probability plots and box plots of the data sets.

The results of these studies can also be discussed in the more general context of relating sedimentological models with geostatistical models. First, bounding surfaces tend to separate regions with different mean permeability. There were enough cases that supported this to warrant considering it as a model of the spatial variation and similarly, there were enough exceptions to this to indicate that the tendency requires further study and quantification. One hypotheses in statistical terms is: "The probability that a bounding surfaces separates regions with different permeability is associated with the hierarchical class of the bounding surface."

In addition, the behavior of the variogram appears to coincide with the magnitude of the variation across the bounding surfaces. In the paleosols, no bounding surfaces were observed as they were destroyed by pedogenic processes and the variogram estimate appeared "bell-shaped" indicating a smoothly continuous spatial process. In the channel studies, the differences in permeability across the bounding surfaces were statistically significant but small, and the bounding surfaces defined regions of variable thickness. The observed exponential behavior of the variogram estimates can be interpreted as resulting from an equally weighted process acting over non-constant ranges. Finally, the results of the ES1 study, that was undertaken because of the observed contrast in materials separated by the bounding surfaces, indicate that the marked contrast observed resulted in distinct breaks in the correlation structure.

The main implication of these findings is that hierarchical bounding surfaces may provide a link between sedimentological models and geostatistical models of heterogeneity. In the following chapters the theme of bounding surfaces as they relate to geostatistical models is investigated further through studies of architectural elements at the same field site and then two supplementary studies in alluvial fan and eolian deposits.

Another model of interest is the threshold-crossing model of Phillips and Wilson (1989). This model represents the spatial variation of a property as a single continuously varying process with an inherent correlation structure. Phillips and Wilson (1989) demonstrated that for a "bell-shaped" correlation structure, the correlation length can be estimated from the average dimensions of contiguous regions exceeding some threshold of the probability

distribution. They presented the relationship between the average dimensions of the regions of excursion above or below the mean value. **Table 5.8** extends the relationship to two additional threshold values located one and two standard deviations away from the mean.

As was discussed, the correlation structure in the paleosol studies exhibits a "bell-shaped" behavior, and is interpreted as more continuous in space than the undisturbed sedimentary deposits. It is then instructive to assess the threshold crossing approach for

Table 5.8. Ratio of the average dimensions ($E(l_b)_i$) of regions exceeding a threshold (b) in the estimating the correlation length (λ_i) in the direction, *i*th direction. $G^c(b)$ is the complimentary cumulative probability of the standardized variable, Z, at the threshold, b. See Phillips and Wilson (1989)

Threshold (b)	Z : $G^c(b)$	$E(l_b)_i / \lambda_i$
μ	0 : 0.5000	$\sqrt{2\pi}$
$\mu+\sigma$	1 : 0.1587	2.325
$\mu+2\sigma$	2 : 0.0228	1.497

estimating the variogram parameters. There are insufficient data to accurately define a threshold value of permeability associated with the presence of observable proxy. However, for SS4 an estimate can be made of a threshold value associated with the carbonate nodules. The permeability of the calcite nodules is below the detection of the LSAMP (< 0.5 darcy). The average size of the observable calcite deposits is approximately 10 centimeters. If these regions are used as the proxy for the threshold two standard deviations below the mean, the corresponding correlation length (Table 5.1) is approximately 6.7 centimeters. This matches very well the seven centimeter correlation length used to fit the variogram model.

This same strategy does not work as well for SS6 where the carbonate nodules are much smaller (two centimeters in diameter) and the range of the variogram estimate appears much larger. This problem could also arise from the poor estimate of the correlation structure due to the biased sampling or it could illustrate one of the fundamental problems of the threshold crossing approach. Namely, the estimate is very sensitive to the threshold value and if the

variability appears sufficiently continuous to assume a Gaussian random field with a bell-shaped covariance, then an abrupt, distinctly discernable boundary of the region of excursion may not exist. Unfortunately when regions of excursion are mappable, they are usually associated with discrete boundaries and the presence of discrete boundaries inhibits the application of theory based on spatially continuous processes.

CONCLUSIONS

Results of the small-scale studies of heterogeneity in the three different types of deposits indicate that the permeability probability distribution and the overall behavior of the correlation structure differs between the types of deposits. The paleosols exhibit the lowest mean log-permeability and the smoothest spatial process. The low-energy channel element exhibits a higher mean log-permeability and a spatial distribution with abrupt interfaces resulting in an exponential variogram. The high-energy channel deposits exhibits the highest mean log-permeability and the abrupt spatial changes in permeability result in a nested linear correlation structure.

The bounding surface classification appears to provide insight into the correlation structure of the different types of deposits and may prove a link between sedimentological models and geostatistical models of heterogeneity. Larger-scale two and three-dimensional studies would allow further testing and refinement of the bounding surface-correlation model.

CHAPTER 6: ARCHITECTURAL-ELEMENT SCALE HETEROGENEITY[4]

INTRODUCTION

Effective use of sedimentological studies for the characterization of heterogeneity requires a framework of analysis that possesses both geological and hydrogeological significance. In Chapter 5, results of the facies-scale study suggest that first and second-order bounding surfaces may provide insight into geostatistically modeling heterogeneity. In this chapter, third and fourth-order bounding surfaces are investigated at the larger spatial scale. These higher-order bounding surfaces separate the architectural elements described in Chapter 4.

Several workers (e.g. Phillips et al., 1989; Anderson 1991a) have suggested architectural element analysis as an appropriate sedimentological framework for fluvial deposits. An architectural element is "a lithosome characterized by its geometry, facies composition and scale [that] represents a particular process or suite of processes occurring within a depositional system" (Miall, 1988). The geological significance of architectural elements is well documented (Miall, 1985; Miall, 1988).

Architectural elements are attractive from a hydrogeological perspective because they provide a means of studying fluvial deposits at scales of meters to kilometers. Architectural element external geometries define large-scale hydrogeological trends and, as a suite of genetically related lithofacies, they may be the most suitable geological units for the analysis of hydrogeological effective properties. Outcrop studies of geology and permeability provide the most comprehensive source of two- and three-dimensional information on hydrogeological heterogeneity (Goggin et al. 1988a, Chandler et al., 1989; Dreyer et al., 1990; Kittridge et al., 1989).

The objective of the architectural element study of heterogeneity was to develop a better understanding of how information about larger scale depositional processes can be used to quantify hydrogeological heterogeneity. The outcrop of the Pliocene-Pleistocene Sierra

---

[4]Davis, J.M., R.C. Lohmann, F.M. Phillips, J.L. Wilson, and D.W. Love, 1993, Architecture of the Sierra Ladrones Formation, central New Mexico: Depositional controls on the permeability correlation structure, Geol. Soc. Amer. Bull, v. 105, p. 988-1007.

Ladrones Formation provided the site for this study.

Three main steps of analysis were employed. First, a general understanding of the depositional environment was developed by reviewing previous studies in the area. The second step was to characterize mean air-permeability within architectural elements and map the elements over a 0.16 km^2 peninsular section of the outcrop. Third, the statistical properties of the element-scale heterogeneity were related to the depositional processes by geostatistical analysis of the architectural element map and air-permeability data.

SITE GEOLOGY

The Albuquerque Basin is located in the central portion of New Mexico (inset of Figure 4.1). Structurally, the Albuquerque Basin is one of several en echelon basins resulting from extension of the Rio Grande Rift. The Sierra Ladrones Formation (Pliocene-Pleistocene) records the later stages of basin infilling with alluvial fan and fluvial sediments.

Basin filling ceased by mid-Pleistocene time (Lozinsky et al., 1991) and the Rio Grande and its tributaries began to entrench. This entrenchment left a large portion of the upper basin fill isolated from deposition or erosion creating the Llano de Albuquerque, a broad low-gradient geomorphic surface. Subsequent incision of the Rio Puerco and Rio Grande dissected the Llano de Albuquerque forming the extensive Ceja del Rio Puerco and Cejita Blanca escarpments.

Results of previous studies of the upper Sierra Ladrones Formation exposed within the Ceja del Rio Puerco and the Cejita Blanca suggest that during the late Pliocene to early-Pleistocene, the positions of the Rio Grande and its tributaries (Rio San Jose and Rio Puerco) were similar to their current configuration. Figure 4.2 summarizes the drainage system which Lozinsky et al. (1991) hypothesize deposited the upper Sierra Ladrones Formation. From the hypothetical drainage configuration of Figure 6.2, it is possible to infer the orientation and distribution of ancestral Rio Grande system deposits in the vicinity of the field site (Figure 4.8).

The field site for this study is located along the east-facing Cejita Blanca, just west of

Bosque, New Mexico (Figures 4.1 and 4.2). The portion of the escarpment chosen for study extends eastward as a peninsula from the north-south trending Cejita Blanca. The outcrop studied is approximately 20 meters high and covers 0.16 km^2. The slopes on the outcrop are at the angle of repose or steeper. Overbank clays and paleosols as well as some cemented lenses of gravels and sands lend structural stability to the outcrop. The majority of the sediments however are uncemented. Slope wash is present in some locations as a thin veneer, generally less than 10 centimeters thick, and can be removed easily with a trowel or small shovel.

In a previous study, Davis et al. (1991) defined architectural elements (Miall, 1985) at the field site from a facies study of a 50 meter wide by 20 meter high outcrop. This earlier work identified four main types of elements: two types of channel elements, an overbank fine element, and a paleosol element (Table 6.1). Miall (1985) includes the paleosol facies in the overbank fine element. Davis et al. (1991) treats paleosols as a distinct architectural element. Allen (1974) demonstrated the utility of paleosols in terms of studying the depositional environment of an alluvial sequence. In addition, the permeability of the sandy paleosols is much greater than the overbank clays and silt. Since the objective of this study is to relate depositional processes to hydrogeological heterogeneity, it is preferable to treat paleosols separately from overbank clays and silts.

METHODS

Empirical characterization of the geological heterogeneity observed in outcrop involved detailed mapping of architectural elements, quantitative measurements of permeability, and geostatistical analysis of the combined data.

Mapping

Mapping of the architectural elements described in this chapter corresponds to Phase I of the mapping described in Chapter 2. Traditional surveying techniques were employed to maintain adequate control on the spatial locations of architectural elements and permeability

measurements. A topographic base map of the area was prepared by surveying approximately one thousand points on the outcrop from twenty-two survey stations encompassing the peninsular escarpment. About three-fourths of the survey locations corresponded to architectural element contacts while the remaining one-fourth corresponded to topographically important features. The surveyed architectural element contacts were superimposed on the base topographic map. Mapping was completed by measuring numerous vertical sections up the outcrop with a five-foot Jacob staff and tracing units laterally between the vertical sections.

Air-Permeability

Air-permeability measurements were also made along the outcrop in order to obtain quantitative hydrogeological information. An air-minipermeameter developed for this study enables rapid, in-situ, and non-destructive sampling of air-permeability. The air-minipermeameter principle follows that of Goggin et al. (1988b), in which a constant pressure is applied to a prepared surface via flexible tubing attached to a tip seal. However, our device uses lower pressure, different design principles, and is more portable (Chapter 3). The permeability is calculated from Darcy's law using the applied pressure, measured flow rate, and geometry of the tip seal.

Calibration of the air-minipermeameter was conducted on laboratory fabricated standards. Permeability measurements obtained with the air-minipermeameter were compared with measurements obtained using the same tip-seal (i.e. flow geometry) but utilizing a continuous air source and directly measuring the applied pressure and flow rate. Thirty-three measurements of the different materials ranging from 0.5 to 250 darcy were made with the two devices. The correlation (r^2=0.99) between the two measurement techniques was excellent.

Geostatistical Analysis

Univariate statistical analysis of the air-permeability measurements within architectural elements was performed to estimate the mean permeability for each element. The mean permeability values for each element were then used in conjunction with the architectural element map data for geostatistical analysis. The purpose of the geostatistical analysis is to quantify the hydrogeological heterogeneity by estimating the statistical correlation structure of log-permeability, specifically to examine the spatial variability in log-permeability that results from the structure of the architectural elements. While permeability within architectural elements does vary spatially and analysis of the within-element variability is a subject of continuing investigation, in this study the individual architectural elements are represented by a single mean value.

A dense grid of test points (one point every meter in the x and the y directions) was overlain on the architectural element map. The (x,y) coordinates of the test points as well as the coordinates of digitized polygons defining the areal distribution of architectural elements were then introduced into a computer program (Lohmann, 1992) to determine within which element (represented as a polygon) each test point lay. The programs TRIMAKE and TRIMAT (Macedonio and Pareshci, 1991) were used to estimate the elevation (z) of each horizontal data point. TRIMAKE constructs triangles from the irregularly spaced digitized topographic contour data. Then the triangulation data is used in TRIMAT to estimate elevations on the rectangular test point grid yielding an (x, y, z) value for each point. A mean log-permeability value was then assigned to each test point according to element type (Table 6.1). The resulting data set consists of 54,402 records of three-dimensional location, each with an assigned mean log(k).

Three additional indicator data sets were constructed for the elements CH-II, OF, and P. The indicator data sets consist of the locations and assigned values of ones and zeros depending on the presence or absence of the element of interest. For example, in the CH-II indicator data set, the value of one is assigned to locations where the CH-II element is present and zero where one of the other elements is present. Indicator data sets are valuable in

assessing how the various external geometries of the elements contribute to the overall correlation structure. The spatial correlation structure is summarized by the experimental variogram, and is fundamental to a variety of geostatistical models (see Journel and Huijbregts, 1978; Isaaks and Srivastava, 1989; Cressie, 1991; Cristakos, 1992). Variograms of the four data sets were estimated with GAMV3 (Deutsch and Journel, 1992). GAMV3 allows the user to specify the direction of the search window, angle and distance tolerances, and horizontal and vertical bandwidths. Variogram analysis of the data set was performed in six equally-spaced horizontal directions and the vertical direction. Six directional horizontal variograms were separated by 30 degrees. Horizontal and vertical angle tolerances were 15 and 20 degrees, respectively. To obtain pairings as true to horizontal as possible, a vertical bandwidth was set at 0.5 meters. In the vertical direction, due to the sloping topography, a cone-shaped search window with a 50 degree vertical angle tolerance was employed. A 50 degree vertical angle tolerance results in the pairing of points whose spatial separations vary from the true vertical displacement to 1.55 times the true vertical displacement. The large variability in separations for a given lag hinders the ability to assess the true vertical correlation structure. Since the elements exhibit a large aspect ratio, the vertical correlation structure is analyzed in terms of absolute vertical distances. GAMV3 was modified to record the absolute vertical displacement as the separation lag. Essentially, this is equivalent to a horizontal extrapolation of the architectural elements of a few meters.

RESULTS AND DISCUSSION

Architectural Element Type Descriptions

The four principal architectural elements delineated (Table 6.1) are: 1) high-energy channel element (CH-I); low-energy channel element (CH-II); overbank-fine element (OF); and paleosol element (P). The CH-I elements are dominated by coarse sand and gravel, are generally between 1 and 3 meters thick and pinchout abruptly. The CH-II elements are characterized by very fine to medium sand with locally abundant clay drapes (0.5 to 1.5

centimeters thick). Clay drapes interbedded with very fine sand and laminated clay and silt are common towards the top of these elements. The CH-II elements range in thickness from 0.5 to 9 meters. The overbank-fine elements (OF) are composed of dark brown clay locally interbedded with tan silt and thin immature sand and clay paleosols. Interbeds of immature paleosols are common higher in the section. The OF elements range from one to seven meters thick. The paleosol element is divided into two sub-element classes based on whether the parent material is dominantly sand or clay. The elements Ps and Pgs are the result of pedogenesis of sand and gravelly-sand parent material, respectively. The most common paleosol element is Ps and consists of moderately to well-sorted, very-fine to fine sand. Due to the distinct hydrogeological properties of the clays and silts, paleosols with overbank fine parent material are mapped separately as element Pc. The architectural elements are defined and described in greater detail in Lohmann (1992) and in Chapter 4.

The empirical cumulative probability distribution of log-permeability measured in the elements CH-I, CH-II, and P are presented in **Figure 6.1**. In general, log-permeability approximates normal distributions. However, measurements obtained in the CH-II elements exhibit a pronounced tail of high log-permeability. Conversely, measurements obtained in the Paleosol elements lack high-and-low extreme values. As indicated by the figure, and verified by a Student t-test, log-permeability in these three elements exhibit different means (Table 6.1). Sufficient samples were not collected for analysis of full population statistics of the low-permeability OF element. However, measurements of two independent samples of the OF material were conducted in the lab using a triaxial cell apparatus and a falling head apparatus. Both methods on both samples yielded permeability values on the order of 10^{-6} darcys. Table 6.1 also summarizes the population statistics for log-permeability measured in the architectural elements.

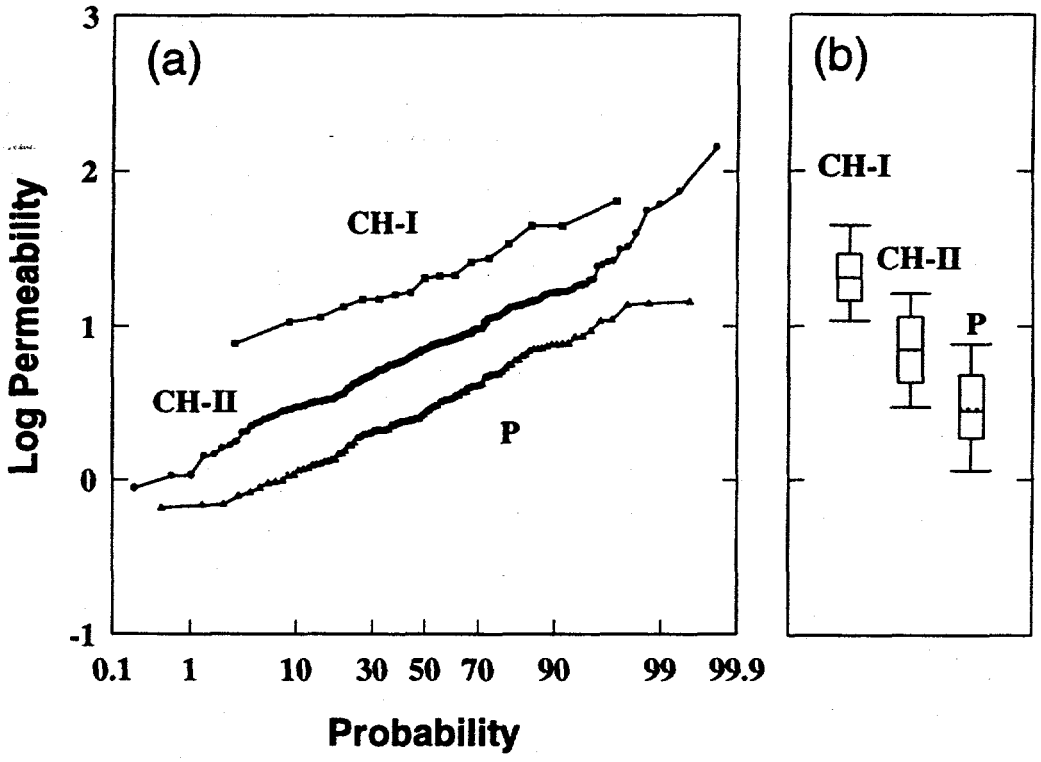

Figure 6.1. (a) Empirical cumulative probability plot of architectural element log-permeability data; (b) Box plots of log permeability data. Boxes represent the 25th and 75th percentiles. Bars extend to the 5th and 95th percentiles. Horizontal lines correspond to the means.

Table 6.1. Summary of lithologic facies groupings and log-permeability statistics for architectural elements.

Element	Facies Present	Description Comments	Log(k) mean	Log(k) stand dev	N	Student t
CH-I	Massive gravel (Gm) Trough cross-bedded gravel (Gt) Planar laminated sand (Sp) Trough cross-bedded sand (St) Low angle cross-bedded sand (Sl) Massive sand and gravel (Sgm)	Channel element is dominantly gravelly and coarse sand facies.	1.32	0.24	17	6.06
CH-2	Gms, St, Sp, Sl, Horizontally laminated sand (Sh) Fining upward v. fine to coarse sand (Sfl) Fine to medium sand with mud balls (Smb) Finely laminated sand, silt and clay (Fl) Clay and silt, massive, desiccated (Fm) Laminated silt, sand, and clay (Fsc)	Sand dominates with rare sand size clay clasts and gravel lag.	0.84	0.32	245	10.9
P	Paleosol, fine to pebbly sand, massive, carbonate stringers and nodules (P) Massive sand, immature paleosol (Sm) Fsc	Soils and stacked soils	0.44	0.32	110	n/a
OF	Silt, clay with rootlets (Fr) Fm, Fsc, P	Overbank fines	-6	n/a	2	

Architectural Element Map

The architectural element map (**Figure 6.2**) was prepared by a combination of extensive surveying and traditional geological mapping. Details of the geometries of the elements are not readily apparent on the architectural element map due to the map scale and the relatively steep topography. An analysis of the three dimensional character of the deposits was aided by construction of cross sections (**Figure 6.3**) along the principal faces. The cross sections represent a projection of mapped elements onto the planes shown on the architectural element map. Since the scale of the elements greatly exceeds the projection distances, this method provides an accurate means of studying the geometry of the elements in a series of two-dimensional maps.

Analysis of the cross sections (Figure 6.3) shows that the architectural elements at the field site exhibit a large degree of lateral continuity with occasional scours by the sand and gravel elements into the underlying units. Two axes of deposition are apparent from the cross sections and the Architectural Element Map. First, the orientation of sand scours estimated by

NEXT PAGE

Figure 6.2. Architectural Element Map.

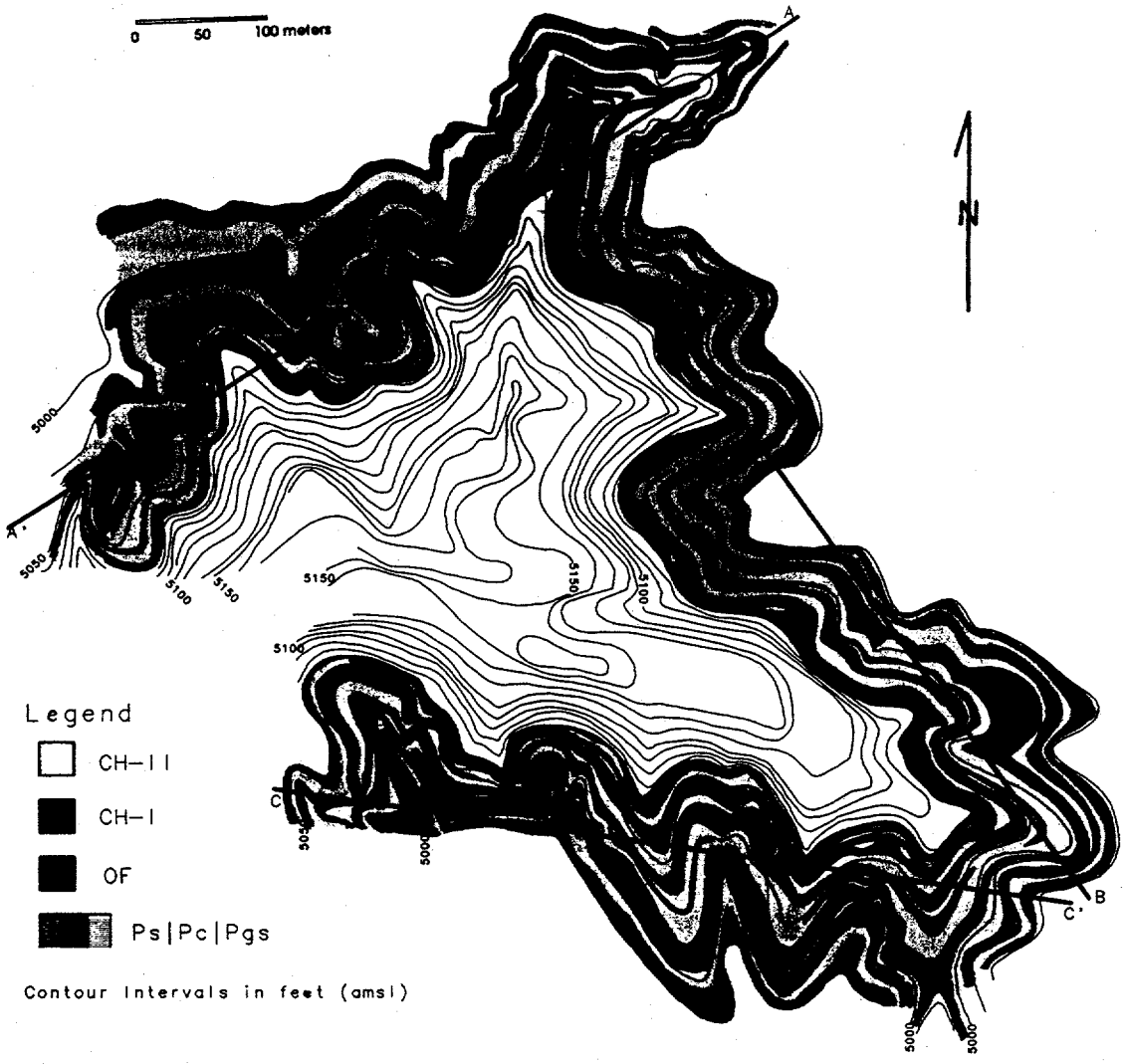
0 50 100 meters
A
B
C
A'
B'
C'
N
5000
5050
5100
5150
Legend
CH-II
CH-I
OF
Ps|Pc|Pgs
Contour Intervals in feet (amsl)

NEXT PAGE

Figure 6.3. Cross-sectional views of Architectural Element Map: (a) Cross Section A-A'; (b) Cross Section B-B'; (c) Cross Section C-C'. Cross-section locations shown on Figure 6.2.

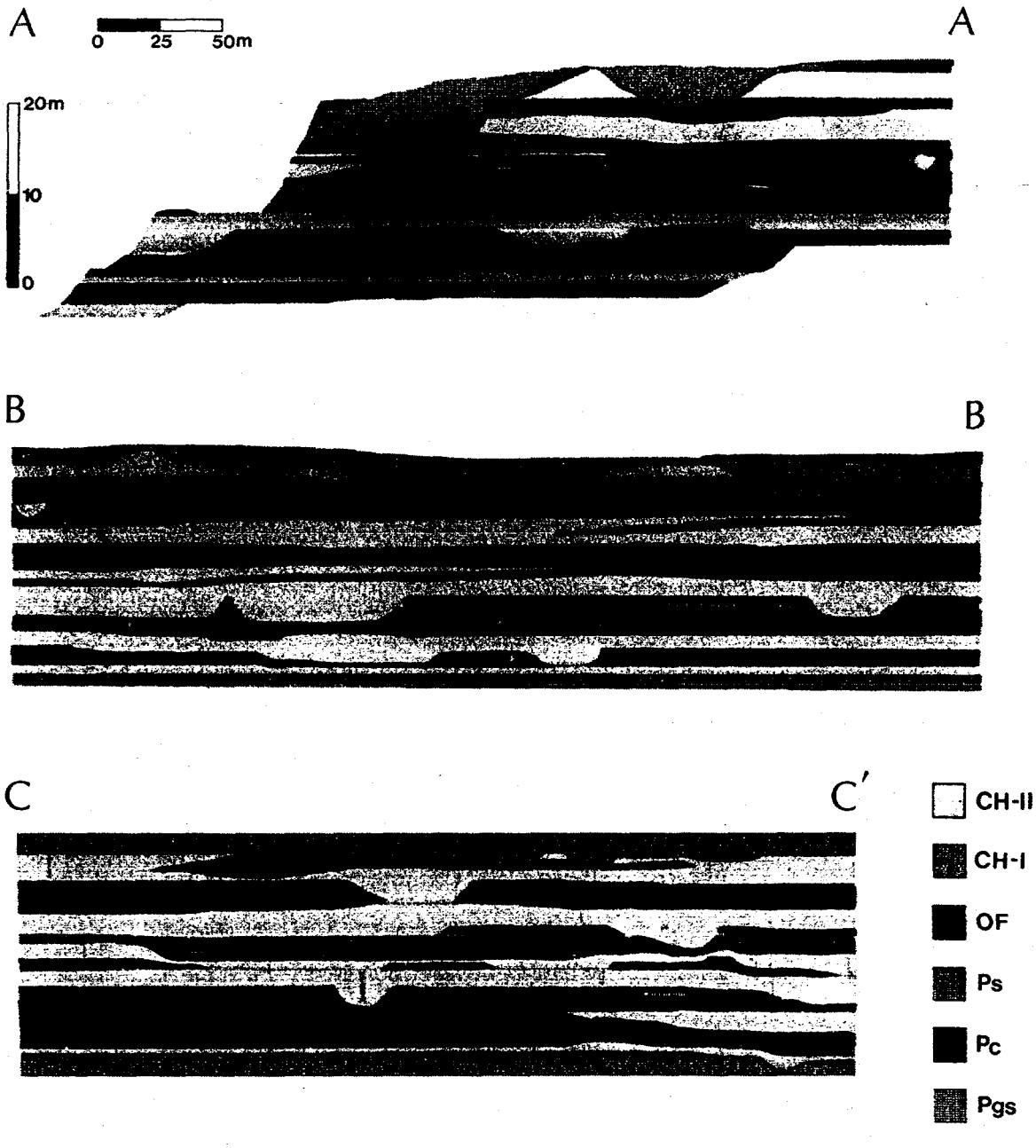
A
0 25 50m
A
20m
10
0
B
B
C
C′
CH-II
CH-I
OF
Ps
Pc
Pgs

correlating sand scours across the field site ranges from S10W to S70E, with an average flow direction of S30E. The other axis is north-south resulting in westerly pinchouts of CH-II elements. In general, the abundance of laterally continuous sands with occasional scours suggests that during large flood events, the flood waters overtopped the banks and moved across the floodplain in sheetlike flow in some areas, and channelized flow in others.

Geostatistical Analysis

The horizontal variograms of mean log-permeability in the directions N90E and N30W are presented in **Figure 6.4**. The horizontal variogram estimates exhibit a similar exponential behavior for lags up to 50 meters. In the N90E direction (Figure 6.4a), the variogram continues to increase for lags greater than 50 meters, reaching a sill of approximately 9 at lag 65 meters. In the N30W direction, the variogram for lags greater than 50 appears to increase in a linear fashion, not attaining the value of 9 in the 200 meters analyzed. Larger-scale analysis would be necessary to determine if the variogram reaches a constant sill, or continues to increase as expected of a non-stationary process. The directional dependence of the variogram represents statistical anisotropy of the log(k) data set in the horizontal direction.

This statistical anisotropy is better revealed by contouring the variogram estimates for the six different horizontal orientations. In the azimuthal variograms presented in **Figure 6.5**, zero lag is located at the center. The radius from the origin corresponds to the lags in the six different orientations. Since the variogram is symmetric, the six orientations result in twelve rays emanating from the origin separated by 30 degrees.

The correlation structures for the log(k) data set (Figure 6.5a), the CH-II indicator data set (Figure 6.5b), and the OF indicator data set (Figure 6.5c) exhibit non-perpendicular anisotropy. The principal orientations of correlation are N30W and N90E. The correlation structure of the log(k) data set most closely resembles the OF indicator correlation structure resulting from the large relative difference of the OF mean log(k). The correlation in the N30W orientation corresponds to the average direction of the CH-II scours (S30E).

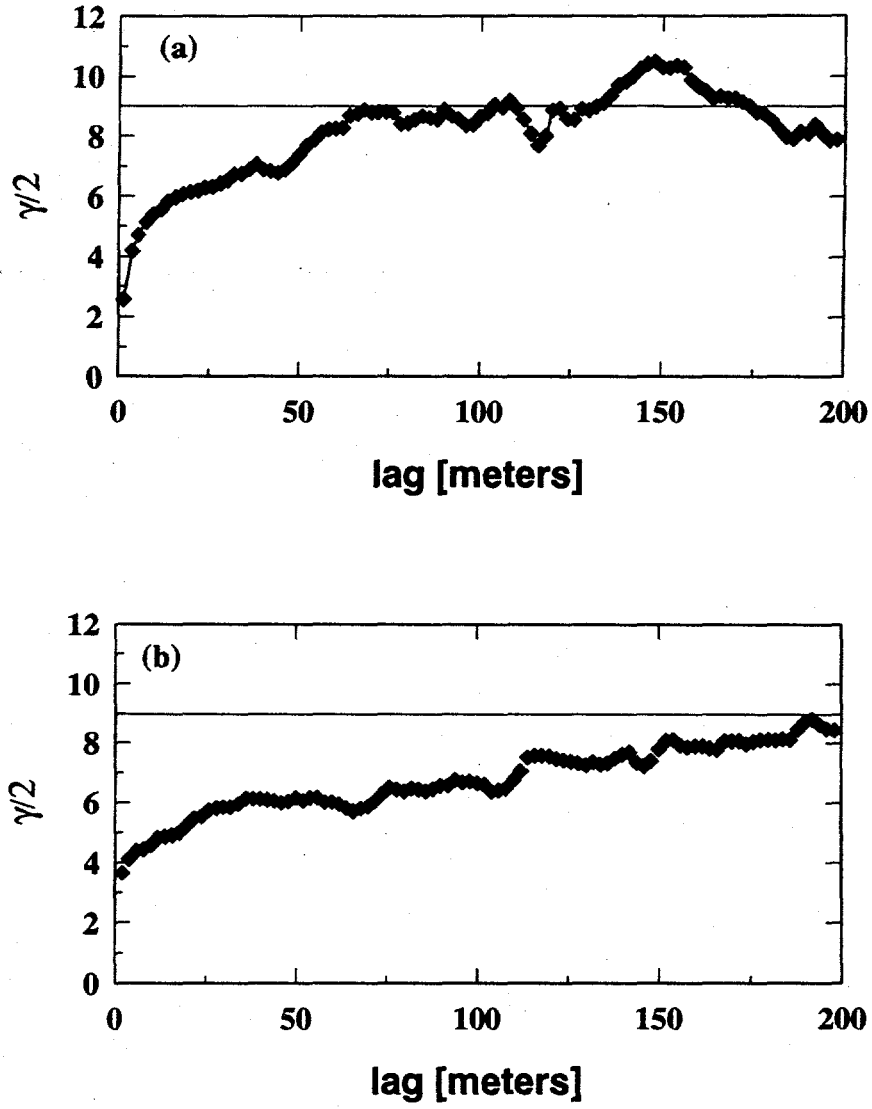

Figure 6.4. Horizontal variograms of the log-permeability data set: (a) N90E; (b) N30W.

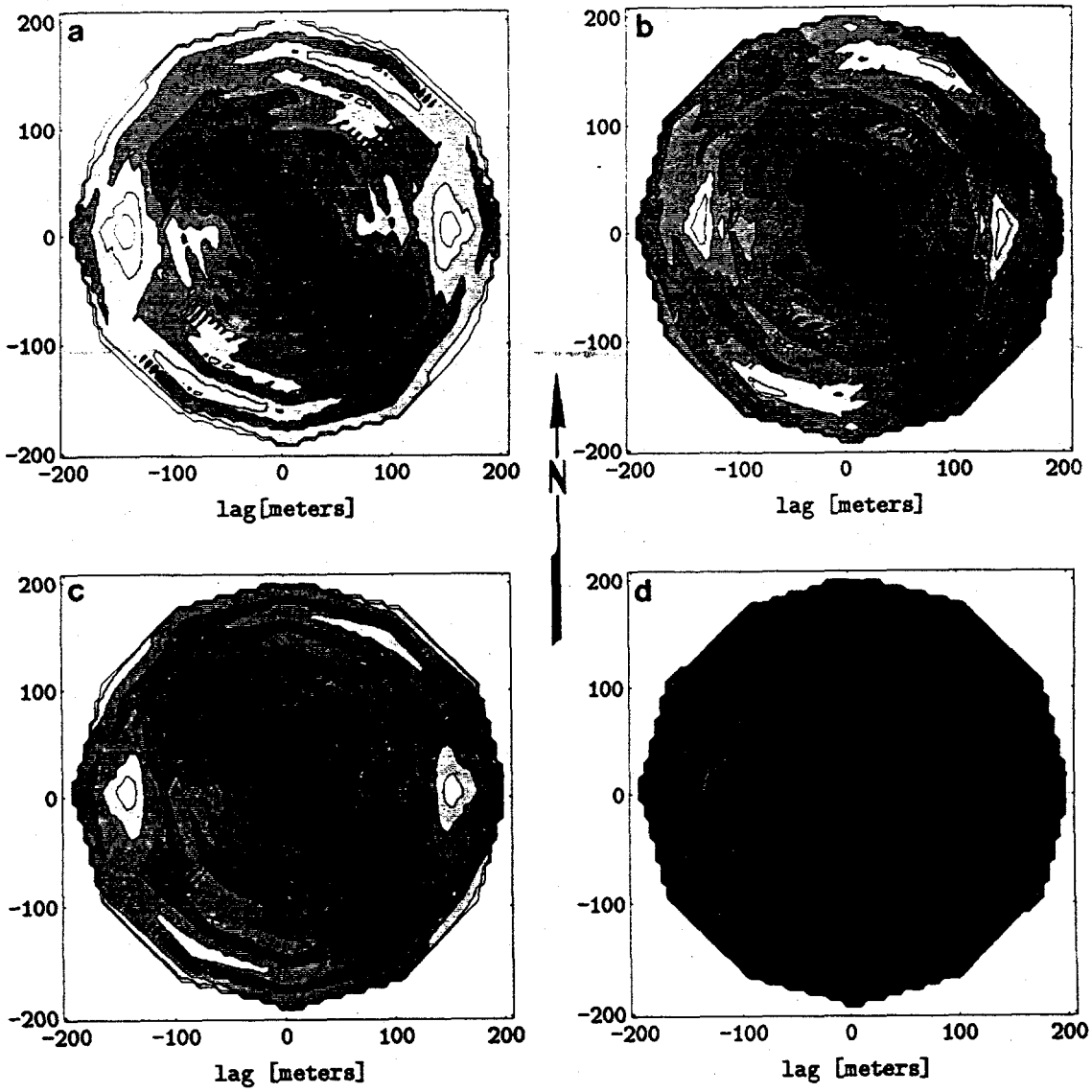

Figure 6.5. Azimuthal horizontal variograms constructed by combining horizontal variogram estimates with orientations N0E, N30E, N60E, N90E, N30W, and N60W. (a) log-permeability data set; (b) CH-II element indicator data set; (c) OF element indicator data set; (d) P element indicator data set. Contour ranges and intervals (range, interval): (a) (0 - 10, 1); (b-d) (0 - 0.25, 0.025).

Significantly less correlation exists in the N90E direction. This is believed to be controlled by the lateral relationship between the CH-II and OF elements. The CH-II element grades laterally into the OF element as the interbedded sands and clays become dominated by clays to the west. This lateral gradation was probably controlled by the transition from the proximal sandy floodplain to the distal mud-dominated floodplain, as illustrated in the block diagram shown in Figure 4.8. The azimuthal variogram for the P (Figure 6.3d) indicator data set differs from the CH-II and OF indicator variograms in two ways. First, the overall variability is lower, and second, anisotropy appears to be orthogonal with strongest correlation in the N0E orientation. The lower overall variability is partly attributed to the proportional effect (Journel and Huijbregts, 1978) in that the P element occupies a smaller volume fraction of the deposits and thus has a lower indicator mean. Also contributing to the lower overall variability is the tabular geometry of the P elements. The N90E orientation of the minimum correlation is consistent with east-west relationship between the zones of overbank deposition and pedogenesis. In the horizontal direction, the correlation structure of the mean log-permeability and the indicator data sets appears to correspond with the configuration of the paleo-drainage system.

The vertical variograms for the four data sets are shown in **Figure 6.6**. The shape of the log(k) variogram is seen to closely mimic the OF element indicator variogram as was the case with the horizontal variograms. Also, the correlation structure is again largely controlled by the external geometry (i.e. thickness) of the elements. The average thicknesses of the OF and P elements are two meters, coinciding with the observed range. Similarly, the CH-II element has an average thickness of three meters and is cyclic on a six meter interval.

The architectural elements defined appear to exhibit different mean log permeabilities indicating that these elements may serve as suitable hydrogeologic units. The specific effective hydrologic properties associated with each element would be a function of the internal structure of lithologic facies. Results from the within-element studies (Chapter 5) indicate that the lower order bounding surfaces associated with cross-bed sets and lithofacies may provide a framework for quantifying the within-element heterogeneity.

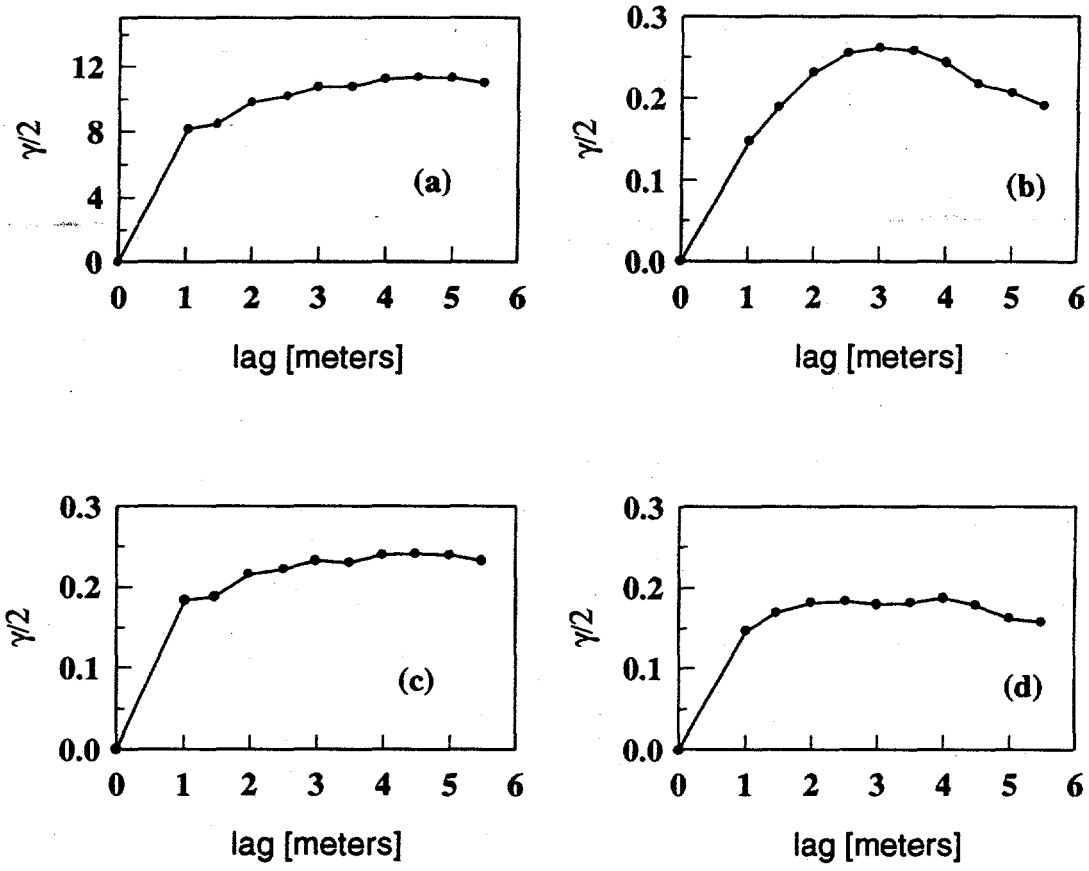

Figure 6.6. Vertical variograms of the log-permeability data set: (a) log-permeability data set; (b) CH-II element indicator data set; (c) OF element indicator data set; (d) P element indicator data set.

In the analysis of the architectural-element scale heterogeneity presented in this chapter, the log-permeability spatial distribution is represented by the spatial distribution of the architectural elements and the mean log-permeabilities of the elements. The geostatistical analyses of this data suggest that the external geometries of the elements may exhibit a significant control on the spatial correlation structures of the log-permeability. While this relationship between deposit geometries and correlation structure has not been previously well documented in studies with abundant geologic control, it is consistent with findings of Johnson and Dreiss (1989) who attributed statistical anisotropy of subsurface soil classification data to elongate paleochannel deposits.

Results of this chapter provide field-based support for the approaches to subsurface characterization proposed by Anderson (1989) and Phillips et al. (1989). Large-scale trends in the heterogeneity are seen to be directly related to the large-scale depositional processes. In addition, the relationship between the element-scale correlation structure and depositional processes appears strong. However, the amount of geologic information necessary to delineate trends depends largely on the understanding of the depositional process-product relationship. Poeter and Gaylord (1991) concluded that in the deposits at the Hanford Site which were dominated by catastrophic flood events, the existing understanding of depositional process-product relationship was not sufficient to predict three-dimensional configuration of deposits.

Overall, results of this study suggest that effective use of information about depositional processes may be used to minimize the data requirements necessary for subsurface characterization of heterogeneity. The results of the statistical analysis of the exhaustive data set obtained in this study appear consistent with the observed and previously documented geology. Specifically, the orientations of the statistical anisotropy appear to correspond to the configuration of the paleo-drainage system, and the variogram ranges in the vertical direction correspond to the average element thicknesses. In the characterization of subsurface heterogeneity where site specific outcrop information is unavailable, the paleo-drainage configuration and average bed thicknesses could be estimated from a variety of sources including local geological investigations, provenance studies, analog outcrop studies, and

borehole data.

CONCLUSIONS

The detailed hydrogeological study of the Sierra Ladrones outcrop demonstrates that architectural element analysis is a useful tool in assessing hydrogeological heterogeneity at scales commonly of interest in aquifer and reservoir problems. Architectural elements deposited by the ancestral Rio Grande system are on the order of one meter thick and are laterally extensive over 100's of meters. There is a good correlation between architectural element type and mean log-permeability.

The external geometry and spatial assemblage of the elements appear to be the dominant control on the element-scale spatial correlation structure. The horizontal variograms estimated from mean log-permeability data exhibit non-orthogonal anisotropy, with the orientation of greatest correlation (N30W) corresponding to the paleoflow direction of the tributary system (S30E). The direction of poorest correlation (N90E) is perpendicular to the paleoflow direction of the ancestral Rio Grande. This direction (N90E) corresponds to the lateral transition of ancestral Rio Grande floodplain deposits from the proximal overbank sands to the most distal paleosols. The vertical variograms appear to be controlled by average element thicknesses.

Results of the small-scale (Chapter 5) and the architectural-element scale study represent a first step in increasing our understanding of how information about depositional processes can aid in characterizing the spatial structure of fluvial/interfluvial deposits. Similar studies in different depositional environments are necessary to better understand how information about depositional processes can be used to quantify aquifer and reservoir heterogeneity. Two similar, but significantly shorter, studies conducted in alluvial fan and eolian deposits are presented in Part IV of this dissertation.

SUMMARY OF SIERRA LADRONES STUDY

The studies of the Sierra Ladrones Formation resulted in an improved understanding of the geology and hydrogeology of the specific field site study and provide a basis for investigating the relationship between sedimentological models and geostatististical models of heterogeneity.

The Sierra Ladrones Formation in the vicinity of the field site is interpreted as resulting from a combination of fluvial and interfluvial depositional processes. The occurrence of the four main architectural element types indicates deposition resulting from a high-energy channel system (CH-I), a lower energy channel and proximal flood plain system (CH-II), a distal flood plain (OF), and a stable interfluvial environment (P). The spatial assemblage of the architectural elements and the orientation of the channel scours indicate that the fluvial system was responding to some large-scale changes of the basin, probably either climate or tectonic variations.

Statistical analysis of permeability within the sandy elements indicates that the architectural elements exhibit different mean log-permeability values. In addition, the mapped lithologic facies also tend to exhibit different mean log-permeability. However, the magnitude of the difference is less and occasionally a difference in the mean log-permeability between two adjacent facies cannot be detected. From a sedimentological viewpoint, this information may be generalized according to the hierarchical bounding surfaces that separate the lithologic facies and architectural elements. That is, the second-order bounding surfaces that separate lithologic facies correspond to boundaries of hydrogeologic regions exhibiting different mean log-permeability. Third and fourth-order bounding surfaces that separate architectural elements correspond to boundaries of larger-scale hydrogeologic regions exhibiting different mean log-permeability. Qualitatively, the magnitude of the difference of means also appears to correlate to the order of the bounding surfaces in the deposits studied.

In addition to defining hydrogeologic regions of different mean log-permeability, results of the geostatistical analysis indicate that the bounding surfaces may also provide a framework for relating geologic information to the permeability correlation structure. In the facies-scale

studies, the behavior of the variogram differed in locations that exhibited different bounding surface characteristics. Namely, the paleosols do not contain internal bounding surfaces and tend to exhibit a fairly smooth spatial variation of log-permeability as indicated by the "bell-shaped" variogram. The fluvial sand deposits do contain internal bounding surfaces and tend to exhibit more short range variability as indicated by the exponential variogram. In the sand and pebble deposits where the bouding surfaces are well defined and mark distinct changes in mean log-permeability, the variogram exhibits a nested linear behavior with the dimension of the nested ranges closely corresponding to the respective average distances between the bounding surfaces.

In the architectural-element scale study, the behavior of the variogram closely corresponds to the inferred depositional environment. Based on a method of assigning mean log-permeability values to the architectural elements, the correlation structure in the horizontal direction exhibited maximum correlation in the N30W direction corresponding to the inferred direction of the ancestral tributary system. The shortest correlation length was in the N90E direction corrsponding to the direction of the transition between proximal and distal floodplain deposition. In the vertical direction correlation lengths were observed on the order of a few meters corresponding with the average thickness of the architectural elements.

In terms of geostatistical modeling, the study of the Sierra Ladrones Formation indicates that models representing the spatial variation of permeability as a log-normal spatially continuous process with one dominant scale of correlation may be inappropriate at the scale of meters to hundreds of meters. Permeability changes by several orders of magnitude over distances of centimeters at architectual element contacts. In addition, the occurence of the four elements exhibiting different mean log-permeability indicates that a multi-modal probability distribution function is more appropriate than the normal distribution. The occurence of the overbank fine element and the sandy channel and paleosol elements certainly warrants a bi-modal model.

In addition to the abrupt spatial changes in permeability and the multi-modal nature of the probability distribution, the correlation structure appears to exhibit multiple scales. The

correlation at the facies-scale studies exhibited a single simple sill in the vertical and, with one exception, horizontal directions. The correlation structure of the mean log-permeability values at the architectural-element scale exhibited a non-orthogonal anisotropy. The desired characteristics of a geostatistical model of the heterogeneity of the Sierra Ladrones formation would exhibit abrupt spatial changes in permeability (discrete model), a multi-modal probability distribution, and a nesting of a finite number of scales corresponding to the dimensions of the lithologic facies and architectural element.

PART IV

OTHER STUDIES

CHAPTER 7: HETEROGENEITY OF ALLUVIAL FAN DEPOSITS[5]

INTRODUCTION

The study of heterogeneity of the Sierra Ladrones Formation (Part III) is supplemented by smaller studies of heterogeneity in deposits of different sedimentary origin. This chapter describes the methodology and results of a study of alluvial fan deposits at the Nevada Test Site (NTS) in conjunction with Reynold's Electrical and Engineering Company (REECo) and Sandia National Laboratory (SNL). The two primary objectives of this study were first to obtain information on the gross geologic features including the location and spatial dimensions of mappable units and second to obtain spatially distributed measurements of permeability for geostatistical analysis.

Geologic mapping and permeability sampling was performed in two existing trenches in the Radioactive Waste Management Site Area 5, NTS (**Figure 7.1**). The geologic mapping for the study of heterogeneity was performed in consultation with Raytheon Services Nevada. The geologic mapping delineated three types of deposits: sheet-flood, debris flow, and channel stream.

In each trench studied (Pits 3 and 4), a portion of one of the trench walls (approximately 50 meters wide by 10 meters high) was the focus of study. For each wall, field observations of the gross hydrogeologic features were mapped on a series of photographs. Measurements of permeability were obtained with a prototype of the LSAMP (Chapter 3) at approximately 250 locations on each of the trench walls studied. The air-minipermeameter used in this study differed in the electronic timing of piston fall. The locations of clusters of permeability measurements were recorded on the photographs. Some locations on the trench walls were not measurable with the air-minipermeameter. For these locations, comments were recorded regarding the nature of the non-measurement (e.g. material too coarse, or not consolidated enough).

---

[5]After Davis, J.M., 1992, Greater confinement disposal heterogeneity study, Nevada Test Site, Area 5, Radioactive Waste Management Site, DOE/NV/10630-26 UC-721, 57p.

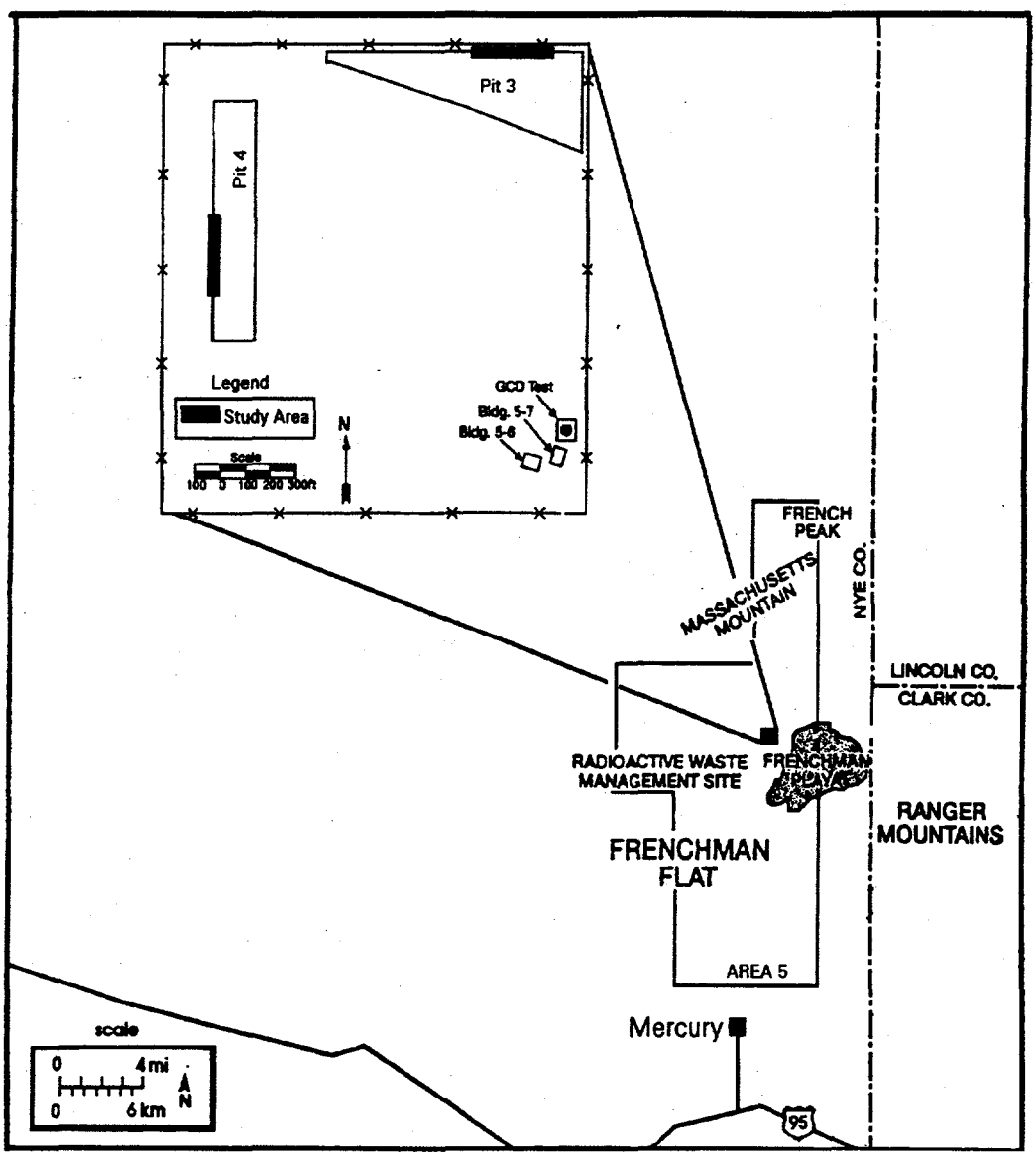

Figure 7.1. Location map of the waste pits and study areas at the Nevada Test Site.

In a subsequent and independent geological investigation of the alluvial fan deposits exposed in the pit walls, Snyder et al. (1993) concluded that the alluvial fan deposits are Quaternary and are characteristic of lower-middle to distal alluvial fan deposits. The mapping performed by Snyder et al. (1993) was on opposite walls of where the heterogeneity studies were performed. While the general classification and gross geologic features mapped by Snyder et al. (1993) were similar to those of the heterogeneity study, a direct comparison of the detailed mapping results and those of original study is not possible at present since the two studies were conducted on different walls of the trenches.

Both the original and subsequent geologic studies are used in the analysis of permeability data. The original hydrogeologic classification is used to test the hypothesis of different mean permeability in the sheet flood and debris flow deposits. The subsequent and more detailed geologic data is used to test two methods of estimating correlation structure based solely on soft geologic information. The first method follows the method employed in Chapter 6 where mean permeabilities are assigned to different lithologic units, a tight sampling grid is overlain on the digitized geologic map, and the variogram is estimated. The second method is the threshold crossing theory proposed by Phillips and Wilson (1989) where the average dimensions of contiguous regions exceeding some threshold of the probability distribution can be used to estimate the correlation length.

METHODS

One of the constraints of this study was the use of photo-mosaics for determining locations on the outcrop. A methodology was developed to correct for the distortion of scale resulting from photos taken at an oblique angle to the outcrop. A methodology was also developed for the unbiased sampling of air-permeability at a variety of spatial scales. The methods developed for this study are directly applicable to studies of similar nature.

Photogrammetric transformation

For any study involving the spatial distribution of properties (in this case permeability and

geology), a mapping technique is required. The technique used here is a crude form of photogrammetry. Photographs of the pit wall were provided as base maps. The photographs are 20 x 25 centimeter (8 x 10 inch) color prints each covering approximately 10-12 horizontal meters of the pit walls. Sufficient overlap was provided so that the photos could be combined into a photo-mosaic of the entire study area.

The photographs on which the mapping was performed were taken from the bottom of the pits looking up at the wall. The result of the oblique angle of projection is a distortion in scale from the top of the photographs to the bottom. When the photos are placed together, a significant concavity results. That is, the photo-mosaic of a largely rectangular region approximates a section of an annular ring. Given that the photographs were the only economical means of locating control points and geologic contacts and the distortion was too significant to be neglected, it was necessary to transform the data digitized from the photo-mosaics into a new set of coordinates. Photogrammetric approaches were considered, however not enough information regarding camera lens characteristics and projection of the photographs were available.

A transformation was developed to correct for the photographic distortion. The goal of the transformation was to map each point of the annular ring onto an associated rectangular region. The conformal mapping technique of complex analysis provides us with such a transformation (Spiegel, 1964). The complex natural logarithm is defined as:

$$w = \ln(r) + i\theta$$

Using this identity, any point in the z plane ($z=x+iy$) can be mapped into the w plane by converting the x and y coordinates into cylindrical coordinates according to:

$$r = \sqrt{x^2+y^2} \qquad \theta = \tan^{-1}\frac{y}{x}$$

Each point in the annulus of the ring is defined according to cylindrical coordinates. Then using the complex natural logarithm, the points are transformed into a rectangular region.

Conceptually, each radius of the annulus corresponds to an elevation on the outcrop and each vertical transect is represented by an angle. Thus the conformal mapping translates the cylindrical coordinates of the photo-mosaic to the rectangular coordinates desired. The transformation is summarized in **Figure 7.2**.

In practice, the transformation was performed as follows. First, the photo-mosaic was aligned on a digitizing table so that the tangent of the bottom of the mosaic was coincident with the horizontal axis of the digitizing table. The origin was placed at the bottom center of the photo-mosaic so that points to the left of center were in Quadrant II and points to the right of center were in Quadrant I. All points had positive y-coordinates. The points of interest were then digitized from the photo-mosaics in rectangular coordinates with units of centimeters. In order to apply the transformation, the locations of the digitized points were converted to cylindrical coordinates and translated downward so that the region occupied an annular ring centered at the origin. The constant of translation in the y direction was equal to the radius of curvature of the photo-mosaic. In principle, the radius of curvature can be obtained given two points on the ring (a and b) and the arclength between them, L, from the equation:

$$L = R\left[\sin^{-1}\left(\frac{b}{|R|}\right) - \sin^{-1}\left(\frac{a}{|R|}\right)\right]$$

The radius of curvature, R, can be solved for numerically given two horizontal locations, a and b, on the photograph and the arclength, L. However, it was difficult to obtain accurate measurements of the arclength. In addition, it was found that the transformation is very sensitive to the radius of curvature and a graphical method of trial and error was preferred. In the trial and error method, the corners of the overlay grid were digitized and were used as the basis for estimating the transform parameters.

Figure 7.3b presents the best fit rectangular grid to the original Pit 3 overlay grid corner data (**Figure 7.3a**). Certain imperfections are apparent in the transformed grid that result from a combination of several factors. The most important factor is that the transform is only an approximate transform as it is not based on principles of photogrammetry but rather

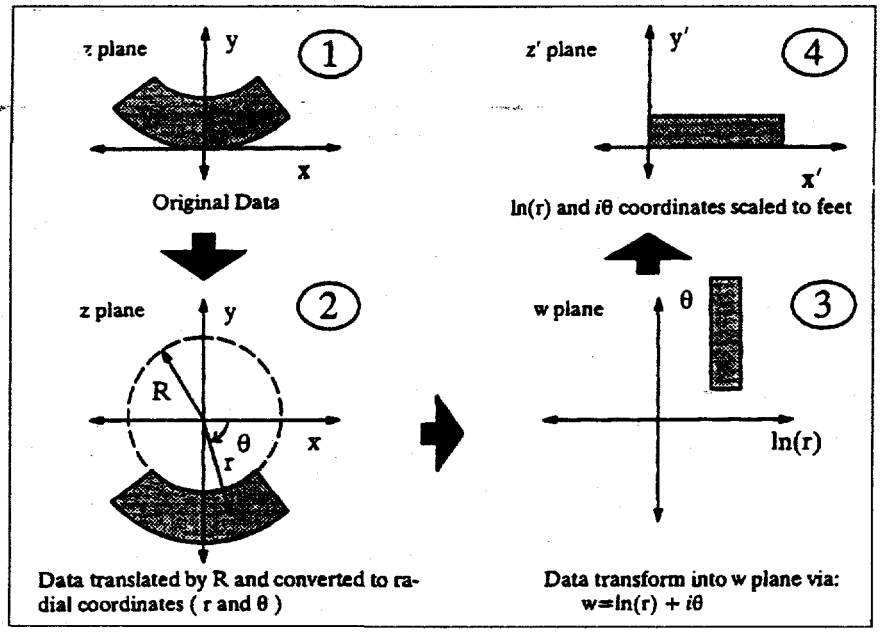

Figure 7.2. Schematic illustration of transformation used to obtain locations from photomosaics. Sequence of operations is counterclockwise.

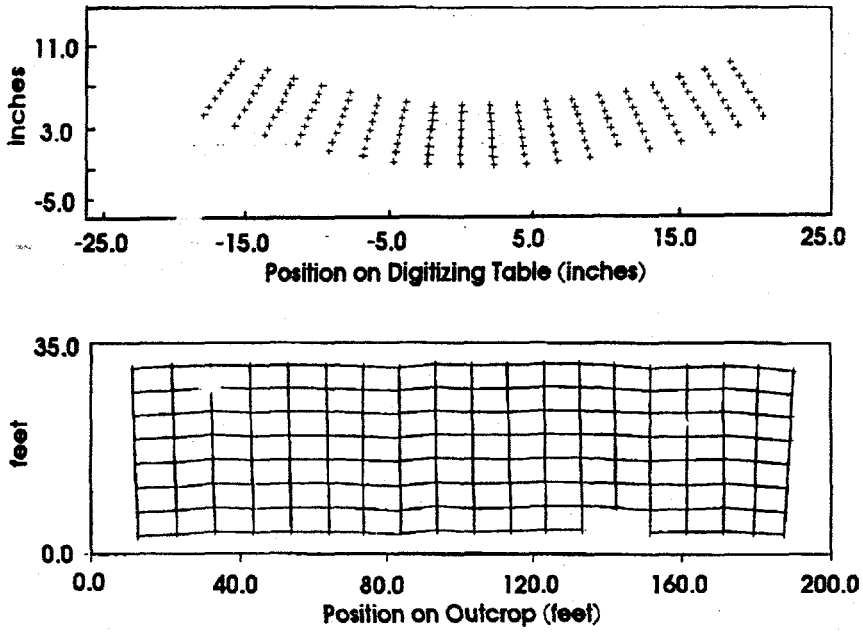

Figure 7.3. (a) Original grid corners of photo-mosaic, Pit 3. (b) Best fit transformed grid.

on the appearance of the photo-mosaics and the appearance of the actual outcrop. Another reason for the slight deviations of the transformed grid to that of a true grid result from the way the grid was prepared on the photographs. The grids on the photograph were established by measuring from the top of the photograph down in 1.22 meter increments but a variable scales. For example, the scale of the photographs of Pit 3 was 0.62 meters per centimeter at the top of the photos and 0.54 meters per centimeter at the bottom of the photos, a vertical scale gradient of 0.008 meters per centimeter per meter. For each 1.22 vertical interval, the scale changes by 0.01 meters per centimeter. In the case of Pit 4, the vertical scale gradient is estimated to be 0.001 meters per centimeter per meter. In both cases the vertical scale gradient was taken into account when plotting the grid corners on the photos. Since the top of the wall is of variable elevation, this is translated downward throughout the grid.

Sampling Strategy

A stratified random sampling approach was developed for the unbiased sampling of air-permeability at a variety of spatial scales. Estimation of the spatial correlation of permeability requires sampling at spacings below the correlation length. Since the correlation structure was unknown at the outset, it was desirable to measure permeability at a variety of spacings. To accomplish sampling at a variety of spacings without introducing bias, a two step random approach was developed to determine sampling locations. This method is similar to that used in the facies-scale studies of Chapter 5.

First, a fixed orthogonal grid was set up on the entire trench wall. Then a random deviation (horizontal and vertical) from the lower left node of each element was generated. This was determined by generating two uniform random numbers from zero to one (U(0,1)) and multiplying each by the horizontal and vertical dimensions of the overlay grid elements (**Figure 7.4**). The location of the control points were then marked directly on the photograph by measuring from the lower left corner of overlay grid elements the horizontal and vertical deviations determined by the stratified random approach described above. Considering the stratified nature of the deposits along with the time constraints, the grid dimension were set at 3.05 meters (horizontal) and 1.22 meters (vertical).

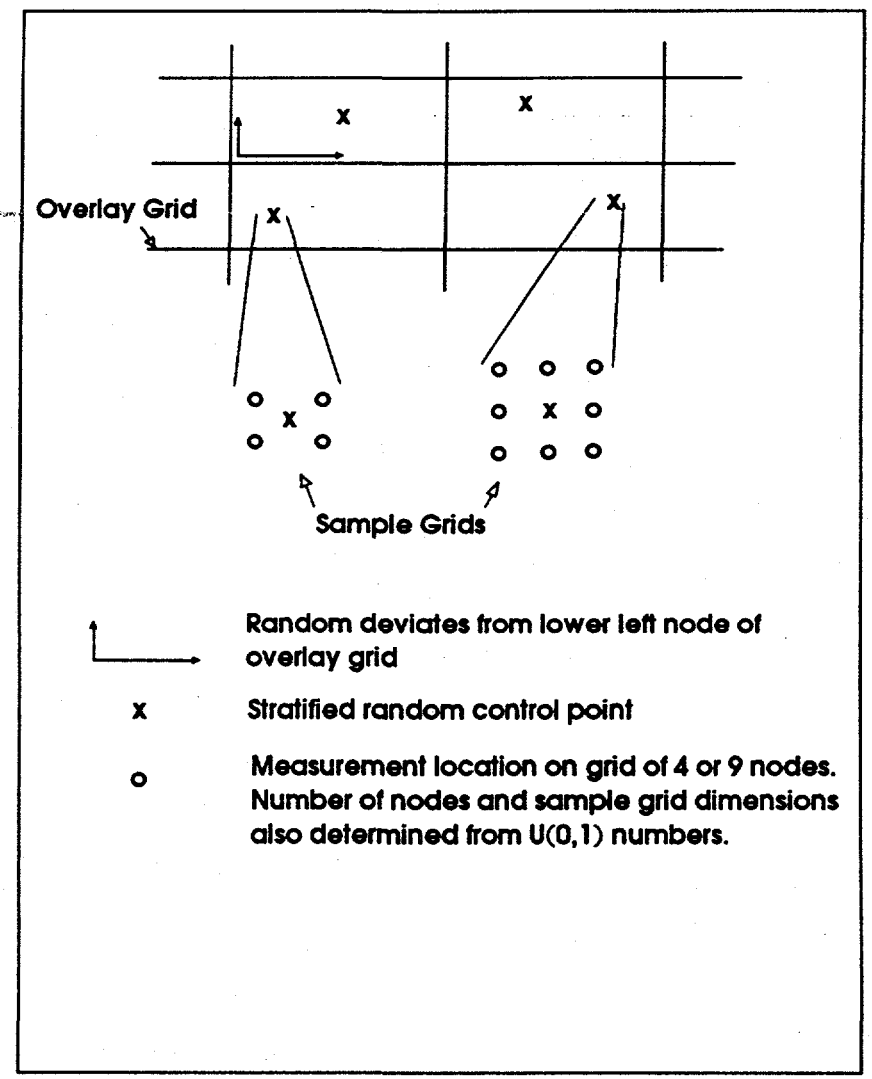

Figure 7.4. Schematic illustration of method used for determining contol point locations and sampling grid characteristics (dimensions and number of nodes)

For each control point, measurements were taken on a grid with the control point at the center of the grid. The characteristics of the sampling grids around each control point were also determined randomly. The grid characteristics were determined by first generating a U(0,1) random number. If the number was less than one-half, the grid contained four nodes; if the number was greater than or equal to one-half, the grid contained nine nodes. The horizontal and vertical dimensions of the sampling grids were determined by generating two additional U(0,1) random numbers and multiplying each by the overlay dimensions.

The grid elements were numbered consecutively from left-to-right and top-to-bottom on the photo-mosaics. For each grid element, the set of random horizontal and vertical offsets were plotted on the photo-mosaics from the overlay-grid corners. In the field, each control point was located by identifying the physical location on the outcrop that corresponded to the control point marked on the photomosaic. The final locations of the control points were obtained by digitizing the locations on the photo-mosaics and applying the same transform used in the mapping exercise.

Sampling of Air-Permeability and Mapping of Hydrogeologic Units

The equipment for this task included the prototype of the air-minipermeameter (Chapter 3), a lift for accessing the trench wall, a small shovel for preparing sampling locations, and a two meter flexible tape measure for locating measurements relative to the control points. A minimum of two personnel were required: one to operate the air-permeameter and another to operate the lift. In order to assess malfunction or drift of the air-permeameter, a standard was taken into the field and sampled regularly. The standard was a porous stone fabricated in the laboratory from sieved sand and epoxy. The times measured with the air-minipermeameter on the standard and were recorded on the data sheets as a "sample standard".

The air-flow-rate data measured with the air-minipermeameter were converted to permeability according to the equations presented in Chapter 3. The standard used in the field was measured under laboratory conditions to have a permeability of 105 darcys. When the mean measured air-flow-rates of the field standard for Pits 3 and Pit 4 (see **Table 7.1**,

Standard mean) were used to calculate permeability, values of 81 and 70 darcys were obtained, respectively. It is also noted that the mean free-fall time (Table 7.1) differed for the two pit studies indicating that there was a change in the permeameter.

First, it is important to note that the air-minipermeameter used for the NTS study was the prototype device for the LSAMP described in Chapter 3. The main differences between the two was the electronic timing of the piston fall. The device used in the NTS study used flashlight bulbs and photoresistors connected to a circuit board as the timing device as described by Davis et al. (1991). The upgrade of the timing device was performed prior to the discovery of the discrepency in measurements between the two Pit studies.

Table 7.1. Means and variances of repeated measurements in units of seconds and seconds-squared, respectively.

	Free-fall mean	Free-fall variance	Standard mean	Standard variance
Pit 3 (n=11)	1.16	0.0022	1.44	0.0042
Pit 4 (n=15)	1.22	0.0025	1.54	0.0047

As a result, the cause for the discrepancy between the standard measured under laboratory and field calibration conditions as well as the difference in free-falls times measured in Pit 3 and 4 is unclear. The permeameter was disassembled and shipped to REECo (Mercury, NV) for each pit study. The device was reassembled in the Mercury dormitories the evening prior to the first day of sampling. The same components configured in the same manner were used for both pit studies. After sampling was completed, the permeameter was disassembled and shipped back to New Mexico Tech (Socorro, NM). There is no clear indication of which parameter changed to result in different response of the air-minipermeameter to free-fall and standard measurements. The sensors were not moved between the sampling campaigns so it is unlikely that the measured volume changed. One possibility is that the photoresister connections were reversed between the Pit 3 and Pit 4 studies. If there was a delay in one of the electronic switches to the stopwatch then this could account for the observed difference.

Without a physical explanation of the difference in the standard and free-fall measurements obtained in Pits 3 and 4, the coefficient of friction, β was used as a fitting parameter. With all other parameters held constant, β, was varied until the time measured for the standard in the field resulted in the permeability obtained with the calibrated device under calibration conditions. This was performed using the mean measured time for the standard for each pit study. The resulting values for the coefficient of friction, β, for Pits 3 and 4 are 210 and 275 [Ns^2/m^2], respectively.

From the field measured free-fall and standard times, the permeameter measurement error was assessed. One possible source of measurement error was instrument drift. For each of the Pit studies, there was no apparent correlation of measurement values with time of day so drift of the instrument is regarded as negligible. Another form of measurement error is the repeatability of the instrument. To test the repeatability of the instrument triplicate measurements were performed in three locations. At control points (3-19 and 3-78) either the horizontal or vertical grid spacing were less than one centimeter. Instead of obtaining very closely spaced measurements, three sets of triplicate measurements were taken at these control points. This set of repeated measurements is used in assessing permeameter repeatability at a given location on the outcrop.

An analysis of variance (ANOVA) was performed on the six groups of data, each group containing three measurements. The natural log transform was applied to the permeability measurements since it is expected to exhibit a log-normal distribution. The result of the analysis indicates a much smaller variance within groups (0.068) than between groups (0.419). The F statistic, which is defined as the ratio of the between group variance to the within group variance, is 6.16 indicating that the variability of the population is much greater than the variability associated with measurement error. The error associated with repeatability is expected to contribute to the nugget of the variogram estimates.

RESULTS

The hydrogeologic units were mapped in Pits 3 and 4 concurrent with permeability data

acquisition. The location of the contacts were recorded on the photo-mosaics of the pit walls and were digitized and transformed. Three basic types of geologic material were mapped: sheet flood, debris flow, and channel deposits. In general, the sheet flood material was characterized by clast supported material exhibiting sedimentary structures; the debris flow material was characterized by matrix-supported clasts without any apparent sedimentary structures, and the channel deposits consisted of large clasts (cobbles and some boulders) with infilling sands.

For the study in Pit 3, Stuart Rawlinson (Raytheon, Las Vegas, NV) produced a line geologic map on the pit wall photo-mosaic. While this was performed concurrent with permeability sampling, the tasks were separate.

The result was two slightly different interpretations of the geology and hydrogeology. When collecting permeability measurements, the locations on the pit wall were recorded as debris flow (DF) or sheet flood (SF) depending on the absence or presence of sedimentary structure (no permeability measurements were obtained in the channel (CH) deposits). The presence or absence of sedimentary structure was the hydrogeologic definition of the sheet flood and debris flow deposits, respectively. The geologic map of Pit 3 by Rawlinson (**Figure 7.5**) delineates two sheet flood deposits in the upper part of the pit wall. The muddy sheet flood (MSF) and very-muddy sheet flood (VMSF) were interpreted hydrogeologically as debris flow as they exhibit no apparent sedimentary structure. There is a strong possibility that the MSF and VMSF deposits were genetically sheet flood and have undergone pedogenic processes destroying the primary sedimentary structures. Another region of considerable disagreement between the two interpretations occurs in the lower sheet flood (PSF) unit. At control points in this lower unit, material interpreted by Rawlinson as sheet flood were recorded as debris flow when air-permeability measurements were taken. Most of these discrepancies occur near a mapped contact and may be the result of slight errors in mapping the contact.

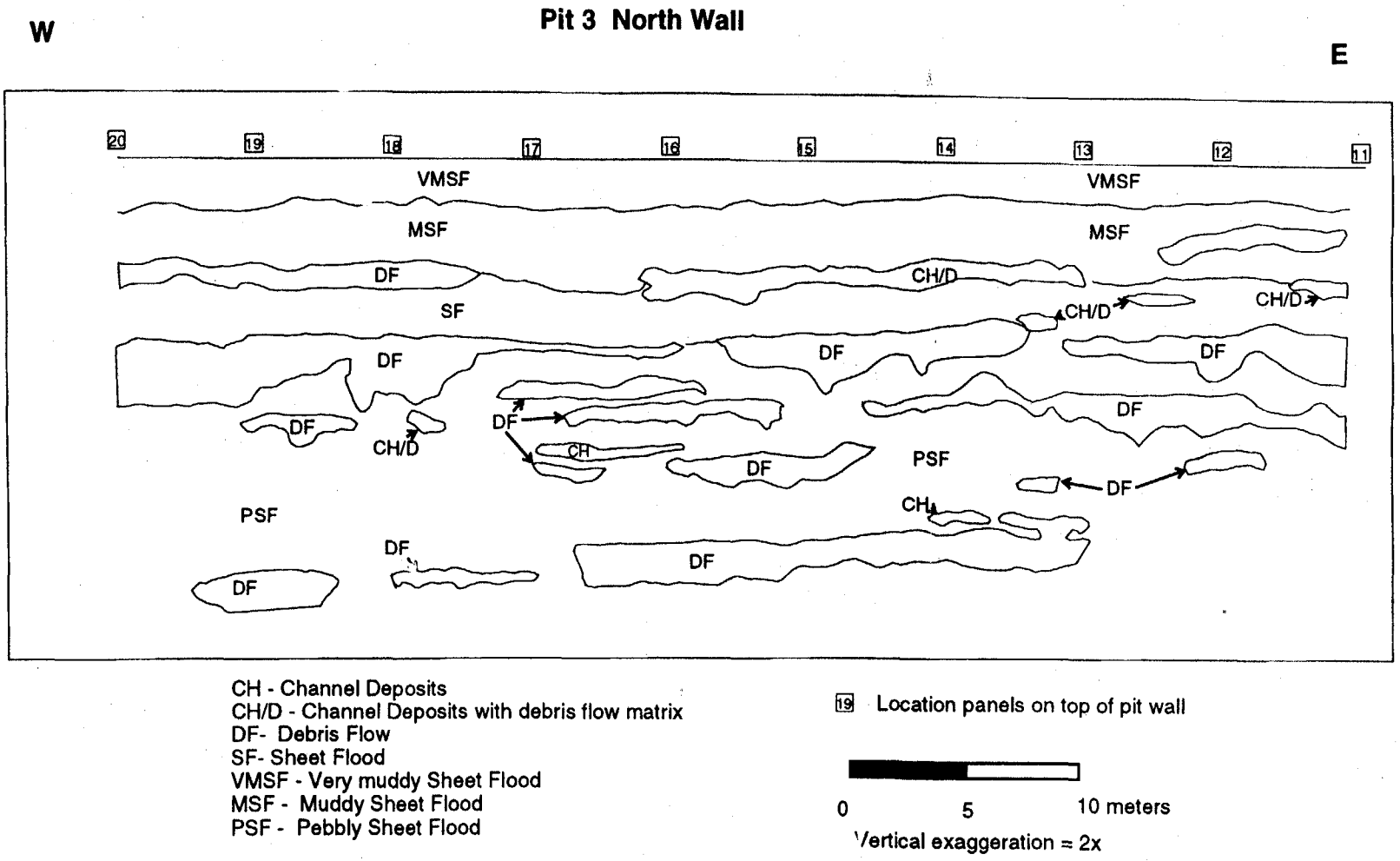

Figure 7.5. Hydrogeologic map of Pit 3.

The hydrogeologic map for Pit 4 (**Figure 7.6**) was produced by the author with the assistance of Warren Cox (REECo, Mercury, NV) and Erik Webb (DOE Fellow/Sandia National Labs). The same three units (SF, DF, and CH) were observed and mapped in Pit 4. The mapping was performed after sampling of permeability was complete. Since the map was constructed by the same personnel that performed the permeability measurements, the hydrogeology mapped is consistent with the hydrogeology recorded during sampling.

Pit 3

On the first trip (January 23 - January 25, 1991), permeability measurements were made on the north wall of Area 5, Pit 3. The wall was approximately 10 meters high and well over 250 meters long. A 55 meter segment of the wall extending from wall-marker 11 to wall-marker 20 was targeted for measurement. The wall itself consisted of unconsolidated alluvial fan sediments that maintain some slight cohesion possibly due to calcite cementation and minor compaction. The surface of the wall is essentially vertical (approximately three meters off vertical) with local irregularities such as cavities and crevasses.

Of the total 384 data locations, 292 successful measurements were made (76% success ratio). There were 60 missed measurements in the sheet flood material and 32 in the debris flow material. **Table 7.2** summarizes the distribution and reason for the non-measurements. In both types of material (debris flow and sheet flood) there were a significant number of non-measurements due to friable surfaces and large rocks. A smaller number of non-measurements were caused by poor seals on rough surfaces (blow out), caliche, slope cover, burrows and instrument problems. However, in the sheet flood unit, the major cause of non-measurements was a dense matrix of pebbles. It is not entirely understood what effect these missing data have on the shape of the resulting statistical distributions. However, if the rock and caliche represent the lowest permeability and the pebbly and "too friable" regions represent the highest permeability, the estimated probability distribution would tend to underestimate the tails of the actual distribution. The locations of the "missed" values seem to be evenly distributed in space and are not taken into account in the geostatistical analysis.

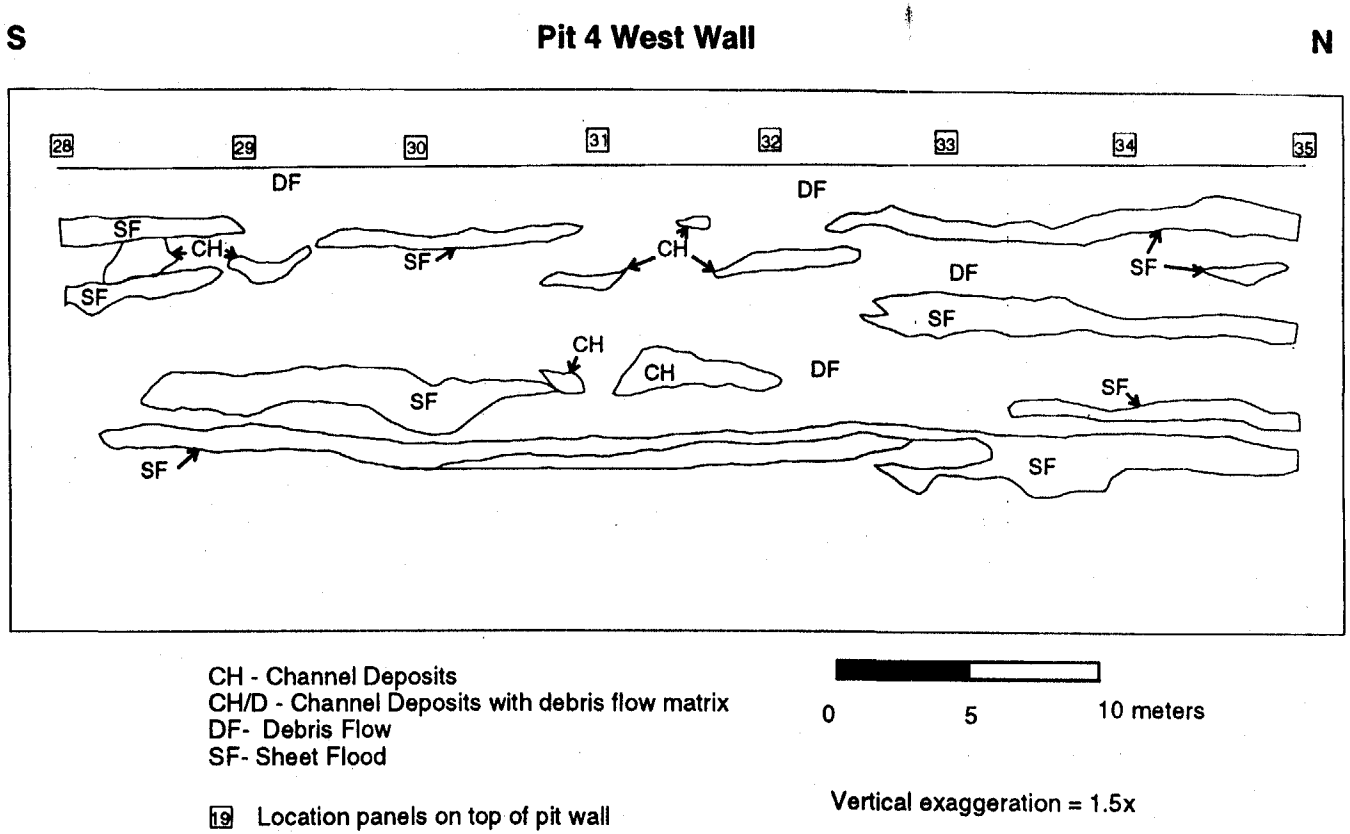

Figure 7.6. Hydrogeologic map of Pit 4.

Table 7.2. Summary of non-measurements in Pit 3.

TYPE OF PROBLEM	NO. IN SHEET FLOOD	NO. IN DEBRIS FLOW
Friable surface	5	6
Large rocks	11	10
Poor seal (blow out)	1	2
Caliche	3	1
Slope cover	3	0
Burrows	0	2
Instrument Problems	0	3
Pebbles	37	7
TOTAL	60	32
Success rate	70%	83%

Permeability measurements were made beginning at the lower left hand corner of the gridded area of the outcrop. Given the time constraints of two days of sampling per pit and the objective of obtaining a sufficient number of data points distributed over as much of the wall as possible, alternating columns of control points were skipped after the first two columns were completed. Thus, of the 124 control points mapped in Pit 3, permeability measurement were made at only 59.

Pit 4

Permeability measurements were made in Pit 4 on February 12-13, 1991, under the same conditions as described for Pit 3. Of the 56 mapped control points, 48 were used, and of the 337 attempted measurements, 213 were successful (63% success ratio). **Table 7.3** summarizes the distributions and reasons for the non-measurements at Pit 4. The problems encountered in making permeability measurements in Pit 4 were similar to those in Pit 3.

However, in comparing the two data sets, Pit 4 had a lower overall percentage of sheet flood

deposits. These were generally of coarser, more friable material and difficult to sample. Of the 213 successful permeability measurements from Pit 3, only 11% were from sheet flood deposits.

Pit 4 was not as deep as Pit 3, the pit wall dimensions were only 6.1 meters high by approximately 43 meters long. The same sampling design was used in Pit 4 as that used in Pit 3. While the practice of skipping every other column was followed in Pit 4, the lowest control point in each skipped column was occupied.

Table 7.3. Summary of non-measurements in Pit 4.

TYPE OF PROBLEM	NO. IN SHEET FLOOD	NO. IN DEBRIS FLOW
Friable surface	9	17
Large rocks	10	27
Poor seal (blow out)	3	8
Caliche	0	0
Slope cover	0	0
Burrows	0	0
Instrument Problems	0	25
Pebbles	12	3
TOTAL	34	80
Success rate	42%	70%

DATA ANALYSIS AND INTERPRETATION

Hydrogeologic maps were generated based on the field mapping of geologic units. Classical statistical analysis was performed on the permeability data and compared with the theoretical normal distribution for associated means and standard deviations. In the cases of both data sets, the hypotheses of log-normal distributions appears valid. Variogram estimates were also performed with the GAMV3 routine (Deutch and Journel, 1992).

The sampling strategy employed appears to have worked very well. The locations of the successful measurements in Pit 3 and Pit 4 are presented in **Figures 7.7**. The data set is believed to be largely unbiased and very amenable to variogram estimation. Variogram analysis of the entire Pit 3 data set was performed at two scales. Small-scale correlation (< 1 meter) was estimated with an omni-directional variogram to obtain as many pairings as possible. The lag interval of the small-scale variogram was 0.2 ± 0.1 meters. The large-scale variogram were then estimated in the horizontal and vertical directions with lag intervals of 0.5 ± 0.25 meters and search window tolerance angle of ± 25 degrees. For Pit 3, each lag estimate had at least 50 pairs with a vast majority of lags containing more than 200 pairs. For Pit 4, again all variogram estimates except lag #1 are based on more than 50 pairs with most lags containing more than 200 pairs.

Pit 3

The Pit 3 data consists of 292 permeability measurements taken from two different hydrogeologic units. The measurements are distributed evenly between the two types of deposits with 157 from the debris flow and 133 from the sheet flood.

Distribution analysis of the Pit 3 data indicate a skewed right distribution of the original data. A natural-logarithm transform was applied and apparently normal distributions resulted. The empirical cumulative probability distribution of log-permeability are presented in **Figure 7.8a**. The log-data were then split into two hydrogeologic sub-sets. Empirical distributions of the hydrogeologic data sub-sets were also estimated and are presented in **Figure 7.8b**. The population statistics are summarized in **Table 7.4**. The variance of the Pit 3 log-permeability data is much larger than that observed in the within-facies studies of Chapter 5. When the data is split according to debris flow and sheet flood, the variances associated with the subsets is much less than the total variance but still larger than the variance observed within the fluvial and paleosol facies. The difference is attributed to the higher variability of depositional and diagenetic (pedogenenic) processes of an alluvial fan over the scale of tens of meters versus the variability of the fluvial and pedogenic processes

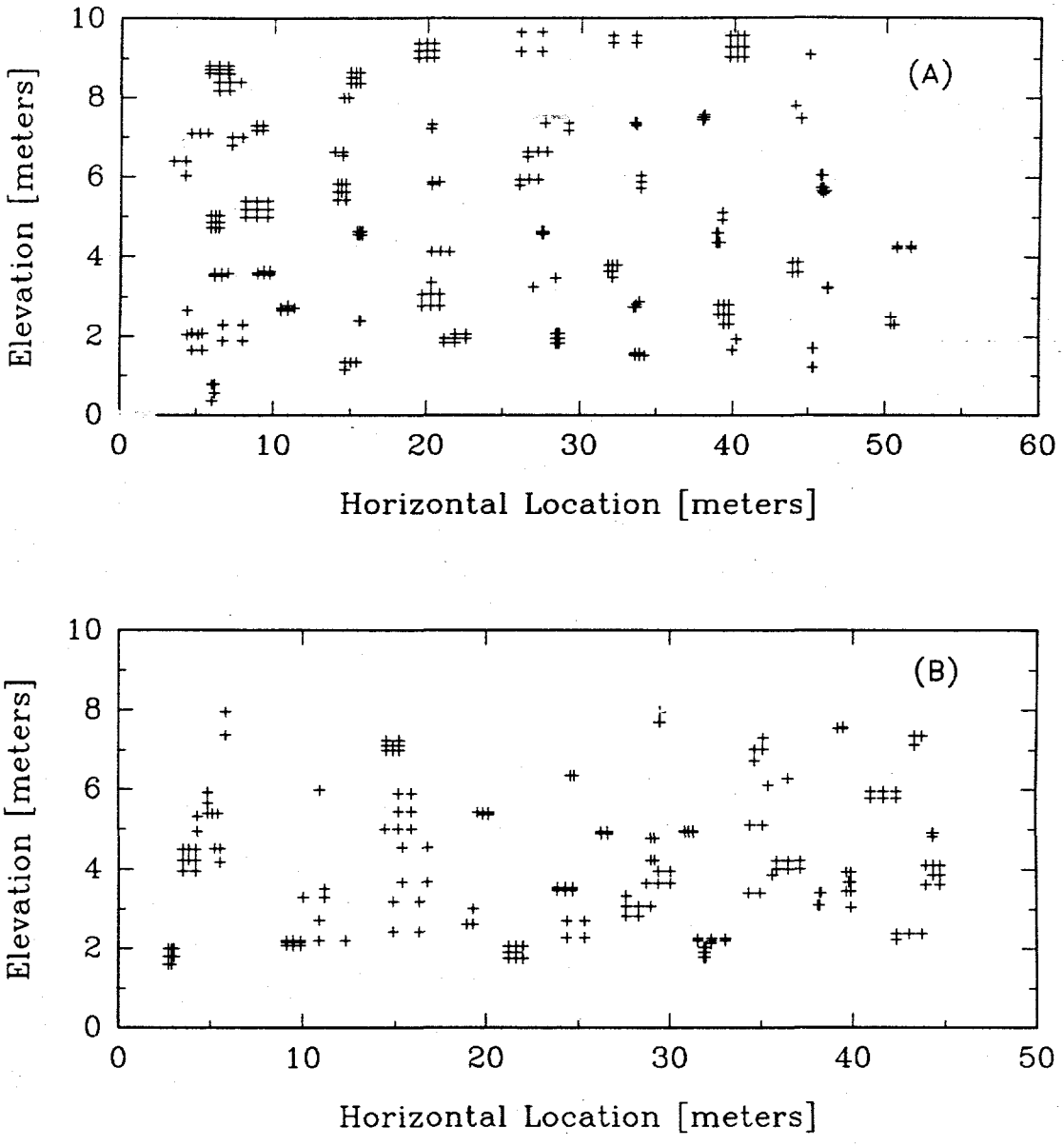

Figure 7.7. Sampling locations for Pit 3 and Pit 4.

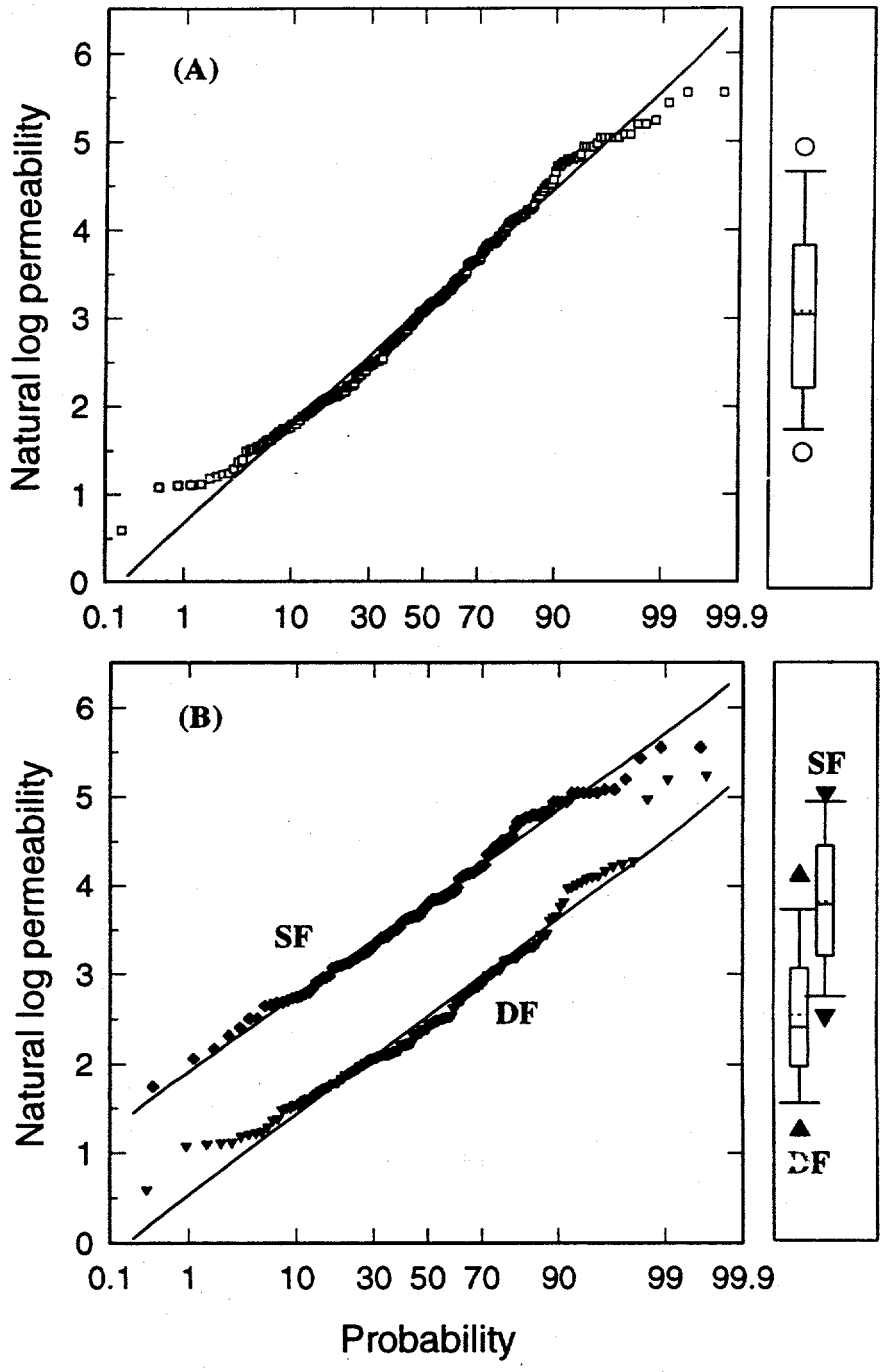

Figure 7.8. (a) Empirical cumulative distributions for Pit 3 data. The maximum difference observed between the empirical and theoretical distributions is 0.066. (b) Empirical cumulative distributions for Pit 3 sheet flood (SF) and debris flow (DF) sub-populations. The maximum difference in the estimated and theoretical probabilities are 0.092 (debris flow) and 0.058 (sheet flood).

acting over the scale of tens of centimeters in fluvial/interfluvial environments. The correlation structure was investigated at two scales. The results of the small-scale variogram estimate are presented in **Figure 7.9a**. The small-scale variogram exhibits fairly consistent values between lags of 0.1 and 0.8 meters, however, the first variogram estimate at 0.1 meters is slightly lower than the others. If the measurement error of the field study is equivalent to the apparent sill (0.4), then no inference can be drawn regarding the small-scale correlation structure. However, this value is larger than that observed in the other field studies. The variance of repeated field measurements of standards presented in Chapter 3 indicates that the measurement variance of log-permeability (base-*e*) is less than 0.03. In the small-scale studies presented in Chapter 5, a nugget of 0.04 is consistently observed and overall population variances do not exceed 0.3. In addition, the triplicate measurements obtained in this study indicate a variance associated with instrument repeatability on the order of 0.07. As a result, the small-scale variogram is likely to reflect small-scale correlation. An exponential model is fit to the estimate with a nugget of 0.07 and correlation length of 0.08 meters. An important feature of the small-scale correlation is that a single simple sill is apparently reached for lags between 0.1 and 0.8 meters. The increase in the variogram estimate at lag 0.87 is interpreted as the onset of the larger-scale correlation structure.

The large-scale horizontal and vertical variograms are presented in **Figures 7.9b and 7.9c**, respectively. At the scale of meters, the correlation structure also exhibits an exponential behavior. The modeled nugget (0.4) results from the sill of the small-scale correlation structure. Some periodicity is seen in the variogram estimate that may result from periodic horizontal variations in permeability. However, with the significant amount of noise in the variogram estimate it is difficult to discern the cause of the periodicity. One possibility is that the periodicity is an artifact of the sampling every other column on the overlay grid. Recall that the horizontal dimension of the overlay grid elements was 3.05 meters. Skipping every other column may have resulted in a poor pairings for lags that are multiples of three.

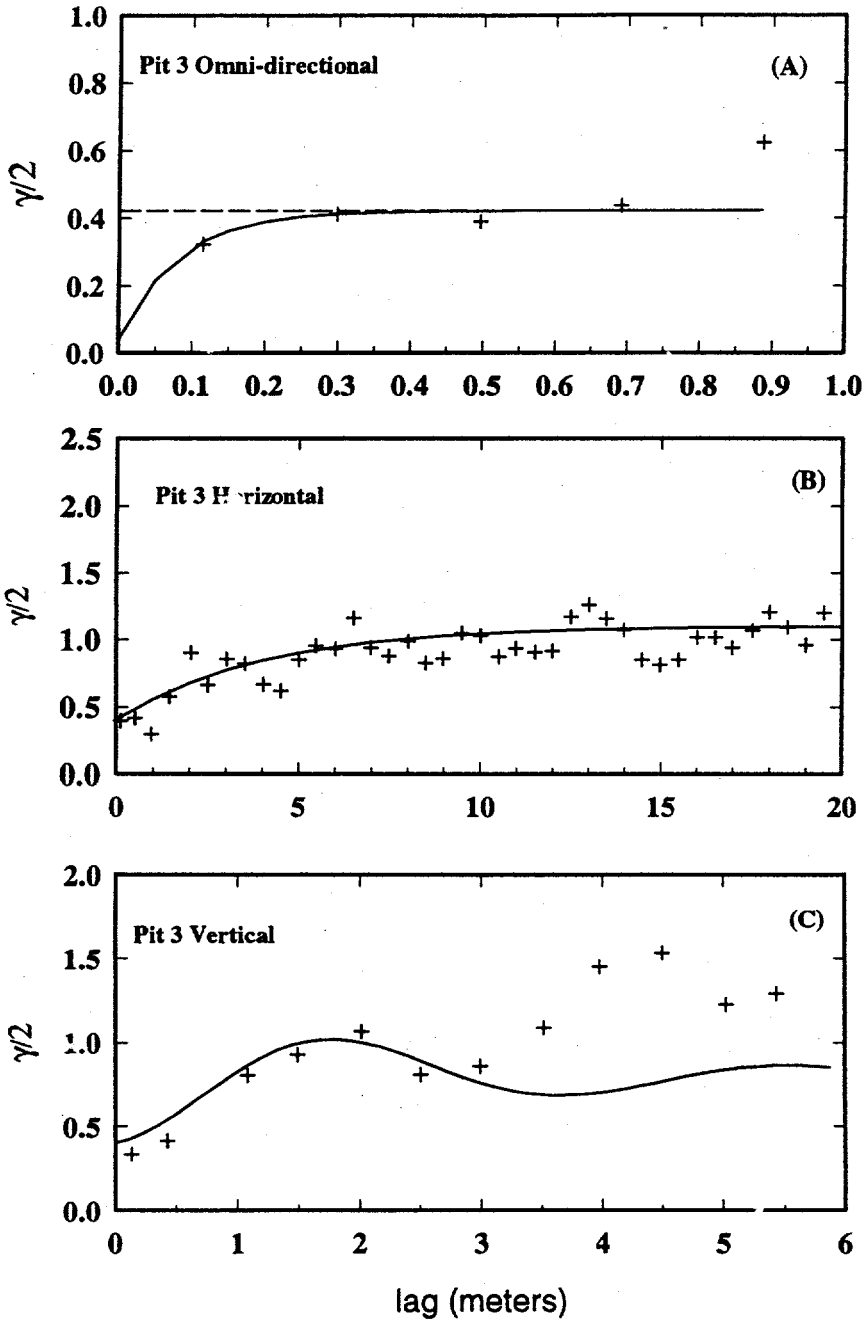

Figure 7.9. Small-scale (a) omni-directional, (b) horizontal, and (c) vertical variogram estimates of Pit 3 logarithmic data.

The horizontal variogram is fit with:

$$\gamma_h(\xi) = 0.4 + 0.7\ [1 - \exp(\frac{-|\xi|}{4})]$$

The vertical variogram (Figure 7.9c) exhibits periodic structure and is fit with a cosine-exponential variogram model.

$$\gamma_v(\xi) = 0.4 + 0.4\ [1 - \exp(\frac{-|\xi|}{3})\cos(\frac{|\xi|}{0.6})]$$

The deviation from the model at large lags may result from a vertical trend in the data. The anisotropic nature of the variogram is consistent with the field observations of a stratified medium.

Table 7.4. Summary of permeability statistics for Pit 3 data. Permeability values are in darcys.

Data Set	Mean [ln(k)]	Var [ln(k)]	N
All	3.12	1.104	292
Debris flow	2.53	0.735	159
Sheet flood	3.81	0.664	133

Pit 4

The Pit 4 data consist of 213 permeability measurements taken from two different hydrogeologic units. Unlike Pit 3, the measurements obtained from Pit 4 are not evenly distributed between the two types of deposits sampled. Only 25 measurements were obtained from the sheet flood deposits in Pit 4 while 188 measurements were obtained from the debris flow deposits.

Distribution analysis of the Pit 4 data was performed. As with Pit 3, the original data resulted in a skewed right distribution. A natural logarithm transform was applied and the resulting empirical and theoretical normal distributions are presented in **Figure 7.10a**. The data set was split into two subsets for analysis of the population statistics. The resulting distributions are shown in **Figure 7.10b** and summarized in Table 7.5 .

Table 7.5. Summary permeability statistics for Pit 4 Data.
Permeability values are in darcys.

Data Set	Mean [ln(k)]	Var [ln(k)]	N
All	2.03	0.667	213
Debris flow	1.88	0.424	188
Sheet flood	3.21	1.106	25

As in the case of Pit 3, small-scale and large-scale variograms were estimated with the same variogram search window parameters. The small-scale variogram of the Pit 4 data (**Figure 7.11a**) is very similar to that of the Pit 3 data and is modeled in a similar fashion. The small-scale variogram reaches a sill of approximately 0.3 at lags greater than 0.2 meters. This sill value is used as the nugget for the large scale directional variograms. The horizontal variogram exhibits exponential behavior with a correlation length of 2 meters (**Figure 7.11b**). The vertical variogram is presented in **Figure 7.11c** and exhibits a crude periodic behavior.

$$\gamma_h(\xi) = 0.25 + 0.5[1 - \exp(\frac{-|\xi|}{2})]$$

$$\gamma_v(\xi) = 0.25 + 0.4\ [\ 1 - \exp(\frac{-|\xi|}{3})\cos(\frac{|\xi|}{0.6})\ ]$$

An exponential-cosine model is used to model the vertical variogram :

The sill of the Pit 4 horizontal variogram is less than the sill estimated in the horizontal variogram of Pit 3 reflecting the apparent difference in overall log-permeability variance of the two pit walls (Tables 7.4 and 7.5). The correlation length of the horizontal

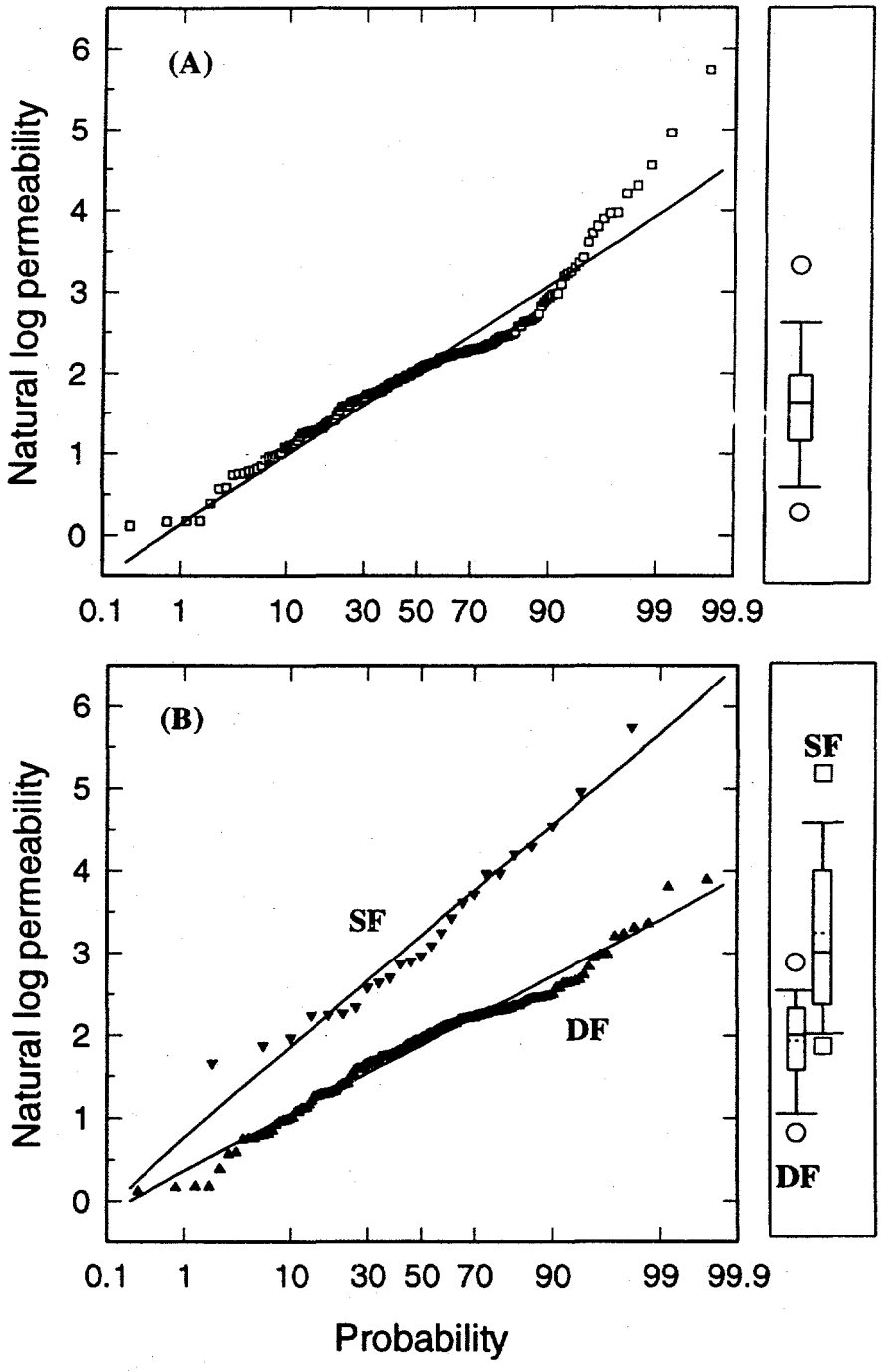

Figure 7.10. (a) Empirical cumulative distributions for Pit 4 data. The maximum difference observed between the empirical and theoretical distributions is 0.129. (b) Empirical cumulative distributions for Pit 4 sheet flood (SF) and debris flow (DF) sub-populations. The maximum difference in the estimated and theoretical probabilities are 0.074 (debris flow) and 0.121 (sheet flood).

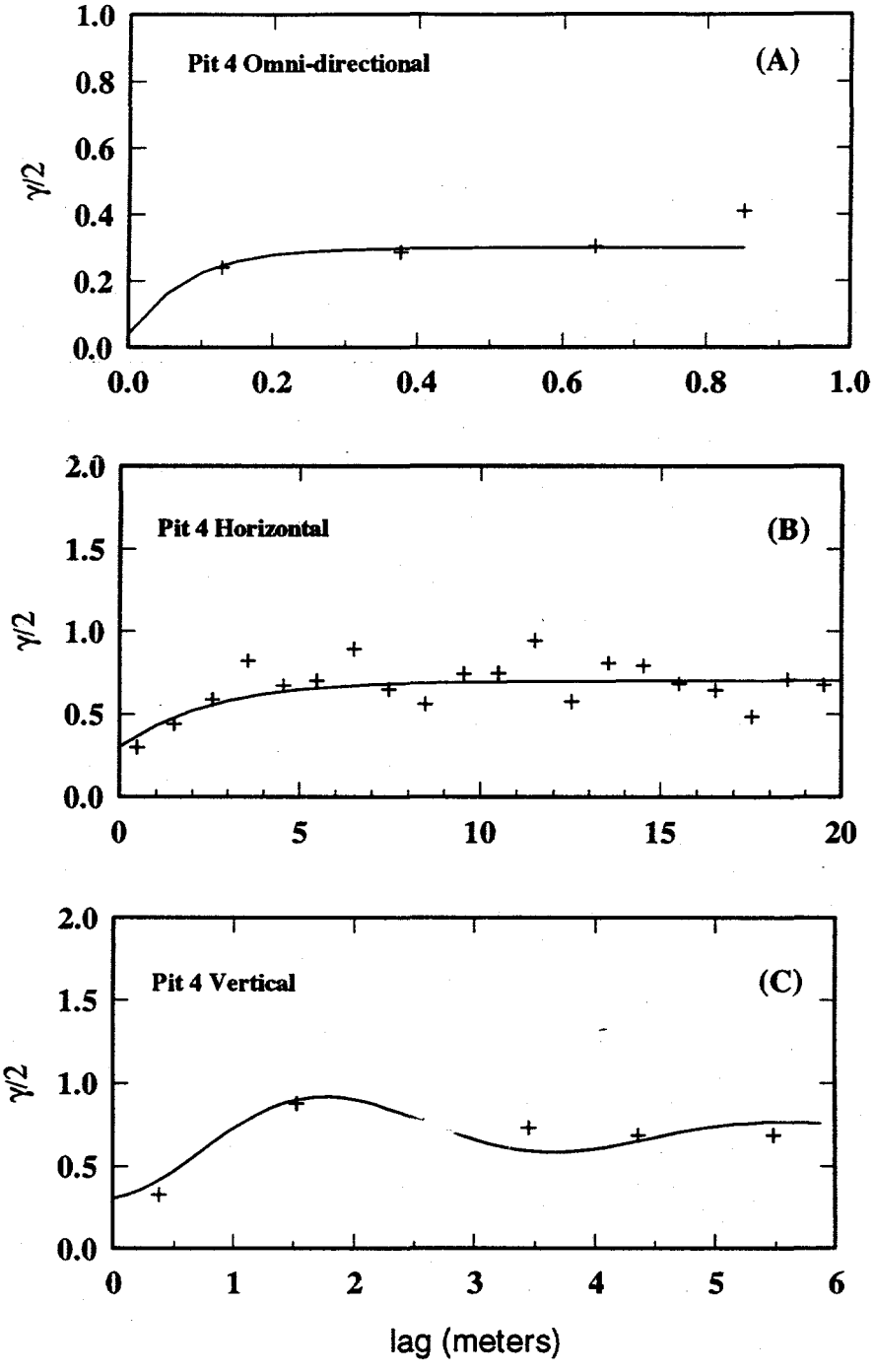

Figure 7.11. Small-scale (a) omni-directional, (b) horizontal, and (c) vertical variogram estimates of Pit 4 logarithmic data.

variogram in Pit 4 is also shorter than the estimated correlation length of the Pit 3 data. Since the Pit 4 data set is dominated by debris flow units, the smaller correlation length is interpreted as reflecting the correlation length of the debris flow deposits more than the correlation length of the spatial assemblage of the debris flow and sheet flood observed in Pit 3. The vertical variograms in Pits 3 and 4 are fit with the same model indicating that the average thickness of the deposits does not vary appreciably over the 400 horizontal meters separating the two pits.

Geological Approaches to Estimating the Variogram

With the permeability data collected and the geologic information available through this work and the subsequent work by Snyder et al. (1993), two approaches are investigated for incorporating geologic information into the estimation of the correlation structure. Since the Pit 3 data contain fewer "non-measurements" and the instrument calibration is closer to the laboratory calibration, it is probably more representative of the actual permeability distribution. For both approaches, the Pit 3 data are used.

The first method was to represent the spatial variation of permeability as a function solely of the spatial distribution of lithologic facies. The detailed geologic mapping of Snyder et al. (1993) delineated nine lithologic facies each differing slightly in sorting and grain-size. From the descriptions of the lithologic facies, they are binned into five groups based on sorting and grain size. The groups were then qualitatively ranked according to permeability and assigned mean log-permeability values differing by one-quarter of an order of magnitude. Since the lithologic map and facies descriptions used in this excercise were performed on the opposite pit wall of the permeability measurements, the measured permeability values were not used in the assigning of the mean log-permeability values. The descriptions and assigned mean permeabilities are listed in **Table 7.6**.

The geostatistical analysis of the assigned mean permeabilities was performed in a similar manner to the analysis in Chapter 6. The two-dimensional cross-section of Snyder et al. (1993) was digitized using GSMAP. The PTPOLY routine was used to assign mean

permeabilities to the regions occupied by different lithologic facies. The variogram estimate of the assigned mean permeabilities employed the same search window angle as the variogram estimate (± 25 degrees). The results of the analysis are compared with the variogram estimate of the data in **Figure 7.12**. The resulting variogram shapes in the horizontal and vertical direction closely mimic the shape of the variogram estimate of the data. The variogram of the model in the vertical direction appears slightly out-of- phase with the variogram estimate

Table 7.6. Summary of lithologic facies descriptions, ranking of estimated permeability and assigned mean log-permeability.

Facies designation	Description [Snyder et al., (1993)]	Permeability Class	Assigned mean log(k)
a	soil structure, translocation of $CaCO_3$, occasional cementation of matrix	5	0.50
b	structureless, mod. to poorly sorted, fine grained sediments	4	0.75
c	structureless, mod. to poorly sorted, coarse grained sediments	3	1.00
d	bedded, mod. to poorly sorted, fine grained sediment	3	1.00
e	bedded, mod. to well sorted, coarse grained sediments	2	1.25
f	poorly sorted, little bedding, coarsest grained material, large clasts (25-50%)	1	1.50
g	poorly sorted, little bedding, coarsest grained material, large clasts (50-75%)	1	1.50
h	poorly sorted, little bedding, coarsest grained material, large clasts (>75%)	1	1.50
i	mod. sorted, predom. pebbles with some fine sand, silt, clay.	2	1.25

of the data. This could be attributed to non-stationarity in the average unit thickness between the pit wall where measurements were taken and the pit wall where the mapping was

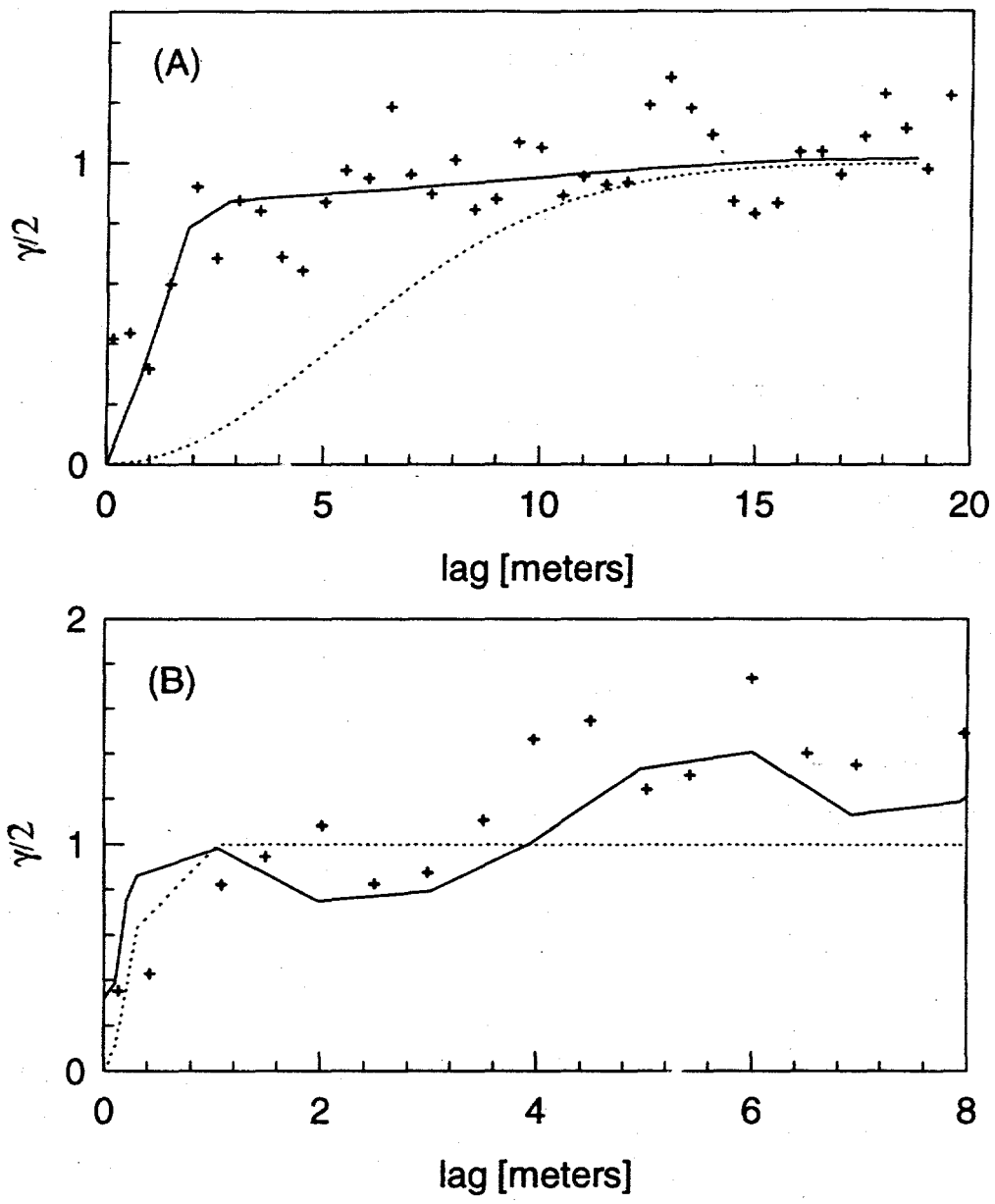

Figure 7.12. Normalized horizontal (a) and vertical (b) variogram results of assigned mean permeabilities (solid line) and theshold crossing (dotted line). Variogram estimates normalized to respective sill values.

performed. However, the results of the vertical variogram estimates from the permeability data in Pits 3 and 4 indicate uniformity in average thicknesses over a larger distance. The overall underestimation of the variogram is attributed to the lack of variability within the lithologic units and more importantly the lack of tails on the resulting assigned probability distribution.

The second geological approach tested with the Pit 3 data is the threshold crossing approach (Phillips and Wilson, 1989) described in Chapter 5. Here, the map of Snyder et al. (1993) is again used to estimate the average dimensions of regions exceeding some threshold of the permeability probability distribution. The facies assigned with the highest mean permeabilities (f,g,h) are taken as a proxies for the threshold of the mean plus one standard deviation ($\mu+\sigma$). Again since the lithologic descriptions and mapping were performed on the opposite pit wall, the assigned theshold is not based on measured permeability values.

Twenty-four of these "extreme valued" facies occur on the map of Snyder et al. (1993). The average horizontal and vertical dimensions of the designated facies are 17 and 0.7 meters, respectively. For these average dimensions and the specified threshold, the estimated correlation lengths of the bell-shaped variogram in the horizontal and vertical directions are 7.4 and 0.3 meters, respectively, and are presented in Figure 7.10. In general, the threshold crossing approach with a bell-shaped variogram appears to yield an overestimate of the observed correlation length. However, the search window imposed on the variogram estimates of the data and the assigned means may result in an underestimation of the "actual" correlation length.

While both approaches appear to provide reasonable estimates of the correlation length, the method of assigning mean permeabilities to lithologically different units appears to provide a better estimate of the overall correlation structure and the effective range. In addition, this method does not require a priori assumptions regarding the correlation structure. This experiment indicates that the correlation structure is strongly controlled by the spatial assemblage of lithologic facies. This result can be of practical importance in estimating the correlation structure at sites where a spatial representation of the lithologic facies can be

obtained either from a conceptual geological model or an analog outcrop.

CONCLUSIONS

Five hundred and five measurements of air-permeability were collected to assess the spatial variability of permeability in the alluvial fan deposits of the Radioactive Waste Management Site, Area 5, Nevada Test Site. A two-step random sampling strategy was developed and implemented. Based on the number of pairs obtained in the estimation of the variogram and the ability to estimate the variogram at several scales, the goal of the sampling strategy was achieved. In addition the method of conformal mapping the control points and geologic contacts recorded on photo-mosaics to a rectangular region appears to have worked well.

Geostatistical analysis of the data collected indicates 1) permeability is log-normally distributed in the areas studied, 2) the means of the debris flow and sheet flood material appear to be different, and 3) correlation length structure exhibits two distinct scales. The first structure reaches a sill at approximately 0.2 meters and the larger-scale horizontal structure attains a sill at approximately five meters.

The method of assigning mean permeabilities to different lithologic facies appears to provide an adequate data base for the estimation of the shape of the correlation structure. However, the method does not provide information on the small variability represented in the nugget or the overall population statistics, both of which may be important in modeling applications.

CHAPTER 8: HETEROGENEITY STUDY OF EOLIAN DEPOSITS

INTRODUCTION

An additional outcrop study of heterogeneity was conducted on the Miocene Popotosa Formation. The study site is located 14 miles south of San Antonio, New Mexico on State Highway 1 where the railroad tracks cross the highway (**Figure 8.1**). The outcrop is a result of the railroad track excavation.

The purpose of this study was to provide a third type of depositional environment for the analysis of the relationship between observed geological features and the spatial statistics of permeability. The primary objectives were to 1) estimate the mean and variance of air-permeability for comparison with deposits of other depositional origin, and 2) assess the relationship between the correlation structure of air-permeability with observable geological features.

The deposits in the outcrop are interpreted to be of eolian origin based on the large-scale cross-bed sets that are steeply dipping at the top and tangential to horizontal at the base. (**Figure 8.2**). The lamination within sets is crudely defined and contacts between laminae are gradational indicating that the sediments were deposited by grainfall on the upper lee-side part of the dune (Collinson, 1986). In outcrops of various orientations in the vicinity of the study site, the dip of the cross-bed sets appears variable indicating that the dune was of rather complex morphology.

METHODS

A photo-mosaic of the outcrop was constructed from four 10 x 12 centimeter color prints. Spatial control of set boundaries and permeability control points was maintained with traditional surveying techniques. Air permeability measurements were obtained with the LSAMP (Chapter 3). Permeability measurements were taken on rectangular grids around each

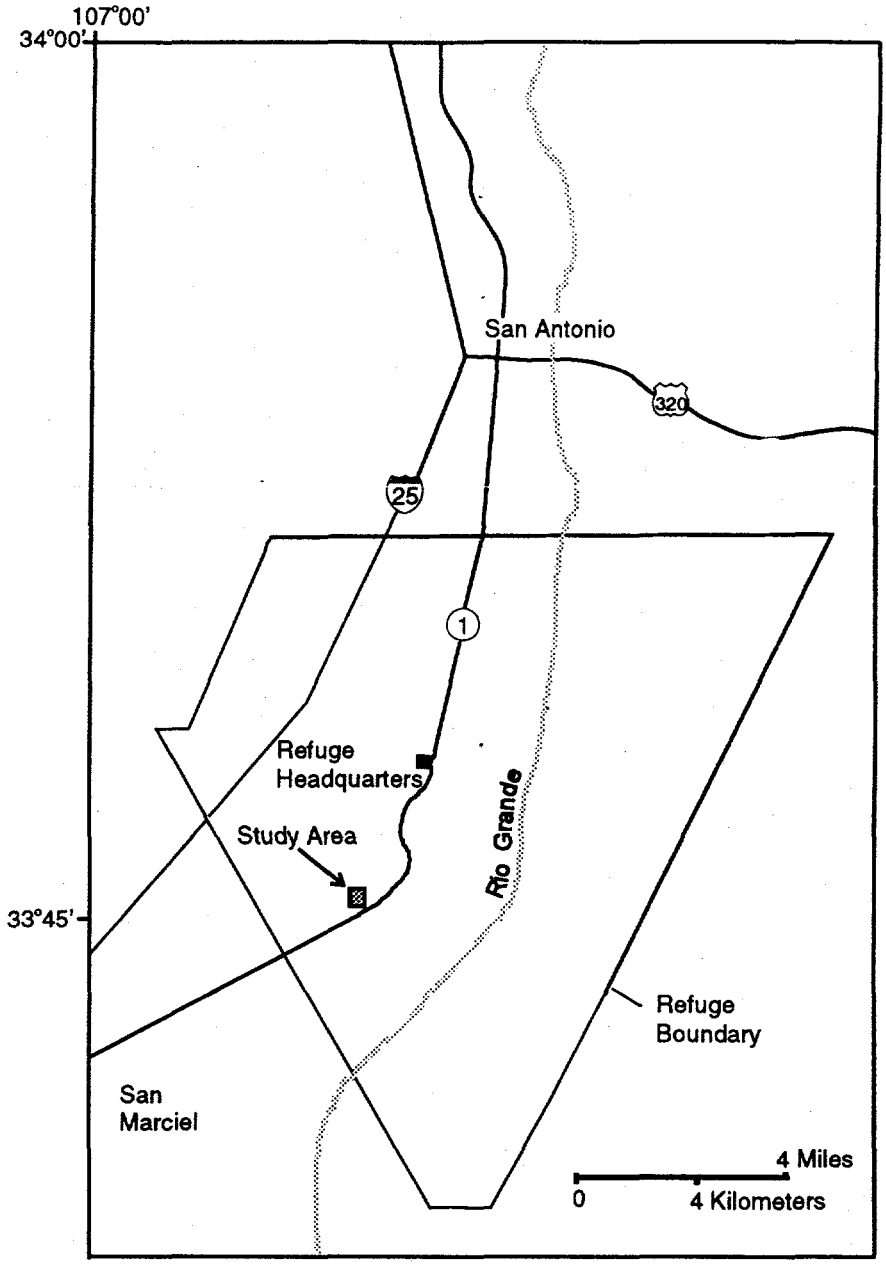

Figure 8.1. Location map of study site on the Bosque del Apache National Wildlife Refuge.

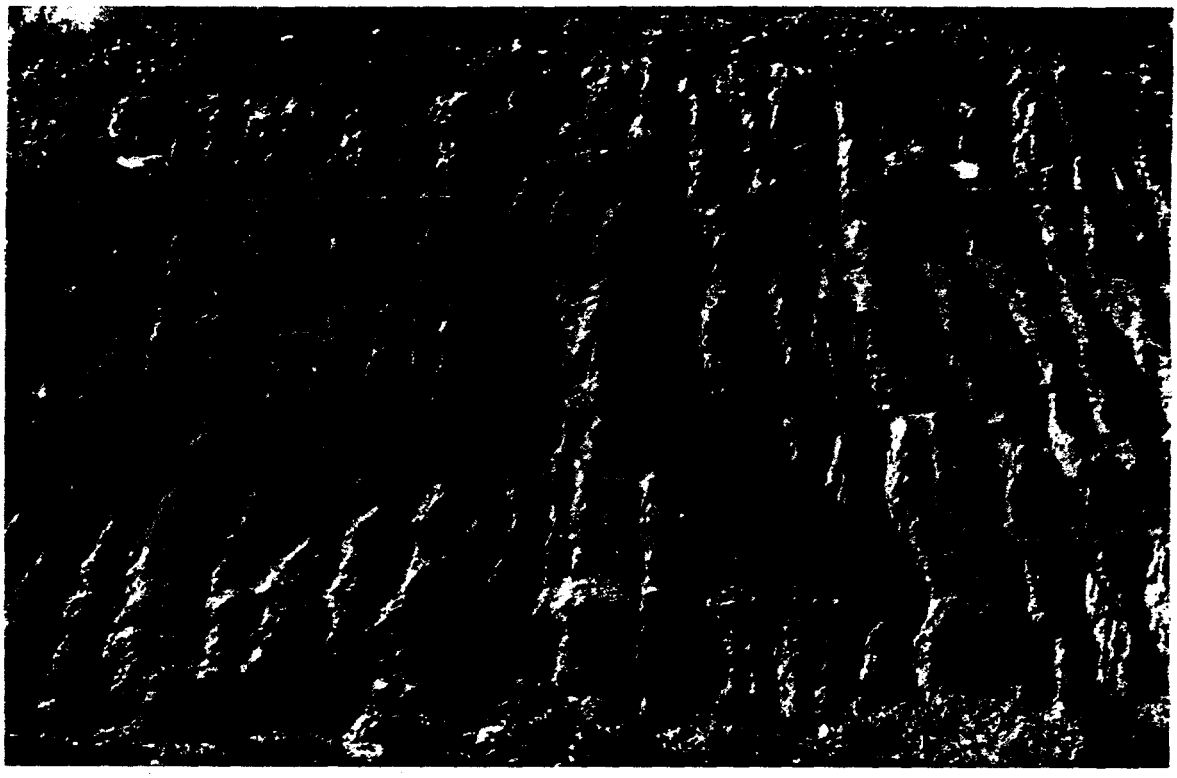

Figure 8.2. Photograph of eolian outcrop studied. Outcrop is approximately 5 meters high.

control point. The location of these control points was also marked on the photo-mosaic with a permanent marker.

RESULTS

The map of the lithologic facies and control point locations is presented in **Figure 8.3**. Four lithofacies were identified. The lithofacies represent cross-bed sets and are all of similar type. Facies 1 (F1) and Facies 4 (F4) were subdivided into two sub-facies along surfaces exhibiting marginal erosion. All facies consist of laminated fine to medium sand. The angle of lamination is variable with the steepest dipping laminae near the top of each facies. The observed facies are interpreted as grain-fall deposits of an eolian dune field. The variability of the prevailing wind direction and thus the type of dune field has not been ascertained. While cementation is more prevalent in these deposits than any of the others presented here, the deposits were still workable with a small trowel. Cementation appeared relatively uniform with isolated well-cemented concretions on the order of a few centimeters in length.

The sampling of permeability was performed by scrambling up the outcrop to reasonably accessible locations. Once a location for sampling was identified, a sampling grid was determined with an effort to sample over a variety of spacings. The unbiased method used in Chapters 5 and 7 was not employed. Sampling locations are shown in **Figure 8.4**. Two hundred and eleven permeability measurements were obtained. The empirical cumulative probability distribution of the entire data set appears to exhibit log-normal behavior (**Figure 8.5a**). Separating the data according to facies, F1, F2, and F4 exhibit similar means while F4 exhibits a significantly lower mean (**Figure 8.5b** and **Table 8.1**).

The variance of the log-permeability is much smaller than the variances observed in the alluvial fan deposits and comparable to the variances observed in the fluvial/interfluvial facies-scale studies. This is consistent with the difference in depositional processes between the three environments. Since all of the facies originated from the same type of process the interfacies variability is small. Similarly, eolian deposits tend to be well sorted resulting in low intrafacies variability.

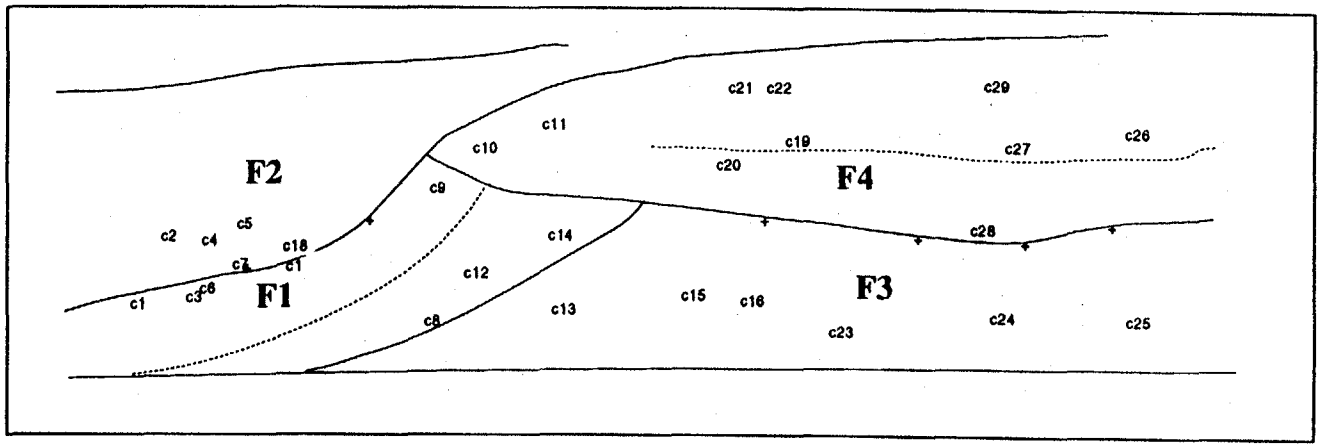

Figure 8.3. Map of lithologic facies and control points

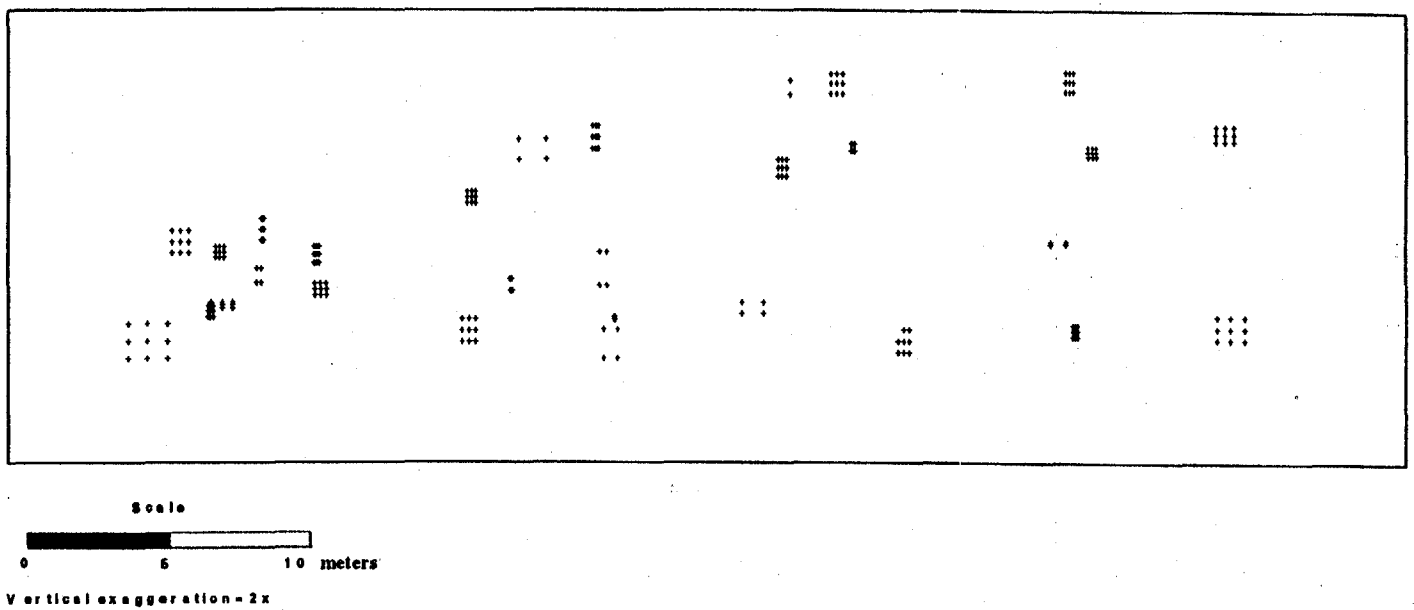

Figure 8.4. Permeability sample locations for eolian study

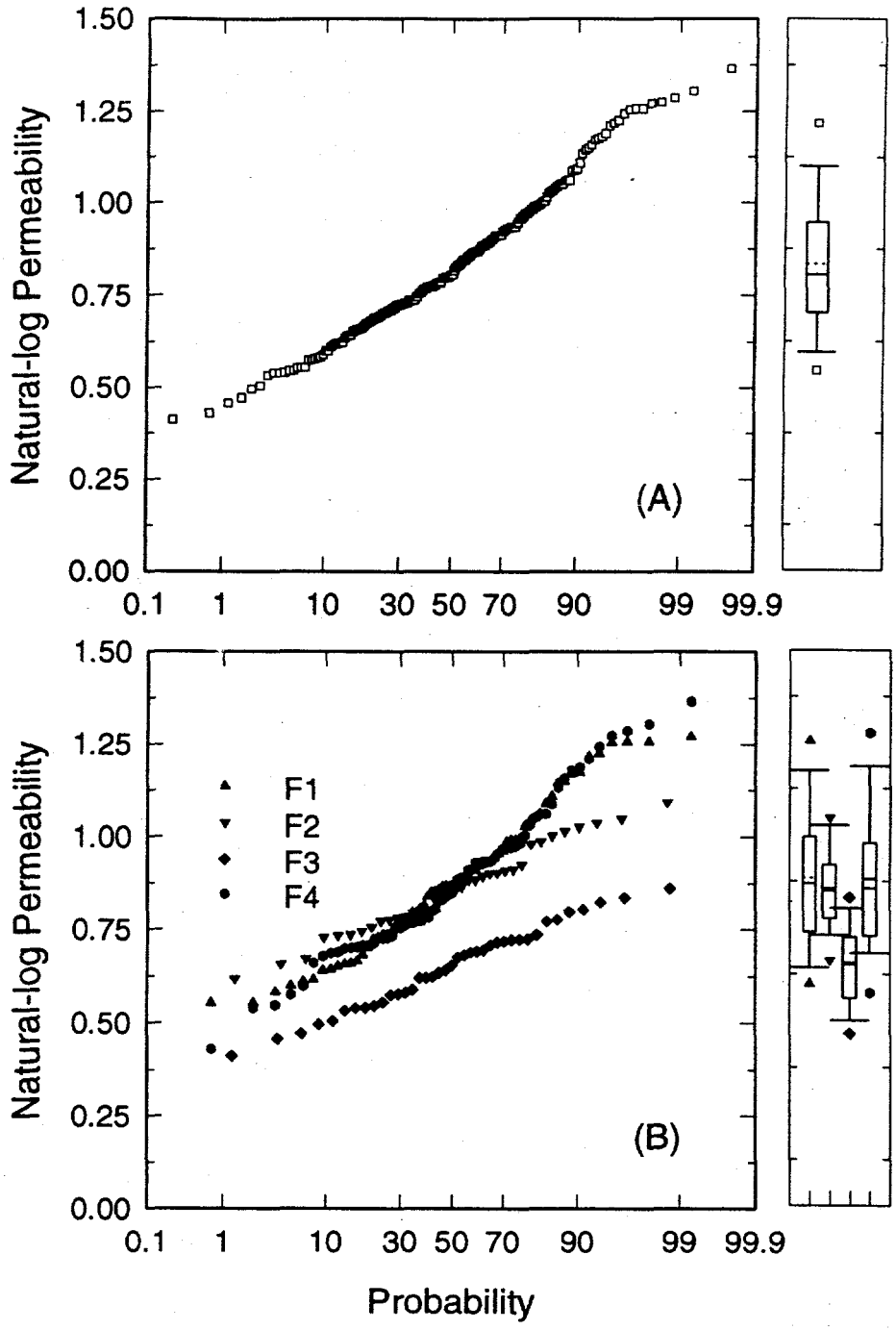

Figure 8.5. (a) Probability plot of log-permeability. N=211. (b) Probability plots of air-permeability separated according to lithologic facies.

Table 8.1 Summary of statistics for eolian log-permeability data set. Permeability in darcy units.

Data Set	N	μ [ln(k)]	σ^2
ALL	211	1.92	0.19
F1	68	2.04	0.19
F2	36	1.97	0.07
F3	39	1.49	0.07
F4	68	2.05	0.22

The variograms were estimated with variable lag spacing and are presented in **Figure 8.6.** For lags up to one meter, the unit lag was 0.20 meters. For lags greater than one meter, the unit lag was 2.5 meters. For the horizontal variogram, a search window with an angle tolerance of 45degrees and maximum bandwidth of two meters was also imposed. The same lag progression was used for the vertical variogram and a 45 degrees search window was used for the search window but no bandwidth was imposed.

A nested correlation structure is apparent for both variograms at small lags. A nugget of 0.04 is employed to represent measurement error and correlation below the detection of the LSAMP. A nested exponential-"bell-shaped" model is used to fit the variogram estimates.

$$\gamma_h(\xi) = 0.04 + 0.06\,[1 - \exp(\frac{-|\xi|}{0.15})] + 0.11\,[1 - \exp(\frac{-|\xi|^2}{(5.3)^2})]$$

$$\gamma_v(\xi) = 0.04 + 0.06\,[1 - \exp(\frac{-|\xi|}{0.02})] + 0.10\,[1 - \exp(\frac{-|\xi|^2}{(0.8)^2})])]$$

The "bell-shaped" correlation structure is similar to that observed in the paleosol facies studies (Chapter 5). The eolian deposits differ from the paleosols in that internal bounding surfaces are present in the eolian deposits. However, those surfaces separate regions with similar mean permeability and thus do not greatly inhibit the smoothness of the variability.

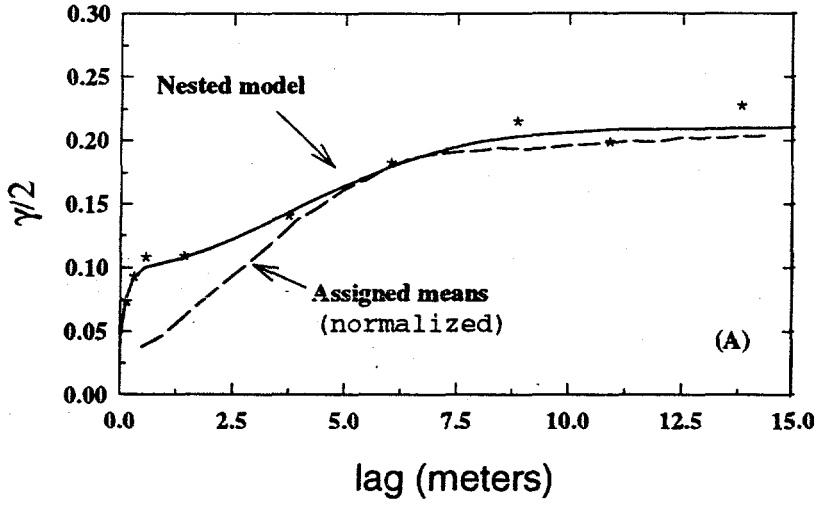

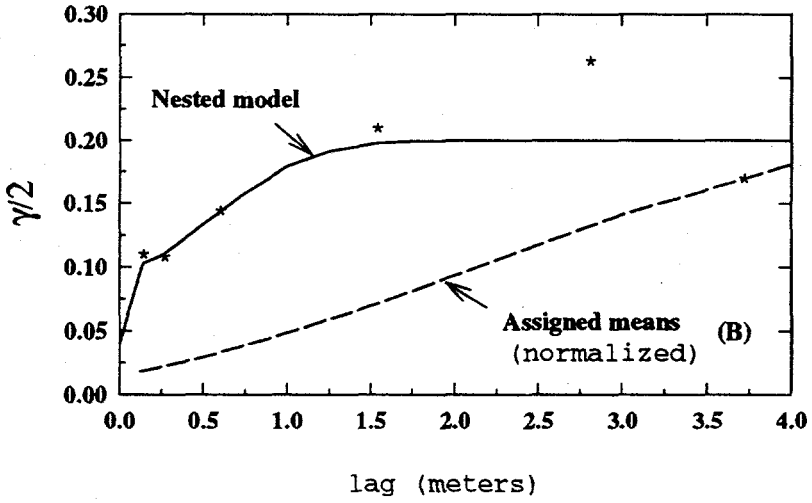

Figure 8.6. (a) Horizontal, and (b) vertical variogram estimates (*) of logarithmic permeability data with fitted model (solid line) and the assigned mean log-permeability model (dotted line).

The appearance of the "bell-shaped" variogram estimates and the relatively smooth nature of the heterogeneity, prompted the investigation of the threshold crossing approach to estimate correlation lengths from the observed geological features. Log-permeability in only one of the mapped facies (F3) is consistently below the mean. The log-permeability in the other facies is on average slightly higher than the mean. The mean was taken as the threshold and the facies boundaries were taken as the boundaries of regions that, on average, separate regions above and below the mean. In addition, since the mean was the threshold used, both regions above and below the mean were used in estimating the average dimensions. This results from the symmetry of the threshold crossing theory. The average dimensions of the facies were estimated from the facies shown in Figure 8.2 and are 18.5 and 3.2 meters in the horizontal and vertical directions, respectively. This translates into estimated "bell-shaped" correlation lengths of 4.2 and 0.7 meters. These values correspond well to the fitted values of 5.3 and 0.8 meters. At the present time the influence of the nugget and the small-scale exponential correlation structure on the threshold crossing theory is unclear. However, a pure nugget representing a lack of small-scale correlation would be expected to diminish the clarity of the boundaries of the regions of excursion.

The assigned mean methodology was also employed to estimate correlation structure from the observed geological features. The facies map of Figure 8.2 was digitized and respective estimated means of the facies were assigned. The variogram estimate for the assigned mean data set used the same search window as the variogram estimate of the data. As in Chapter 7 this method provides a good estimate of the range in the horizontal direction but in this case overestimates the correlation at small lags since the assigned means are perfectly correlated within facies.

CONCLUSIONS

The study in the eolian deposits of the Popotosa Formation is a good illustration of the differences in permeability statistics for a different depositional setting. The variance of log-permeability of the eolian deposits is much lower than the variance of log-permeability of the

alluvial fan deposits of the Nevada Test Site and the interfluvial/fluvial deposits of the Sierra Ladrones Formation.

The correlation structure of log-permeability in the eolian deposits appears to exhibit a large nugget and "bell-shaped" variogram. Both of these differ from the results of the other deposits studied.

PART V

DISCUSSION AND CONCLUSIONS

CHAPTER 9: CONCEPTUAL MODEL

INTRODUCTION

The challenge facing hydrogeologists of predicting fluid flow through heterogeneous media is two-fold. First, a quantitative representation of the spatial variation of hydrologic properties is necessary. Then, a body of theory is necessary for predicting fluid flow and solute transport through heterogeneous media. The development of theory has experienced significant progress in the last two decades with the application of stochastic models to flow and transport through heterogeneous media (e.g. Gelhar and Axness, 1983; and Neuman, 1990).

This theoretical advance provides a quantitative framework and a set of specific questions for the investigation of the nature of heterogeneity. The quantitative framework adopted here is that of stochastic groundwater hydrology. This framework is preferred over deterministic facies modeling (e.g. Anderson, 1989) since the models explicitly account for the uncertainty associated with the subsurface. One of the main objectives of this study was to develop a framework for incorporating geological information into the characterization of heterogeneity. This chapter utilizes the results of the outcrop studies to develop a generalized conceptual model of the relationship between sedimentological features and geostatistical properties. Here, geostatistical properties refer primarily to the univariate probability distribution, the spatial correlation structure, and a qualitative ranking of the continuity of regions exhibiting similar mean permeabilities.

The proposed conceptual model addresses two aspects of geostatistical characterization. First, a geostatistical characterization entails the selection of a random field model. In this aspect, the overall spatial characteristics of a deposit as inferred from sedimentological models can yield insight into which model is best suited to represent heterogeneity in a particular type of deposit. While at present the relationship between sedimentological models and random field models is largely qualitative, it is in many respects superior to incorporating no physical

information. The second aspect of geostatistical characterization is the estimation of the random field model parameters. The correlation structure is an important feature of many of the random field models and was the focus of this study.

BACKGROUND

The conceptual model is an attempt to provide some integration of the fields of stochastic subsurface hydrology and clastic sedimentology, particularly the aspects of the disciplines that focus on the spatial distribution of properties. For stochastic subsurface hydrology, this is the adoption of a random field model of heterogeneity for either analytical or numerical modeling of flow and transport. In sedimentology, this is the study of the relationship between the observed spatial distribution of lithologic units and the physical processes of deposition.

Geostatistical Framework

In recent years a wide variety of statistical models have been proposed in the literature to represent the spatial variation of permeability. Each model is based on a different method for mathematically representing or computationally generating spatially-correlated random variables and each exhibits overall differences in appearance. The most common model is the multi-variate Gaussian model that represents the hydraulic conductivity as a log-normal distribution at each location with a single scale of correlation. The spatial variation of hydraulic conductivity in these models is continuous and relatively smooth. The primary benefit of such a conceptualization is that the equations of flow and transport can be solved analytically (e.g. Bakr et al., 1978; Gelhar and Axness; 1983). Results of field tracer experiments generally show good comparison between the theoretical models and the observed plume behavior (e.g. Freyberg, 1986; Garabedian et al., 1991). The main disadvantage of the multi-variate Gaussian model is the tendency for regions of extreme (high and low) values to be isolated and volumetrically under-represented (Journel and Alabert, 1988).

Deviations of the macrodispersivity predicted by the multi-variate Gaussian model and that observed in the field have been attributed a variety of unmodeled physical processes (e.g.

non-uniform or time-varying flow field, or spatial variability of porosity) and uncertainty associated with the estimation of the hydraulic conductivity correlation length and variance (Hess et al., 1992). These various factors could undoubtedly result in the observed difference. However, another possible reason for the discrepancy between predicted and observed dispersivities is the appropriateness of the multi-variate Gaussian conceptualization of heterogeneity.

The multi-variate Gaussian model can also be used to represent multiple scale heterogeneity. Several workers (e.g. Wheatcraft and Tyler, 1988; Hewitt and Behrens, 1990; Neuman, 1990) have proposed that the fractal model may be more appropriate for geological media. Geological features are known to occur at a variety of scales, however the degree to which this is manifested in a self-similar correlation structure of permeability has yet to be evaluated. Results of the field studies presented here indicate that the fractal model may be useful as a special case but generally is not warranted.

Burrough (1983a, 1983b) assessed the applicability of the fractal model to the spatial variation of soil properties along a one-dimensional transect but preferred a nested non-fractal model in which a finite number of correlation lengths correspond to the scales of the dominant pedogenic processes. The non-fractal nested model (Burrough, 1983b) preserves the abrupt change in soil properties at the large scale that result from abrupt changes in parent material and the smaller-scale processes such as bioturbation and chemical weathering.

Also, in an effort to simulate abrupt spatial changes in properties, Colarullo and Gutjahr (1991) have proposed a multi-dimensional model of heterogeneity based on a discrete Markov random field. The Markov RF model enables the definition of a finite number of states which can be thought of as lithologic types. Each lithologic type then corresponds to a characteristic permeability. The Markov RF model is fundamentally a single-scale, multi-modal, discrete representation of heterogeneity.

The random field models of heterogeneity described differ in their mathematical formulation and the details of implementation. In this context however, the point of interest is how they differ in their overall spatial statistical properties. Such statistical properties include

the permeability probability distribution, the spatial correlation of permeability, and the spatial continuity of relatively homogeneous regions. Incidentally, while each model differs in their basic characteristics, they can be superposed in varying combinations to honor a variety of spatial properties. **Table 9.1** summarizes the characteristics of some of the proposed random field models.

Table 9.1. Summary of random field model characteristics with respect to modality and spatial correlation.

Random Field Model	Multi-modal	Multi-scale	Continuity
Multivariate Gaussian	No	No	Low
Fractal	No	Yes	Low
Nested non-fractal	Yes	Yes	High
Indicator	Yes	Yes	Moderate
Markov	Yes	Yes	High

Sedimentological Framework

The sedimentological framework of interest is the process/product relationship of clastic sedimentology. The underlying premise of sedimentology is that a suite of sedimentary features observed over a variety of scales can be associated with a suite of depositional processes. Based on field observations of sedimentary deposits of modern and well-understood processes, sedimentologists have developed a set of models relating the overall sedimentological characteristics to the depositional environment (suite of processes). The relationship from modern environments is then applied to observations in ancient deposits to infer the depositional processes. In the context of the conceptual model relating sedimentological models to geostatistical models, the process/product relationship is extended to relate the depositional product with a suite of geostatistical properties (process/product/properties). This provides a physical basis for the stochastic modeling of

heterogeneity.

GENERALIZED CONCEPTUAL MODEL

The conceptual model is based on the general hypothesis that there exists a relationship between observable geological features and quantitative parameters suitable for characterizing the spatial distribution of permeability. Observable geological features include sedimentary structures, lithologic facies, architectural elements and the surfaces separating these volume filling entities. Quantitative hydrogeological parameters include the permeability probability distribution, the spatial statistical correlation of permeability, and the spatial continuity of relatively homogeneous regions.

The field of sedimentology is based on the premise that deposits resulting from different combinations of depositional processes differ in 1) the type of lithofacies, 2) the spatial dimensions of the lithofacies, and 3) the spatial association of the lithofacies. A corollary to the general hypothesis can then be stated in that: "the geological controls governing the occurrence and spatial distribution of geologic features also govern the overall geostatistical properties".

Results of the outcrop studies presented indicates relationships between 1) the occurrence of lithofacies with the modality of the permeability distribution, and 2) the spatial dimensions and orientations of hierarchical bounding surfaces with the permeability correlation structure. From these relationships, two aspects of geostatistical characterization are addressed. First, the selection of the most appropriate model of heterogeneity under a given set of geological conditions, and second, the estimation of the correlation structure.

Selection of random field model

Currently, in hydrologic studies of the influence of heterogeneity on solute transport, the selection of random field models is not based on any compelling field evidence. Much debate has arisen from various workers speculating on the stochastic models best suited to represent heterogeneity and universal laws for the estimation of hydrologic effective properties (e.g.

Journel and Alabert, 1988; Gelhar et al., 1992; Neuman, 1990, 1993; and Gelhar et al., 1993). These studies often concede that a better understanding of the nature of heterogeneity is necessary before an educated choice of model can be made.

Figure 9.1 suggests a framework for selecting a random field model based on geological information. Essentially, two geostatistical properties are used in the selection. One is the permeability univariate behavior, and the second is the nature of the correlation structure. The arrows drawn to the various types of random field models based on different combinations of modality and scaling are only examples; many more combinations exist.

The "modality" refers to the number of discernable sub-populations within the overall population. The results of the field studies presented indicate that the different observed lithologic facies tend to exhibit different mean permeability. As a result, it is proposed that the "modality" can be inferred from an understanding of the specific lithologic facies present and their relative abundances.

In addition, the results of this study indicate a relationship between the spatial dimensions and orientations of the sediments separated by a hierarchy of bounding surfaces and the overall characteristics of the correlation structure. This is the second component proposed for the selection of the most appropriate random field model.

For example, in the Sierra Ladrones study, the occurrence of the four main architectural element conprised of fluvial sand/gravel, sand, silt/clay, and paleosols indicate a multi-modal distribution of permeability. In addition, the results of Chapters 5 and 6 indicate a multi-scale correlation structure arising from the hierarchical bounding surfaces. From Figure 9.1, a hybrid Markov-Multivariate Gaussian random field model appears most appropriate for representing the heterogeneity.

The alluvial fan deposits presented in Chapter 7 exhibit a weakly multi-modal distribution arising from the occurrence of two depostional units that exhibit different mean log-permeability: sheet floods and debris flows. The continuity of regions exhibiting similar mean permeability, that is the hydrogeologic units, was observed to be on the order of tens of meters and the spatial changes in permeability were not extremely abrupt. Based on the

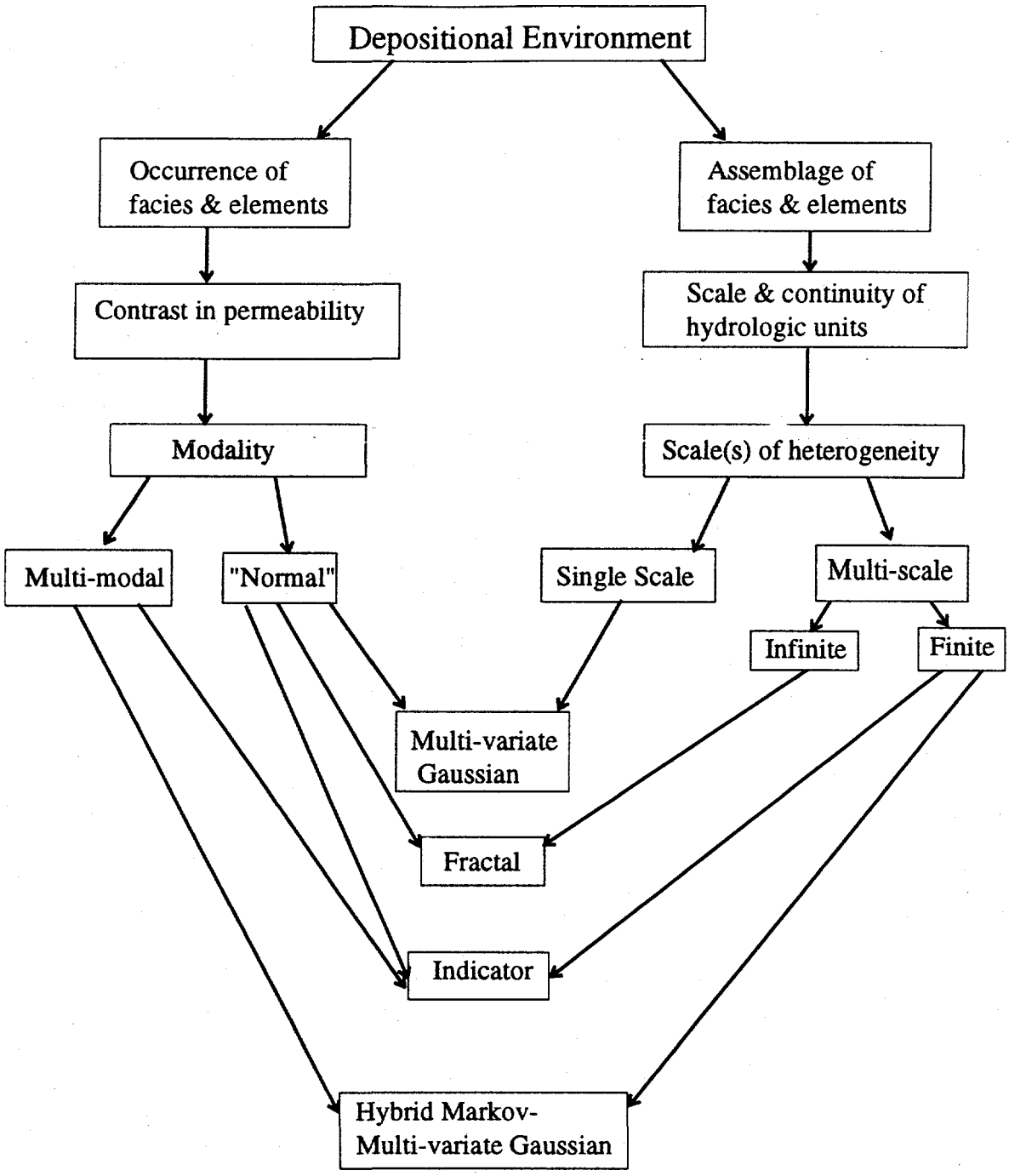

Figure 9.1. Conceptual model relating the characteristics of depositional environment and sedimentological model to random field models of heterogeneity.

occurrence of two main types of lithologic (hydrogeologic) units of different depositional mechanisms, the conceptual model (Figure 9.1) would suggest a multi-modal distribution of log-permeability. The spatial assemblage of lithologic units can be characterized as relatively uniform over scales of tens of meters and, according to the conceptual model, a single scale of variability would be sufficient. Given the characteristics of the modality and the correlation structure, a random field model could be chosen. In this case, a random field based on the indicator approach may be most applicable.

The eolian deposits on the other hand consist of one type of lithologic facies separated by bounding surfaces of a single level in the hierarchy. A "normal", single-scale process would be a reasonable first selection for characterizing the heterogeneity in that deposit. From the conceptual model, this would imply that a multi-variate Gaussian model would be most appropriate for these deposits. The small-scale correlation observed in the actual deposits may be the result of diagenetic alteration which is not explicitly accounted for in the current conceptual framework. However, if the spatial distribution of the diagenesis and the effects of the specific diagenetic alteration on permeability were better understood, they could be superimposed to arrive at a nested model.

Incorporating the results of this study into the selection of the most appropriate random field model is still somewhat subjective. However this model provides a physically-based framework on which to ground the continued debate of the most appropriate random field model for the characterization of geological heterogeneity. In the future quantitative methods of discriminating between random field models based on field data would enable some degree a validation of the proposed model. The measure of spatial entropy (Journel and Deutsch, 1993) may be of some assistance. To date, the estimation has been performed only on exhaustive data sets of simulated fields and only subtle (15%) differences in entropy were reported. Application to sparse data sets with measurement error is expected to be of limited use.

Quantitative estimates of correlation statistics

In addition to developing a framework for the selection of the most appropriate random field model of heterogeneity, the results of the studies indicate that some aspects of the correlation structure can be estimated from geological information. One approach is the method of assigning mean permeabilities to a map of the spatial distribution of lithofacies to estimate the variogram. This approach appears to provide a reasonable estimate of the overall shape and range of the correlation structure. Another method for estimating the correlation length from geological information is the threshold crossing approach. This approach appears to work reasonably well, however it is difficult to define regions of excursion above or below a threshold and maintain confidence in the underlying assumption of a continuously varying and smooth process.

While both of these approaches may prove useful in the estimation of correlation parameters, they do not have a physical geological basis. As such, they do not provide a geological foundation on which to investigate the presence or absence of a fundamental relationship between depositional processes and statistical models of heterogeneity. Clearly, such a relationship must be investigated within a geological framework that physically relates depositional processes and products and allows for quantitative analysis of geostatistical characteristics.

The results of the facies-scale (Chapter 5) and architectural-element-scale studies (Chapter 6) of heterogeneity indicate that the hierarchical bounding surface framework may provide such a foundation for investigating the basic quantitative relationship between the depositional processes and the characteristics of the spatial correlation structure. For the vertical variograms, the ranges appear to coincide with the average dimensions of regions bounded by first and second order surfaces. For the lower variability deposits, the variogram exhibited exponential behavior, and for deposits exhibiting more variability (ES1), the variogram exhibited a nested linear behavior with the second-order bounding surfaces contributing the majority of the overall variability. The paleosols did not contain internal bounding surfaces and exhibited a smoothly varying permeability as indicated by the "bell-shaped" correlation

structure. At the larger scale, the correlation structure of the architectural-element mean permeability coincided with the directions of the large-scale depositional processes.

The relationship between bounding surfaces and geostatistical models appears amenable to theoretical development. In the studies that possess bounding surfaces, the model of Burrough (1983b) presented in Chapter 5 provides a simple example of the spatial correlation of soil properties as a function of a hierarchy of pedogenic controls. Also the lack of bounding surfaces is reflected in the observed "bell-shaped" correlation structure. For Gaussian random fields exhibiting a "bell-shaped" correlation structure, theoretical models such as the threshold crossing are applicable.

For the model of discrete heterogeneity presented by Burrough (1983b), further theoretical development is necessary. Some important characteristics of such theoretical development include: 1) extension to multiple spatial dimensions; 2) accounting for variable ranges of processes in the hierarchy; and 3) further work on the physical significance of the weighting parameters.

CONCLUSIONS

The results of the outcrop studies of heterogeneity provide insight into a relationship between sedimentological properties and geostatistical characteristics. From these results, a generalized conceptual model was constructed to relate two fundamental characteristics of sedimentological models of depositional environment with two fundamental properties of geostatistical models of heterogeneity. Specifically, sedimentological models are based on the occurrence and spatial distribution of lithofacies and/or architectural elements. The occurrence of a suite of lithofacies can be used to estimate the basic properties of the probability distribution function of a geostatistical model. Information about the spatial distribution of these lithofacies can be used to infer basic characteristics of an appropriate spatial correlation structure.

The results of the outcrop studies also indicate that the geological classification of hierarchical bounding surfaces may provide a means of better understanding geological

heterogeneity under different depositional settings.

CHAPTER 10: CONCLUSIONS

The objective of this study was two-fold. The first objective was to obtain intensive data sets of the spatial distribution of permeability and observed geological features in a variety of geological settings then, second, to investigate the relationship between the observed sedimentological characteristics and quantitative models of heterogeneity. Three outcrop studies were conducted in which the spatial distribution of permeability was mapped along with geological features. The main field site was at an outcrop of the Pliocence-Pleistocene Sierra Ladrones Formtion in central New Mexico. Four main architectural elements were defined and mapped over a 20 meter vertical section along two kilometers of outcrop. Approximately 2,000 permeability measurements were obtained. Two other studies were conducted on outcrops of different depositional origin. The first of the supplemental studies was conducted on walls of waste pits cut into alluvial fan deposits at the Nevada Test Site. Two subperpendicular pit walls were mapped and approximately 500 permeability measurements were obtained. The other supplemental study was conducted south of Socorro, New Mexico on an outcrop of Miocene eolian dune deposits. Approximately 200 permeability measurements were obtained. In the process of these various studies, a set of methods for the data collection and analysis were developed. The methods are applicable to other studies of similar nature. Geostatistical anlaysis of the data provides important information and insight into the nature of the spatial variation of permeability in clastic sedimentary materials. The results of the various studies collectively provide a basis for constructing a conceptual model relating sedimentological models and geostatistical models of heterogeneity.

SIGNIFICANT METHODS DEVELOPED

Air-Minipermeameter

The lighweight, syringe-based, air-minipermeameter (LSAMP) represents another significant contribution to the methods of outcrop studies of heterogeneity in weakly lithified, high permeability materials in rugged terrain. The device developed weighs two kilograms and provides rapid and accurate measurements of permeability for materials ranging from 0.5 to 200 darcy. The LSAMP is an improvement over previous similar devices in its portability and ability to operate at very small pressures (approximately one kilopascal).

Sampling Strategy

In the collection of field data, a sampling strategy was developed for the unbiased sampling of permeability over a variety of scales. The method was employed in various forms in the facies-scale studies (Chapter 5), the alluvial fan studies (Chapter 7), and the eolian study (Chapter 8). The two stage sampling of the facies-scale studies where additional data was collected one year after the initial sampling to improve the estimates for very small lags provide a means of assessing the method. Results of five facies-scale studies were presented. In the four studies that employed the unbiased nested sampling method, the variogram estimates of the secondary sampling coincide with the variogram estimates of the initial sampling. In the one study that did not employ the unbiased nested sampling method, the two variogram estimates differed considerably.

Approximate Photogrammetric Transform

An approximate photrammetric transformation was developed for the correction of the distortion associated with oblique photographs of outcrops. The complex natural logarithm transformation appears to provide an adequate means of projecting information on the distorted photo-mosaic to a rectangular grid. The method is advantageous in situations where the camera characteristics or the projection angle are not known.

CHARACTERISTICS OF HETEROGENEITY IN THE THREE DEPOSITIONAL ENVIRONMENTS

Sierra Ladrones: Interfluvial/fluvial deposits

The Sierra Ladrones Formation in the vicinity of the field site is interpreted as resulting from a combination of fluvial and interfluvial depositional processes. The occurrence of the four main architectural element types indicates deposition resulting from a high-energy channel system (CH-I), a lower energy channel and proximal flood plain system (CH-II), a distal flood plain (OF), a stable interfluvial environment (P). The spatial assemblage of the the architectural elements and the orientation of the channel scours indicate that the fluvial system was responding to some large-scale change of the basin, probably either climate or tectonic variations.

Statistical analysis of permeability within the sandy elements indicates that the architectural elements exhibit different mean log-permeability values. In addition, the mapped lithologic facies also tend to exhibit different mean log-permeability; however, the magnitude of the difference is less and occasionally a difference in the mean log-permeability between two adjacent facies cannot be detected. From a sedimentological perspective, this information may be generalized according to the hierarchical bounding surfaces that separate the lithologic facies and architectural elements. That is, the second-order bounding surfaces that separate lithologic facies correspond to boundaries of hydrogeologic regions exhibiting different mean log-permeability. Third and fourth-order bounding surfaces that separate architectural elements correspond to boundaries of larger-scale hydrogeologic regions exhibiting different mean log-permeability. Qualitatively, the magnitude of the difference of means also appears to correlate to the order of the bounding surfaces in the deposits studied.

In addition to defining hydrogeologic regions of different mean log-permeability, results of the geostatistical analysis indicate that bounding surfaces may provide a framework for relating geologic information to the permeability correlation structure. In the facies-scale studies, the behavior of the variogram differed in locations that exhibited different bounding surface characteristics. Namely, the paleosols do not contain internal bounding surfaces and

tend to exhibit a fairly smooth spatial variation of log-permeability as indicated by the "bell-shaped" variogram. The fluvial sand deposits do contain internal bounding surfaces and tend to exhibit more short range variability as indicated by the exponential variogram. In the sand and pebble deposits where the bounding surfaces are well defined and mark distinct changes in mean log-permeability, the variogram exhibits a nested linear behavior with the dimension of the nested ranges closely corresponding to the respective average distances between the bounding surfaces.

The relationship between the bounding surfaces and the correlation structure was also observed in the architectural-element scale study. The behavior of the variogram closely corresponded to the inferred depositional environment. Based on a method of assigning mean log-permeability values to the architectural elements, the correlation structure in the horizontal direction exhibited maximum correlation in the N30W direction corresponding to the inferred direction of the ancestral tributary system. The shortest correlation length was in the N90E direction corresponding to the direction of the transition between proximal and distal floodplain deposition. In the vertical direction correlation lengths were observed on the order of a few meters corresponding with the average thickness of the architectural elements.

Nevada Test Site: Alluvial fan

The heterogeneity in the alluvial fan deposits of the Nevada Test Site can be characterized as relatively high variance, two-scale heterogeneity. The high variance is attributed to the high degree of variability within and between the depositional processes of sheet flood, debris flow, and subsequent pedogenesis. Collectively, these processes result in deposits ranging from very coarse and moderately sorted to fine and poorly sorted. Based on 505 measurements of air-permeability, the geostatistical analysis of the data collected indicates 1) permeability is log-normally distributed in the areas studied, 2) the means of the debris flow and sheet flood material appear to be different, and 3) correlation length structure exhibits two distinct scales. The first structure reaches a sill at approximately 0.2 meters and the larger-scale horizontal structure attains a sill at approximately five meters.

Popotosa: Eolian deposits

The heterogeneity in the eolian deposits of the Popotosa Formation can be characterized as low variance with a nested correlation structure. The low variance is attributed geologically to the predominance of one type of lithologic facies (grain-fall) that is relatively homogeneous. The multi-scale correlation structure was fit with a nested exponential-"bell-shaped" model. Of the deposits studied, diagenetic alteration is most pronounced in this deposit. From macroscopic observations, the amount of cement appears to vary in a continuous fashion ranging from well cemented concretions to friable sand. Without a more detailed study of the impact of diagenesis on permeability, it is difficult to assess what role the alterations play in the overall correlation structure.

GENERAL CONCLUSIONS

The heterogeneity in the three deposits studied differed significantly. In each case, the characteristics of the heterogeneity can be explained in terms of the processes of deposition and subsequent alteration. From this exercise, it was possible to construct a conceptual model relating the processes of deposition to the general characteristics of geostatistical models. The conceptual model serves several functions. First, it provides a framework for interpreting information on the form of sedimentological models for application in geostatistical modeling. Second, it provides a physical basis for developing and testing further hypotheses regarding geostatistical modeling of heterogeneity.

The conceptual model presented is largely qualitative. However, the results of the data analyses indicate that the classification scheme of hierarchical bounding surfaces may provide an important quantitative component to the link between depositional processes and geostatistical models.

FUTURE WORK

Recommendations for future work fall into three main categories. The first area coincides with the emphasis of this study, namely investigations of the physical heterogeneity of

geological material. Second, future work is needed in the area of theoretical developments focusing on specific quantitative tools that would aid in the analysis and prediction of realistic distributions of permeability.

Several issues regarding the physical heterogeneity of geological deposits deserve further attention. First, the relationship between the hierarchical bounding surfaces and correlation structure may provide a powerful tool in the characterization of aquifer heterogeneity. Field studies of continuous exposures will be necessary to understand how the small-scale bounding surfaces progress with increased scale and the influence on the correlation structure. Such studies will require intensive field sampling so that the probability distribution and correlation statistics can be estimated at a variety of scales.

Transporting the results of the bounding surface-correlation structure model to the subsurface will need to be tested via tracer tests. In this phase, appropriate geophysical methods should be investigated to condition the model on a particular level of bounding surface.

Another related area of research that will require future work is the sedimentology of recent geologic deposits. Quantitative mapping of bounding surfaces in deposits with well-understood depositional processes will not only enhance the process/product relationship of sedimentology but will also provide valuable information for the characterization of aquifer heterogeneity. Also, studies of the diagenesis of aquifer material will be necessary to understand heterogeneities resulting from post-depositional processes. Both of these types of information will be vital for the successful incorporation of geologic information into quantitative models.

In the area of theoretical developments, the primary need is a quantitative framework for multi-dimensional nested processes exhibiting discrete behavior. Such a framework is necessary for 1) quantification of field studies of heterogeneity, 2) simulation of realistic random fields exhibiting nested, non-fractal correlation, and 3) quantification of the uncertainty associated with the different levels of the nested structures.

REFERENCES CITED

Adamson, A.W., 1979, A textbook of physical chemistry: Academic Press, New York.

Allen, J.R.L.. 1974, Studies in fluviatile sedimentation: Implication of pedogenic carbonate units, Lower Old Red Sandstone, Anglo-Welsh Outcrop: Journal of Geology, v. 9, p. 181-208.

Allen, J.R.L., 1983, Studies in fluviatile sedimentation: bars, bar-complexes and sandstone sheets (low sinuosity braided streams) in the Brownstones (L.Devonian), Welsh Borders: Sedimentary Geology, v. 33, p. 237-293.

Anderson, M.P., 1989, Hydrogeologic facies models to delineate large-scale spatial trends in glacial and glaciofluvial sediments: Geological Society of America Bulletin, v. 101, p. 501-511.

Anderson, M.P., 1991a, Aquifer heterogeneity -- a geological perspective, *in* Bachu, S., ed., Proceedings Fifth Canadian/American Conference on Hydrogeology, Parameter Identification and Estimation for Aquifer and Reservoir Characterization, Calgary, Alberta, Canada, Sept. 18-20, National Water Well Association, Dublin, Ohio. p. 3-22.

Anderson, M.P., 1991b, Comment on "Universal scaling of hydraulic conductivities and dispersivities in geologic media" by S.P. Neuman: Water Resources Research, v. 27, p. 1381-1382.

Armstrong, M., 1984, Common problems seen in variograms: Mathematical Geology, v. 16, p. 305-313.

Bakr, A.A., Gelhar, L.W., Gutjahr, A.L., and MacMillan, J.R., 1978, Stochastic analysis of spatial variability in subsurface flows 1. Comparison of one- and three-dimensional flows: Water Resources Research, v. 14, p. 263-271.

Bates, R.L and J.A. Jackson, 1984, Dictionary of Geological Terms, 3rd ed.: The American Geological Institute, Doubleday, New York, 571 p.

Bear, J. 1972, Dynamics of fluids in porous media: American Elsevier, New York, 764 p.

Birkeland, P.W., 1984, Soils and Geomorphology: Oxford University Press, London, 372 p.

Bryan, K., 1938, The Ceja del Rio Puerco: A border feature of the Basin and Range Province in New Mexico, Part II: Journal of Geology, v. 45, p. 1-16.

Bryan, K., and McCann, F.T., 1937, The Ceja del Rio Puerco: A border feature of the Basin and Range Province in New Mexico: Journal of Geology, v. 45, p. 801-828.

Burrough, P.A., 1983a, Multiscale sources of spatial variation in soil I. The application of fractal concepts to nested levels of soil variation: Journal of Soil Science, v. 34, p. 577-597.

Burrough, P.A., 1983b, Multiscale sources of spatial variation in soil II. A non-Brownian fractal model and its application in soil survey: Journal of Soil Science, v. 34, p. 599-620.

Chapin, C.E and Zidek, Jiri (editors), 1989, Field excursions to volcanic terrains in the Western United States, Volume I, Southern Rocky Mountain region: June 25-July 1, 1989, Santa Fe, NM: New Mexico Bureau of Mines and Mineral Resources, Memoir 46, 486 p.

Chandler, M.A., Kocurek, G., Goggin, D.J., and Lake, L.W., 1989, Effects of stratigraphic heterogeneity on permeability in eolian sandstone sequence, Page Sandstone, Northern Arizona: American Association of Petroleum Geologists Bulletin, v. 73, p. 658-668.

Colarullo, S.J., and Gutjahr, A.L., 1991, Characterization of aquifer heterogeneities using discrete Markov random fields (abstract), Eos, Trans. Amer. Geophysical Union, v. 72, p.

227.
Collinson, J.D., and Thompson, D.B., Sedimentary Structures: George Allen and Unwin, London, 194 p.
Collinson, J.D., 1986, Chapter 5: Deserts, *in* Reading, H.G., ed., Sedimentary Environments and Facies, Second Edition: Blackwell Scientific Publications, Boston. p. 95-122.
Cressie, N.A.C., 1991, Statistics for spatial data: John Wiley and Sons, New York, 900 p.
Cristakos, G., 1992, Random field models in earth sciences: Academic Press, New York, 474 p.
Davis, J.M., 1990, An approach to the characterization of spatial variability of permeability in the Sierra Ladrones Formation, Albuquerque Basin, Central New Mexico: M.S. Thesis, New Mexico Institute of Mining and Technology, Socorro, New Mexico, 136 p.
Davis, J.M., Colarullo, S.J., Phillips, F.M., and Lohmann, R.C., 1991, Alluvial aquifer heterogeneities in the Rio Grande valley: Implications for groundwater contamination: New Mexico Water Resources Research Institute Technical Completion Report No. 256, 111 p.
Davis, J.M., 1992, Greater confinement disposal heterogeneity study, Nevada Test Site, Area 5, Radioactive Waste Management Site, DOE/NV/10630-26 UC-721, 57 p.
Davis, J.M., Lohmann R.C., Phillips F.M., Wilson, J.L., and Love, D.W., 1993, Architecture of the Sierra Ladrones Formation, central New Mexico: Depositional controls on the permeability correlation structure: Geological Society America Bulletin, v. 105, p. 998-1007.
Davis, J.M., Wilson, J.L., and Phillips, F.M., 1994, A portable air-minipermeameter rapid in-situ field measurements: Ground Water, in press.
Denny, C.S., 1940, Tertiary geology of the San Acacia area, New Mexico: Journal of Geology, v. 48, p. 73-106.
Deutsch, C.V., and Journel, A.G., 1992, GSLIB: Geostatistical Software Library User's Guide: Oxford University Press: New York, 336 p.
Dickinson, W.T., Rudra, R.P., and Wall, G.J., 1985, Discrimination of soil erosion and fluvial sediment areas: Canadian Journal of Earth Scienes, v. 22, p. 1112-1117.
Dreyer, T., Scheie, A., and Walderhaug, O., 1990, Minipermeameter-based study of permeability trends in channel sand bodies: American Association of Petroleum Geologists Bulletin, v. 74, p. 359-374.
Eijpe, R., and Weber, K.J., 1971, Mini-permeameters for rock and unconsolidated sand: American Association of Petroleum Geologists Bulletin, v.55, p. 307-309.
Englund, E., and Sparks, A, 1988, Geo-EAS 1.2.1 User's Guide: EPA Report # 60018-91/008. EPA-EMSL, Las Vegas, Nevada.
Freyberg, D.L., 1986, A natural gradient experiment on solute transport in a sand aquifer 2. Spatial moments and the advection and dispersion of nonreactive solutes: Water Resources Research, v. 22, p. 2031-2046.
Garabedian, S.P., LeBlanc, D.R., Gelhar, L.W., and Celia, M.A., 1991, Large-scale natural gradient tracer test in sand and gravel 2. Analysis of spatial moments for a nonreactive tracer: Water Resources Research, v. 27, p. 911-924.
Gelhar, L.W., and Axness, C.L., 1983, Three dimensional stochastic analysis of macrodispersion in aquifers: Water Resources Research, v. 19, p. 161-180.
Gelhar, L.W., Welty, C., and Rehfeldt, K.R., 1992, A critical review of data on field-scale dispersion in aquifers: Water Resources Research, v. 28, p. 1955-1974.

Gelhar, L.W., Welty, C., and Rehfeldt, K.R., 1993, Reply: Water Resources Research, v. 29, p. 1867-1869.

Goggin, D.J., Chandler, M.A., Korcurek, G., and Lake, L.W., 1988a, Patterns of permeability in eolian deposits: Page Sandstone (Jurassic), Northeastern Arizona: Society of Petroleum Engineers Formation Evaluation, v. 3, p. 297-306.

Goggin, D.J., Thrasher, R., and Lake, L.W., 1988b, A theoretical and experimental analysis of minipermeameter response including gas slippage and high velocity flow effects: In Situ, v. 12, p. 79-116.

Gotkowitz, M.B., 1993, A study of the relationship between permeability distributions and small scale sedimentary features in a fluvial formation: Hydrology Program Open Report, New Mexico Institute of Mining and Technology, Socorro, New Mexico, 71 p.

Haldorsen, H.H., and Damsleth, D., 1990, Stochastic modeling: Journal of Petroleum Technology, April, p. 404-412.

Hess, K.M., Wolf, S.H., Celia, M.A., 1992, Large-scale natural gradient tracer test in sand and gravel, Cape Cod, Massachusetts 3. Hydraulic conductivity variability and calculated macrodispersivities: Water Resources Research, v. 28, p. 2011-2027.

Hewett, T.A., and Behrens, R.A., 1990, Conditional simulation of reservoir heterogeneity with fractals: Society of Petroleum Engineers Formation Evaluation, v. 5, p. 217-225.

Hirst, J.P.P, 1991, Variations in alluvial architecture across the Oligo-Miocene Huesca fluvial system, Ebro Basin, Spain: *in* Lidz, B.H., ed., The three-dimensional facies architecture of terrigenous clastic sediments and its implications for hydrocarbon discovery and recovery, Concepts in Sedimentology and Paleontology, v. 3: , Society of Economic Paleontologists and Mineralogists, Tulsa, Oklahoma.

Ingersoll, R.V., 1978, Petrofacies and petrologic evolution of the late Cretaceous fore-arc basin, Northern and Central California: Journal of Geology, v. 86, p. 335-352.

Isaaks, E.H., and Srivastava, R.M., 1989, An Introduction to Applied Geostatistics: Oxford University Press, New York, 561 p.

Johnson, N.M., and Dreiss, S.J., 1989, Hydrostratigraphic interpretation using indicator geostatistics: Water Resources Research, v. 25, p. 2501-2510.

Journel A.G., and Alabert, F.G., 1988, Focusing on spatial connectivity of extreme-value attributes: Stochastic indicator models of reservoir heterogeneities: Society of Petroleum Engineers paper 18324 presented at the 63rd Annual Technical Conference and Exhibition, Houston, October 2-5, p. 621-632.

Journel, A.G., and Huijbregts, Ch. J., 1978, Mining Geostatistics: Academic Press, New York, 600 p.

Journel, A.G., and Deutsch, C.V., 1993, Entropy and spatial disorder: Mathematical Geology, v. 25, p. 329-355.

Karara, H.M., ed., 1989, Non-topographic photogrammetry -Second Edition: American Society for Photogrammetry and Remote Sensing, Falls Church, Virginia, 445 p.

Katz, D.L. and Lee, R.L., 1990, Natural gas engineering: production and storage: McGraw-Hill Publishing Company, New York, 760 p.

Kerr, P.F., and Wilcox, J.T., 1963, Structure and volcanism, Grants Ridge area: *in* Kelley, V.C., (compiler), Geology and technology of the Grants Uranium Region: New Mexico Bureau of Mines and Mineral Resources Memoir 15, p. 205-213.

Kittridge, M.G., Lake, L.W., Lucia, F.J., and Fogg, G.E., 1989, Outcrop-subsurface comparisons of heterogeneity in the San Andres Formation: Society of Petroleum Engineers paper 19596, presented at 64th Annual Technical Conference, October 8-11, San Antonio, Texas, p. 259-273.

Lake, L.W., Carroll, H.B., and Wesson, T.C., 1991, Reservoir Characterization II: Academic Press, New York, 726 p.

Lipman, P.W., and Mehnert, H.H., 1980, Potassium-argon ages from the Mount Taylor volcanic field, New Mexico: U.S. Geological Survey Professional Paper 1124-B, 8 p.

Lohmann, R.C., 1992, A sedimentological approach to hydrologic characterization: A detailed three-dimensional study of an outcrop of the Sierra Ladrones Formation, Albuquerque Basin: Hydrology Program Open Report H92-5, New Mexico Institute of Mining and Technology, Socorro, New Mexico, 129 p.

Love, D.W., and Young, J.D., 1983, Progress report on the Late Cenozoic evolution of the Lower Rio Puerco: *in* New Mexico Geological Society Guidebook, 34th Field Conference, Socorro Region II, p. 277-284.

Lozinsky, R.P., 1988, Stratigraphy, sedimentology, and sand petrology of the Santa Fe Group and pre-Santa Fe Tertiary deposits in the Albuquerque Basin, Central New Mexico: Ph.D. Dissertation, New Mexico Institute of Mining and Technology, Socorro, New Mexico, 298 p.

Lozinsky, R.P., Hawley, J.W., and Love, D.W., 1991, Geologic overview and Pliocene-Quaternary history of the Albuquerque Basin, Central New Mexico: *in* Hawley J.W., and Love, D.W., eds., Quaternary and Neogene landscape evolution: A transect across the Colorado Plateau and Basin and Range provinces in West-Central and Central New Mexico: New Mexico Bureau of Mines and Mineral Resources Bulletin 137, p. 157-162.

Macedonio, G., and Pareschi, M.T., 1991, An algorithm for the triangulation of arbitrarily distributed points: Applications to volume estimate and terrain fitting: Computers and Geoscience, v. 17, p. 859-874.

Machette, M.N., 1978, Geologic map of the San Acacia quadrangle, Socorro County, New Mexico: U.S. Geological Survey Map GQ-1415, scale 1:24,000.

Mack, G.H. and Seager, W.R., 1990, Tectonic control on facies distribution of the Camp Rice and Palomas Formations (Pliocene-Pleistocene) in the southern Rio Grande Rift: Geological Society of America Bulletin, v. 102, p. 45-53.

McGrath, D.G., and Hawley, J.W., 1987, Geomorphic evolution and soil-geomorphic relationships in the Socorro area, Central New Mexico: *in* Mclemore, V.T., and Bowie, M.R., eds., Guidebook to the Socorro Area, New Mexico: New Mexico Bureau of Mines and Mineral Resources, Socorro, New Mexico, p. 55-67.

McKee, E.D., 1966, Significance of climbing-ripple structure: U.S. Geological Survey Professional Paper 550-D, p. D94-D103.

McKee, E.D., Crosby, E.J., and Berryhill H.L., Jr., 1967, Flood deposits, Bijou Creek, Colorado, June 1965: Journal of Sedimentary Petrology, v. 37, p. 829-851.

Miall, A.D., 1978, Lithofacies types and vertical profile models of braided river deposits. A summary: *in* A.D. Miall ed., Fluvial Sedimentology: Canadian Society of Petroleum Geologists Memoir 5, p. 597-604.

Miall, A.D., 1985, Architectural element analysis: A new method of facies analysis applied to fluvial deposits: Earth Science Reviews, v. 22, p. 261-308.

Miall, A.D., 1988, Facies Architecture in Clastic Sedimentary Basins: *in* Kleinsphen, K.L., and Paola, C., (eds.), New Perspectives in Basin Analysis: Springer-Verlag, New York, 452 p.

Miall, A.D. , and Tyler, N., 1991, The three-dimensional facies architecture of terrigenous clastic sediments and its implications for hydrocarbon discovery and recovery: *in* Lidz, B.H., ed., Concepts in Sedimentology and Paleontology, v. 3: Society of Economic Paleontologists and Mineralogists, Tulsa, Oklahoma.

Neuman, S.P., 1990, Universal scaling of hydraulic conductivities and dispersivities in geologic media: Water Resources Research, v. 26, p. 1749-1758.

Neuman, S.P., 1991, Reply: Water Resources Research, v. 27, p. 1383-1384.

Neuman, S.P., 1993, Comment on "A critical review of data on field-scale dispersion in aquifers" by L.W. Gelhar, C. Welty, and K.R. Rehfeldt: Water Resources Research v. 29, p. 1863-1865.

Phillips, F.M., Wilson, J.L., and Davis, J.M., 1989, Statistical analysis of hydraulic conductivity distributions: A quantitative geological approach: *in*, Molz, F., ed., Proceedings of the Conference on New Field Techniques for Quantifying the Physical and Chemical Properties of Heterogeneous Aquifers, Dallas, Texas, March 20-23, National Water Well Association, Dublin, Ohio, p. 19-31.

Poeter, E., and Gaylord, D.R., 1991, Influence of aquifer heterogeneity on contaminant transport at the Hanford Site: Ground Water, v. 28, p. 900-909.

Rehfeldt, K.R. and Gelhar, L.W., 1992, Stochastic analysis of dispersion in unsteady flow in heterogeneous aquifers: Water Research Research, v. 28, p. 2085-2099.

Rehfeldt, K.R., Gelhar, LW., Southard, J.B., and Dasinger, A.M., 1989, Estimates of macrodispersivity based on analysis of hydraulic conductivity variability at the MADE Site: Interim Rep. EN-6405, Electrical Power Research Institute, Palo Alto, Calif. , 132 p.

Sedgewick, R., 1990, Algorithms in C: Addison-Wesley Publishing, New York, 657 p.

Selner, G.I., and Taylor, R.B., 1991a, GSMAP Version 7: Graphics programs and related utility programs for the IMB PC and compatible microcomputers to assist compilation and publication of geologic maps and illustrations using geodetic or cartesian coordinates: U.S. Geological Survey Open File Report 91-1, Denver, Colorado, 151 p.

Selner, G.I., and Taylor, R.B., 1991b, GSMAP, GSMEDIT, GSMUTIL, GSPOST, GSDIG, and other programs version 8: For the IBM PC and compatible microcomputers to assist workers in the earth sciences: U.S. Geological Survey Open File Report 91-217, Denver, Colorado, 214 p.

Snyder, K.E., Parsons, and Gustafson, D.L., 1993, Field results of subsurface geologic mapping at the Area 5 Radioactive Waste Management Site DOE/Nevada Test Site, Nye County, Nevada: Report prepared by Raytheon Services Nevada Environmental Restoration and Waste Management Division, Las Vegas, Nevada, 144 p.

Spiegel, M.R., 1964, Schaum's outline of theory and problems of complex variables with an introduction to conformal mapping and it applications: McGraw-Hill, New York, 313 p.

Spiegel, Z., and Baldwin, B., 1963, Geology and water resources of the Santa Fe area, New Mexico: U.S. Geological Survey Water Supply Paper 1525, 258 p.

Stearns, C.E., 1953, Tertiary geology of the Galisteo-Tonque area, New Mexico: Geological Society of America Bulletin, v. 64, p. 459-507.

Sudicky, E.A., 1986, A natural gradient experiment on solute transport in a sand aquifer: Spatial variability of hydraulic conductivity and its role in the dispersion process: Water Resources Research, v. 23, p. 2069-2082.

Symon, K.R., 1971, Mechanics: Addison-Wesley, Menlo Park, 639 p.

Till, R.T., 1974, Statistical Methods for the earth scientist: Wiley and Sons, New York, 154.

Wheatcraft, S.W., and Tyler, S.W., 1988, An explanation of scale-dependant dispersivity in heterogeneous aquifers using concepts of fractal geometry: Water Resources Research, v. 24, p. 566-578.

Wright, H.E., Jr., 1946, Tertiary and Quaternary geology of the lower Rio Puerco area, New

Mexico: Geological Society of America Bulletin, v. 57, p. 383-456.
Young, J.D., 1982, Late Cenozoic geology of the lower Rio Puerco, Valencia and Socorro Counties, New Mexico: M.S. Thesis, New Mexico Institute of Mining and Technology, Socorro, New Mexico, 126 p.

APPENDIX A: AIR-MINIPERMEAMETER CIRCUITRY

The circuitry of the prototype device measures the time that is required for the piston to displace a known distance. From the measured time, the piston velocity and volumetric flow rate are obtained for the calculation of permeability.

The prototype circuitry consists of two sets of miniature photo-sensors (Microswitch®). Each set of sensors consists of an infrared light emitter and receiver. The sensors are insensitive to ambient light and operate on a 9 volt direct current (VDC) source. The photo-sensor pairs act as switches and are connected to a stop-watch via the circuitry shown in Figure A1. The photo-sensor "switch" (Figure A1) is open (9VDC) when the sensors are in contact and closed (ground) when the piston passes. This hi-lo signal is sent to a bounceless switch circuit (Figure A1). When the piston passes either pair of sensors, the photo-sensor switch closes, and the bounceless switch sends a square-wave pulse of duration 0.1 second to the OR-GATE. When the OR-GATE receives a square-wave pulse from either set of sensors, a 1.5 VDC pulse of duration 0.1 second is sent to the start-stop switch of the stopwatch. While the duration of the pulse is controlled by the circuitry, the shortest measurement time is approximately one-half second. Thus, the first pulse of 0.1 second ceases prior to the piston passing the second set of sensors.

The circuitry of the prototype device provides one example of how the signal from the photo-sensors can be sent to the stopwatch. The circuitry shown generally works well under laboratory and field conditions. However, a more sophisticated design would likely improve the power efficiency and minimize instrument problems in the field.

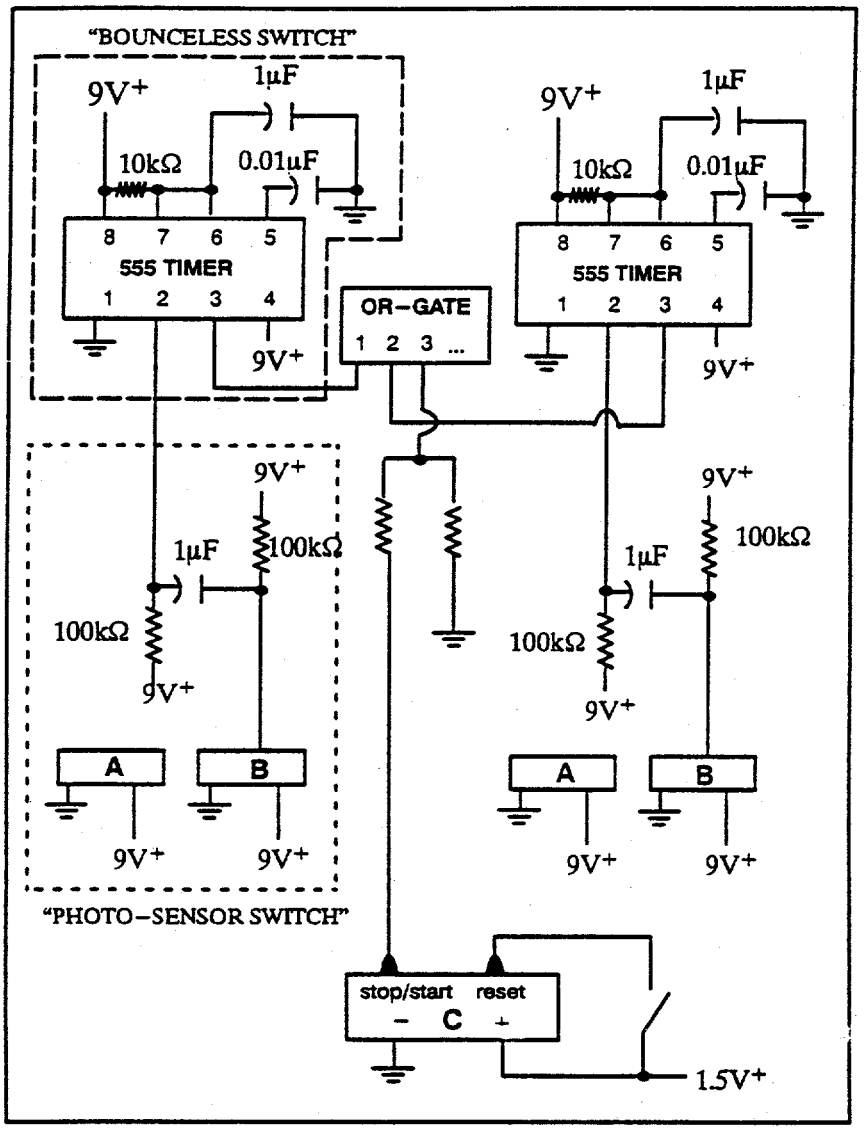

Figure A1. Circuit diagram for timing device. A=modulated light emitter; B=modulated light receiver; C=stopwatch.

APPENDIX B: AIR-PERMEAMETER DATA[6]

Sierra Ladrones Study

Nevada Test Site

Popotosa Formation (Eolian)

[6]Facies-scale data sets (Chapter 5) can be found in Gotkowitz (1993).

Date [yr mo dy]	Control Point	Facies	Arch. Element	Northing [meters]	Easting [meters]	Elev. [meters]	Perm. [darcy]
910516	14-1	p	p	-28.19	47.58	1526.10	1.06
910516	14-2	p	p	-28.19	47.58	1526.40	2.65
910516	14-3	p	p	-28.73	47.44	1526.10	1.66
910516	14-4	p	p	-28.73	47.44	1526.40	1.34
910516	14-5	p	p	-27.52	47.76	1526.10	1.25
910516	14-6	p	p	-27.52	47.76	1526.40	1.18
910516	15-1	p	p	-32.49	45.23	1526.10	1.26
910516	15-2	p	p	-32.71	45.11	1526.10	0.66
910516	15-3	p	p	-32.49	45.23	1526.40	5.53
910516	15-4	p	p	-32.71	45.11	1526.40	4.60
910516	15-5	p	p	-32.36	45.31	1526.10	1.23
910516	15-6	p	p	-32.36	45.31	1526.40	4.09
910516	16-1	sh	ch2	-33.25	45.99	1527.70	12.04
910516	16-2	sh	ch2	-33.50	46.43	1527.70	14.21
910516	16-3	sh	ch2	-33.50	46.43	1527.60	13.39
910516	16-4	p	p	-33.50	46.43	1526.90	1.47
910516	16-5	sh	ch2	-33.70	46.77	1527.70	16.61
910516	16-6	sh	ch2	-33.70	46.77	1527.60	13.76
910516	16-7	sh	ch2	-33.78	46.90	1527.60	16.89
910516	16-8	sh	ch2	-33.78	46.90	1527.60	13.51
910516	16-9	p	p	-33.88	46.90	1526.90	1.07
910516	16-10	p	p	-33.65	46.69	1526.90	2.36
910516	17-1	sh	ch2	-36.49	44.17	1528.60	7.49
910516	17-2	sh	ch2	-36.83	44.11	1528.60	4.72
910516	17-3	sh	ch2	-36.09	44.24	1528.60	7.82
910516	17-4	s	ch2	-36.09	44.24	1529.00	4.66
910516	17-5	p	p	-36.49	44.17	1529.00	4.83
910516	17-6	p	p	-36.49	44.17	1528.80	0.97
910516	17-7	p	p	-36.78	44.11	1528.80	3.94
910516	18-1	sp	ch2	-45.99	38.34	1528.60	14.93
910516	18-2	sp	ch2	-45.99	38.34	1528.90	12.70
910516	18-3	sr	ch2	-45.99	38.34	1529.30	8.20
910516	18-4	sr	ch2	-45.99	38.34	1529.50	4.51
910516	18-5	sp	ch2	-45.99	38.34	1529.40	17.50
910516	18-6	sh	ch2	-46.20	37.78	1528.60	17.09
910516	18-7	sr	ch2	-46.20	37.78	1529.30	5.52
910516	18-8	sp	ch2	-46.20	37.78	1529.40	16.80
910516	18-9	sr	ch2	-46.20	37.78	1529.50	5.86
910516	18-10	sh	ch2	-46.20	37.78	1529.00	11.19
910516	19-1	sr	ch2	-46.12	45.84	1533.80	8.89
910516	19-2	sr	ch2	-46.12	45.84	1534.00	14.28
910516	19-3	sr	ch2	-46.12	45.84	1534.20	5.11
910516	19-4	sr	ch2	-46.12	45.84	1534.40	3.28
910516	19-5	sr	ch2	-45.54	46.24	1533.80	7.64
910516	19-6	sr	chg	-45.54	46.24	1534.00	7.74
910516	19-7	sr	ch2	-45.54	46.24	1534.20	4.66
910516	19-8	sr	ch2	-45.54	46.24	1534.40	1.65

Date [yr mo dy]	Control Point	Facies	Arch. Element	Northing [meters]	Easting [meters]	Elev. [meters]	Perm. [darcy]
910516	19-9	sr	ch2	-44.97	46.65	1533.80	9.68
910516	19-10	sr	ch2	-44.97	46.65	1534.00	12.09
910516	19-11	sr	ch2	-44.97	46.65	1534.20	5.57
910516	19-12	sr	ch2	-44.97	46.65	1534.40	2.73
910516	19-13	sr	ch2	-44.68	46.85	1533.80	8.86
910516	19-14	sr	ch2	-44.68	46.85	1534.00	8.42
910516	19-15	sr	ch2	-44.68	46.85	1534.20	4.51
910516	19-16	sr	ch2	-44.68	46.85	1534.40	1.42
910520	20-1	p	p	-42.89	43.68	1529.10	1.31
910520	20-2	p	p	-42.29	43.78	1529.10	3.94
910520	20-3	p	p	-42.15	43.81	1529.10	1.98
910520	20-4	p	p	-41.65	43.90	1529.10	6.41
910520	20-5	p	p	-43.28	43.61	1529.50	1.96
910520	20-6	p	p	-43.48	43.57	1529.70	5.04
910520	20-7	p	p	-43.67	43.54	1529.10	2.40
910520	20-8	p	p	-44.46	43.40	1529.90	3.17
910520	20-9	p	p	-44.46	43.40	1529.70	4.69
910520	20-10	p	p	-46.43	43.05	1529.70	3.69
910520	20-11	p	p	-45.74	43.17	1528.80	3.22
910523	21-1	p	of	-23.93	48.68	1524.60	0.001
910523	21-2	p	of	-24.73	48.68	1524.60	0.001
910523	21-3	p	of	-23.33	48.68	1524.60	0.001
910523	21-4	fs	of	-23.93	48.68	1524.10	0.001
910523	21-5	fs	of	-24.73	48.68	1524.10	0.001
910523	21-6	fs	of	-23.33	48.68	1524.10	0.001
910523	21-7	fr	of	-23.93	48.68	1524.90	0.001
910523	21-8	fr	of	-24.73	48.68	1524.90	0.001
910523	21-9	fr	of	-23.33	48.68	1524.90	0.001
910523	22- 1	xx	xx	-52.03	43.68	1525.50	0.001
910523	22- 2	xx	xx	-52.03	43.68	1525.00	0.001
910523	22- 3	xx	xx	-52.03	43.68	1525.80	0.001
910523	22- 4	xx	xx	-52.17	43.30	1525.50	0.001
910523	22- 5	xx	xx	-52.17	43.30	1525.00	0.001
910523	22- 6	xx	xx	-52.17	43.30	1525.80	0.001
910523	23- 1	xx	xx	-52.58	30.75	1525.50	0.001
910523	23- 2	xx	xx	-52.58	30.75	1525.00	0.001
910523	23- 3	xx	xx	-52.58	30.75	1526.00	0.001
910523	23- 4	xx	xx	-52.40	31.74	1525.50	0.001
910523	23- 5	xx	xx	-52.40	31.74	1525.00	0.001
910523	23- 6	xx	xx	-52.40	31.74	1526.00	0.001
910523	24- 1	p	of	-34.87	78.79	1525.20	1.86
910523	24- 2	fs	of	-34.87	78.79	1525.60	0.001
910523	24- 3	p	of	-34.87	78.79	1525.90	2.75
910523	24- 4	fs	of	-34.87	78.79	1526.10	0.001
910523	24- 5	p	of	-34.87	78.79	1526.20	3.02
910523	24- 6	fsc	of	-34.87	78.79	1524.90	0.001
910523	24- 7	p	of	-33.39	78.53	1525.20	1.16

Date [yr mo dy]	Control Point	Facies	Arch. Element	Northing [meters]	Easting [meters]	Elev. [meters]	Perm. [darcy]
910523	24- 8	p	of	-33.39	78.53	1525.80	1.75
910523	24- 9	fs	of	-33.39	78.53	1525.40	0.001
910523	24- 10	fs	of	-33.39	78.53	1524.70	0.001
910523	25- 1	fs	of	-42.86	97.14	1525.10	0.001
910523	25- 2	fs	of	-42.86	97.14	1525.70	0.001
910523	25- 3	p	of	-42.86	97.14	1524.30	0.89
910523	25- 4	fsc	of	-42.56	97.66	1525.10	0.001
910523	25- 5	p	of	-42.56	97.66	1524.30	0.95
910523	26- 1	p	of	-71.08	126.03	1525.50	2.10
910523	26- 2	fs	of	-71.08	126.03	1525.70	0.001
910523	26- 3	p	of	-71.08	126.03	1526.00	2.25
910523	26- 4	fsc	of	-71.08	126.03	1526.10	0.001
910523	26- 5	p	of	-70.60	126.31	1525.50	2.95
910523	26- 6	fs	of	-70.60	126.31	1525.70	0.001
910523	26- 7	p	of	-70.60	126.31	1525.90	2.90
910523	26- 8	fsc	of	-70.60	126.31	1526.10	0.001
910523	26- 9	p	of	-71.60	125.73	1525.50	2.47
910523	26- 10	fs	of	-71.60	125.73	1525.20	0.001
910523	27- 1	p	of	-91.14	133.56	1525.50	2.02
910523	27- 2	st	ch2	-91.14	133.56	1525.90	39.76
910523	27- 3	fs	of	-91.14	133.56	1525.00	0.001
910524	28-1	p	p	-26.52	56.69	1531.60	3.94
910524	28-2	p	p	-26.52	56.69	1531.20	3.31
910524	28-3	p	p	-26.52	55.69	1531.60	6.87
910524	28-4	p	p	-26.52	55.69	1531.20	2.09
910524	28-5	sm	p	-26.52	55.69	1531.00	14.15
910524	28-6	p	p	-26.52	57.84	1531.60	4.03
910524	28-7	p	p	-26.52	57.84	1531.20	2.07
910524	29-1	p	p	-30.25	53.06	1531.60	2.82
910524	29-2	p	p	-29.22	53.77	1531.60	3.26
910524	29-3	p	p	-29.22	53.77	1531.10	5.60
910524	29-4	p	p	-30.25	53.06	1531.20	7.66
910524	29-5	p	p	-31.20	52.39	1531.60	2.09
910524	29-6	p	p	-31.20	52.39	1531.10	4.88
910524	29-7	p	p	-31.56	52.14	1531.60	2.10
910524	29-8	p	p	-31.56	52.14	1531.20	3.55
910524	29-9	p	p	-33.60	50.71	1531.60	3.96
910524	29-10	p	p	-33.60	50.71	1531.30	3.28
910524	30-1	sh	ch2	-38.25	53.83	1534.10	10.49
910524	30-2	sh	ch2	-38.06	53.88	1534.10	13.15
910524	30-3	sh	ch2	-38.45	53.78	1534.10	12.60
910524	30-4	sh	ch2	-38.45	53.78	1534.00	11.32
910524	30-5	sh	ch2	-38.25	53.83	1534.00	11.49
910524	30-6	sh	ch2	-38.06	53.88	1534.00	8.26
910524	30-7	sr	ch2	-38.25	53.83	1535.00	3.31
910524	30-8	sr	ch2	-37.85	53.94	1535.00	2.84
910524	30-9	sr	ch2	-38.54	53.75	1535.00	3.89

Date [yr mo dy]	Control Point	Facies	Arch. Element	Northing [meters]	Easting [meters]	Elev. [meters]	Perm. [darcy]
910524	31-3	sp	ch2	-28.65	57.76	1531.70	8.52
910524	31-4	sp	ch2	-29.05	57.07	1531.70	14.63
910524	31-5	sp	ch2	-29.05	57.07	1532.00	3.11
910524	31-6	sp	ch2	-29.05	57.07	1531.70	0.001
910524	31-7	sp	ch2	-29.05	57.07	1531.60	6.50
910524	31-8	sp	ch2	-29.05	57.07	1531.30	2.48
910524	32-1	p	p	-39.69	46.24	1532.20	0.001
910524	32-2	p	p	-39.69	46.24	1532.00	2.37
910524	32-3	p	p	-38.87	46.62	1532.00	1.54
910524	32-4	p	p	-37.87	47.08	1532.00	3.69
910524	32-5	p	p	-41.95	45.18	1532.00	5.98
910527	33-1	sh	ch2	-50.90	43.16	1534.10	9.44
910527	33-2	sh	ch2	-50.20	44.37	1534.10	6.46
910527	33-3	sh	ch2	-50.90	43.16	1534.60	8.76
910527	33-4	sr	ch2	-50.90	43.16	1534.90	8.22
910527	33-5	sr	ch2	-50.90	43.16	1535.00	6.78
910527	33-6	sr	ch2	-50.20	44.37	1534.90	7.90
910527	33-7	sr	ch2	-50.20	44.37	1535.00	5.75
910527	33-8	sr	ch2	-50.60	43.68	1535.00	3.91
910527	34-1	sh	ch2	-57.33	38.92	1534.10	7.92
910527	34-2	sr	ch2	-58.48	37.96	1534.10	8.49
910527	34-3	sr	ch2	-60.01	36.67	1534.10	13.33
910527	34-4	ssc	ch2	-60.01	36.67	1534.60	6.21
910527	34-5	sh	ch2	-58.48	37.96	1534.70	8.09
910527	34-6	sr	ch2	-58.48	37.96	1535.10	6.23
910527	34-7	sh	ch2	-57.33	38.92	1534.70	7.90
910527	34-8	sx	ch2	-57.33	38.92	1535.10	5.54
910527	34-9	fsc	ch2	-57.33	38.92	1535.20	0.001
910527	35-1	sr	ch2	-64.47	34.56	1534.70	5.78
910527	35-2	sr	ch2	-64.12	34.76	1534.70	3.35
910527	35-3	sl	ch2	-63.51	35.11	1534.70	2.60
910527	35-4	sh	ch2	-64.12	34.76	1534.40	7.45
910527	35-5	sx	ch2	-63.51	35.11	1534.30	7.01
910527	35-6	sl	ch2	-64.12	34.76	1533.70	8.09
910527	35-7	sl	ch2	-63.51	35.11	1533.70	7.12
910527	35-8	sx	ch2	-64.47	34.56	1535.00	11.44
910527	35-9	sx	ch2	-64.12	34.76	1535.00	18.04
910527	36-1	p	p	-52.24	37.58	1530.70	6.04
910527	36-2	p	p	-52.14	37.86	1530.70	7.72
910527	36-3	p	p	-52.14	37.86	1531.00	8.59
910527	36-4	p	p	-52.14	37.86	1531.40	4.18
910527	36-5	p	p	-52.24	37.58	1531.40	4.03
910527	36-6	p	p	-52.35	37.30	1531.40	3.37
910527	36-7	p	p	-52.35	37.30	1531.20	8.47
910527	36-8	p	p	-52.24	37.58	1531.20	3.48
910527	36-9	p	p	-52.24	37.58	1530.40	7.58
910527	36-10	fx	of	-52.24	37.58	1531.90	0.001

Date [yr mo dy]	Control Point	Facies	Arch. Element	Northing [meters]	Easting [meters]	Elev. [meters]	Perm. [darcy]
910527	36-11	fx	of	-52.14	37.86	1531.90	0.001
910527	37-1	p	p	-50.32	39.53	1530.70	5.29
910527	37-2	p	p	-50.17	40.11	1530.70	7.36
910527	37-3	p	p	-50.32	39.53	1531.80	7.09
910527	37-4	p	p	-50.22	39.92	1531.80	7.07
910527	38-1	sm	ch2	-60.66	43.59	1540.10	1.77
910527	38-2	sp	ch1	-60.66	43.59	1540.90	26.30
910527	38-3	st	ch1	-60.66	43.59	1541.10	64.14
910527	38-4	sm	ch2	-60.45	44.57	1540.20	2.94
910527	38-5	sp	ch1	-60.45	44.57	1540.90	7.70
910527	38-6	st	ch1	-60.63	43.68	1541.10	34.13
910527	39-1	sl	ch2	-55.29	46.45	1540.80	9.65
910527	39-2	sl	ch2	-55.01	46.55	1540.80	14.71
910527	39-3	sx	ch2	-55.29	46.45	1541.00	74.28
910527	39-4	sx	ch2	-55.01	46.55	1541.00	55.34
910527	39-5	st	ch2	-55.29	46.45	1541.30	60.88
910527	39-6	st	ch2	-55.01	46.55	1541.30	141.19
910527	40-1	p	p	-51.88	47.98	1538.40	2.48
910527	40-2	fsc	of	-51.88	47.98	1538.80	0.001
910527	40-3	sr	ch2	-51.88	47.98	1539.00	3.60
910527	40-4	p	p	-51.26	48.49	1538.40	2.09
910527	40-5	fsc	of	-51.26	48.49	1538.80	0.001
910527	40-6	sr	ch2	-51.26	48.49	1539.00	1.06
910527	40-7	p	p	-50.35	49.26	1538.40	2.41
910527	40-8	fsc	of	-50.35	49.26	1538.80	0.001
910527	40-9	sm	ch2	-50.35	49.26	1539.00	2.00
910527	41-1	sh	ch2	-41.03	79.46	1527.00	7.84
910527	41-2	sh	ch2	-41.03	79.46	1527.50	18.61
910527	41-3	sm	ch2	-41.03	79.46	1527.90	5.90
910527	41-4	st	ch2	-41.03	79.46	1528.30	4.93
910527	41-5	st	ch2	-41.23	79.12	1528.30	5.29
910527	41-6	st	ch2	-41.58	78.51	1528.30	11.32
910527	41-7	fx	ch2	-41.03	79.46	1528.50	0.001
910527	41-8	fx	ch2	-41.23	79.12	1528.50	0.001
910527	41-9	st	ch2	-41.58	78.51	1528.60	7.07
910527	42-1	sx	ch2	-46.09	82.21	1528.00	7.96
910527	42-2	sx	ch2	-46.41	81.82	1528.00	4.66
910527	42-3	sx	ch2	-46.73	81.44	1528.20	11.03
910527	42-4	sr	ch2	-46.73	81.44	1528.40	5.57
910527	42-5	sx	ch2	-46.73	81.44	1528.60	3.09
910527	42-6	sx	ch2	-46.41	81.82	1528.60	3.94
910527	43-1	sx	ch2	-50.38	87.26	1528.00	5.68
910527	43-2	sx	ch2	-50.68	87.90	1528.00	5.11
910527	43-3	sx	ch2	-50.68	87.90	1527.80	5.11
910527	43-4	sx	ch2	-50.53	87.58	1528.00	4.29
910527	43-5	sx	ch2	-50.68	87.90	1528.90	3.33
910527	43-6	sx	ch2	-50.68	87.90	1528.90	3.21

Date [yr mo dy]	Control Point	Facies	Arch. Element	Northing [meters]	Easting [meters]	Elev. [meters]	Perm. [darcy]
910527	43-7	sx	ch2	-50.38	87.26	1528.60	1.06
910527	43-8	sx	ch2	-50.38	87.26	1529.00	2.36
910527	43-9	sx	ch2	-50.38	87.26	1529.30	6.35
910527	43-10	p	p	-50.38	87.26	1531.30	1.67
910527	43-11	p	p	-50.38	87.26	1531.90	2.24
910527	44-1	sh	ch2	-59.28	85.44	1535.00	6.95
910527	44-2	sh	ch2	-59.58	86.07	1535.00	4.26
910527	44-3	sh	ch2	-59.28	85.44	1535.20	7.64
910527	44-4	sh	ch2	-59.45	85.80	1535.20	5.06
910527	44-5	sh	ch2	-59.58	86.07	1535.20	8.81
910527	44-6	sfc	ch2	-59.28	85.44	1535.40	0.001
910527	44-7	sfc	ch2	-59.58	86.07	1535.40	0.001
910527	44-8	sfc	ch2	-59.45	85.80	1535.40	0.001
910527	44-9	sm	ch2	-59.28	85.44	1535.90	2.07
910527	44-10	sm	ch2	-59.58	86.07	1535.90	3.14
910527	45-1	p	r	-66.42	94.12	1531.60	2.36
910527	45-2	p	r	-66.42	94.12	1532.00	0.83
910527	45-3	p	r	-66.42	94.12	1532.40	0.69
910527	45-4	p	r	-66.42	94.12	1532.60	1.30
910527	45-5	p	r	-66.68	95.60	1531.60	1.35
910527	45-6	p	r	-66.68	95.60	1532.00	1.14
910527	45-7	p	r	-66.68	95.60	1532.40	0.79
910527	46-1	sp	ch	-46.06	65.11	1542.50	21.52
910527	46-2	sp	ch1	-46.06	65.11	1542.60	16.15
910527	46-3	sp	ch1	-46.06	65.11	1542.80	11.40
910527	46-4	sp	ch1	-46.06	65.11	1542.90	21.20
910527	46-5	p	of	-46.06	65.11	1542.10	4.79
910527	47-1	sr	ch2	-40.81	39.20	1534.70	6.08
910527	47-2	sr	ch2	-40.42	39.13	1534.70	4.27
910527	47-3	sx	ch2	-39.83	39.02	1534.60	16.61
910527	47-4	sx	ch2	-40.42	39.13	1535.20	5.99
910527	47-5	sp	ch2	-40.42	39.13	1535.40	11.58
910527	47-6	sp	ch2	-40.81	39.20	1535.20	14.15
910527	47-7	fsc	ch2	-40.81	39.20	1535.80	0.001
910527	47-8	sx	ch2	-40.81	39.20	1536.10	3.28
910527	48-1	p	p	-47.24	76.72	1532.50	14.49
910527	48-2	p	p	-47.44	77.07	1532.50	13.82
910527	48-3	p	p	-47.59	77.32	1532.60	7.60
910527	48-4	p	p	-47.24	76.72	1532.90	6.53
910527	48-5	p	p	-47.44	77.07	1532.90	4.81
910527	48-6	p	p	-47.59	77.32	1532.90	10.79
910624	1-1	p	p	-86.87	140.21	1524.00	9.36
910624	1-2	fr	p	-86.87	140.21	1524.30	0.001
910624	1-3	p	p	-86.45	140.56	1524.00	10.95
910624	1-4	p	p	-86.45	140.56	1524.30	3.04
910624	1-5	fr	p	-86.45	140.56	1524.40	0.001
910624	1-6	p	p	-86.45	140.56	1524.50	2.42

Date [yr mo dy]	Control Point	Facies	Arch. Element	Northing [meters]	Easting [meters]	Elev. [meters]	Perm. [darcy]
910624	1-7	p	p	-85.99	140.95	1524.00	7.16
910624	1-8	p	p	-85.99	140.95	1524.30	4.12
910624	1-9	fr	p	-85.99	140.95	1524.40	0.001
910624	1-10	p	p	-85.99	140.95	1524.60	1.48
910626	2-1	sh	ch2	-76.81	127.71	1523.10	12.34
910626	2-2	sh	ch2	-77.20	127.81	1523.10	11.71
910626	2-3	sh	ch2	-76.81	127.71	1523.30	11.49
910626	2-4	sh	ch2	-76.81	127.71	1523.60	7.35
910626	2-5	sh	ch2	-77.34	127.85	1523.60	5.92
910626	2-6	p	p	-76.62	127.66	1523.90	2.47
910626	2-7	p	p	-77.20	127.81	1523.90	3.74
910626	2-8	fx	of	-77.20	127.81	1524.30	0.001
910626	2-9	fx	of	-76.62	127.66	1524.30	0.001
910626	4-1	p	p	-85.04	114.00	1533.00	0.001
910626	4-2	sr	ch2	-85.04	114.00	1533.40	1.61
910626	4-3	sr	ch2	-85.04	113.90	1533.60	2.77
910626	4-4	sr	ch2	-85.04	114.25	1533.60	5.29
910626	4-5	p	p	-85.04	114.25	1533.90	0.001
910626	4-6	st	ch2	-85.04	113.75	1533.90	2.46
910626	4-7	st	ch2	-85.04	113.75	1534.20	13.76
910626	4-8	st	ch2	-85.04	113.55	1534.20	7.21
910626	4-9	sr	ch2	-85.04	113.70	1534.40	2.94
910626	4-10	sr	ch2	-85.04	113.50	1534.40	4.33
910626	5-1	p	ru	-89.21	111.64	1542.80	0.70
910626	5-2	p	ru	-88.39	111.17	1542.80	0.98
910626	5-3	fr	of	-88.39	111.17	1542.30	0.001
910626	5-4	fr	of	-89.21	111.64	1542.30	0.001
910626	3-1	p	p	-82.91	118.87	1529.50	0.001
910626	3-2	sr	ch2	-82.91	118.87	1529.80	5.43
910626	3-3	st	ch2	-82.91	118.87	1529.40	16.80
910626	3-4	st	ch2	-82.91	118.87	1529.00	6.75
910626	3-5	st	ch2	-82.91	118.87	1528.60	16.33
910626	3-6	sh	ch2	-83.86	118.58	1529.50	5.57
910626	3-7	p	p	-83.86	118.58	1529.40	0.001
910626	3-8	sr	ch2	-83.86	118.58	1529.70	3.17
910626	3-9	sr	ch2	-83.86	118.58	1529.90	2.97
910626	3-10	sh	ch2	-83.86	118.58	1529.20	4.61
910626	3-11	p	p	-83.86	118.58	1529.10	0.001
910626	3-12	sr	ch2	-83.86	118.58	1529.10	8.86
910626	3-13	sx	ch2	-83.86	118.58	1528.60	32.49
910626	3-14	sh	ch2	-84.82	118.29	1529.50	4.59
910626	3-15	sm	ch2	-84.82	118.29	1529.80	2.22
910626	3-16	p	p	-84.82	118.29	1529.40	0.001
910626	3-17	sh	ch2	-84.82	118.29	1529.20	6.38
910626	3-18	p	p	-84.82	118.29	1529.00	0.001
910626	3-19	sx	ch2	-84.82	118.29	1528.90	15.98
910626	3-20	p	p	-84.82	118.29	1528.80	0.001

Date [yr mo dy]	Control Point	Facies	Arch. Element	Northing [meters]	Easting [meters]	Elev. [meters]	Perm. [darcy]
910626	3-21	sh	ch2	-84.82	118.29	1528.70	13.57
910626	6-1	sh	ch2	-148.35	140.75	1528.60	16.33
910626	6-2	sh	ch2	-147.95	140.68	1528.60	18.73
910626	6-3	st	ch2	-148.35	140.75	1529.00	7.11
910626	6-4	st	ch2	-147.95	140.68	1529.00	2.85
910626	6-5	fr	of	-148.74	140.82	1527.70	0.001
910626	6-6	fr	of	-148.35	140.75	1527.70	0.001
910626	6-7	sh	ch2	-148.86	140.49	1528.60	15.81
910626	6-8	sp	ch2	-148.86	140.49	1528.90	9.65
910626	6-9	sh	ch2	-149.03	140.02	1528.60	15.31
910626	6-10	st	ch2	-149.03	140.02	1528.90	10.07
910626	6-11	sh	ch2	-149.15	139.69	1528.60	13.27
910626	6-12	st	ch2	-149.15	139.69	1528.90	6.56
910626	6-13	sh	ch2	-149.29	139.31	1528.60	13.63
910626	6-14	st	ch2	-149.29	139.31	1528.90	5.09
910626	6-15	sm	ch2	-149.15	139.69	1529.30	4.13
910626	6-16	sm	ch2	-149.03	140.02	1529.30	2.99
910626	7-1	p	p	-142.34	135.33	1534.60	1.99
910626	7-2	p	p	-142.91	135.54	1534.50	2.59
910626	7-3	sx	ch2	-142.34	135.33	1534.90	2.63
910626	7-4	fx	ch2	-142.34	135.33	1535.10	0.001
910626	7-5	fx	ch2	-142.62	135.43	1535.10	0.001
910626	8-1	sr	ch2	-72.54	192.94	1533.20	6.70
910626	8-2	sm	ch2	-72.54	192.94	1533.50	5.68
910626	8-3	sx	ch2	-72.54	192.94	1533.70	6.42
910626	8-4	sr	ch2	-72.54	192.94	1533.00	1.47
910626	8-5	sp	ch2	-72.54	192.94	1532.80	2.32
910626	8-6	sp	ch2	-72.93	192.83	1532.90	3.06
910626	8-7	sh	ch2	-72.93	192.83	1533.20	5.81
910626	8-8	sx	ch2	-72.93	192.83	1533.50	3.51
910626	8-9	sx	ch2	-73.80	192.60	1533.20	7.76
910626	8-10	sx	ch2	-73.80	192.60	1533.40	7.84
910626	9-1	sp	ch2	-45.72	205.74	1525.50	14.49
910626	9-2	sp	ch2	-45.72	205.74	1525.80	7.45
910626	9-3	sp	ch2	-46.01	206.08	1525.40	11.40
910626	9-4	sp	ch2	-46.01	206.08	1525.80	9.65
910626	9-5	sp	ch2	-46.36	206.51	1525.40	5.60
910626	9-6	sp	ch2	-46.36	206.51	1525.70	7.01
910703	10-1	st	ch2	-123.14	186.23	1528.80	7.82
910703	10-2	st	ch2	-123.14	186.23	1528.90	3.03
910703	10-3	sh	ch2	-123.14	186.23	1529.40	5.11
910703	10-4	sh	ch2	-123.14	186.23	1529.50	5.26
910703	10-5	sh	ch2	-122.98	185.35	1528.80	8.86
910703	10-6	sh	ch2	-122.98	185.35	1529.30	9.59
910703	10-7	sh	ch2	-122.98	185.35	1529.40	3.49
910703	10-8	st	ch2	-122.98	185.35	1529.50	3.67
910703	10-9	sh	ch2	-122.98	185.35	1529.60	3.59

Date [yr mo dy]	Control Point	Facies	Arch. Element	Northing [meters]	Easting [meters]	Elev. [meters]	Perm. [darcy]
910703	10-10	sh	ch2	-122.98	185.35	1529.80	4.13
910703	10-11	sh	ch2	-122.86	184.66	1528.80	11.80
910703	10-12	st	ch2	-122.79	184.26	1529.30	4.52
910703	10-13	sh	ch2	-122.79	184.26	1529.50	3.28
910703	10-14	sh	ch2	-122.71	183.77	1528.80	4.38
910703	10-15	sh	ch2	-122.71	183.77	1529.40	5.71
910703	10-16	sh	ch2	-122.71	183.77	1529.50	3.20
910703	10-17	sh	ch2	-122.57	182.98	1529.50	3.23
910703	10-18	sx	ch2	-122.57	182.98	1529.60	18.38
910703	10-19	sh	ch2	122.57	182.98	1529.60	70.80
910703	10-20	sh	ch2	-122.60	183.18	1528.80	3.19
910703	10-21	fr	of	-123.14	186.23	1530.50	0.001
910703	10-22	fr	of	-122.98	185.35	1530.50	0.001
910703	10-23	fr	of	-122.79	184.26	1530.50	0.001
910703	10-24	fr	of	-122.71	183.77	1530.50	0.001
910703	10-25	fr	of	-122.57	182.98	1530.50	0.001
910703	11-1	sx	ch2	-117.35	198.12	1529.10	7.58
910703	11-2	sh	ch2	-117.35	198.12	1529.40	14.49
910703	11-3	sh	ch2	-117.48	197.64	1529.00	16.33
910703	11-4	sh	ch2	-117.48	197.64	1529.40	5.96
910703	11-5	sx	ch2	-117.48	197.64	1529.70	8.26
910703	11-6	sh	ch2	-117.66	196.96	1528.80	13.69
910703	11-7	sp	ch2	-117.66	196.96	1529.30	4.90
910703	11-8	sx	ch2	-117.66	196.96	1529.70	3.27
910703	11-9	sh	ch2	-117.89	196.09	1528.80	9.41
910703	11-10	sx	ch2	-117.89	196.09	1529.10	7.22
910703	11-11	sx	ch2	-117.89	196.09	1529.30	9.00
910703	11-12	sh	ch2	-117.89	196.09	1529.60	4.80
910703	11-13	sx	ch2	-112.35	198.12	1529.70	8.40
910703	11-14	fsc	of	-117.35	198.12	1530.50	0.001
910703	11-15	fsc	of	-117.48	197.64	1530.50	0.001
910703	11-16	fsc	of	-117.66	196.96	1530.50	0.001
910703	11-17	fsc	of	-117.89	196.09	1530.50	0.001
910703	12-1	p	p	-110.95	196.60	1533.50	0.001
910703	12-2	p	p	-110.79	194.80	1533.50	0.001
910703	12-3	sx	ch2	-110.95	196.60	1534.00	5.95
910703	12-4	sx	ch2	-110.95	196.60	1534.20	7.58
910703	12-5	sx	ch2	-110.95	196.60	1534.40	3.41
910703	12-6	fr	of	-110.95	196.60	1534.80	0.001
910703	12-7	sx	ch2	-110.79	194.80	1533.90	2.90
910703	12-8	sx	ch2	-110.79	194.80	1534.20	8.69
910703	12-9	sx	ch2	-110.79	194.80	1534.50	8.40
910703	12-10	fr	of	-110.79	194.80	1534.80	0.001
910703	13-1	gx	ch1	-108.20	190.50	1538.10	300.00
910703	13-2	sh	ch2	-108.20	190.50	1537.60	25.12
910703	13-3	sh	ch2	-108.20	190.50	1537.30	10.49
910703	13-4	pc	p	-108.20	190.50	1536.80	0.001

Date [yr mo dy]	Control Point	Facies	Arch. Element	Northing [meters]	Easting [meters]	Elev. [meters]	Perm. [darcy]
910703	13-5	gx	ch1	-108.36	189.92	1538.10	300.00
910703	13-6	sh	ch2	-108.36	189.92	1537.60	31.37
910703	13-7	sh	ch2	-108.36	189.92	1537.30	20.02
910703	13-8	pc	p	-108.36	189.92	1536.80	0.001
910703	14-1	gm	ch1	-113.08	178.31	1538.70	300.00
910703	14-2	sh	ch1	-113.08	178.30	1537.90	27.88
910703	14-3	pc	p	-113.08	178.31	1536.90	0.001
910703	14-4	gm	ch1	-113.13	178.11	1538.70	300.00
910703	14-5	sh	ch1	-113.13	178.11	1537.90	44.54
910703	14-6	pc	p	-113.13	178.11	1536.90	0.001
910703	14-7	gm	ch1	-113.24	177.73	1538.70	300.00
910703	14-8	pc	p	-113.24	177.73	1536.90	0.001
910703	14-9	sh	ch1	-113.24	177.73	1537.90	44.54
910703	15-1	sx	ch1	-119.48	150.27	1544.60	20.59
910703	15-2	sx	ch1	-119.56	150.20	1544.60	15.00
910703	15-3	sx	ch1	-121.40	148.66	1544.60	10.68
910703	15-4	sx	ch1	-121.47	148.60	1544.60	16.61
910703	15-5	fx	of	-119.48	150.27	1543.80	0.001
910703	15-6	fx	of	-121.40	148.66	1543.80	0.001
910703	15-7	p	ru	-121.40	148.66	1543.30	3.54
910703	15-8	p	ru	-122.16	148.02	1543.30	2.31
910703	15-9	sh	ch1	-121.40	148.66	1542.10	15.16
910703	15-10	sh	ch1	-122.16	148.02	1542.10	13.45
910703	16-1	sx	ch2	-120.40	169.77	1535.10	9.27
910703	16-2	sx	ch2	-120.40	169.77	1534.90	3.57
910703	16-3	p	p	-120.40	169.77	1534.60	1.90
910703	16-4	p	p	-120.40	169.77	1534.20	1.75
910703	16-5	sx	ch2	-120.63	169.58	1535.10	6.90
910703	16-6	sx	ch2	-120.63	169.58	1534.90	2.53
910703	16-7	p	p	-120.63	169.58	1534.60	2.13
910703	16-8	p	p	-120.70	169.52	1534.60	2.33
910703	17-1	st	ch2	-125.58	174.65	1529.90	9.56
910703	17-2	sx	ch2	-125.58	174.65	1529.70	0.88
910703	17-3	sh	ch2	-125.58	174.65	1529.50	2.78
910703	17-4	sp	ch2	-125.58	174.65	1529.30	26.30
910703	17-5	sp	ch2	-125.58	174.65	1529.20	24.68
910703	17-6	sh	ch2	-125.58	174.65	1529.10	4.87
910703	17-7	st	ch2	-125.75	174.35	1529.90	20.16
910703	17-8	sh	ch2	-125.75	174.35	1529.50	4.01
910703	17-9	sp	ch2	-125.75	174.35	1529.30	26.05
910703	17-10	sp	ch2	-125.75	174.35	1529.20	13.21
910703	17-11	st	ch2	-125.85	174.17	1529.90	5.33
910703	17-12	sh	ch2	-125.85	174.17	1529.60	3.16
910703	17-13	sp	ch2	-125.85	174.17	1529.30	16.24

Nevada Test Site Data

Nevada Test Site -- Pit 3

N	Control Point	X [meters]	Y [meters]	Hydro Geo	time [seconds]	perm [darcy]
1	3-124-1	6.04	0.79	DF	8.66	7.98
2	3-124-6	6.22	0.57	DF	4.00	18.70
3	3-124-7	6.04	0.36	DF	8.51	8.13
4	3-124-9	6.22	0.79	DF	7.31	9.55
5	3-109-1	4.74	2.08	SF	4.93	14.69
6	3-109-2	5.41	2.08	SF	2.60	32.59
7	3-109-3	4.74	1.65	SF	2.70	30.89
8	3-109-4	5.41	1.65	SF	4.30	17.18
9	3-91-1	4.39	2.65	SF	8.75	7.89
10	3-91-3	4.39	2.04	SF	4.67	15.62
11	3-91-4	5.12	2.04	SF	2.52	34.10
12	3-73-1	6.16	3.58	SF	4.49	16.34
13	3-73-2	6.62	3.58	SF	3.14	25.22
14	3-73-3	7.07	3.58	SF	2.36	37.63
15	3-73-4	6.16	3.54	SF	4.71	15.47
16	3-73-5	6.62	3.54	SF	2.33	38.39
17	3-73-7	6.16	3.51	SF	2.31	38.91
18	3-73-8	6.62	3.51	SF	5.77	12.33
19	3-55-1	5.93	5.03	DF	7.52	9.26
20	3-55-2	6.20	5.03	DF	5.59	12.77
21	3-55-3	6.47	5.03	DF	8.30	8.34
22	3-55-4	5.93	4.87	DF	1.80	60.75
23	3-55-5	6.20	4.87	DF	5.75	12.38
24	3-55-6	6.47	4.72	DF	7.95	8.73
25	3-55-7	5.93	4.72	DF	1.68	70.69
26	3-55-8	6.20	4.72	DF	2.30	39.17
27	3-55-9	6.47	4.72	DF	6.81	10.30
28	3-37-1	3.45	6.39	SF	2.09	45.85
29	3-37-2	4.25	6.39	SF	1.49	96.95
30	3-37-4	4.25	6.03	DF	6.42	10.98
31	3-19-01	4.62	7.10	DF	3.78	20.01
32	3-19-02	5.15	7.10	DF	4.47	16.42
33	3-19-03	5.68	7.10	DF	3.28	23.85
34	3-19-04	4.62	7.10	DF	5.92	11.99
35	3-19-05	5.15	7.10	DF	9.96	6.89
36	3-19-06	5.68	7.10	DF	4.64	15.74
37	3-19-07	4.62	7.10	DF	5.62	12.69
38	3-19-08	5.15	7.10	DF	8.61	8.03
39	3-19-09	5.68	7.10	DF	3.95	18.98
40	3-1-01	5.78	8.81	DF	22.75	2.95
41	3-1-02	6.40	8.81	DF	21.99	3.06
42	3-1-03	7.03	8.81	DF	14.48	4.68
43	3-1-04	5.78	8.71	DF	9.84	6.98
44	3-1-05	6.40	8.71	DF	11.96	5.70
45	3-1-06	7.03	8.71	DF	7.62	9.13
46	3-1-07	5.78	8.62	DF	6.40	11.01
47	3-1-08	6.40	8.62	DF	9.30	7.40

N	Control Point	X [meters]	Y [meters]	Hydro Geo	time [seconds]	perm [darcy]
48	3-1-09	7.03	8.62	DF	13.44	5.05
49	3-2-01	6.41	8.61	DF	22.10	3.04
50	3-2-02	7.11	8.61	DF	8.34	8.30
51	3-2-04	6.41	8.39	DF	11.29	6.05
52	3-2-05	7.11	8.39	DF	19.74	3.41
53	3-2-06	7.82	8.39	DF	9.38	7.34
54	3-2-07	6.41	8.18	DF	8.16	8.49
55	3-2-08	7.11	8.18	DF	13.63	4.98
56	3-20-01	8.81	7.30	SF	5.03	14.36
57	3-20-02	9.24	7.30	SF	2.89	28.14
58	3-20-03	8.81	7.18	DF	6.41	10.99
59	3-20-04	9.24	7.18	DF	11.91	5.72
60	3-38-1	7.25	7.00	SF	1.30	161.4
61	3-38-3	7.92	7.00	SF	1.40	118.96
62	3-38-7	7.25	6.79	SF	1.99	50.01
63	3-56-1	8.14	5.39	DF	4.09	18.22
64	3-56-2	8.87	5.39	DF	10.41	6.58
65	3-56-3	9.60	5.39	DF	9.70	7.08
66	3-56-4	8.14	5.19	DF	9.49	7.25
67	3-56-5	8.87	5.19	DF	10.81	6.33
68	3-56-6	9.60	5.19	DF	4.40	16.73
69	3-56-7	8.14	4.99	DF	3.59	21.31
70	3-56-8	8.87	4.99	DF	7.49	9.30
71	3-56-9	9.60	4.99	DF	8.36	8.28
72	3-74-1	9.73	3.64	SF	2.06	47.02
73	3-74-2	9.33	3.64	SF	2.17	43.03
74	3-74-4	9.73	3.59	SF	1.31	155.74
75	3-74-5	9.33	3.59	SF	2.31	38.91
76	3-74-6	8.94	3.59	SF	1.39	122.11
77	3-74-7	9.73	3.55	SF	2.03	48.25
78	3-74-8	9.33	3.55	SF	1.79	61.46
79	3-74-9	8.94	3.55	SF	1.76	63.71
80	3-92-2	10.91	2.76	DF	2.09	45.85
81	3-92-4	10.48	2.72	DF	2.97	27.13
82	3-92-5	10.91	2.72	DF	2.38	37.15
83	3-92-6	11.34	2.72	DF	1.66	72.71
84	3-92-7	10.48	2.66	DF	2.67	31.38
85	3-92-8	10.91	2.66	DF	4.37	16.86
86	3-110-1	8.01	2.29	SF	2.41	36.45
87	3-110-2	6.73	2.29	SF	2.63	32.06
88	3-110-3	8.01	1.89	DF	1.88	55.66
89	3-110-4	6.73	1.89	SF	2.38	37.15
90	3-58-1	14.12	5.83	DF	5.16	13.96
91	3-58-2	14.38	5.83	DF	12.23	5.57
92	3-58-3	14.64	5.83	DF	8.41	8.23
93	3-58-4	14.12	5.63	DF	12.38	5.50
94	3-58-5	14.38	5.63	DF	4.26	17.37

Nevada Test Site -- Pit 3

N	Control Point	X [meters]	Y [meters]	Hydro Geo	time [seconds]	perm [darcy]
95	3-58-6	14.64	5.63	DF	3.53	21.75
96	3-58-7	14.12	5.43	DF	13.00	5.23
97	3-58-9	14.64	5.43	DF	1.27	181.51
98	3-40-1	14.43	6.63	SF	2.70	30.89
99	3-40-2	13.91	6.63	SF	1.54	88.14
100	3-40-3	14.43	6.53	SF	3.42	22.62
101	3-22-01	14.48	8.00	DF	8.79	7.85
102	3-22-02	14.79	8.00	DF	5.83	12.19
103	3-32-1	44.04	7.79	DF	1.33	145.57
104	3-32-4	44.43	7.46	DF	5.19	13.87
105	3-14-03	45.00	9.08	SF	7.91	8.78
106	3-106-1	50.37	2.50	DF	3.32	23.48
107	3-106-3	50.37	2.31	DF	3.59	21.31
108	3-106-4	50.61	2.31	DF	3.27	23.94
109	3-88-1	50.76	4.28	DF	3.25	24.13
110	3-88-2	51.65	4.28	DF	10.06	6.82
111	3-88-3	50.76	4.22	DF	2.93	27.62
112	3-88-4	51.65	4.22	DF	7.53	9.25
113	3-86-1	43.91	3.86	SF	3.24	24.22
114	3-86-2	44.28	3.86	SF	3.09	25.75
115	3-86-3	43.91	3.62	SF	3.06	26.08
116	3-86-4	44.28	3.62	SF	1.70	68.79
117	3-68-1	45.76	5.66	SF	1.38	125.44
118	3-68-2	45.92	5.66	SF	1.56	85.08
119	3-68-3	46.07	5.66	SF	4.45	16.51
120	3-68-5	45.92	5.63	SF	1.34	141.00
121	3-68-8	45.92	5.60	SF	1.30	161.43
122	3-50-4	45.72	6.04	SF	2.06	47.02
123	3-50-5	45.83	6.04	SF	2.57	33.14
124	3-50-7	45.72	5.73	SF	2.73	30.42
125	3-50-8	45.83	5.73	SF	1.73	66.14
126	3-50-9	45.93	5.73	SF	2.25	40.56
127	3-12-01	39.74	9.57	DF	6.02	11.77
128	3-12-02	40.20	9.57	DF	7.36	9.48
129	3-12-03	40.65	9.57	DF	6.67	10.53
130	3-12-04	39.74	9.29	DF	9.07	7.60
131	3-12-05	40.20	9.29	DF	11.37	6.01
132	3-12-06	40.65	9.29	DF	10.25	6.69
133	3-12-07	39.74	9.02	DF	12.73	5.34
134	3-12-08	40.20	9.02	DF	17.14	3.94
135	3-12-09	40.65	9.02	DF	11.71	5.83
136	3-122-1	45.28	1.71	SF	3.20	24.61
137	3-122-2	45.30	1.71	SF	3.38	22.96
138	3-122-3	45.28	1.22	DF	7.45	9.36
139	3-122-4	45.30	1.22	DF	5.64	12.64
140	3-104-1	46.23	3.25	SF	2.04	47.83
141	3-104-2	46.26	3.25	SF	1.78	62.19

Nevada Test Site -- Pit 3

N	Control Point	X [meters]	Y [meters]	Hydro Geo	time [seconds]	perm [darcy]
142	3-104-3	46.23	3.22	SF	2.31	38.91
143	3-104-4	46.26	3.22	SF	1.61	78.36
144	3-66-2	39.27	5.11	SF	1.41	115.99
145	3-66-3	39.27	4.93	SF	1.22	230.34
146	3-30-02	38.01	7.55	DF	3.06	26.08
147	3-30-03	38.08	7.55	DF	2.16	43.36
148	3-30-04	37.93	7.49	DF	4.75	15.32
149	3-30-05	38.01	7.49	DF	3.22	24.41
150	3-30-06	38.08	7.49	DF	14.87	4.56
151	3-30-07	37.93	7.43	DF	2.84	28.81
152	3-30-08	38.01	7.43	DF	3.23	24.32
153	3-120-3	40.24	1.94	DF	8.36	8.28
154	3-120-4	39.97	1.66	DF	10.39	6.59
155	3-102-1	39.04	2.81	SF	2.56	33.33
156	3-102-2	39.40	2.81	SF	1.60	79.61
157	3-102-3	39.75	2.81	SF	3.47	22.22
158	3-102-4	39.04	2.57	SF	4.59	15.93
159	3-102-5	39.40	2.57	SF	1.97	50.94
160	3-102-6	39.75	2.57	SF	2.82	29.09
161	3-102-8	39.40	2.32	DF	2.93	27.62
162	3-102-9	39.75	2.32	DF	3.14	25.22
163	3-84-1	38.90	4.61	SF	1.52	91.45
164	3-84-2	39.03	4.61	SF	4.81	15.10
165	3-84-4	38.90	4.37	SF	1.31	155.74
166	3-84-5	39.03	4.37	SF	1.42	113.17
167	3-84-6	39.15	4.37	SF	1.39	122.11
168	3-28-01	33.49	7.36	DF	6.69	10.50
169	3-28-02	33.61	7.36	DF	8.95	7.71
170	3-28-04	33.61	7.30	DF	9.11	7.56
171	3-10-01	32.09	9.57	DF	6.66	10.55
172	3-10-02	33.61	9.57	DF	5.74	12.40
173	3-10-03	32.09	9.39	DF	8.01	8.66
174	3-10-04	33.61	9.39	DF	14.91	4.54
175	3-100-3	33.88	2.89	SF	6.89	10.17
176	3-100-5	33.68	2.82	DF	4.81	15.10
177	3-100-7	33.49	2.75	DF	6.88	10.19
178	3-100-8	33.68	2.75	DF	2.33	38.39
179	3-82-1	31.83	3.79	SF	1.74	65.31
180	3-82-2	32.12	3.79	SF	4.91	14.76
181	3-82-3	32.41	3.79	SF	1.76	63.71
182	3-82-4	31.83	3.64	SF	1.70	68.79
183	3-82-5	32.12	3.64	SF	1.69	69.73
184	3-82-8	32.12	3.49	SF	1.31	155.74
185	3-64-1	33.94	6.02	DF	6.08	11.64
186	3-64-2	33.94	6.02	DF	5.74	12.40
187	3-64-3	33.94	6.02	DF	1.85	57.46
188	3-64-4	33.94	5.87	DF	3.77	20.07

N	Control Point	X [meters]	Y [meters]	Hydro Geo	time [seconds]	perm [darcy]
189	3-64-5	33.94	5.87	DF	4.20	17.66
190	3-64-6	33.94	5.87	DF	8.22	8.43
191	3-64-7	33.94	5.72	DF	8.38	8.26
192	3-64-8	33.94	5.72	DF	3.74	20.27
193	3-64-9	33.94	5.72	DF	6.00	11.81
194	3-26-01	27.64	7.36	DF	1.91	53.98
195	3-26-02	29.16	7.36	DF	1.70	68.79
196	3-26-04	29.16	7.18	DF	4.77	15.25
197	3-8-01	27.44	9.66	DF	4.52	16.22
198	3-8-02	26.07	9.66	DF	36.97	1.81
199	3-8-03	27.44	9.17	DF	22.35	3.01
200	3-8-04	26.07	9.17	DF	20.56	3.27
201	3-118-1	33.62	1.58	SF	1.51	93.20
202	3-118-2	33.92	1.58	SF	4.04	18.48
203	3-118-4	33.62	1.55	SF	2.30	39.17
204	3-118-5	33.92	1.55	SF	2.10	45.48
205	3-118-7	33.62	1.52	SF	5.08	14.20
206	3-118-8	33.92	1.52	SF	1.37	128.97
207	3-118-9	34.23	1.52	SF	1.27	181.51
208	3-80-1	27.43	4.64	SF	1.20	258.78
209	3-80-2	27.50	4.64	SF	1.39	122.11
210	3-80-3	27.58	4.64	SF	1.77	62.94
211	3-80-4	27.43	4.61	SF	2.06	47.02
212	3-80-5	27.50	4.61	SF	1.56	85.08
213	3-80-6	27.58	4.61	SF	1.42	113.17
214	3-80-7	27.43	4.58	SF	1.34	141.00
215	3-80-8	27.50	4.58	SF	1.91	53.98
216	3-80-9	27.58	4.58	SF	1.31	155.74
217	3-62-1	26.01	5.94	SF	3.54	21.68
218	3-62-2	26.60	5.94	SF	1.59	80.91
219	3-62-3	27.20	5.94	SF	3.53	21.75
220	3-62-4	26.01	5.79	SF	1.40	118.96
221	3-44-1	26.53	6.63	SF	3.87	19.45
222	3-44-2	27.15	6.63	SF	1.77	62.94
223	3-44-3	27.78	6.63	SF	2.02	48.68
224	3-44-4	26.53	6.50	SF	3.34	23.31
225	3-6-01	19.37	9.38	DF	7.44	9.37
226	3-6-02	19.89	9.38	DF	16.82	4.02
227	3-6-03	20.40	9.38	DF	18.54	3.64
228	3-6-04	19.37	9.19	DF	19.49	3.46
229	3-6-05	19.89	9.19	DF	20.13	3.35
230	3-6-06	20.40	9.19	DF	7.98	8.70
231	3-6-07	19.37	9.01	DF	8.12	8.54
232	3-6-08	19.89	9.01	DF	10.87	6.29
233	3-6-09	20.40	9.01	DF	14.44	4.70
234	3-116-1	28.40	2.08	SF	2.72	30.58
235	3-116-2	28.52	2.08	SF	1.82	59.39

N	Control Point	X [meters]	Y [meters]	Hydro Geo	time [seconds]	perm [darcy]
236	3-116-3	28.65	2.08	SF	3.82	19.76
237	3-116-4	28.40	1.95	SF	3.40	22.79
238	3-116-5	28.52	1.95	SF	2.55	33.52
239	3-116-6	28.65	1.95	SF	1.96	51.42
240	3-116-7	28.40	1.83	SF	2.93	27.62
241	3-116-8	28.52	1.83	SF	3.87	19.45
242	3-116-9	28.65	1.83	SF	3.12	25.43
243	3-98-3	28.37	3.47	SF	2.35	37.88
244	3-98-4	26.94	3.25	SF	3.01	26.65
245	3-60-1	20.28	5.88	DF	5.94	11.94
246	3-60-2	20.76	5.88	DF	3.67	20.74
247	3-60-4	20.28	5.81	DF	3.60	21.23
248	3-24-03	20.24	7.32	SF	1.52	91.45
249	3-24-04	20.21	7.21	SF	1.51	93.20
250	3-114-2	21.88	2.06	SF	1.34	141.00
251	3-114-3	22.60	2.06	SF	1.38	125.44
252	3-114-4	21.17	1.95	SF	2.05	47.42
253	3-114-5	21.88	1.95	SF	1.45	105.55
254	3-114-6	22.60	1.95	SF	2.33	38.39
255	3-114-7	21.17	1.85	SF	11.91	5.72
256	3-114-8	21.88	1.85	SF	1.34	141.00
257	3-96-2	20.26	3.36	SF	1.81	60.06
258	3-96-4	19.68	3.07	SF	5.78	12.31
259	3-96-5	20.26	3.07	SF	4.00	18.70
260	3-96-6	20.84	3.07	SF	2.14	44.04
261	3-96-7	19.68	2.78	SF	6.35	11.11
262	3-96-8	20.26	2.78	SF	3.49	22.06
263	3-96-9	20.84	2.78	SF	1.97	50.94
264	3-78-1	20.26	4.13	DF	3.20	24.61
265	3-78-2	20.85	4.13	DF	5.70	12.50
266	3-78-3	21.45	4.13	DF	2.91	27.88
267	3-78-4	20.26	4.13	DF	4.20	17.66
268	3-78-5	20.85	4.13	DF	4.08	18.27
269	3-78-6	21.45	4.13	DF	2.66	31.55
270	3-78-7	20.26	4.13	DF	4.27	17.32
271	3-78-8	20.85	4.13	DF	5.64	12.64
272	3-78-9	21.45	4.13	DF	2.64	31.89
273	3-4-01	14.99	8.64	DF	15.30	4.43
274	3-4-02	15.28	8.64	DF	4.91	14.76
275	3-4-03	15.57	8.64	DF	6.43	10.96
276	3-4-04	14.99	8.51	DF	13.49	5.04
277	3-4-05	15.28	8.51	DF	11.37	6.01
278	3-4-07	14.99	8.37	DF	6.10	11.60
279	3-4-08	15.28	8.37	DF	8.60	8.04
280	3-4-09	15.57	8.37	DF	14.03	4.84
281	3-112-1	14.68	1.35	SF	2.19	42.38
282	3-112-2	15.04	1.35	SF	1.31	155.74

Nevada Test Site -- Pit 3

N	Control Point	X [meters]	Y [meters]	Hydro Geo	time [seconds]	perm [darcy]
283	3-112-3	15.41	1.35	SF	2.76	29.96
284	3-112-4	14.68	1.16	SF	2.05	47.42
285	3-94-1	15.55	2.40	SF	3.26	24.03
286	3-94-2	15.65	2.40	SF	1.20	258.78
287	3-76-1	15.42	4.64	DF	3.02	26.53
288	3-76-2	15.57	4.64	DF	1.92	53.45
289	3-76-3	15.72	4.64	DF	1.26	189.45
290	3-76-4	15.42	4.56	DF	1.79	61.46
291	3-76-5	15.57	4.56	DF	1.74	65.31
292	3-76-6	15.72	4.56	DF	1.82	59.39

Nevada Test Site -- Pit 4

N	Control Point	X [meters]	Y [meters]	Hydro Geo	time [seconds]	perm [darcy]
1	4-43-1	2.73	2.00	DF	12.66	5.38
2	4-43-2	2.89	2.00	DF	6.99	10.07
3	4-43-3	3.04	2.00	DF	13.72	4.95
4	4-43-4	2.73	1.80	DF	9.20	7.51
5	4-43-5	2.89	1.80	DF	9.86	6.98
6	4-43-6	3.04	1.80	DF	7.14	9.84
7	4-43-7	2.73	1.60	DF	6.91	10.19
8	4-43-8	2.89	1.60	DF	11.56	5.91
9	4-29-01	3.50	4.50	DF	7.01	10.03
10	4-29-02	3.85	4.50	DF	8.16	8.53
11	4-29-03	4.20	4.50	DF	6.96	10.11
12	4-29-04	3.50	4.23	DF	8.38	8.29
13	4-29-05	3.85	4.23	DF	6.33	11.22
14	4-29-06	4.20	4.23	DF	2.91	28.85
15	4-29-07	3.50	3.95	DF	8.76	7.91
16	4-29-09	4.20	3.95	DF	6.13	11.62
17	4-15-02	4.32	5.33	SF	9.58	7.20
18	4-15-04	4.32	4.94	DF	6.72	10.51
19	4-30-01	5.24	4.52	DF	5.17	14.06
20	4-30-02	5.54	4.52	DF	3.89	19.68
21	4-30-04	5.54	4.18	SF	2.03	52.69
22	4-16-01	4.89	5.92	SF	7.35	9.53
23	4-16-04	4.89	5.66	DF	26.75	2.51
24	4-16-07	4.89	5.40	DF	5.85	12.24
25	4-16-08	5.16	5.40	DF	8.19	8.49
26	4-16-09	5.43	5.40	DF	9.93	6.93
27	4-2-01	5.84	7.95	DF	24.85	2.70
28	4-2-02	5.84	7.95	DF	25.33	2.65
29	4-2-03	5.84	7.37	DF	29.68	2.26
30	4-2-04	5.84	7.37	DF	18.58	3.63
31	4-45-1	9.13	2.21	DF	30.35	2.21
32	4-45-2	9.51	2.21	DF	7.43	9.42
33	4-45-3	9.89	2.21	DF	19.03	3.54
34	4-45-4	9.13	2.15	DF	9.22	7.49
35	4-45-5	9.51	2.15	DF	8.66	8.00
36	4-45-6	9.89	2.15	DF	19.18	3.52
37	4-45-7	9.13	2.08	DF	8.71	7.96
38	4-45-8	9.51	2.08	DF	22.90	2.94
39	4-45-9	9.89	2.08	DF	5.47	4.38
40	4-32-2	11.19	3.50	DF	7.08	9.93
41	4-32-3	10.03	3.29	DF	13.92	4.88
42	4-32-4	11.19	3.29	DF	13.02	5.23
43	4-18-01	10.94	5.98	DF	11.03	6.21
44	4-46-1	10.90	2.72	DF	16.61	4.07
45	4-46-3	10.90	2.20	DF	17.60	3.84
46	4-46-4	12.33	2.20	DF	7.66	9.12
47	4-47-1	14.92	3.19	SF	2.46	37.23

N	Control Point	X [meters]	Y [meters]	Hydro Geo	time [seconds]	perm [darcy]
48	4-47-2	16.36	3.19	DF	11.89	5.74
49	4-47-3	14.92	2.43	DF	3.27	24.57
50	4-47-4	16.36	2.43	DF	30.41	2.20
51	4-33-1	15.41	4.55	SF	10.50	6.54
52	4-33-2	16.79	4.55	DF	5.22	13.91
53	4-33-3	15.41	3.67	SF	2.02	53.22
54	4-33-4	16.79	3.67	SF	1.45	142.44
55	4-19-02	15.20	5.89	DF	10.41	6.60
56	4-19-03	15.93	5.89	DF	11.88	5.75
57	4-19-05	15.20	5.45	DF	9.58	7.20
58	4-19-06	15.93	5.45	DF	11.41	6.00
59	4-19-07	14.47	5.01	DF	4.41	16.91
60	4-19-08	15.20	5.01	DF	6.12	11.64
61	4-19-09	15.93	5.01	DF	10.99	6.23
62	4-5-01	14.56	7.24	DF	56.17	1.19
63	4-5-03	15.26	7.24	DF	55.84	1.19
64	4-5-04	14.56	7.11	DF	31.32	2.14
65	4-5-05	14.91	7.11	DF	7.06	9.96
66	4-5-06	15.26	7.11	DF	37.34	1.79
67	4-5-07	14.56	6.99	DF	45.59	1.47
68	4-5-08	14.91	6.99	DF	31.86	2.10
69	4-5-09	15.26	6.99	DF	19.24	3.51
70	4-48-2	19.29	3.01	DF	12.60	5.41
71	4-48-3	18.96	2.62	DF	10.28	6.68
72	4-48-4	19.29	2.62	DF	8.30	8.37
73	4-49-1	21.23	2.07	DF	11.58	5.90
74	4-49-2	21.63	2.07	DF	13.87	4.90
75	4-49-3	22.02	2.07	DF	10.58	6.49
76	4-49-4	21.23	1.92	DF	9.88	6.97
77	4-49-5	21.63	1.92	DF	11.74	5.82
78	4-49-7	21.23	1.76	DF	12.68	5.37
79	4-49-8	21.63	1.76	DF	18.30	3.69
80	4-49-9	22.02	1.76	DF	11.84	5.77
81	4-21-01	19.56	5.43	DF	9.91	6.94
82	4-21-02	19.86	5.43	DF	7.32	9.58
83	4-21-03	20.17	5.43	DF	7.50	9.33
84	4-21-05	19.86	5.40	DF	12.79	5.33
85	4-21-06	20.17	5.40	DF	10.71	6.40
86	4-21-08	19.86	5.37	DF	6.11	11.66
87	4-21-09	20.17	5.37	DF	11.07	6.19
88	4-50-1	24.37	2.71	SF	4.92	14.88
89	4-50-2	25.35	2.71	SF	1.29	312.20
90	4-50-3	24.37	2.28	DF	3.03	27.26
91	4-50-4	25.35	2.28	DF	13.87	4.90
92	4-36-1	23.85	3.54	DF	28.59	2.35
93	4-36-2	24.26	3.54	DF	12.56	5.43
94	4-36-3	24.67	3.54	DF	9.02	7.67

N	Control Point	X [meters]	Y [meters]	Hydro Geo	time [seconds]	perm [darcy]
95	4-36-4	23.85	3.49	DF	10.45	6.57
96	4-36-5	24.26	3.49	DF	18.53	3.64
97	4-36-6	24.67	3.49	DF	8.43	8.24
98	4-36-7	23.85	3.45	DF	17.12	3.95
99	4-36-8	24.26	3.45	DF	9.44	7.31
100	4-36-9	24.67	3.45	DF	16.50	4.10
101	4-22-01	24.56	6.35	DF	7.74	9.02
102	4-22-02	24.77	6.35	DF	13.12	5.19
103	4-51-1	27.63	3.32	SF	4.24	17.72
104	4-51-4	27.63	3.07	DF	20.06	3.36
105	4-51-5	28.30	3.07	DF	7.70	9.07
106	4-51-6	28.97	3.07	DF	31.46	2.13
107	4-51-7	27.63	2.83	DF	10.01	6.87
108	4-51-8	28.30	2.83	SF	1.82	67.16
109	4-37-1	28.97	4.78	DF	7.59	9.21
110	4-37-2	29.16	4.78	DF	9.20	7.51
111	4-37-3	28.97	4.23	DF	7.63	9.16
112	4-37-4	29.16	4.23	DF	18.74	3.60
113	4-23-01	26.26	4.94	DF	4.03	18.84
114	4-23-02	26.62	4.94	DF	8.81	7.86
115	4-23-04	26.26	4.91	DF	7.80	8.95
116	4-23-05	26.62	4.91	DF	13.91	4.89
117	4-23-07	26.26	4.88	DF	59.41	1.12
118	4-23-08	26.62	4.88	DF	25.52	2.63
119	4-52-1	31.84	2.03	DF	12.38	5.51
120	4-52-2	31.89	2.03	DF	8.56	8.10
121	4-52-3	31.93	2.03	DF	18.81	3.59
122	4-52-4	31.84	1.91	DF	9.13	7.57
123	4-52-5	31.89	1.91	DF	6.00	11.90
124	4-52-6	31.93	1.91	DF	7.06	9.96
125	4-52-7	31.84	1.79	DF	10.34	6.64
126	4-52-8	31.89	1.79	DF	7.02	10.02
127	4-52-9	31.93	1.79	DF	9.12	7.58
128	4-38-2	29.37	3.95	DF	11.40	6.00
129	4-38-3	30.03	3.95	DF	10.28	6.68
130	4-38-4	28.72	3.64	DF	18.09	3.73
131	4-38-5	29.37	3.64	DF	13.13	5.18
132	4-38-6	30.03	3.64	DF	8.38	8.29
133	4-24-01	30.83	4.96	DF	7.24	9.69
134	4-24-02	31.04	4.96	DF	5.20	13.97
135	4-24-03	31.26	4.96	DF	12.00	5.69
136	4-24-04	30.83	4.94	DF	11.69	5.85
137	4-24-05	31.04	4.94	DF	7.43	9.42
138	4-24-06	31.26	4.94	DF	6.08	11.72
139	4-24-07	30.83	4.93	DF	11.18	6.12
140	4-24-08	31.04	4.93	DF	7.13	9.85
141	4-24-09	31.26	4.93	DF	6.20	11.47

Nevada Test Site -- Pit 4

N	Control Point	X [meters]	Y [meters]	Hydro Geo	time [seconds]	perm [darcy]
142	4-10-04	29.42	7.96	DF	18.50	3.65
143	4-10-05	29.45	7.96	DF	37.95	1.76
144	4-10-06	29.48	7.96	DF	7.16	9.81
145	4-10-07	29.42	7.70	DF	24.56	2.74
146	4-10-08	29.45	7.70	DF	21.09	3.19
147	4-10-09	29.48	7.70	DF	9.58	7.20
148	4-53-1	31.52	2.26	DF	11.97	5.70
149	4-53-2	32.26	2.26	DF	6.40	11.08
150	4-53-3	33.01	2.26	DF	16.36	4.14
151	4-53-4	31.52	2.20	DF	5.13	14.18
152	4-53-5	32.26	2.20	DF	7.74	9.02
153	4-53-6	33.01	2.20	DF	8.51	8.15
154	4-53-8	32.26	2.14	DF	12.00	5.69
155	4-39-3	35.59	3.86	SF	3.15	25.84
156	4-39-7	34.27	3.40	DF	6.17	11.54
157	4-39-8	34.93	3.40	DF	7.74	9.02
158	4-25-02	34.38	5.11	SF	5.44	13.27
159	4-25-03	35.08	5.11	SF	2.31	41.37
160	4-25-05	34.38	5.11	SF	7.24	9.69
161	4-25-06	35.08	5.11	SF	6.75	10.45
162	4-25-08	34.38	5.11	SF	3.93	19.43
163	4-25-09	35.08	5.11	SF	2.78	30.83
164	4-11-03	35.08	7.31	DF	5.94	12.03
165	4-11-05	34.62	7.02	DF	21.94	3.07
166	4-11-06	35.08	7.02	DF	22.14	3.04
167	4-11-08	34.62	6.73	DF	22.13	3.04
168	4-54-2	38.18	3.40	SF	5.16	14.09
169	4-54-3	38.25	3.40	SF	1.61	94.75
170	4-54-4	38.10	3.10	SF	1.75	74.21
171	4-54-5	38.18	3.10	SF	3.55	22.08
172	4-40-1	35.81	4.22	DF	5.50	13.11
173	4-40-2	36.46	4.22	DF	7.41	9.45
174	4-40-3	37.12	4.22	DF	6.84	10.31
175	4-40-4	35.81	4.01	DF	3.20	25.30
176	4-40-5	36.46	4.01	DF	7.84	8.90
177	4-40-6	37.12	4.01	DF	6.69	10.56
178	4-26-02	36.46	6.28	DF	8.24	8.44
179	4-26-03	35.37	6.10	DF	14.81	4.58
180	4-55-4	39.88	3.05	SF	12.92	5.27
181	4-41-1	39.64	3.93	DF	7.35	9.53
182	4-41-3	39.88	3.93	DF	6.52	10.86
183	4-41-5	39.76	3.68	SF	4.14	18.24
184	4-41-6	39.88	3.68	SF	7.38	9.49
185	4-41-7	39.64	3.44	DF	7.91	8.81
186	4-41-9	39.88	3.44	DF	56.31	1.18
187	4-27-04	40.96	5.95	DF	6.69	10.56
188	4-27-05	41.66	5.95	DF	3.88	19.74

Nevada Test Site -- Pit 4

N	Control Point	X [meters]	Y [meters]	Hydro Geo	time [seconds]	perm [darcy]
189	4-27-06	42.36	5.95	DF	14.75	4.60
190	4-27-07	40.96	5.79	DF	9.58	7.20
191	4-27-08	41.66	5.79	DF	5.02	14.54
192	4-27-09	42.36	5.79	DF	16.96	3.99
193	4-13-03	39.45	7.58	DF	12.85	5.30
194	4-13-05	39.17	7.55	DF	8.27	8.40
195	4-13-06	39.45	7.55	DF	2.10	49.26
196	4-56-1	42.36	2.38	DF	18.08	3.73
197	4-56-2	43.05	2.38	DF	25.81	2.60
198	4-56-3	43.74	2.38	DF	6.03	11.83
199	4-56-4	42.36	2.23	DF	9.91	6.94
200	4-42-1	43.96	4.10	DF	7.67	9.11
201	4-42-2	44.35	4.10	DF	8.16	8.53
202	4-42-3	44.73	4.10	DF	4.79	15.35
203	4-42-5	44.35	3.86	DF	11.78	5.80
204	4-42-6	44.73	3.86	DF	7.59	9.21
205	4-42-7	43.96	3.61	DF	8.47	8.19
206	4-42-9	44.73	3.61	DF	2.20	45.13
207	4-28-01	44.31	4.91	DF	7.31	9.59
208	4-28-02	44.35	4.91	DF	6.88	10.24
209	4-28-03	44.40	4.91	DF	13.62	4.99
210	4-28-04	44.31	4.82	DF	6.66	10.61
211	4-14-01	43.33	7.36	DF	5.46	13.22
212	4-14-03	43.75	7.36	DF	22.95	2.93
213	4-14-04	43.33	7.13	DF	16.53	4.09

Popotosa

I.D.	x [m]	z [m]	y [m]	k [darcy]	facies
1-1	-5.68	1.87	-16.06	8.11	1
2-1	-4.98	1.87	-16.06	11.01	1
3-1	-4.28	1.87	-16.06	16.5	1
4-1	-5.68	2.17	-16.06	8.58	1
5-1	-4.98	2.17	-16.06	4.64	1
6-1	-4.28	2.17	-16.06	9.92	1
7-1	-5.68	2.47	-16.06	16.79	1
8-1	-4.98	2.47	-16.06	6.57	1
9-1	-4.28	2.47	-16.06	10.69	1
1-2	-4.11	3.72	-16.85	4.15	2
2-2	-3.81	3.72	-16.85	6.99	2
3-2	-3.51	3.72	-16.85	5.72	2
4-2	-4.11	3.92	-16.85	8.18	2
5-2	-3.81	3.92	-16.85	5.58	2
6-2	-3.51	3.92	-16.85	6.23	2
7-2	-4.11	4.12	-16.85	5.93	2
8-2	-3.81	4.12	-16.85	6.29	2
9-2	-3.51	4.12	-16.85	8.11	2
1-3	-2.83	2.59	-15.97	7.12	1
2-3	-2.73	2.59	-15.97	4.57	1
3-3	-2.63	2.59	-15.97	7.36	1
4-3	-2.83	2.69	-15.97	6.92	1
5-3	-2.73	2.69	-15.97	7.36	1
6-3	-2.63	2.69	-15.97	9.06	1
7-3	-2.83	2.79	-15.97	7.21	1
8-3	-2.73	2.79	-15.97	13.93	1
9-3	-2.63	2.79	-15.97	7.93	1
1-4	-2.54	3.64	-16.93	5.42	2
2-4	-2.39	3.64	-16.93	10.34	2
3-4	-2.24	3.64	-16.93	5.35	2
4-4	-2.54	3.74	-16.93	7.34	2
5-4	-2.39	3.74	-16.93	5.97	2
6-4	-2.24	3.74	-16.93	5.46	2
7-4	-2.54	3.84	-16.93	11.18	2
8-4	-2.39	3.84	-16.93	6.27	2
9-4	-2.24	3.84	-16.93	8	2
1-5	-0.88	3.95	-17.15	4.54	2
2-5	-0.83	3.95	-17.15	7.14	2
3-5	-0.78	3.95	-17.15	7.64	2
4-5	-0.88	4.15	-17.15	8.41	2
5-5	-0.83	4.15	-17.15	6.81	2
6-5	-0.78	4.15	-17.15	7.83	2
7-5	-0.88	4.35	-17.15	4.7	2
8-5	-0.83	4.35	-17.15	6.11	2
9-5	-0.78	4.35	-17.15	7.66	2
1-6	-2.71	2.75	-16.36	9.72	1
2-6	-2.31	2.75	-16.36	6.25	1

I.D.	x [m]	z [m]	y [m]	k [darcy]	facies
3-6	-1.91	2.75	-16.36	8.18	1
4-6	-2.71	2.8	-16.36	5.35	1
5-6	-2.31	2.8	-16.36	7.09	1
6-6	-1.91	2.8	-16.36	9.17	1
7-6	-2.71	2.85	-16.36	5.98	1
8-6	-2.31	2.85	-16.36	7.43	1
9-6	-1.91	2.85	-16.36	7.34	1
1-7	-1.05	3.2	-16.58	11.22	1
2-7	-0.9	3.2	-16.58	12.87	1
3-7	-1.05	3.45	-16.58	7.49	1
4-7	-0.9	3.45	-16.58	7.81	1
1-8	6.3	2.15	-16.24	7.62	1
2-8	6.55	2.15	-16.24	4.08	1
3-8	6.8	2.15	-16.24	6.25	1
4-8	6.3	2.35	-16.24	5.91	1
5-8	6.55	2.35	-16.24	4.48	1
6-8	6.8	2.35	-16.24	4.55	1
7-8	6.3	2.55	-16.24	3.59	1
8-8	6.55	2.55	-16.24	4.13	1
9-8	6.8	2.55	-16.24	6.4	1
1-9	6.49	4.62	-18.06	9.79	1
2-9	6.64	4.62	-18.06	18.08	1
3-9	6.79	4.62	-18.06	14.79	1
4-9	6.49	4.72	-18.06	8.87	1
5-9	6.64	4.72	-18.06	14.94	1
6-9	6.79	4.72	-18.06	18.08	1
7-9	6.49	4.82	-18.06	17.96	1
8-9	6.64	4.82	-18.06	18.67	1
9-9	6.79	4.82	-18.06	14.06	1
1-10	8.31	5.39	-18.69	20.15	4
2-10	9.31	5.39	-18.69	14.34	4
3-10	8.31	5.74	-18.69	13.6	4
4-10	9.31	5.74	-18.69	19.32	4
1-11	10.98	5.57	-19.33	5.33	4
2-11	11.08	5.57	-19.33	6.4	4
3-11	11.18	5.57	-19.33	3.52	4
4-11	10.98	5.77	-19.33	8.18	4
5-11	11.08	5.77	-19.33	7.76	4
6-11	11.18	5.77	-19.33	8.51	4
7-11	10.98	5.97	-19.33	5.03	4
8-11	11.08	5.97	-19.33	8.58	4
9-11	11.18	5.97	-19.33	11.49	4
1-12	7.99	3.05	-17.16	11.49	1
2-12	8.04	3.05	-17.16	6.06	1
3-12	8.09	3.05	-17.16	5.05	1
4-12	7.99	3.25	-17.16	4.39	1
5-12	8.04	3.25	-17.16	4.82	1
6-12	8.09	3.25	-17.16	3.98	1

I.D.	x [m]	z [m]	y [m]	k [darcy]	facies
13-1	11.37	1.87	-16.76	6.86	3
13-2	11.87	1.87	-16.76	3.78	3
13-3	11.37	2.37	-16.76	3.59	3
13-4	11.87	2.37	-16.76	4.73	3
14-1	11.24	3.14	-17.82	5.82	1
14-2	11.49	3.14	-17.82	5.46	1
14-3	11.24	3.74	-17.82	5.44	1
14-4	11.49	3.74	-17.82	5.56	1
15-1	16.33	2.64	-17.33	5.2	3
15-2	17.13	2.64	-17.33	5.45	3
15-3	16.33	2.84	-17.33	4.2	3
15-4	17.13	2.84	-17.33	5.98	3
16-4	11.74	2.54	-17.38	2.58	3
16-2	11.79	2.54	-17.38	3.76	3
16-3	11.74	2.59	-17.38	4.37	3
16-4	11.79	2.59	-17.38	3.41	3
17-1	1.02	2.97	-17.05	12.27	1
17-2	1.22	2.97	-17.05	8.34	1
17-3	1.42	2.97	-17.05	3.83	1
17-4	1.02	3.07	-17.05	3.58	1
17-5	1.22	3.07	-17.05	8.46	1
17-6	1.44	3.07	-17.05	9.82	1
17-7	1.02	3.17	-17.05	8.56	1
17-8	1.22	3.17	-17.05	5.29	1
17-9	1.42	3.17	-17.05	4.37	1
18-1	0.98	3.54	-17.16	9.72	2
18-2	1.08	3.54	-17.16	10.89	2
18-3	1.18	3.54	-17.16	12.37	2
18-4	0.98	3.69	-17.16	9.56	2
18-5	1.08	3.69	-17.16	6.81	2
18-6	1.18	3.69	-17.16	7.95	2
18-7	0.98	3.84	-17.16	10.61	2
18-8	1.08	3.84	-17.16	6.07	2
18-9	1.18	3.84	-17.16	10.06	2
19-1	20.28	5.54	-20.74	17.52	4
19-2	20.4	5.54	-20.74	8.58	4
19-3	20.28	5.66	-20.74	18.8	4
19-4	20.4	5.66	-20.74	6.76	4
20-1	17.64	5.08	-19.86	11.22	4
20-2	17.79	5.08	-19.86	4.77	4
20-3	17.94	5.08	-19.86	4.86	4
20-4	17.64	5.23	-19.86	5.75	4
20-5	17.79	5.23	-19.86	12.21	4
20-6	17.94	5.23	-19.86	10.76	4
20-7	17.64	5.38	-19.86	3.77	4
20-8	17.79	5.38	-19.86	5.42	4
20-9	17.94	5.38	-19.86	5.02	4
21-1	18.09	6.52	-21.73	9.44	4

I.D.	x [m]	z [m]	y [m]	k [darcy]	facies
21-2	18.09	6.77	-21.73	10.09	4
22-1	19.55	6.53	-21.81	11.44	4
22-2	19.75	6.53	-21.81	23.17	4
22-3	19.95	6.53	-21.81	16.21	4
22-4	19.55	6.71	-21.81	9.63	4
22-5	19.75	6.71	-21.81	7.02	4
22-6	19.95	6.71	-21.81	8.58	4
22-7	19.55	6.89	-21.81	9.35	4
22-8	19.75	6.89	-21.81	6.29	4
22-9	19.95	6.89	-21.81	6.99	4
23-1	21.95	1.97	-17.41	3.47	3
23-2	22.15	1.97	-17.41	3.2	3
23-3	22.35	1.97	-17.41	3.88	3
23-4	21.95	2.17	-17.41	2.87	3
23-5	22.15	2.17	-17.41	3.13	3
23-6	22.35	2.17	-17.41	2.97	3
23-7	22.15	2.37	-17.41	5.12	3
23-8	22.35	2.37	-17.41	6.67	3
23-9	22.35	2.37	-17.41	5.92	3
24-1	28.13	2.25	-17.81	3.52	3
24-2	28.23	2.25	-17.81	4.88	3
24-3	28.33	2.25	-17.81	3.81	3
24-4	28.13	2.35	-17.81	3.47	3
24-5	28.23	2.35	-17.81	4.18	3
24-6	28.33	2.35	-17.81	4.17	3
24-7	28.13	2.45	-17.81	4.51	3
24-8	28.23	2.45	-17.81	5.31	3
24-9	28.33	2.45	-17.81	5.24	3
25-1	33.3	2.2	-17.99	4.96	3
25-2	33.8	2.2	-17.99	6.37	3
25-3	34.3	2.2	-17.99	5.29	3
25-4	33.3	2.4	-17.99	7.27	3
25-5	33.8	2.4	-17.99	5.3	3
25-6	34.3	2.4	-17.99	4.92	3
25-7	33.3	2.6	-17.99	4.3	3
25-8	33.8	2.6	-17.99	6.27	3
25-9	34.3	2.6	-17.99	4.8	3
26-1	33.25	5.72	-21.64	5.91	4
26-2	33.58	5.72	-21.64	3.47	4
26-3	33.91	5.72	-21.64	2.69	4
26-4	33.25	5.85	-21.64	5.85	4
26-5	33.91	5.85	-21.64	4.9	4
26-6	33.58	5.85	-21.64	5.1	4
26-7	33.25	5.98	-21.64	5.06	4
26-8	33.58	5.98	-21.64	5.85	4
26-9	33.91	5.98	-21.64	15.1	4
27-1	28.69	5.44	-20.89	5.18	4
27-2	28.84	5.44	-20.89	5.11	4

I.D.	x [m]	z [m]	y [m]	k [darcy]	facies
27-3	28.99	5.44	-20.89	6.06	4
27-4	28.69	5.52	-20.89	7.32	4
27-5	28.84	5.52	-20.89	7.74	4
27-6	28.99	5.52	-20.89	5.67	4
27-7	28.69	5.6	-20.89	9.35	4
27-8	28.84	5.6	-20.89	5.35	4
27-9	28.99	5.6	-20.89	5.68	4
28-1	27.39	3.88	-19.37	5.92	4
28-2	27.91	3.88	-19.37	5.32	4
28-3	27.39	3.93	-19.37	15.42	4
28-4	27.91	3.93	-19.37	9.29	4
29-1	27.88	6.58	-21.9	9.06	4
29-2	28.02	6.58	-21.9	3.98	4
29-3	28.16	6.58	-21.9	6.73	4
29-4	27.88	6.75	-21.9	6.07	4
29-5	28.02	6.75	-21.9	8.79	4
29-6	28.16	6.75	-21.9	4.58	4
29-7	27.88	6.92	-21.9	8.51	4
29-8	28.02	6.92	-21.9	8.13	4
29-9	28.16	6.92	-21.9	7.66	4

APPENDIX C: Survey Data

Survey data for Summer 1992 mapping of the Bosque Site

Horizontal datum taken to be 5000 feet west of Benchmark BM-I25-54 located west of the southbound lane of Interstate 25 near fence on the Socorro/Valencia County line. The Benchmark serves as survey Station-001 with the following coordinates. The instrument was zeroed to the top of a hill to the north also just west of the interstate. The north and east distances to the hill crest were obtained from the U.S.G.S. 7.5 minute topographic map.

STAT 001

INSTRUMENT POSITION		BACKSIGHT	
North	0	Hill peak on topo	
East	5000	North	16600
Elevation	4808.47	East	6950
Instrument Height	5.2		

	DESCRIPTION	N COORD	E COORD	ELEV
01-1	Station 42	1367.93	3667.77	4903.18

STAT 042

INSTRUMENT POSITION		BACKSIGHT	
North	1366.28	Station #01	
East	3669.38	North	0
Elevation	4903.18	East	5000
Instrument Height	3.98		

	DESCRIPTION	N COORD	E COORD	ELEV
42-1	BS to I-25-54	0.01	4999.99	4807.94
42-2	Station 40	1958.63	1797.55	5163.83
42-3	Station 45	3243.19	1047.67	5182.36
42-4	Station 50	4432.70	1508.64	5166.26
42-5	Station 51	4089.74	2363.82	5009.53
42-6	Station 52	4254.00	2759.61	4972.72

STAT 051

INSTRUMENT POSITION		BACKSIGHT	
North	4089.74	Station #52	
East	2363.82	North	4254.00
Elevation	5009.53	East	2759.61
Instrument Height	4.37		

	DESCRIPTION	N COORD	E COORD	ELEV
51-1	backsight to 52	4252.76	2756.61	4970.67

51-2	bs of 106 clay	3583.14	2163.75	4991.63
51-3	tp of stake in P	3651.13	1959.00	5018.25
51-4	top main Org s. soil	3751.55	1785.29	5033.26
51-5	sndy gvl/thck sndy soil	3806.82	1634.19	5059.14
51-6	P/brn cly	3855.60	1557.74	5071.68
51-7	gvl/sand; alcove S. side	3904.78	1527.47	5063.41
51-8	top of rcs on nose	3758.51	1769.19	5043.93
51-9	scour/P	3859.52	1894.02	5010.75
51-10	same scour	3824.35	1849.19	5009.03
51-11	same scour	3632.82	1998.08	5015.74
51-12	brn cly/tan sand	3451.53	1673.41	5019.29
51-13	106 clay/sand/grv	4082.78	2189.59	4990.02
51-14	stake	3065.52	1766.82	5020.45
51-15	clay/sand soil	4054.13	1990.36	4994.89
51-16	top of rcs	3109.09	1604.86	5041.24
51-17	stake	3115.01	1577.90	5053.04
51-18	scour	4149.99	1911.36	5013.81
51-19	top of stake	3012.38	2098.29	4973.53

STAT 052

INSTRUMENT POSITION		BACKSIGHT	
North	4254.00	Station #42	
East	2759.61	North	1366.28
Elevation	4972.72	East	3669.38
Instrument Height	4.62		

	DESCRIPTION	N COORD	E COORD	ELEV
52-1	BS to stat042	1366.11	3669.43	4904.04
52-2	Station 40	1960.30	1797.54	5165.04
52-3	Station 45	3243.93	1047.54	5184.09
52-4	Station 50	4434.48	1510.89	5168.16
52-5	Station 51	4091.18	2366.53	5011.64
52-6	Station 61	5364.38	2014.81	4977.05
52-7	Station 73	6171.94	1614.74	4975.44
52-8	Station 71	6536.53	1888.68	5000.99
52-9	Station 72	6444.72	3098.33	4921.39

STAT 061

INSTRUMENT POSITION		BACKSIGHT	
North	5364.38	Station #52	
East	2014.81	North	4254.00
Elevation	4977.05	East	2759.61
Instrument Height	4.58		

	DESCRIPTION	N COORD	E COORD	ELEV
61-1	backsight to 52	4254.08	2759.56	4972.74

61-2	stake	4542.61	1918.95	4993.64
61-3	station 51	4090.35	2363.66	5011.66
61-4		4209.60	2158.86	5033.16
61-5	gvl ledge/sand (rod=0)	4325.92	2032.02	5066.36
61-6	stake	4420.20	2072.23	5002.63
61-7	top of rcs	4333.92	2062.09	5044.04
61-8	brn cly/org soil; rod=0	4444.80	1891.69	5035.75
61-9	stake	4575.28	1859.79	4994.44
61-10	congl over sand; rod=0	4453.97	1838.75	5065.50
61-11	stake	4672.41	1839.39	4988.78
61-12	top of rcs	4494.12	1812.33	5049.87
61-13	stake	4825.19	1853.75	4988.85
61-14	brn cly/org soil; rod=0	4529.92	1734.33	5038.68
61-15		5084.80	1757.44	4986.42
61-16	brn clay/org s.soil	5017.43	1676.69	5028.64
61-17	top of org s.soil	4630.87	1710.76	5035.52
61-18	top of rcs	4991.95	1607.49	5048.90
61-19	top of rcs	4625.20	1689.90	5048.69
61-20	gvl over sand; rod=0	4607.94	1663.80	5065.72
61-21	top org s.soil	4649.31	1590.83	5033.06
61-22	sand over soil	4957.27	1573.24	5060.92
61-23	top of rcs	4675.92	1558.02	5049.06
61-24	gvl over sand	4673.10	1535.94	5065.90
61-25	gvl of pale s. soil	4693.15	1490.12	5092.20
61-26	brn cly/org s.soil	4791.87	1648.78	5031.41
61-27	top of rcs	4792.77	1602.42	5048.85
61-28	base of gvl; rod=0	4817.06	1572.34	5063.87
61-29	stake in main org sand	5449.75	1634.03	5030.41
61-30	top of rcs	5439.99	1592.49	5049.35
61-31	gvl over s.soil	5431.62	1569.68	5064.96

STAT 071

INSTRUMENT POSITION		BACKSIGHT	
North	6536.53	Station #61	
East	1888.68	North	5364.38
Elevation	5000.99	East	2014.81
Instrument Height	4.51		

	DESCRIPTION	N COORD	E COORD	ELEV
71-1	backsight 61	5364.55	2014.79	4977.12
71-2	stake; s. soil/grv	5496.91	1810.77	4989.43
71-3	stake; tp of same grv	5695.58	1571.89	4991.12
71-4	top of gvl SW of 73	5944.79	1473.49	4990.08
71-5	top of gvl NW of 73	6313.07	1540.24	4990.77
71-6	stk in saddle	7399.46	2702.57	5003.17
71-7	top of orng s. soil	6923.62	1830.41	5030.30
71-8	target @ top of rcs	6937.40	1819.56	5045.18
71-9	tgt @ base of sand&gvl	6958.65	1825.40	5058.92
71-10	sta 11; top of Fred	7720.05	2617.34	5103.86
71-11	gvl over brn cly @ tgt	6809.05	1629.97	5060.52

71-12	sta 9 up on top	7945.40	2193.57	5154.19
71-13	s. grv/org s. soil	6752.16	1652.74	5058.95
71-14	s. soil/rcs	6738.97	1659.39	5047.41
71-15	top of main orng s.soil	6734.27	1678.62	5032.59
71-16	tgt @ top of rcs	6608.33	1412.82	5047.36
71-17	s. grv / org s. soil	6591.16	1415.50	5053.88
71-18	tgt @ top of rcs	6499.40	1537.35	5052.87
71-19	top org s. soil	6486.44	1562.12	5030.90
71-20	top of 106 gvl	6526.35	1690.48	4989.81

STAT 072

INSTRUMENT POSITION		BACKSIGHT	
North	6444.72	Station #52	
East	3098.33	North	4254.00
Elevation	4921.39	East	2759.61
Instrument Height	4.13		

	DESCRIPTION	N COORD	E COORD	ELEV
72-1	BS to Station 52	4254.03	2759.62	4972.81
72-2	Station 51	4092.47	2362.29	5011.69
72-3	Station 50	4435.48	1509.61	5168.17
72-4	Station 70	6360.51	592.30	5189.95
72-5	Base of Grv sim. to FMP	6444.25	1454.16	5064.67
72-6	Station 73	6175.18	1614.27	4975.71
72-7	Station 61	5365.79	2013.72	4977.19
72-8	Station 71	6538.68	1888.80	5001.24

STAT 72B

INSTRUMENT POSITION		BACKSIGHT	
North	6444.72	Station #61	
East	3098.33	North	5364.38
Elevation	4921.39	East	2014.81
Instrument Height	4.33		

	DESCRIPTION	N COORD	E COORD	ELEV
72-9	backsight to 61	5364.47	2014.90	4977.20
72-10	old station 15	7583.07	2884.17	5014.41
72-11	old station 11	7721.95	2617.85	5103.93
72-12	old station 9	7946.29	2194.44	5154.05
72-12	top of escarpment	7711.66	1668.60	5175.21
72-13	gravel over red s.soil	7506.94	2003.51	5057.87
72-14	old station 18	7551.92	2107.44	5013.54
72-15	top of orange s. soil	7476.63	2062.85	5028.79
72-16	base of brn clay ("106")	7416.66	2144.72	4988.63
72-17	rs1	7146.80	1999.50	4989.18
72-18	rs2 ("106" position)	6867.73	1979.24	4991.10
72-19	station 71	6539.35	1888.71	5001.18

STAT070

INSTRUMENT POSITION		BACKSIGHT	
North	6360.51	Station #73	
East	592.30	North	6175.18
Elevation	5189.95	East	1614.27
Instrument Height	4.27		

	DESCRIPTION	N COORD	E COORD	ELEV
70-1	BS to stat 073	6175.10	1614.71	4975.45
70-2	Station 75	6155.41	1069.27	5079.69
70-3	tip promentory E of	6322.43	882.36	5127.10
70-4	gully NE of 70	6443.42	708.07	5137.55
70-5	nose NE of 70	6470.33	903.97	5132.97

STAT075

INSTRUMENT POSITION		BACKSIGHT	
North	6155.41	Station #70	
East	1069.27	North	6360.51
Elevation	5079.69	East	592.30
Instrument Height	4.44		

	DESCRIPTION	N COORD	E COORD	ELEV
75-1	backsight to 70	6360.53	592.26	5189.84
75-2	tp P cut to E by Fred	6416.61	1140.00	5074.58
75-3	base of lwr Fred N of 75	6404.05	1140.75	5061.52
75-4	brn clay/s.soil	6394.56	1108.10	5048.72
75-5	base of red cly soil	6378.64	1128.44	5043.65
75-6	top of white overbnks	6333.30	1107.97	5019.93
75-7	see map in notebook	6308.14	1087.21	5014.65
75-8	bs tsand/brn cly/P	6311.15	1124.17	4997.70
75-9	prism @ level of 106'	6310.37	1180.38	4988.37
75-10	bs s chnl below White	6251.34	1071.33	4999.33
75-11	bs white/p w/ sand to E	6232.93	1058.60	5011.18
75-12	see topo map in notebook	6272.36	1065.90	4983.33
75-13	base sndy chnl/brn cly	6369.89	1049.65	4999.12
75-14	tan sand/red cly	6344.48	1078.96	5003.04
75-15	edge ts chnl rod=3=white	6332.68	1089.35	5011.39
75-16	base of E-W sand chnnl	6351.24	1031.21	5000.53
75-17	south end of E-W chnnl	6319.23	1026.19	5012.38
75-18	base of red cly soil	6305.54	999.16	5042.24
75-19	base of upper Fred	6312.97	964.89	5061.34
75-20	base of Ruth	6316.80	954.34	5067.51
75-21	near top of wht overbnks	6273.08	1025.98	5019.22
75-22	contace: ts ch; mball ch	6270.03	989.51	5023.03
75-23	same	6273.69	996.60	5021.26

75-24	White betwn 2 s. ch	6338.81	1018.37	5019.64
75-25	tp prom cmt white sand	6335.77	1004.50	5027.97
75-26	see topo map in notebook	6365.47	1038.07	4991.18
75-27	bottom of gully	6410.20	1043.31	5000.41
75-28	bs E-W ch/brn cly/ org s. soil/ 106	6385.80	1044.38	4998.57
75-29	bs of white s. ch w/ thck clay @ top/org. s. soil	6300.80	1225.10	4997.35
75-30	target in lam silts & clays; 2' below ch	6424.19	1319.10	5002.70
75-31	station 73	6172.35	1613.66	4975.50
75-32	top of 106'	6312.50	1540.33	4990.73
75-33	top of wht chnnl	6373.09	1488.84	5014.96
75-34	base of red cly soil	6410.48	1458.66	5044.35
75-35	base of upper Fred	6431.53	1444.64	5065.06
75-36	top of wht overbnks	6130.36	1335.81	5019.28
75-37	base of upper Fred	6106.63	1243.96	5063.64
75-38	sand over soil	6117.96	1100.03	5074.74
75-39	edge of sand chnnl	6155.41	1069.27	5084.13

STATN19

INSTRUMENT POSITION		BACKSIGHT	
North	7741.64	Station 18	
East	2002.84	North	7551.92
Elevation	5001.48	East	2107.44
Instrument Height	3.79		

	DESCRIPTION	N COORD	E COORD	ELEV
19-1	BS to old 18	7550.83	2108.04	5013.46
19-2	SW edge MnO chnl	7622.60	2029.44	5014.98
19-3	top orng s.soil	7609.00	2009.58	5029.15
19-4	base sand chnl	7629.38	1975.37	5034.17
19-5	see notes	7724.08	1896.83	5041.08
19-6	see notes	7723.49	1859.22	5051.15
19-7	base lower Fred	7742.01	1837.04	5055.38
19-8	top soil/up Fred	7828.43	1890.57	5067.66
19-9	base lower Fred	7834.86	1921.29	5052.83
19-10	base red cly soi	7841.33	1926.26	5039.74
19-11	base sand/brn cl	7902.20	1955.19	5040.14
19-12	top orng s.soil	7893.00	1951.37	5028.14
19-13	see notes	7849.43	2008.50	5021.38
19-14	top orng s.soil	7803.98	2035.72	5028.18
19-15	see notes	7752.54	2061.75	5009.17
19-16	base M&M chnnl	7697.54	2120.30	5008.90
19-17	see notes	7774.12	2131.93	5050.12
19-18	see notes	7799.73	2059.69	5046.53

STAT 018

INSTRUMENT POSITION		BACKSIGHT	
North	7551.92	Station #19	
East	2107.44	East	7741.64
Elevation	5013.00	East	2002.84
Instrument Height	4.53		

	DESCRIPTION	N COORD	E COORD	ELEV
18-1	BS to 19	7743.07	2002.05	5000.90
18-2	see notes	7734.31	2150.27	5016.97
18-3	up 106 NE of 18	7549.79	2177.39	4983.55
18-4	base low Frd/s.s	7538.30	2020.38	5052.53
18-5	base sand chn/Fr	7550.72	2002.33	5056.45
18-6	stk SW of 18 (81)	7467.48	2034.31	5036.15
18-7	base M&M chnnl	7453.86	2088.62	5014.28

STAT081

INSTRUMENT POSITION		BACKSIGHT	
North	7467.48	Station #18	
East	2034.31	North	7551.92
Elevation	5036.15	East	2107.44
Instrument Height	4.25		

	DESCRIPTION	N COORD	E COORD	ELEV
81-1	BS to old 18	7553.98	2109.22	5012.11
81-2	top edge M&M ch.	7414.90	2013.61	5013.65
81-3	see notes	7373.76	1903.32	4986.77
81-4	base overbnk cly	7409.69	1850.54	5014.48
81-5	base brn cly/ovb	7411.36	1810.99	5036.68
81-6	base Frd/o.s.soi	7403.23	1767.42	5056.78
81-7	see notes	7440.88	1752.27	5045.64
81-8	see notes	7468.84	1733.49	5036.94
81-9	base scour/brncl	7511.31	1715.15	5034.55
81-10	sand/red cly soi	7380.13	1785.53	5043.06
81-11	base of chnnl	7383.22	1793.00	5038.89
81-12	N edge of chnnl	7404.53	1804.04	5041.40
81-13	base of wing	7392.45	1786.71	5046.92
81-14	see notes	7334.52	1741.31	5038.97
81-15	top main o.s.soi	7309.07	1765.46	5028.79
81-16	base red cly soi	7240.16	1783.34	5039.93
81-17	see notes	7206.54	1860.49	5016.56
81-18	stk top of 106	7150.42	2000.43	4987.81

STAT @ Reference Stake #1

INSTRUMENT POSITION		BACKSIGHT	
North	7146.80	Reference	Stake #2
East	1999.50	North	6867.73
Elevation	4989.18	East	1979.24
Instrument Height	4.02		

	DESCRIPTION	N COORD	E COORD	ELEV
81-19	BS to rs-2	6866.50	1979.15	4991.10
81-20	N. side of CH	6889.05	1955.30	4998.04
81-21	S. side of CH	6887.15	1933.55	4998.90
81-22	top O.S.S.	6964.54	1866.05	5030.20
81-23	top R.C.S.	6969.52	1839.18	5043.83
81-24	Base of grvly Fred	6986.79	1823.33	5056.61
81-25	Edge small CH below	6978.66	1914.08	4995.54
81-26	base of small chann	6988.82	1921.15	4992.57
81-27	other edge	7005.69	1925.63	4994.27
81-28	base of channel win	7043.20	1885.26	4996.78
81-29	N edge of little CH	7077.46	1895.73	4992.28
81-30	base of channel	7052.88	1892.17	4993.75

Common Abbreviations:

106 Refers to the stratigraphic level of the base of the study section
BS Backsight
bs Base, as in base ....
FMP Refers to the stratigraphic level of the top of the study section (also referred to, affectionately, as "the Fred")
gvl gravel
lam laminated
M&M sand channel with both manganese and maroon staining
org orange
o s. orange, sandy
rcs red clay soil, used as marker bed
rs reference stake, as in rs1 = reference stake 1
Ruth equivalent to element Pgs
stk stake
tgt prism on survey rod
tp top, as in top of ....
white overbank element type 2 (OF-II) located in the southern part of the mapped area